Magnetic field line connection between the ionosphere and the magnetosphere — Auroral activity and relevant magnetic field variations at geosynchronous orbit —

磁気圏・電離圏間の磁力線の結合関係に関する研究 — オーロラ活動と関連した静止軌道上の磁場変動 —

Nozomu Nishitani
西谷　望
Solar-Terrestrial Environment Laboratory
Nagoya University
名古屋大学太陽地球環境研究所

Abstract

Magnetic field variations, recorded on geosynchronous satellites GOES 5 and GOES 6 during the expansion phase of substorms, are compared with simultaneous auroral activity within the ground conjugate areas of these satellites, in order to examine the magnetic field connection between the ionosphere and the magnetosphere. Auroral image data were acquired by multi-station all-sky TV cameras during the Global Aurora Dynamics Campaign, from December 1985 to February 1986. Twelve examples of simultaneously observed substorm expansions at GOES 5, GOES 6, and the ground-based auroral TV stations have been selected for analysis.

It is found that field-aligned current structures, associated with active auroral forms such as bulges and surges, are highly localized at geosynchronous altitudes. On the basis of this evidence, the ionospheric foot (conjugate) points of magnetic field line passing through the geosynchronous satellites can be examined, by comparing the small-scale field-aligned currents observed at geosynchronous orbit with the simultaneous development of auroral bulges and surges in substorm expansions. The latitude of the foot point of the geosynchronous satellite depends primarily on the Dst index and the inclination angle of the magnetic field vector at the satellite. This indicates the significant role of the intensity of the ring and/or magnetotail currents. The AE and Kp indices are of lesser importance.

The longitude of the foot point of the geosynchronous satellite often deviates by 10 to 15 degrees from the calculated position based on Tsyganenko's magnetic field model (1987). This deviation is eastward (westward) on the west (east) side of the expansion onset meridian. This is most likely due to the effects of large scale Region 1 and Region 2 field-aligned currents on either side of the satellite, which are not explicitly included in Tsyganenko's model.

The characteristics of Tsyganenko's model are examined here, in order to test the validity of the model. As a result of mapping analysis, several shortcomings of the model are evident. Most of them are largely due to the absence from the model of field-aligned currents. They are

also partly due to the limited spatial extent of the observational data set used in establishing the model, and, more essentially, to the inappropriate mathematical expression of the model in some specific magnetospheric regions. A magnetospheric model based on a 3-dimensional MHD simulation is also examined, from which a highly localized magnetic field distortion is found in the near-earth magnetotail, indicating the presence of large scale but localized field-aligned currents. In addition, field-aligned components of the currents in Tsyganenko's model are examined directly. It is shown that large-scale but localized field-aligned currents, which satisfy current continuity along field lines, are not included in Tsyganenko's model.

On the basis of the confirmation of the absence of field-aligned currents, Tsyganenko's magnetic field model is modified by introducing the Region 1 and Region 2 field-aligned currents. For current intensities appropriate to a disturbed period of the magnetosphere, the azimuthal deviation of the foot point of a geosynchronous satellite is about 10° in longitude from that estimated by using Tsyganenko's model. The magnitude of magnetic field line deflection is determined mainly by the intensity of Region 1 and Region 2 field-aligned currents together with the relative location of the magnetic field line of interest to these currents. The mapping characteristics of the Tsyganenko's modified magnetic field model are similar to that of the field model from the MHD simulation, supporting the usefulness of MHD simulation of the magnetosphere to infer the magnetic field distribution in the magnetosphere.

The intensity of field-aligned currents is examined using two available examples from data obtained by the polar-orbiting satellite DMSP-F7. The current observed by the satellite for one event is consistent with the observed magnetic field line deflection of 10° in longitude. For the other event, the current can account for a field line deflection which is only about a half of that observed. This could be attributed to the difference in time relative to the peak of the expansion. The auroral surge of interest for both events was located at the position where a significant deflection of the magnetic field line, by large-scale field-aligned currents, was expected.

Acknowledgements

The author wishes to express a heartly gratitude to Prof. T. Oguti for his continuing guidance and encouragement throughout the course of this study. He is also indebted to Prof. N. Matuura, Dr. T. Ogino, and Dr. K. Yumoto for their valuable discussion and continuing guidance. He is also indebted to Dr. T. Watanabe, Mr. A. Iwata, and the other members in Solar-Terrestrial Environment Laboratory, Nagoya University for their great support for the completion of this thesis.

The author is grateful to Prof. T. Tamao, Prof. S. Kokubun, Dr. T. Iijima, Dr. K. Hayashi, and Dr. Tatsundo Yamamoto for the fruitful discussions. Thanks are due to the other members in GRL (now EPP/STP), University of Tokyo throughout the author's graduate career.

Thanks are due to Prof. M.W.J. Scourfield, Prof. R.E. Horita, and Mr. Gavin Hough for kindly checking and correcting my thesis.

The author wishes to express his thanks to all members of the GADC campaign for their kind support to the observations in Canada, Alaska, and Norway. The author is indebted to Dr. F.J. Rich and Dr. T. Ono for providing DMSP-F7 magnetic field and particle data. Thanks are due to Mr. H. Nakajima for providing the computer programs to analyze DMSP-F7 particle data.

Contents

1. General Introduction

1.1. Magnetospheric Configuration

The earth's magnetic dipole field is continuously interacting with a unidirectionally streaming plasma, namely, the solar wind. This plasma flow confines the geomagnetic field to a cavity called the 'magnetosphere' bounded by the 'magnetopause'. The dayside magnetosphere is compressed by the solar wind, while the nightside is extended antisunward due to the tangential stress of the solar wind and forms the 'magnetotail' as illustrated in Figure 1.1.

As a result of the solar wind-magnetosphere dynamo process, there are four major current systems which form the magnetospheric configuration; the ring, magnetotail, magnetopause, and field-aligned currents. These currents are now briefly summarized.

1.1.1. Magnetopause currents

Magnetopause currents (MPC) flow as shown in Figure 1.2 along the magnetopause from the dawnside to the duskside at low latitudes, while they flow in the opposite direction at dayside high latitudes (Chapman and Ferraro, 1931; Mead and Beard, 1964). As a result two current vortices are formed in the northern and southern hemisphere centered on the magnetic neutral point called the 'cusp', where the magnetic field is perpendicular to the magnetopause surface. These currents shield the earth's magnetic field from the solar wind, while inside the dayside magnetopause the magnetic field is compressed. The approximate location of the magnetopause is determined by the balance of the dynamic pressure of the solar wind by that of the magnetic pressure of the magnetosphere. The geocentric distance of the magnetopause toward the sun averages 10 to 11 R_E (the earth's radius), and it ranges from about 15 R_E to 6 R_E, depending mainly on the variations in dynamic pressure of the solar wind.

1.1.2. Magnetotail currents

As shown in Figure 1.2 the magnetotail current flows through the neutral sheet (NSC)

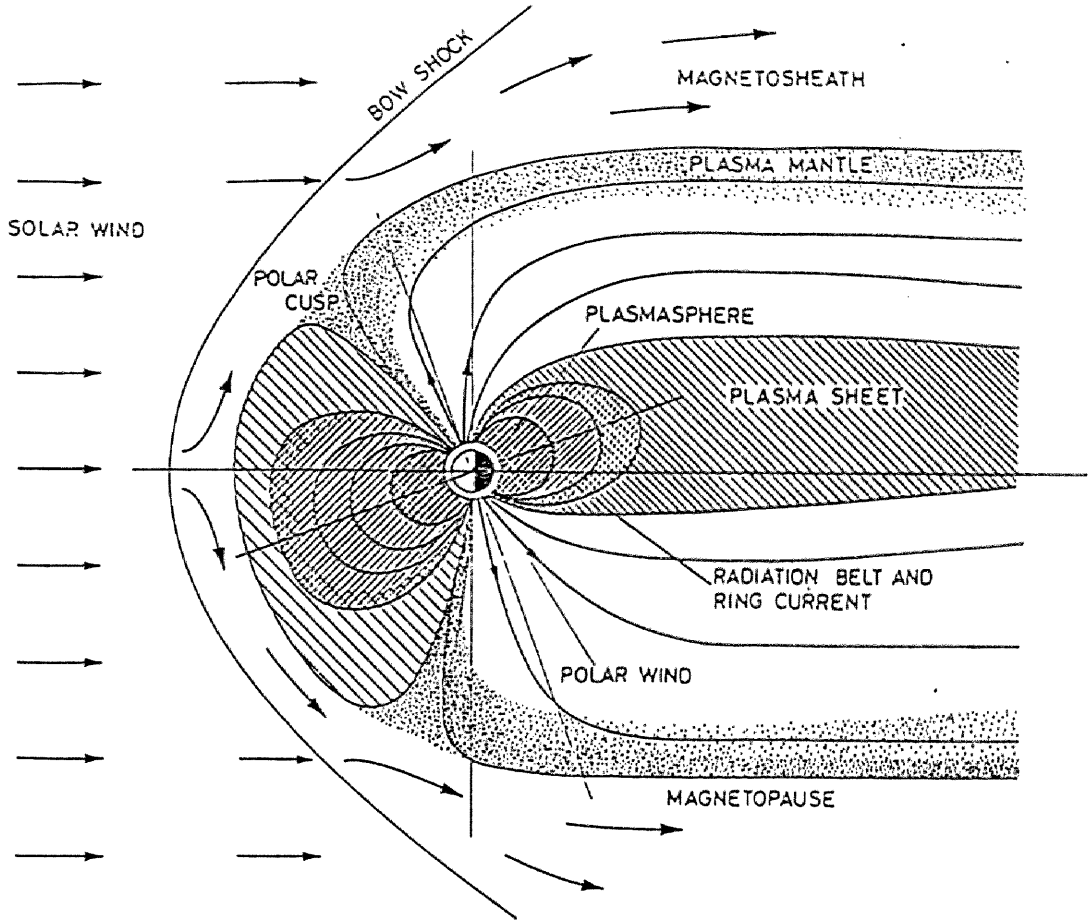

Figure 1.1 Noon-midnight cross section of the magnetosphere (Rosenbauer, 1975).

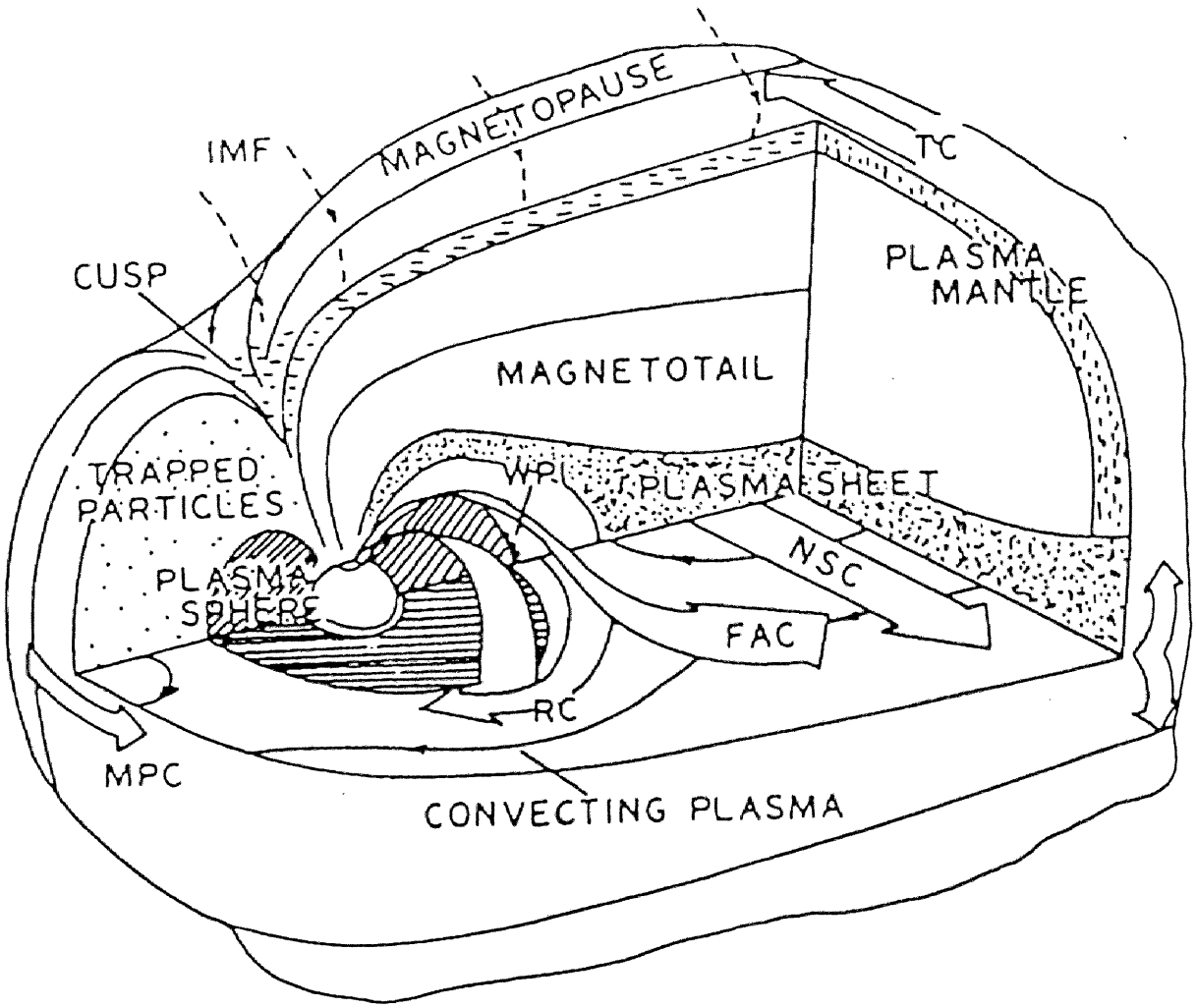

KEY

FAC	FIELD-ALIGNED CURRENT
IMF	INTERPLANETARY MAGNETIC FIELD
MPC	MAGNETOPAUSE CURRENT
NSC	NEUTRAL SHEET CURRENT
TC	TAIL CURRENT
WPI	WAVE PARTICLE INTERACTIONS

Figure 1.2 A schematic view of the magnetosphere (Stern, 1978).

and is closed through the nightside magnetopause (TC). The solar wind flows along the flank of the magnetosphere, and some charged particles enter the magnetosphere. Due to the induction electric field caused by the motion of the solar wind with respect to the earth's geomagnetic field, charge-separation processes occur on both sides of the magnetotail flank. The positively charged particles will drift across the tail toward the dusk side, while the electrons will drift toward the dawn side. Both contribute to form the neutral (or plasma) sheet tail current if the particles' pitch angle is near 90°. On the other hand for pitch angles near 0° or 180°, the particles will move along the magnetic field lines against the mirror force of the magnetic field and enter the loss cone. They consequently contribute to the Region 1 field-aligned currents which will be discussed later. Most of the neutral sheet current is closed with the surface currents flowing on the northern and southern boundary of the magnetotail.

1.1.3. Ring currents

In the near-earth region ($4 \sim 7$ R_E) there is a significant electric current caused either as a consequence of pressure balance or equivalently as the sum of gradient, curvature, and magnetization drifts of charged particles trapped in the geomagnetic field. This is referred to as the ring current (Akasofu and Chapman, 1961), which flows mostly westward around the earth near the equatorial plane. A much weaker eastward current has been observed at ~ 3 R_E (Lui et al., 1987). It is well known that plasma for the ring current is supplied mainly by the inward transport of plasma sheet particles, including both H^+, He^{++}, and O^+ ions of ionospheric origin, together with some H^+ of solar wind origin (Lundin et al., 1980; Stüdemann et al., 1987). This indicates that the ring current is connected, either directly or indirectly, with both the ionosphere and the outer magnetosphere.

1.1.4. Field-aligned currents

It is now well established that the outer region of the magnetosphere is coupled with the ionosphere by field-aligned electric currents, as shown in Figure 1.2 (FAC). From the

beginning of this century, it has been predicted that charged particles or electric currents flow along the field lines at high latitudes. However, the existence of field-aligned currents was not actually confirmed until the beginning of *in situ* satellite observations (Zmuda and Armstrong, 1974; Iijima and Potemra, 1976). Figure 1.3 shows the ionospheric distribution of field-aligned currents observed by the polar orbiting satellite TRIAD (Iijima and Potemra, 1978). The poleward pair of current systems flow into the ionosphere on the dawn side and away from the ionosphere on the dusk side. This is called the Region 1 current system. Equatorward of this Region 1 system is a pair of current systems of the opposite direction to the Region 1 system, i.e., flowing upward on the dawn side and downward on the dusk side. This is called the Region 2 current system. The ionospheric region into and out of which field-aligned currents flow is of high electric conductivity, because of the precipitation of charged particles. Hence, its location is associated with the spatial-temporal distribution of auroras, which is called the "auroral oval" (Feldstein et al., 1967). The latter will be discussed later together with the strong horizontal ionospheric currents, that flow especially during auroral substorms.

The source regions of field-aligned currents (FAC's) in the magnetosphere are not yet understood fully, because the shape (or the stretching) of magnetospheric magnetic field lines depends on several parameters. It is reasonable, however, to expect that the Region 1 currents are connected to the plasma sheet boundary layer, while the Region 2 currents are connected to the near-earth plasma sheet and ring current regions taking into account the polarity of currents; the sign of Region 1 currents is consistent with the charge accumulation in the magnetotail (positive in the dawn side and negative in the dusk side) as mentioned previously in the section 1.1.2. The sign of Region 2 currents is consistent with the charge separation of the plasma injected from the outer region by the dawn-dusk electric field.

The distribution of the FAC system is highly correlated with the interplanetary magnetic field (IMF). When B_Z (north-south component of the IMF) is northward, there is a pair of field-aligned currents located poleward of the dayside Region 1 current system with opposite

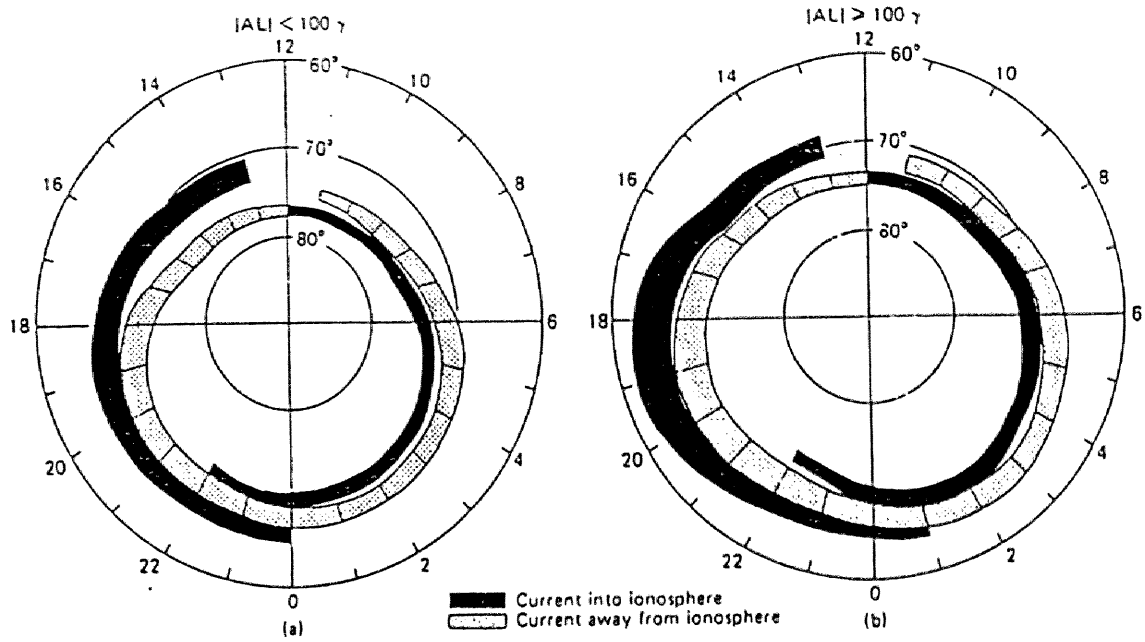

Figure 1.3 Ionospheric distribution of field-aligned currents observed by the polar orbiting satellite (a) for |AL| < 100 γ and (b) for |AL| > 100 γ (Iijima and potemra, 1978).

polarity to the Region 1 currents called NB_Z currents (Iijima, 1984; Iijima and Shibaji, 1987). On the other hand, when B_Z is southward there is little NB_Z current, and the Region 1 and Region 2 currents are intensified. The intensity of these currents depends also on the magnetic activity of the magnetosphere (Iijima and Potemra, 1976; Ohtani et al., 1988). When the magnetic activity is high, the Region 1 and Region 2 field-aligned currents become intense. However, the detailed distribution of the current system is not yet known, in particular, how it varies with the magnetic disturbance level, and how it develops during the course of magnetospheric substorms.

1.2. Magnetospheric Substorm

The earth's magnetosphere is intermittently unstable, and explosively releases a large amount of energy derived from the solar wind-magnetosphere interaction into the auroral ionosphere and the near-earth magnetosphere. This is called a "magnetospheric substorm" (Akasofu, 1968; Akasofu, 1977). Magnetospheric substorms have many manifestations, e.g. magnetic field perturbations on the ground and in the magnetosphere, auroral activity by particle precipitations into the ionosphere, and particle injections into the inner magnetosphere, etc. (Rostoker et al., 1980).

The substorm concept was first introduced by Akasofu (1964). He constructed an "auroral substorm" model, shown in Figure 1.4, by using multi-station all-sky image data. In his model an auroral sudden brightening starts around midnight over a limited longitudinal width in the auroral zone latitude (B), and the "auroral bulge" expands poleward, westward and eastward with the time scale of several tens of minutes (C, D); it is referred to as the "expansion phase" of the substorm. It was found that auroral forms also expand equatorward (Snyder and Akasofu, 1972). In the evening sector the "westward traveling surge" (WTS) develops (C, D, and E) (Akasofu et al., 1965). At the head of the surge intense upward field-aligned currents exist, which will be discussed later in this section. When the expansion ends, the expanded bulges and surges begin to decay, and a stable auroral arcs are

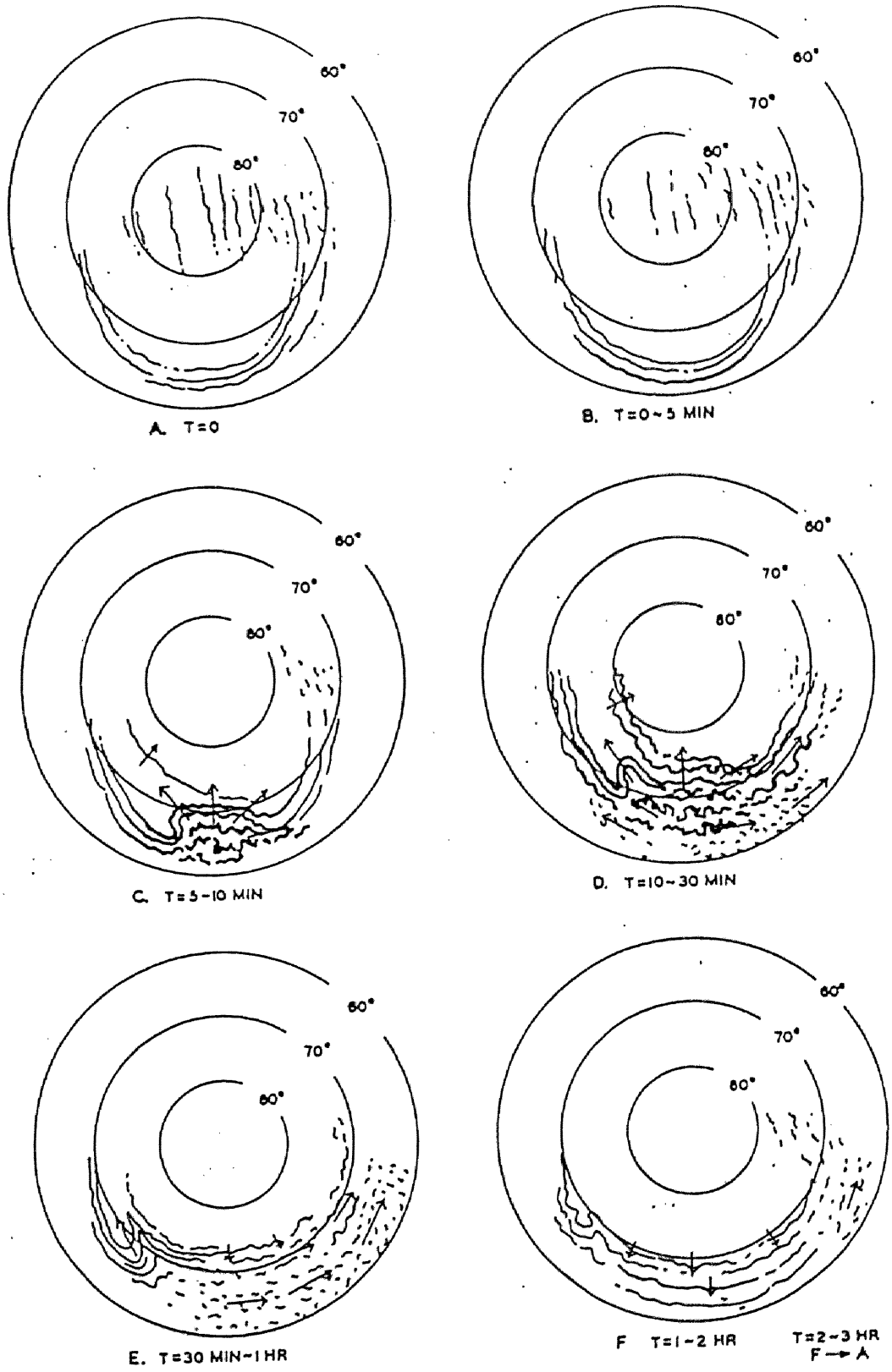

Figure 1.4 A Schematic view of auroral substorm (Akasofu, 1964).

formed again around the geomagnetic pole (F, A), i.e., the "recovery phase". Akasofu (1975) used the auroral image taken by the DMSP satellite to show the development of an auroral substorm on a global scale. The DMSP satellite takes images by a scanning photometer and it takes about 15 minutes to obtain one image, so that the detailed study of the space-time development of auroral morphology was impossible. However, this morphology has been recently confirmed by global imagings via satellites such as DE 1 (Craven and Frank, 1985; Frank and Craven, 1988) and Viking (Rostoker et al., 1987). Rostoker et al. (1987) found that the onset region of an auroral substorm is highly localized in azimuthal extent, with the size of several hundreds of kilometers.

The magnetic field variations at night-side auroral zone stations show sharp decreases in the H (geomagnetic north-south) component at expansion onset, which is the manifestation of the westward electrojet (strong ionospheric current in the auroral zone). As the substorm develops, the westward electrojet expands poleward, westward and eastward (Wiens and Rostoker, 1975; Pytte et al., 1976a). This is referred to as the "(polar) magnetic substorm." Magnetic substorms are found to be highly correlated with auroral substorms (e.g. Kamide and Akasofu, 1975), which will be discussed in detail later in this section. Before the onset the ground magnetograms often show a gradual increase in the H component on the dusk side and a decrease on the dawn side, i.e., the "growth phase." Figure 1.5 shows worldwide time-dependent distribution of ionospheric equivalent currents during a substorm, which is obtained from ground magnetic field variations, by rotating the horizontal magnetic field vectors clockwise by 90°, assuming that the magnetic field perturbation at each ground station is produced by overhead ionospheric current. During the growth phase (Figure 1.5(a)), the equivalent current pattern shows two vortices centered on the dusk and dawn side of the polar cap (DP2 current system). During the expansion phase (Figure 1.5(b)), the pattern is characterized by two vortices with one larger vortex centered at higher latitude around midnight and the other smaller vortex centered at lower latitude (DP1 current system). AU and AL indices, which are defined as the upper and lower envelopes of the superimposed

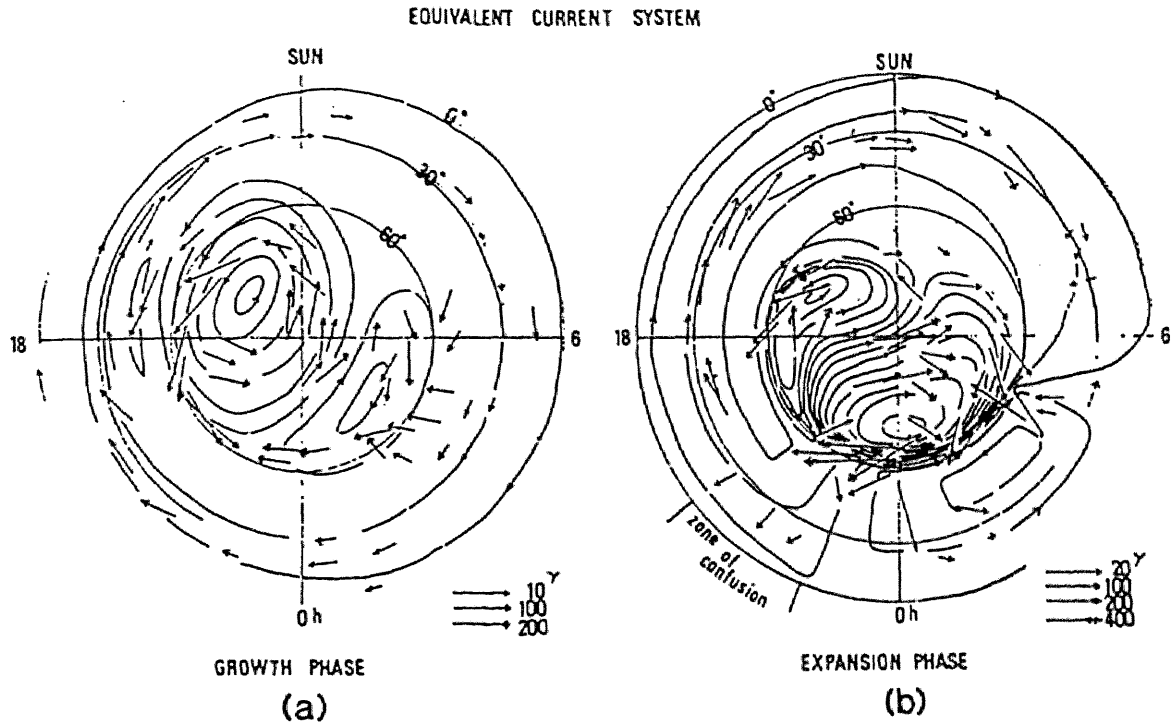

Figure 1.5 Distribution of ionospheric equivalent currents obtained from ground magnetic field variations during the growth phase and the expansion phase of the substorm (Iijima and Nagata, 1972).

plot of the H component magnetograms at auroral latitude stations, represent the maximum eastward and westward electrojet currents, respectively. Then the separation between AU and AL, namely AE, is used as an index of geomagnetic and auroral activity (Davis and Sugiura, 1966).

At middle latitudes an increase in the H component of magnetic field is observed near the meridian where auroral expansion starts, and a decrease (increase) in the D component is observed in the east (west) of the onset meridian. These magnetic variations can be explained either in terms of the effect of a pair of field-aligned currents flowing into and out of the ionosphere, the current wedge or, equivalently, by return currents from the westward electrojet. The beginning time of these magnetic changes is often used for determining the onset time of magnetic substorms (e.g. McPherron et al., 1973; Clauer and McPherron, 1974).

Satellite observations over the last two decades have indicated that several kinds of disturbances occur in the magnetosphere during substorms. These phenomena are prominent in the nightside magnetosphere, suggesting that the source of substorms is in the magnetotail region. The substorm thus includes the magnetospheric phenomena, and has been named the "magnetospheric substorm."

Various kinds of phenomena take place in the magnetotail during a substorm. In the distant magnetotail ($X_{GSM} < -15R_E$, in GSM or geocentric solar magnetospheric coordinates X_{GSM} is toward the sun, Z_{GSM} is in the plane containing sun-earth line and earth's magnetic dipole and positive northward, and Y_{GSM} satisfies the right-handed orthogonal set), the characteristic signature is the burst of energetic particles (> several tens of keV) soon after the onset and the subsequent southward turning of the magnetic field (Terasawa and Nishida, 1976) suggesting plasma sheet thinning. In the near-earth region ($X_{GSM} > -15R_E$) the magnitude of the magnetic field is intensified and the plasma sheet thins during the growth phase. After the onset the magnetic field vector rotates to more dipolar orientation and the plasma sheet expands (Pytte et al., 1976b). Figure 1.6 shows the characteristic particle

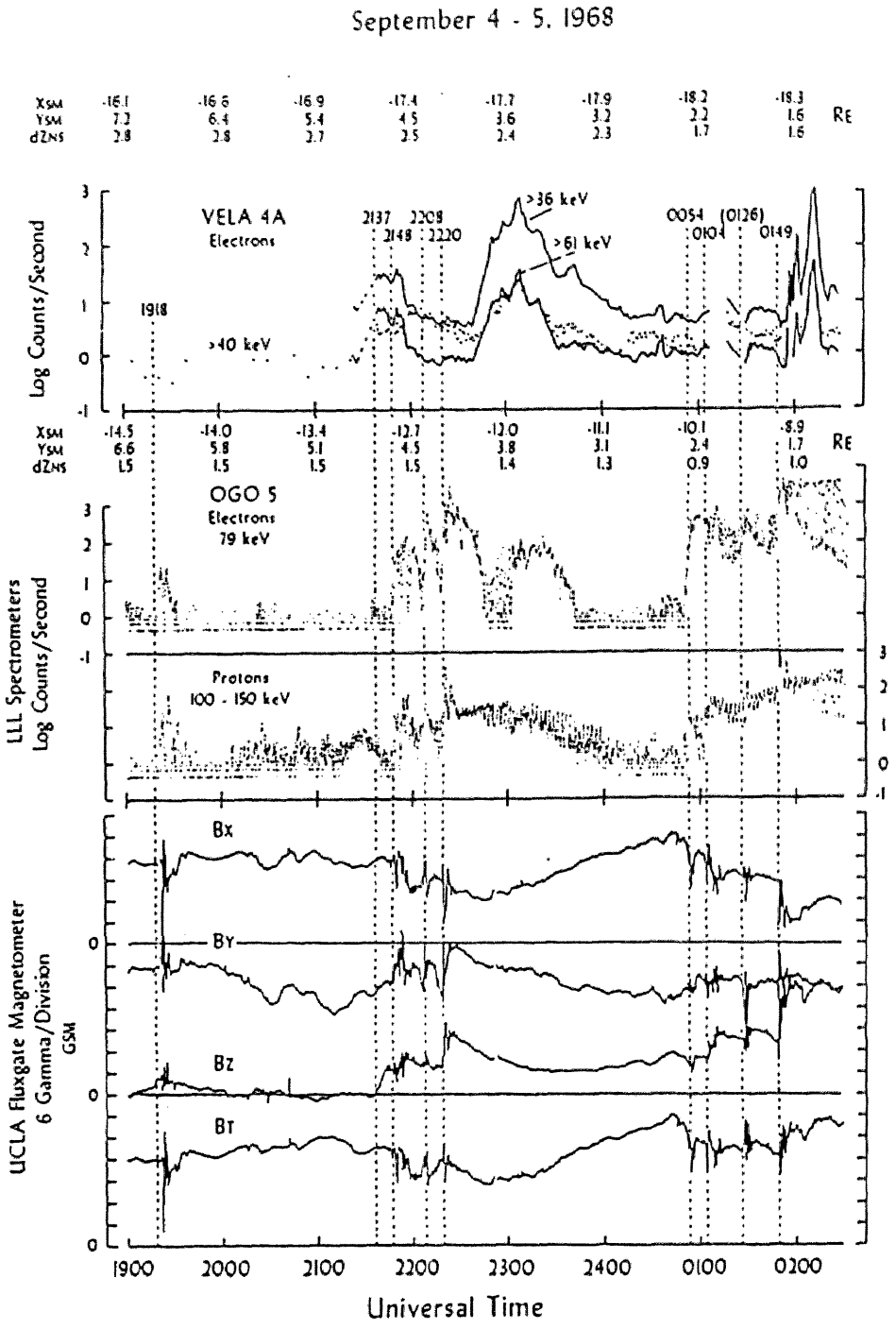

Figure 1.6 Characteristic particle and magnetic field variations in the near-earth ($X_{GSM} > -15R_E$) magnetotail during a substorm. The expansion onsets are denoted by dotted lines. (Pytte et al., 1976a)

and magnetic field variations in the near-earth ($X_{GSM} > -15R_E$) magnetotail during the substorm. The expansion onsets are denoted by dotted lines. At expansion onsets OGO 5 observes increases in the B_Z component magnetic field preceded by decreases, together with increases in electron number density preceded by decreases.

Substorm signatures are clearly observed at geosynchronous orbit (e.g. Sauvaud and Winckler, 1980). One signature is the injection of energetic particles from the more distant region of the magnetosphere (e.g. DeForest and McIlwain, 1971). Another signature is magnetic change indicating a more tail-like geomagnetic field during the growth phase followed by a dipole-like field accompanied by the perturbation of the azimuthal component of the magnetic field. Nagai (1982) analyzed GOES 2 and GOES 3 magnetic field data to show that the substorm-associated magnetic disturbances at geosynchronous altitudes can be explained by the "current wedge model" (McPherron et al., 1973). This model consists of a pair of field-aligned currents and the ionospheric auroral electrojet current produced by the collapse and diversion of the cross-tail current, and the subsequent longitudinal expansion of each field-aligned current. Figures 1.7(a) and (b) show a schematic view of the current system and characteristic signature of magnetic field variations at geosynchronous orbit respectively. The H component is antiparallel to the earth dipole, the V component is perpendicular to H and positive outward, and the D component is perpendicular to H and V and positive eastward. Many other authors also reached the same conclusion (Singer et al., 1985; Barfield et al., 1986; Nagai et al., 1987; Nagai, 1987).

However, magnetic variations during a substorm cannot always be explained by the current wedge model. McPherron and Barfield (1980) showed that the typical D component perturbation is not observed at geosynchronous orbit in winter seasons. They attempted to explain it by the earth dipole tilt effect. Nishitani and Oguti (1988) analyzed GOES 2 and GOES 3 data in the winter season and found that longer-time scale (several tens of minutes to several hours) D component variations show the typical current-wedge-type signature (positive in the dusk side and negative in the dawn side), whereas short-time scale (about a

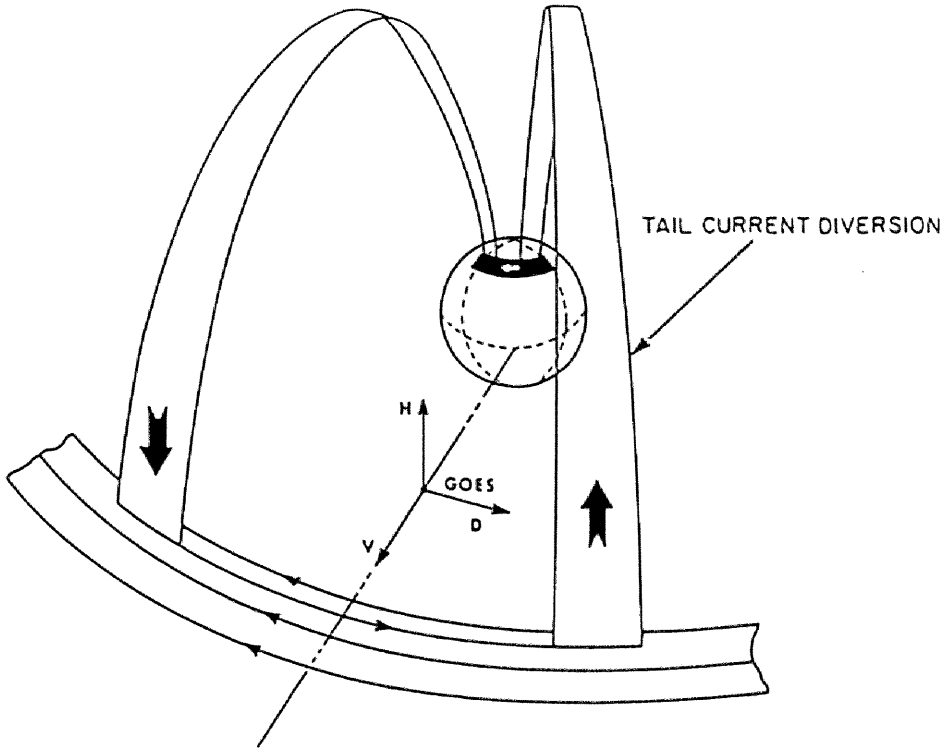

(a)

Figures 1.7 (a) A schematic view of the current wedge model (Barfield et al., 1985) and (b) characteristic magnetic field variations at geosynchronous orbit based on the model (Nagai, 1982). The H component is antiparallel to the earth dipole, the V component is perpendicular to H and positive outward, and the D component is perpendicular to H and V and positive eastward.

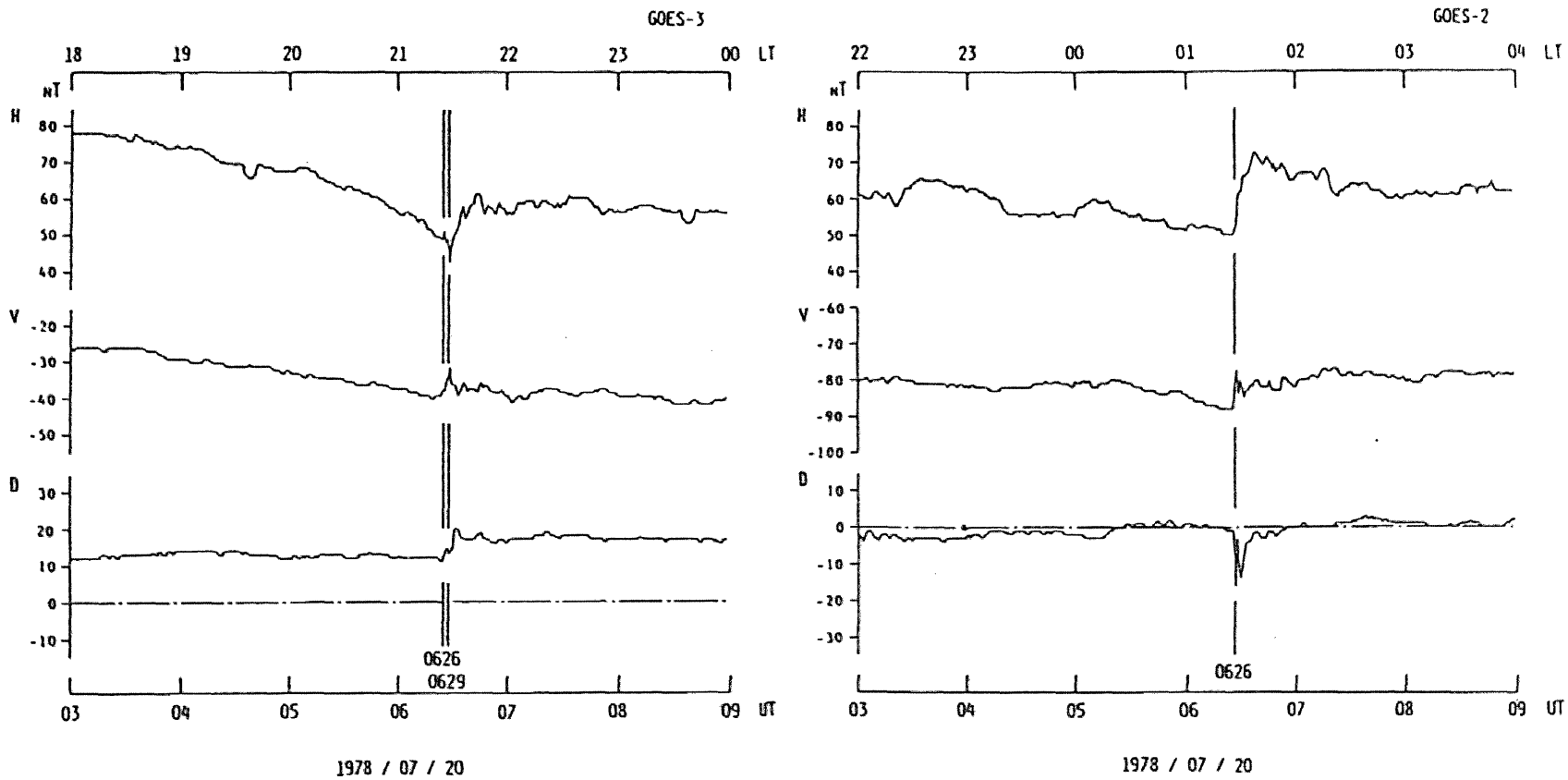
GOES-3
18 19 20 21 22 23 00 LT
nT
H
80 70 60 50 40
V
-20 -30 -40 -50
D
30 20 10 0 -10
0626
0629
03 04 05 06 07 08 09 UT
1978 / 07 / 20
GOES-2
22 23 00 01 02 03 04 LT
nT
H
80 70 60 50 40
V
-60 -70 -80 -90 -100
D
10 0 -10 -20 -30
0626
03 04 05 06 07 08 09 UT
1978 / 07 / 20

(b)

few minutes) magnetic variations do not show such a simplified feature.

Another problem of the model is that it is not yet clear how these current wedges are related to the plasma-sheet thinning observed in the distant magnetotail as described earlier. During the growth phase the plasma sheet thins, while the magnetic field near geosynchronous orbit becomes tail-like, indicating the intensification of magnetotail currents. Baker and McPherron (1990) proposed that, as the magnetotail current becomes intense, the J×B force increases and compresses the plasma sheet until it balances the plasma pressure hence causing the plasma-sheet thinning. However, quantitative estimates of various parameters are quite incomplete.

In addition, the essential shortcoming of the current-wedge model lies in the fact that the model does not take into account the interaction with the ionosphere, e.g. the return currents from the ionosphere.

Since data obtained from the geosynchronous satellites are intrinsically based on one-point observations, the separation of spatial changes from temporal variations is very difficult. It is therefore impossible to determine the distribution of magnetospheric currents uniquely, particularly during the substorm. Nagai et al. (1987) and Fairfield and Zanetti (1989) used geosynchronous and eccentric orbiting satellites to examine the distribution of currents by use of the two or three-point data set. These data sets are still insufficient, however, to determine uniquely the space-time development of the current systems. Hence it is important to combine *in situ* measurements obtained by satellites with two-dimensional data obtained on the ground, such as auroral images and magnetic field variations.

The relationship between the growth phase and the expansion phase has been the subject of continuous controversy. The main problem is whether the expansion phase is a causal consequence of the growth phase. Kokubun and McPherron (1981) and Lopez et al. (1988) showed that the magnitude of magnetic field changes at, or near, geosynchronous orbit during the expansion phase is highly correlated with the magnitude of changes during the growth phase. However, most substorms are multiple-onset substorms, and even one substorm

can have several complicated time-dependent spatial structures. It is impossible to predict the space-time development of auroral substorms by using the growth phase data only. Therefore study of the spatial-temporal development of substorms by using 2-dimensional data is essential.

The 2-dimensional development of substorms has often been examined with ground magnetic data. Kamide et al. (1981) and Kamide et al. (1985) used global magnetic data and, by assuming the distribution of ionospheric conductivity, derived the temporal development of ionospheric currents and field-aligned currents with a temporal resolution of 10 minutes. However, the magnetic data contains the integrated effect of ionospheric and field-aligned currents over a very wide region, and hence they are not appropriate for the detailed study of the small-scale development of substorms. It is thus important to utilize auroral data, which will give the 2-dimensional distribution of particle precipitation with a spatial scale of about 10 km.

For the study of the temporal distribution of the current system during substorms by use of auroral data, an essential requirement is to determine the relationships between auroral structures and ionospheric and field-aligned current systems. Since the ionospheric region where electron precipitation occurs is electrically highly conductive, auroras are associated with ionospheric currents. Kamide and Akasofu (1975) made a comparison of the auroral distribution obtained by the DMSP satellite and the distribution of auroral electrojets to conclude that a strong westward electric current flows along the poleward bulges. Many other observations on the ground show the close relationship between active auroras and westward electrojets.

On the other hand, since the aurora is usually caused by the precipitation of energetic electrons, it is reasonable to believe that the auroral forms are associated with upward field-aligned currents. Armstrong et al. (1975), Kamide and Akasofu (1976), Kamide and Rostoker (1977), and Kamide et al. (1979) compared auroral images taken by ground all-sky TV cameras, or the DMSP satellite, with field-aligned currents observed by the polar-

orbiting satellite TRIAD. They concluded that upward field-aligned currents are collocated with "discrete auroras" (e.g. auroral bulges and surges), which have an energy spectrum with a peak energy of several keV, and that downward field-aligned currents coincide with the region of "diffuse auroras" (e.g. pulsating auroras), which have no prominent energy peak. Baumjohann et al. (1981) combined ground magnetic field data with the STARE electric field data and, by assuming an ionospheric conductivity distribution, showed that the western part of an expanding auroral bulge is collocated with highly localized and intense upward field-aligned currents and the eastern part is collocated with more widespread and less intense downward currents.

From many kinds of observations, there is little doubt that the auroral bulges are collocated with the upward currents. However, it is also evident that upward currents associated with auroral arcs are generally surrounded by downward return currents and are difficult to observe unless the current intensity is very strong and the satellite is within the localized current structure.

WTS's (Westward-Traveling Surges as already mentioned) are the most prominent feature in the western part of substorm expansion aurora, together with intense upward field-aligned currents just mentioned. WTS-associated FAC's have been investigated by many workers. Kisabeth and Rostoker (1973) compared auroral images and ground magnetic data and found Hall currents around the surge associated with upward field-aligned currents. Opgenoorth et al. (1983) used all-sky images, ground magnetic data and electric field data from the STARE radar to find a close relationship between a surge and a strong upward field-aligned current. Bythrow and Potemra (1987) used the DMSP images and magnetic field data to reach the same conclusion. However, the source structure of WTS's is not yet clear. Upward field-aligned currents have been generally believed to form the western part of the substorm current wedge (Nagai, 1982), though there are few studies of detailed comparison between ground and satellite data. Gelpi et al. (1987) compared magnetic signatures at geosynchronous orbit and auroral images taken by the DMSP satellite. They were not able

to find close relationships, however, probably because the DMSP satellite cannot separate spatial and temporal changes of the aurora.

There are some studies of relationships between auroral activity observed on the ground and particle/magnetic field data at geosynchronous orbit. Akasofu et al. (1974), Eather et al. (1976), Mende and Shelley (1976) claimed that the temporal variations in auroral luminosity at the estimated conjugate points of geosynchronous satellites are consistent with the temporal changes in electron fluxes measured by geosynchronous satellites. However, the time resolution in these studies is rather poor (>>1 minute), and the fast evolution of auroral structures such as surges and bulges is barely taken into consideration. Nishitani and Oguti (1988) used auroral data obtained by all-sky TV cameras on the ground and magnetic field data of the GOES 2 and 3 geosynchronous satellites. They found excellent correlation between the magnetic field changes at geosynchronous orbit and the auroral activity near the estimated conjugate point. However, they could not examine in detail the relationship between the surge structure and magnetic variations at geosynchronous orbit, because only three events were studied and the longitudinal extent of the combined fields of view of all-sky TV cameras was limited.

1.3. Modeling of the Magnetosphere

In order to examine relationships between the ionosphere and the magnetosphere, a reliable magnetospheric magnetic field model is essential. Over the past several years many attempts have been made to model the magnetic field configuration of the magnetosphere (see Quantitative modeling of the magnetosphere, edited by Walker, 1979). Sugiura and Poros (1973) used magnetic data of the OGO 3 and 5 satellites to find that there are three main regions where the magnitude of the magnetic field differs considerably from the earth's dipole field. These regions are the near-earth equatorial region, the magnetotail equatorial region, and the cusp region. They also attempted to provide an analytical expression of the magnetic field, in terms of ring currents, magnetotail currents, and magnetopause currents.

They discussed each region separately, so that the validity of the model was insufficient to represent the global magnetosphere quantitatively and consistently.

More refined models were provided by Mead and Fairfield (1975) and Olson and Pfitzer (1977). Mead and Fairfield (1975) derived a quantitative model of the magnetospheric magnetic field by fitting the data, obtained by four IMP satellites, to a quadratic expansion in solar-magnetic coordinates and a linear expansion of the solar wind-dipole tilt angle. The model included four sets of coefficients, representing different degrees of magnetic disturbance as determined by the range of Kp values. Although it was the first model that included both the effect of distributed currents and the dipole tilt angle, the model has many limitations. There were gaps in the data coverage, particularly beyond 17 R_E and at high latitudes. In addition, the terms included in the model were insufficient to represent the effects of relatively localized current systems such as ring currents, magnetotail currents, and field-aligned currents. Olson and Pfitzer (1977) represented the magnetic field by using a 6-order expansion of power series and exponential terms. They used 180 coefficients and the model can describe the magnetopause, tail, and ring currents. The shortcoming of this model is that it is restricted to quiet conditions.

By using the magnetic field data used by Mead and Fairfield (1975), complemented by data from the HEOS satellites, Tsyganenko and Usmanov (1982) applied mathematical description of the magnetic field to the three current regions of the magnetosphere as mentioned by Sugiura and Poros (1973). Their model was more refined than that of Mead and Fairfield (1975), the main point being that it can represent the localized current systems. The shortcoming of the model is that due to the lack of data, it is not applicable to the region $X_{GSM} < -16R_E$ and the high latitude magnetotail region. This model was further improved by Tsyganenko (1987). More data points were added to the original data set, particularly in the distant magnetotail region. In addition, the representation was modified by taking the effect of magnetotail return currents into consideration so that the expression for the high-latitude magnetotail became better. This model has two versions; the long version has

26 coefficients and can describe the magnetic field from about 4 to 70 R_E in the magnetotail, while the truncated version has 20 coefficients and can describe the magnetic field from about 4 to 30 R_E. Tsyganenko (1989) proposed a more elaborate representation of the magnetic field by considering a warped (bent around the moon-midnight meridian) current sheet as a result of dipole tilt effects.

However, the models described still have several limitations. First, these models are based on averaged data sets and thus cannot represent the instantaneous configuration of the magnetosphere. Second, these models are all symmetric with respect to the XZ plane in solar magnetospheric coordinates, although strong asymmetry was evident in the satellite observations (Sugiura and Poros, 1973). Third, and the most important, they do not include explicitly the effects of field-aligned currents in their models. Although they include some features of field-aligned currents, field-aligned current continuity is not taken into account. Large-scale field-aligned currents, such as the Region 1 and Region 2 currents, must have considerable effects on the magnetospheric configuration. However, there are few studies that quantify the effects these currents have on the magnetosphere, especially on the field-line connection between the ionosphere and the magnetosphere.

There is another approach to modeling of the magnetosphere, that is the 3-dimensional MHD computer simulation (e.g. Ogino et al., 1986). The advantage of this kind of modeling is that several variables such as magnetic field, plasma pressure, and plasma bulk velocity satisfy Maxwell's equation and MHD equation. This method can also be applied to the study of the magnetic field line connection between the magnetosphere and the ionosphere.

1.4. Outline of this thesis

In this thesis, we will compare auroral activity observed by multi-station all-sky TV cameras and magnetic field variations at geosynchronous orbit, examine small-scale field-aligned currents associated with individual auroral structures, and examine the field line mapping between the ionosphere and geosynchronous altitudes.

In Chapter 2 we investigate several auroral activities such as bulges and surges and related magnetic variations on the ground and at geosynchronous orbit. In particular we focus attention on the "westward traveling surges" and associated magnetic signatures at geosynchronous orbit. We will demonstrate existence of systematic longitudinal deviation of magnetic field lines connected to the surge from that predicted by Tsyganenko's model field line. In Chapter 3 we will examine Tsyganenko's field line model from two points of view, mapping analysis and examination of field-aligned currents. In addition, these results will be compared with the 3-dimensional MHD simulation results by Ogino (private communication, 1991) to examine the characteristics of Tsyganenko's model. In Chapter 4, Tsyganenko's magnetic field model will be modified by introducing the effect of large-scale field-aligned currents to construct a tentative magnetic model, which is consistent with the relative location of the ionospheric point to the magnetospheric conjugate point obtained from our observation. In the modified model the magnitude of magnetic field deflection will be examined for several parameters of the large-scale field-aligned currents. In Chapter 5 the intensity of field-aligned current estimated from the deviation of conjugacy is compared with that actually observed by the polar-orbiting satellite DMSP-F7. We will mention time-dependent characteristics of the large-scale field-aligned current system in the course of the development of the substorm expansion. Finally, concluding remarks will be presented in Chapter 6.

2. Comparison of auroral activity with the magnetic field variations at geosynchronous orbit

2.1. Introduction

In the course of magnetospheric substorms the magnetosphere releases a large amount of energy derived from the solar wind-magnetosphere interaction in a complex way (e.g. Rostoker et al., 1980). Therefore the magnetosphere shows quite complicated temporal and spatial variations. It is practically impossible to determine the time-dependent 3-dimensional configuration of the magnetosphere (e.g. the current distribution), uniquely, by using satellite data alone, which is based on single-point observations and cannot be used to separate spatial and temporal changes.

The auroral image is a projection of magnetospheric activity on the ionosphere and can provide 2-dimensional information on the time-dependent magnetospheric configuration. However, it is not yet clear where these auroras are actually connected to in the magnetosphere along magnetic field lines, although several attempts have been made to project the auroral image into the magnetosphere using existent magnetic field models such as Tsyganenko's models (e.g. Elphinstone et al., 1991). It is therefore essential to combine 2-dimensional ground-based auroral image data with the *in situ* satellite data in order to study the temporal-spatial variation of the magnetosphere during magnetospheric substorms.

There have been some studies on the relationship between auroral activity and particle/magnetic field data at geosynchronous orbit (Akasofu, 1974; Eather et al., 1976; Mende and Shelley, 1976). However, the time resolution in these studies is rather poor (>>1 minute), and hence the fast evolution of auroral structures such as surges and bulges is rarely taken into consideration. Nishitani and Oguti (1988) used auroral data obtained by all-sky TV cameras on the ground and magnetic field data of the GOES 2 and GOES 3 geosynchronous satellites. They found excellent coincidence between the magnetic field changes at geosynchronous orbit and the auroral activity near the estimated conjugate point within a time resolution of 10 seconds. However, their examination of the relationship between the auroral

surge structure and magnetic variations at geosynchronous orbit still involved some uncertainty, because only three events were studied and, more importantly, the spatial coverage in longitude was provided by only one TV camera.

In this chapter we compare auroral activity observed by multi-station all-sky TV cameras, which cover a very large spatial extent in longitude ($\geq 45°$), and magnetic field variations at geosynchronous satellites during the early stage of the substorm expansion phase. We examine magnetic field variations at geosynchronous orbit associated with individual auroral activity, and then examine the field line connection between ionospheric and geosynchronous altitudes. In particular we will focus attention on "westward traveling surges" and related magnetic field variations at geosynchronous orbit, because it is most likely that these auroral surges are collocated with local enhancements in upward field-aligned currents (e.g. Opgenoorth et al., 1983).

In order to estimate the ionospheric foot point of geosynchronous satellites we use Tsyganenko's magnetospheric magnetic field model (1987), which is an empirical model based on satellite observations. On the other hand, we examine the real foot point of geosynchronous satellites, from the comparison of the magnetospheric and ionospheric phenomena as mentioned above. Then we will test the reliability of Tsyganenko's magnetic field model by determining whether it shows any systematic error in estimating the ionospheric foot points of geosynchronous satellites.

2.2. Auroral and magnetic field data

Auroral data used in this study were obtained by all-sky TV cameras at Fort Smith (60.0°, 248.1°, geographic coordinates; 68.2°, 299.5°, geomagnetic coordinates), Shamattawa (55.9°, 267.9°; 67.8°, 330.1°), Little Grand Rapids(52.0°, 264.5°; 63.5°, 324.8°), and Great Whale River (55.3°, 282.2°; 68.0°, 353.7°), during the Global Aurora Dynamics Campaign which was carried out from December, 1985 to February, 1986 (Oguti et al., 1988a). Magnetic data at geosynchronous orbit were obtained from GOES 5 (74.9° W) and GOES 6 (107.9°

W) satellites, with a time resolution of 3.06 seconds.

Figure 2.1 shows the distribution and field of view of the ground all-sky TV cameras, together with the ionospheric foot points (black dots) of GOES satellites. These foot points are calculated on the basis of IGRF85 internal field model plus the Tsyganenko (1987) external field model (truncated version). This figure shows that the foot point of GOES 5 is located near Great Whale River (GWR) and that of GOES 6 is about 300 km west of Shamattawa (SHM) and Little Grand Rapids (LGR). Tsyganenko's (1987) model contains a Kp-dependent parameter and the foot point of the satellite moves about 3° in geomagnetic latitude approximately along the geomagnetic meridian line depending on the geomagnetic activity level, as shown in Figure 2.1.

The auroral images taken by all-sky TV cameras are projected onto an ionospheric coordinate system, by assuming the auroral height to be 110 km (a detailed description of the data analysis system will be given in the appendix), as demonstrated in Figure 2.2. In this figure auroras are shown in a positive image, so that the black parts represent bright regions. It should be noted that the TV cameras often recorded some light contamination with the auroras. On some days the moon in the field of view of TV cameras was so bright that auroral images were obscured, hence the moon was shaded by a cover. However, the effects of the scattered moon light were considerable especially on hazy nights. In addition there were frequent contaminations due to smoke, especially in the western field of view at LGR.

The magnetic observatories used in this study are listed in Table 2.1, and Figure 2.3 shows the distribution of these observatories. Near the foot point of GOES satellites, the magnetic field data are available every 5 seconds from Great Whale River, Shamattawa, Little Grand Rapids, Churchill, and La Ronge, and every 1 minute from Yellowknife. Data at a 1-minute sampling rate from sub-auroral latitude stations, St. Jones (STJ), Ottawa (OTT), and Victoria (VIC) are used to examine the location of the substorm expansion onset region.

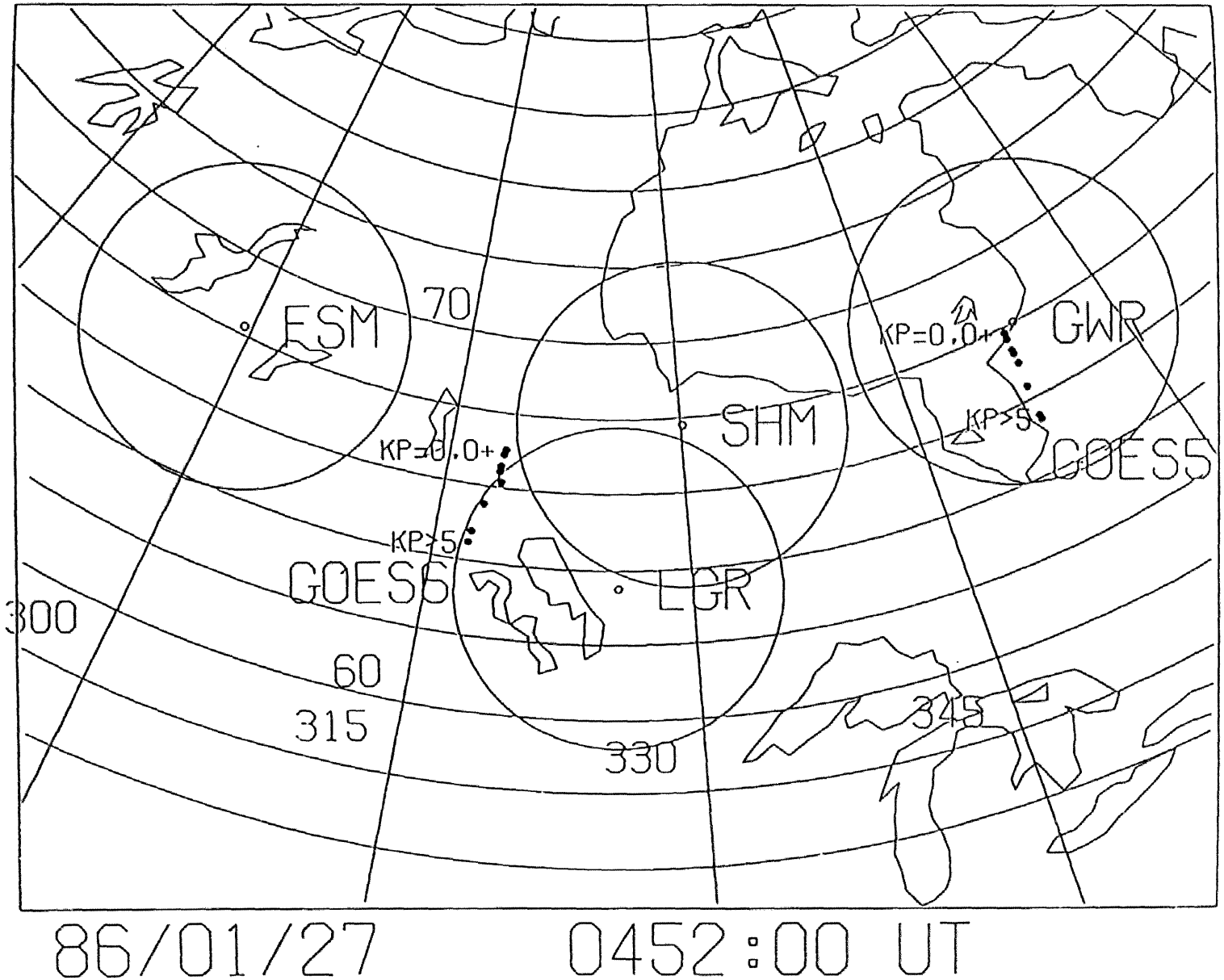

Figure 2.1 Distribution and field of view of ground all-sky TV cameras, together with the ionospheric foot points (black dots) of GOES satellites. These foot points are calculated on the basis of IGRF85 internal field model plus Tsyganenko (1987) external field model (truncated version).

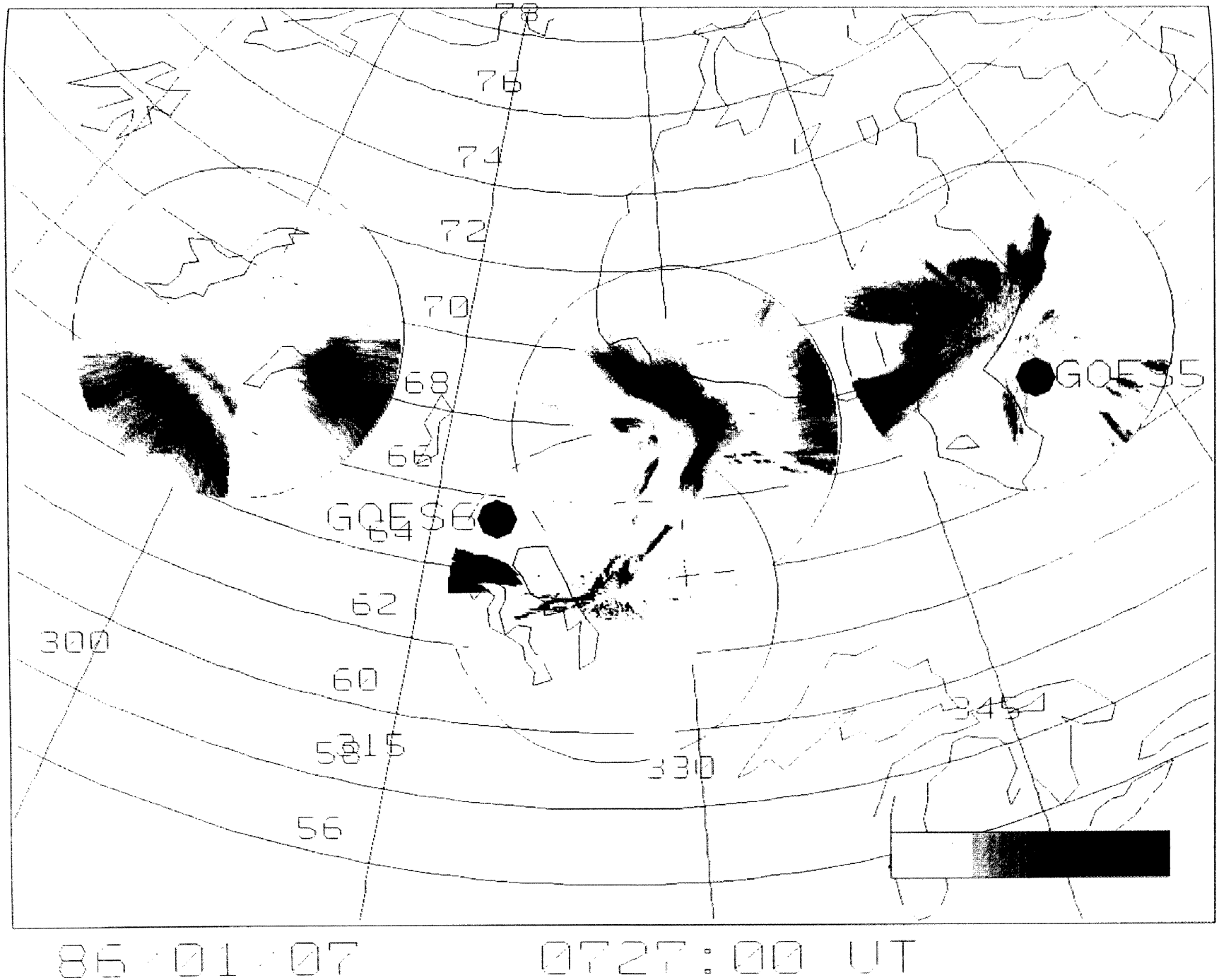

Figure 2.2 An example of the conversion of the auroral images taken by all-sky TV cameras into ionospheric coordinate system. Auroras are shown in a positive image, so that the black parts represent bright regions.

Station Name	Abbrev.	Geographic		Geomagnetic	
		lat.	long.	lat.	long.
Great Whale River	GWR	55.3	282.2	68.0	353.7
Churchill	CHR	58.8	265.9	70.3	326.0
Shamattawa	SHM	55.9	267.9	67.8	330.1
Yellowknife	YLK	62.4	245.6	69.9	294.4
Little Grand Rapids	LGR	52.0	264.5	63.5	325.8
La Ronge	LRG	55.2	254.7	64.9	310.8
Saint Johns	STJ	47.6	307.3	57.6	29.1
Ottawa	OTT	45.4	284.3	58.5	356.0
Victoria	VIC	48.5	236.6	54.1	292.4

Table 2.1 List of the magnetic observatories.

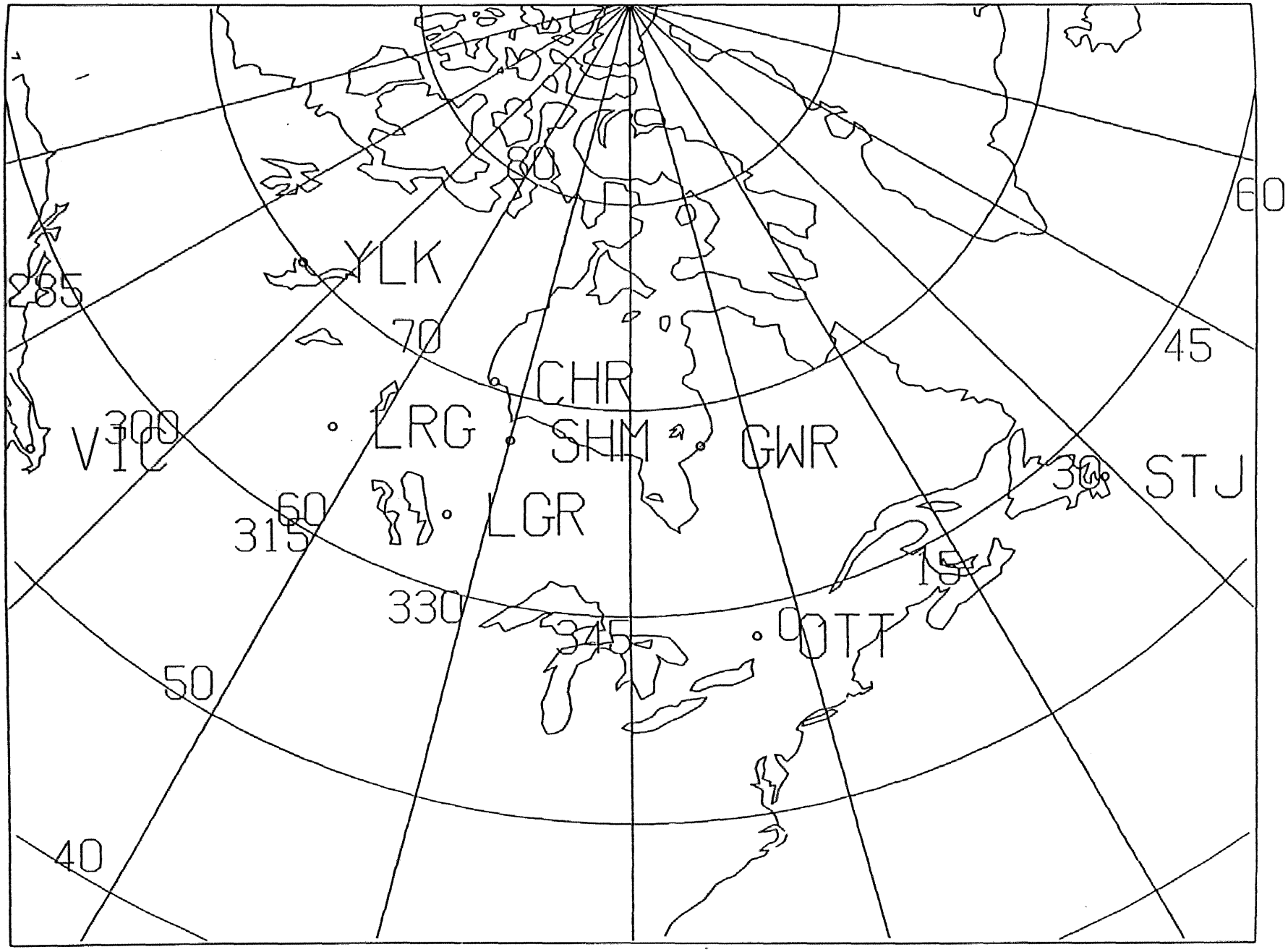

Figure 2.3 Distribution of the magnetic observatories.

The purpose of this thesis is to study the relationships between ground auroral activity and ground magnetic variations over a considerable spatial extent with magnetic changes at geosynchronous orbit. Therefore we have selected the time intervals when both all-sky TV cameras at Shamattawa and Great Whale River, were in operation during the campaign period. Twelve events have been selected from 4 days, i.e., Jan. 01, Jan. 02, Jan. 07 and Jan. 27. The substorms on Jan. 07, 1986 have already been presented in the paper by Oguti et al. (1988b). Here we will examine the substorms on Jan. 27, which involve various characteristic signatures, and then the substorms on Jan. 02, Jan. 01, and on Jan. 07. The summary of substorms used in this study will be given in Table 2.2, in Section 2.4.

2.3. Substorm events

2.3.1. Jan. 27 1986

The AE index on this day is shown in Figure 2.4. The geomagnetic activity is rather high. Several substorms can be identified in the AE index, among which three expansion onsets at about 0250 UT, 0450 UT and 0650 UT were located near the observation sites (see arrows). The onset time cannot be clearly identified from the AE index, but well defined onset times of these expansions are 0249 UT, 0448 UT and 0639 UT as obtained from the sub-auroral latitude magnetograms (Figures 2.9 and 2.14, vertical lines).

2.3.1.1. Substorm at 0448 UT

The auroral image data from GWR, SHM, and LGR are available. During this event GWR was located near geomagnetic midnight and SHM was located near 2200 MLT (magnetic local time). The Kp index is 5+, indicating rather high geomagnetic activity.

This substorm includes two expansion onsets at 0448 UT and at 0500 UT, as can be clearly seen in the magnetic field variations at sub-auroral latitude stations shown in Figure 2.9. In the following we will discuss these two onsets separately.

2.3.1.1a. Expansion onset at 0448 UT

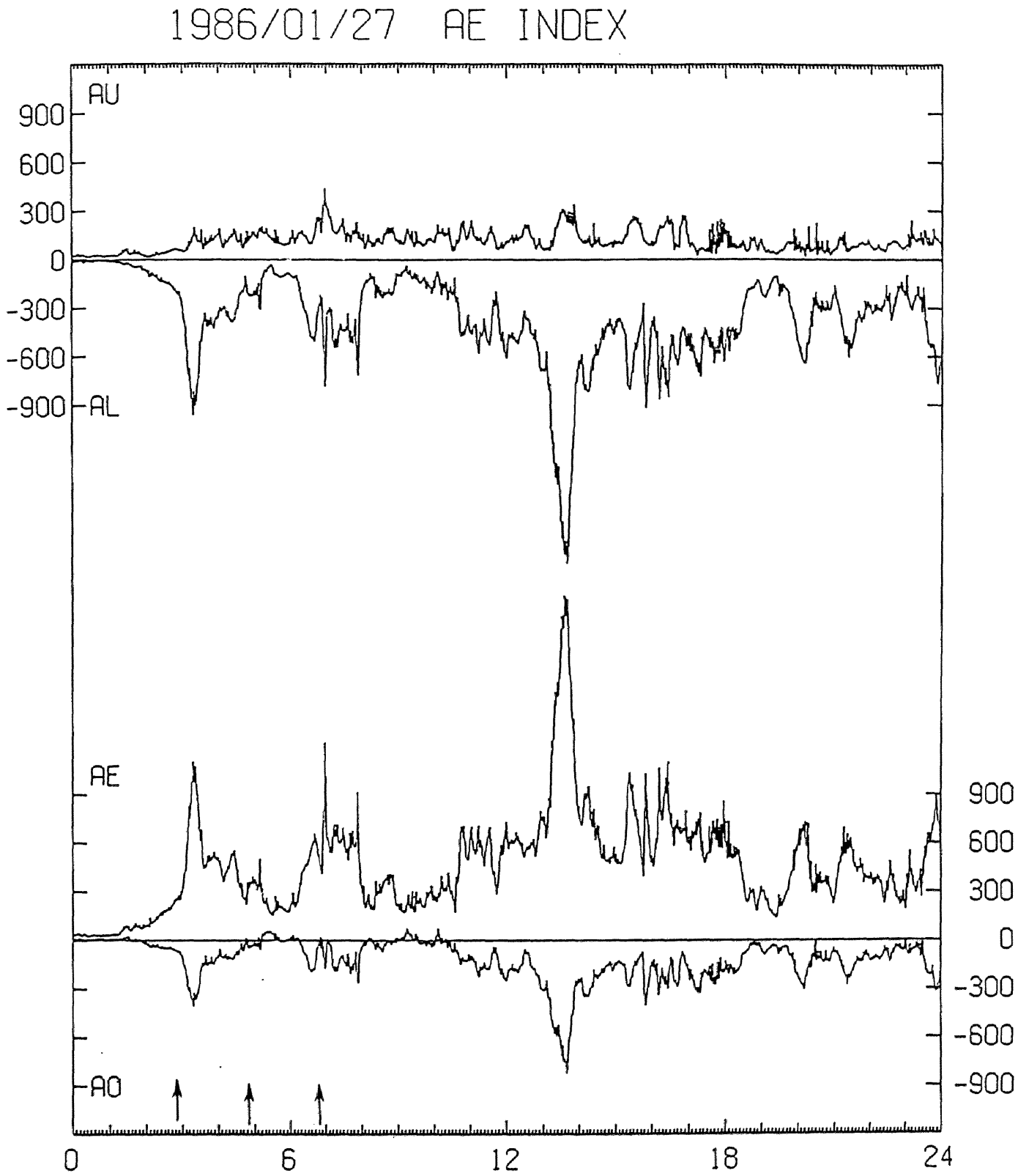

Figure 2.4 The AE index on January 27, 1986.

Figure 2.5 shows the space-time development of auroral images obtained by all-sky TV cameras at SHM, GWR, and LGR. The time interval between images in this figure is 1 minute, although we have examined the images every 5 seconds. Whereas the field of view of the all-sky TV camera actually covers a circular area about 1000 km in radius at an altitude of 110 km, the limit is less than about 500 km where we can determine the auroral distribution with an accuracy of ±100 km because of the change in the height distribution of auroras from 110 km and the error in determining the attitude of the TV camera. Actually we limit the field of view at each station to 470 km at the 110 km altitude level (e.g. Figure 2.5).

The expansion started between GWR and SHM. Prior to the onset, at about 0447 UT, an eastward-moving auroral branch was seen (shown by the arrow) in the western sky of GWR. At first a faint arc gradually brightened, then it moved eastward to reach the estimated foot point of GOES 5 at 0449 UT. This auroral branch vanished by 0452 UT. On the other hand an auroral surge with the spatial scale of 200 km appeared in the eastern field of view of SHM at 0451 UT (shown by the arrow), and then the head of the surge moved westward, changing forms, rotating clockwise as viewed parallel to the magnetic field direction. This surge faded by 0458 UT and a discrete auroral band was left.

The DMSP-F7 satellite passed above SHM at about 0458 UT. The auroral image taken by a scanning imager onboard the satellite is shown in Figure 2.6. This figure shows the only example of the same auroral form simultaneously observed by ground TV cameras and the DMSP satellite, of the events examined in this study. The auroral pattern observed by the satellite is coincident with the pattern observed by the ground TV cameras at 0458 UT (Figure 2.5), indicating the validity of the projection of ground all-sky TV images onto the ionospheric height of 110 km. Above GWR there were a few faint arcs. Above SHM a discrete auroral band was observed, extending from about 200 km east of SHM toward the far west.

Figure 2.7 shows the magnetic field variations at GOES 6 and GOES 5. The magnetic

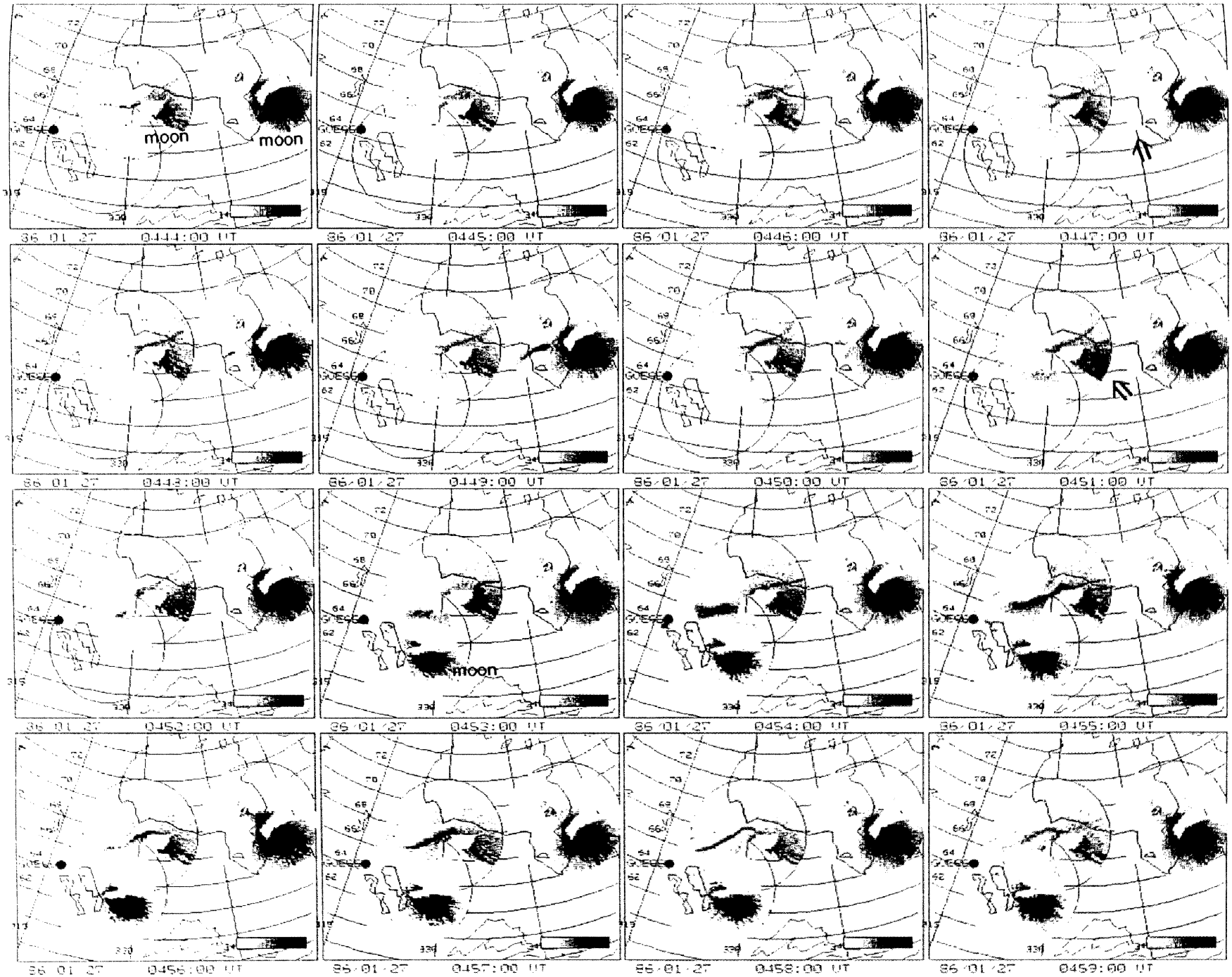

Figure 2.5 Spatial-temporal development of auroras obtained by all-sky TV cameras at SHM, GWR, and LGR, from 0444 UT to 0459 UT on January 27, 1986.

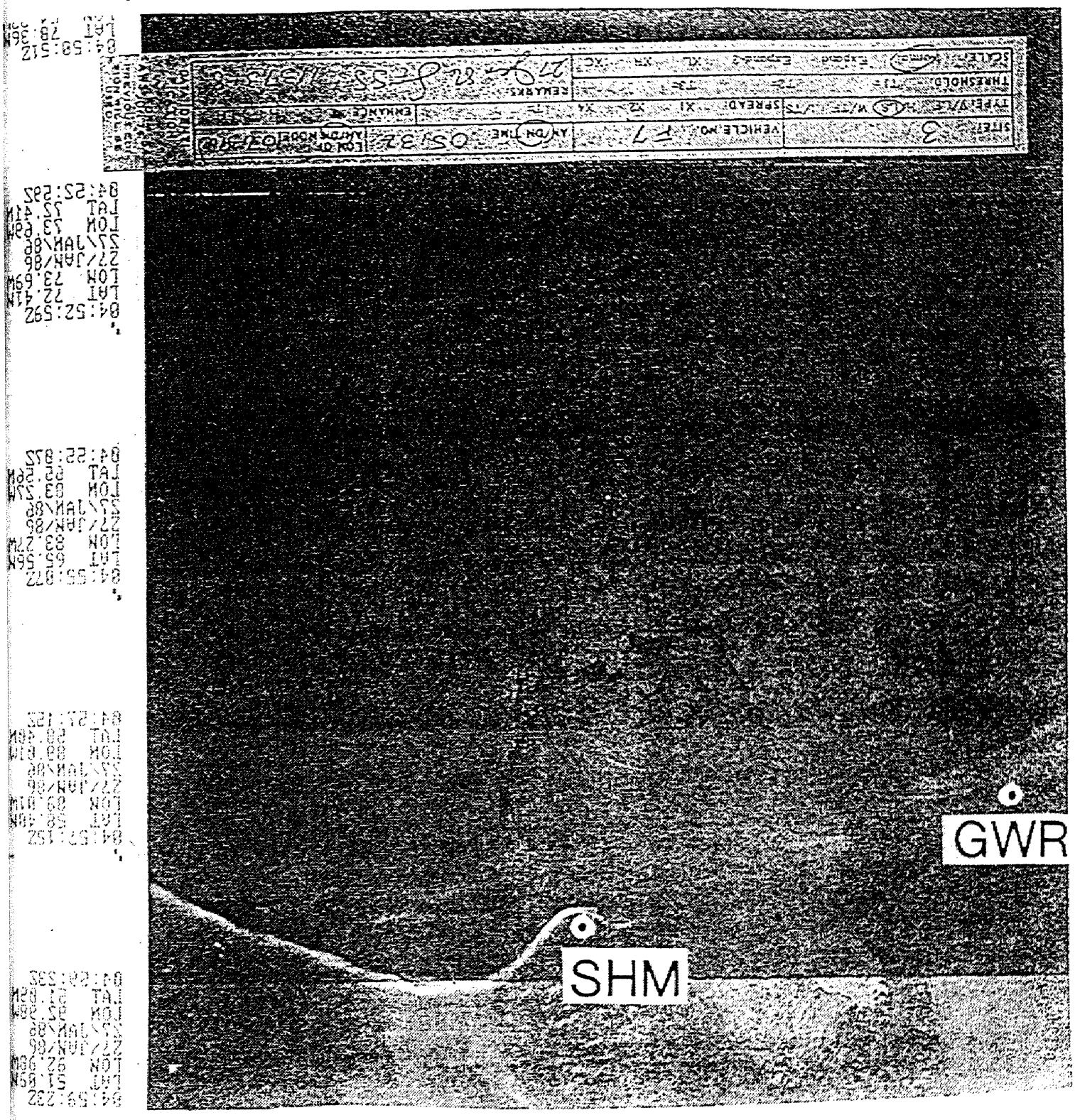

Figure 2.6 The auroral image taken by a scanning imager onboard the DMSP-F7 satellite. The image is positive. The satellite passed above SHM at about 0458 UT.

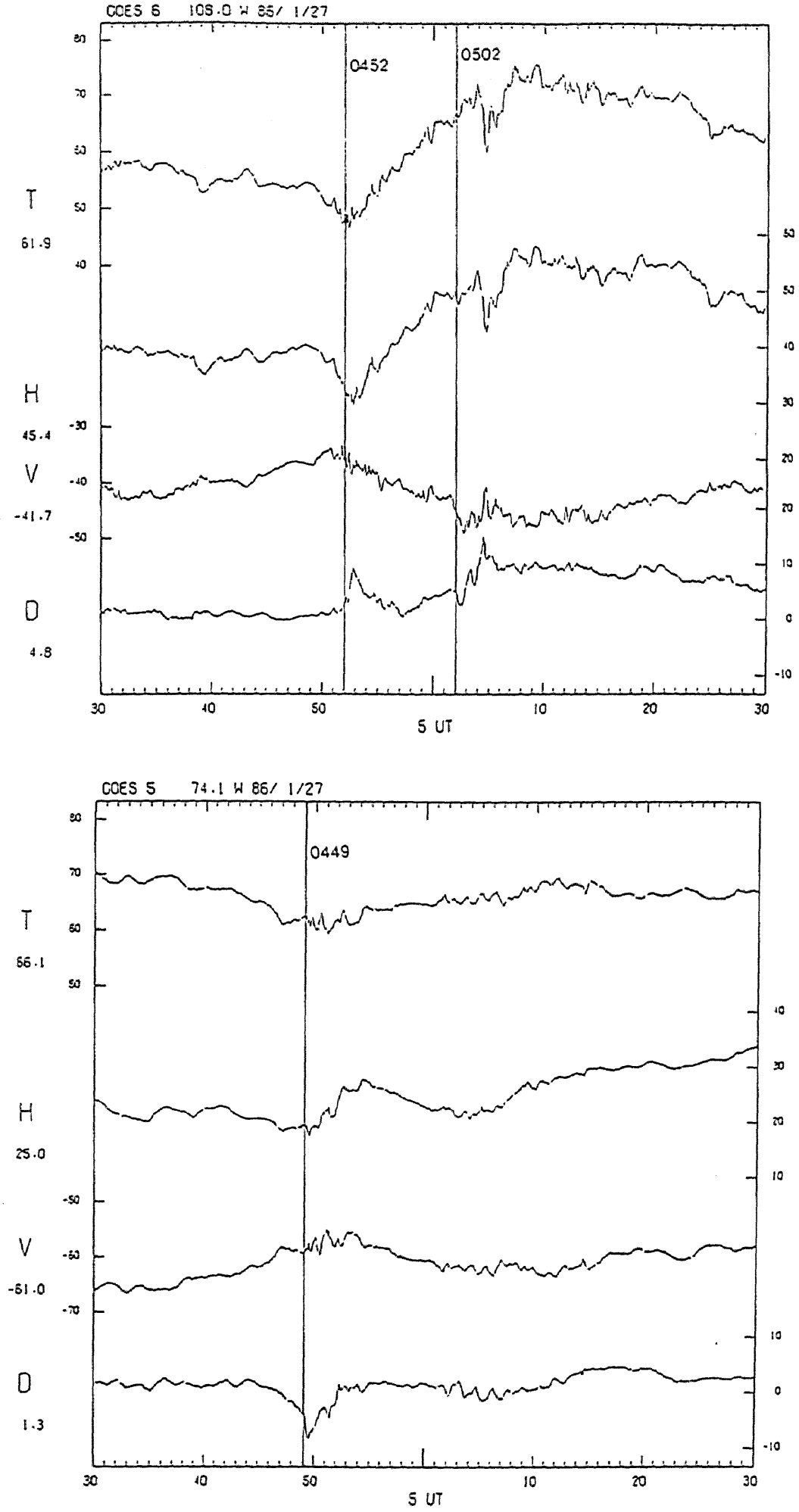

Figure 2.7 Magnetic field variations at GOES 6 and GOES 5 from 0430 UT to 0530 UT on January 27, 1986. The magnetic field components are given in HVD coordinates (see text). T is total intensity of the magnetic field.

field components are given in HVD coordinates; H is antiparallel to the earth's dipole field (positive northward), V is perpendicular to H and positive radially outward, and D is perpendicular to H and V and positive eastward. T is the total intensity of the magnetic field. The initial decrease in the D component occurred at GOES 5 at about 0447 UT. This decrease reached a minimum at 0449 UT and almost simultaneously the H component began to increase. This H increase is coincident with the arrival of the eastward moving auroral branch at the estimated foot point of GOES 5 (Figure 2.5). The D decrease recovered at about 0452 UT while the H component continued to increase until 0454 UT. GOES 6 observed an increase in the D component at 0452 UT, which reached maximum at 0453 UT. The H component first decreased slightly at 0448 UT and then began to increase at 0453 UT. At the time of the D increase at GOES 6 (from 0452 to 0453 UT) the auroral surge was located about 200 km east of SHM, that is, not near but about 500 km (or about 15 degrees in longitude) east of the estimated foot point of GOES 6. This will be described in detail later in this section.

The ground magnetic field variations at auroral latitude stations are shown in Figure 2.8. The Xm component is positive northward in corrected geomagnetic coordinates, the Ym is positive eastward and the Z is positive downward. From this figure it is clear that this event with the onset at 0450 UT was highly localized, observed only at SHM (in the Xm and Z components) and LGR (in the Z). The magnetogram at SHM showed a decrease in the Xm component at 0450 UT, which reached a maximum at 0455 UT, coincident with the passage of an auroral surge above SHM. The magnetic perturbation was therefore probably caused by the current system associated with the surge.

The magnetic field variations at sub-auroral latitude stations (STJ, OTT, and VIC) are shown in Figure 2.9. They showed only small variations (less than 15 nT) in the Xm component until 0500 UT. However there was a slight decrease in the Ym component at OTT and an increase at VIC at 0448 UT, suggesting that the substorm onset region was located between the longitudes of these two stations.

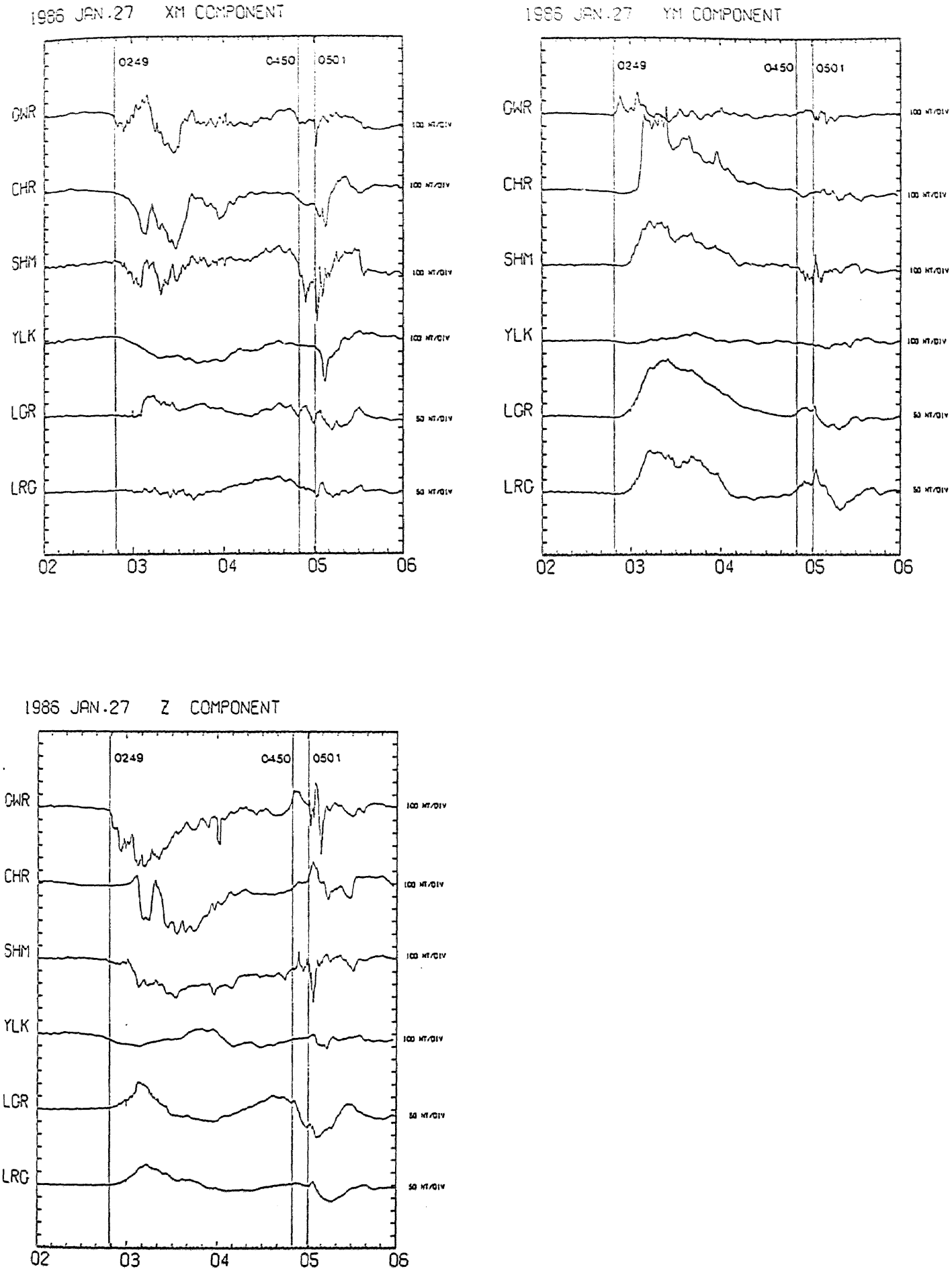

Figure 2.8 Ground magnetic field variations at auroral zone stations from 0200 UT to 0600 UT on January 27, 1986. The Xm component is positive northward in the corrected geomagnetic coordinates, the Ym is positive eastward and the Z is positive downward.

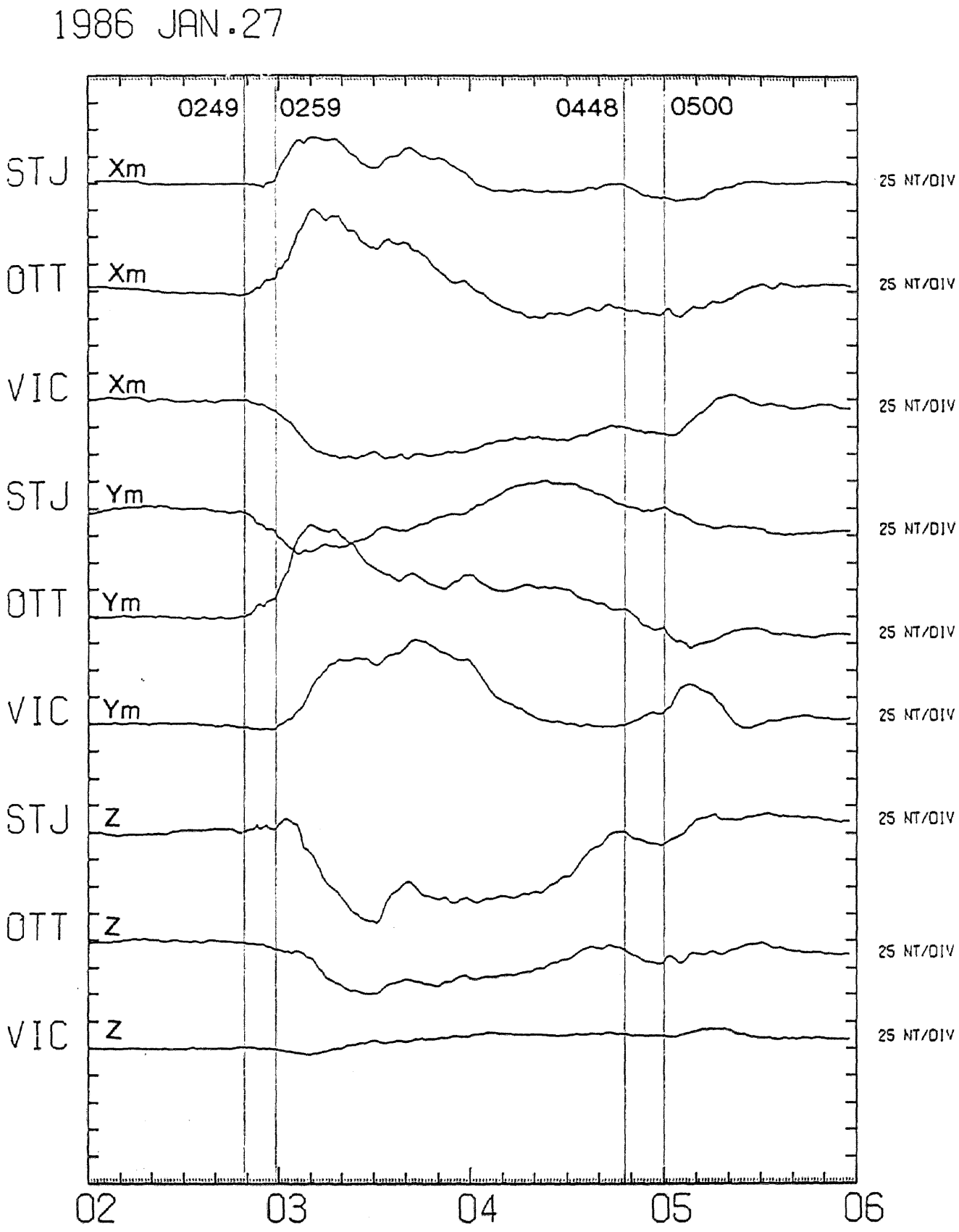

Figure 2.9 Magnetic field variations at sub-auroral zone stations from 0200 UT to 0600 UT on January 27, 1986.

2. Comparison of auroral activity with the magnetic field variations at geosynchronous orbit

The front of the auroral surge when GOES 6 observed the positive D perturbation was located about 200 km east of SHM, while the estimated foot point of GOES 6 was about 300 km west of SHM. That is, the surge was located about 500 km (or about 15 degrees in longitude) east of the estimated foot point of GOES 6 when the satellite observed the D component perturbation probably caused by field-aligned currents associated with the surge. In explaining this, there are two possibilities. One possibility is that there was another field-aligned current structure near the longitude of GOES 6 location. From the ground magnetic observations, however, it is evident that the magnetic field variation at that time was highly localized. Furthermore, as shown in Figure 2.6 the western part of the arc was straight and had no irregular forms such as bulges and surges when observed by the DMSP satellite. Since it usually takes several minutes for the active vortex-type aurora to return to the stable arc, it seems unrealistic that another arc developed and decayed simultaneously near the estimated GOES 6 foot point.

The other and more probable situation is that the magnetic field lines connecting geosynchronous altitudes and the ionosphere deviated from Tsyganenko's model field line in the azimuthal direction, and these two phenomena (magnetic field variation at geosynchronous orbit and auroral activity) occurred at the same time are on the common field line. Let us consider the cause of the spatial deviation of the estimated foot point by Tsyganenko's model from the location of the aurora, which is correlated with the positive D perturbation at GOES 6. The most probable cause is that the real field lines connecting the ionosphere and geosynchronous altitudes azimuthally deviate from the model between the large-scale Region 1 and Region 2 field aligned currents. Tsyganenko's model does not involve the effects of the field-aligned currents flowing from the magnetospheric equator to the ionosphere, which will be described in Chapter 3. Since these currents should considerably affect the large-scale magnetospheric magnetic field distribution, it is necessary to take into consideration the effect of Region 1 and Region 2 field-aligned current systems. The discussion concerned with introducing this effect into Tsyganenko's model will be given in Chapter 4.

2.3.1.1b. Expansion Onset at 0500 UT

The second auroral expansion began at 0501 UT (Figure 2.10). An initial brightening of the arc occurred above SHM at about 0501 UT (see the arrows). The brightening covered a longitudinal extent from the east of GWR to about 500 km west of SHM within 10 seconds, and then the brightened aurora began to move poleward within another 10 seconds. Simultaneously, an equatorward moving arc was seen in the field of view of SHM. Unfortunately owing to some electron beam trouble with the TV camera, the southern field of view of SHM was saturated, and hence the center of the equatorward moving arc was missing.

GOES 6 magnetic field in Figure 2.7 showed a slight decrease in the D component at 0502 UT. This D perturbation returned to positive in 1 minute and continued until 0505 UT, together with irregular fluctuations. For that time there was little fluctuation at GOES 5, indicating the localized nature of the current system near GOES 6.

The ground magnetogram (Figure 2.8) showed a sharp decrease in the Xm component at GWR at about 0501 UT. Almost simultaneously a more gradual decrease was observed at SHM. The magnetograms at CHR and YLK showed negative Xm perturbations several minutes later, indicating subsequent poleward and westward motion of the expansion front.

The magnetic field data in the sub-auroral latitude stations in Figure 2.9 showed the initiation of a positive bay at about 0500 UT. The variation of the Ym component was negative at STJ and OTT, while it is positive at VIC, suggesting the onset region was located between the OTT and VIC meridians. The amplitude of the variation in the Ym component for the second event, with the onset at 0500 UT, was much larger than that at the first event with the onset at 0448 UT. This means that on the ground the amplitude of the magnetic variation is larger for the second event than it is for the first event, while the magnetic variation at geosynchronous orbit is larger for the second event. This is probably due to the localized nature of the observed small-scale field-aligned current systems, as will be discussed in detail in Section 2.4.

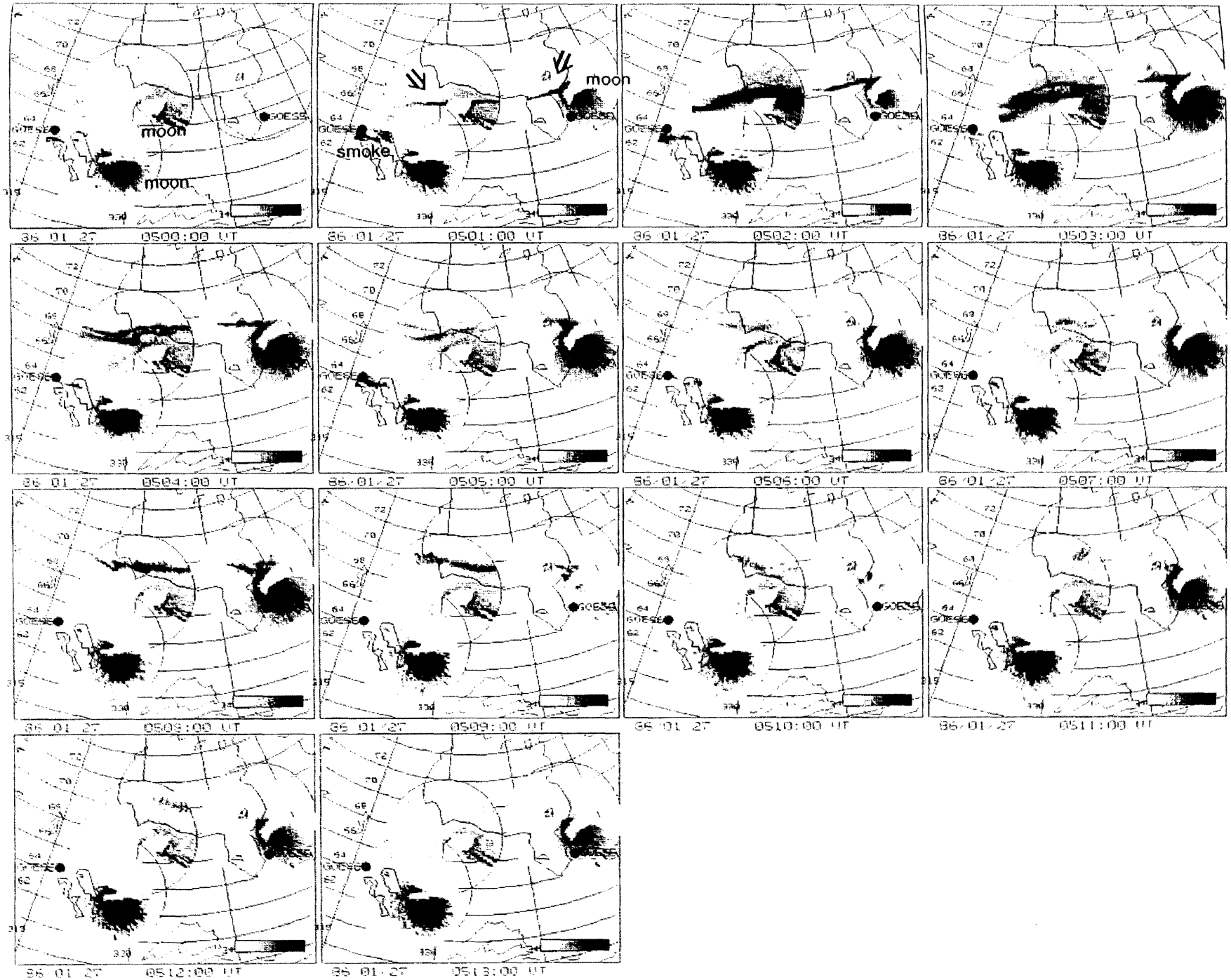

Figure 2.10 Spatial-temporal development of auroras from 0500 UT to 0513 UT on January 27, 1986.

2.3.1.2. Substorm at 0249 UT

During this event GWR was located near 2130 MLT and SHM was located near 2000 MLT. The Kp index was 2+.

Figure 2.11 ((a) and (b)) show sequential images of auroral activity. During the time of this event moon light was intense and scattered by haze, therefore the eastern part of the auroral image of each station was badly contaminated. Most of the image, however, is still useful for examination of the spatial-temporal distribution of auroras.

A stable arc was extending from above GWR to the western horizon of SHM from about 0249 UT. Although at first this arc was rather too weak to be seen in Figure 2.11, it was actually recorded in the original video tape. Within this arc a new auroral surge began to develop above GWR at 0251 UT (indicated by the arrow). This surge expanded both westward and poleward, then faded by 0258 UT. Another auroral surge was observed in the east of SHM from 0259 UT (shown by the arrow). This surge developed and expanded both poleward and westward, then faded gradually by 0308 UT. On the other hand a north-south (N-S) aligned arc was seen at 0305 UT above GWR (see the arrow), which moved westward with the velocity of about 100 km/min., then faded gradually. After that an auroral band extending from the west, through the zenith to the north-east of SHM, was seen from 0312 UT to 0320 UT.

Figure 2.12 shows the magnetic field variations at GOES 6 and GOES 5. Irregular fluctuations in all components began at GOES 5 at 0251 UT, preceded by a gradual decrease in the H component for several minutes. At 0304 UT a large perturbation occurred, positive in the H and D components and negative in the V component (becoming positive again in a few tens of seconds). The perturbation at 0251 UT is coincident with the formation of a surge above GWR (Figure 2.11), while the perturbation at 0305 UT is coincident with the appearance of an N-S aligned arc above GWR. This indicates that these perturbations at GOES 5 are highly correlated with the auroral activity at the estimated foot point of GOES 5. At GOES 6 small irregular fluctuations in all components occurred at 0253 UT,

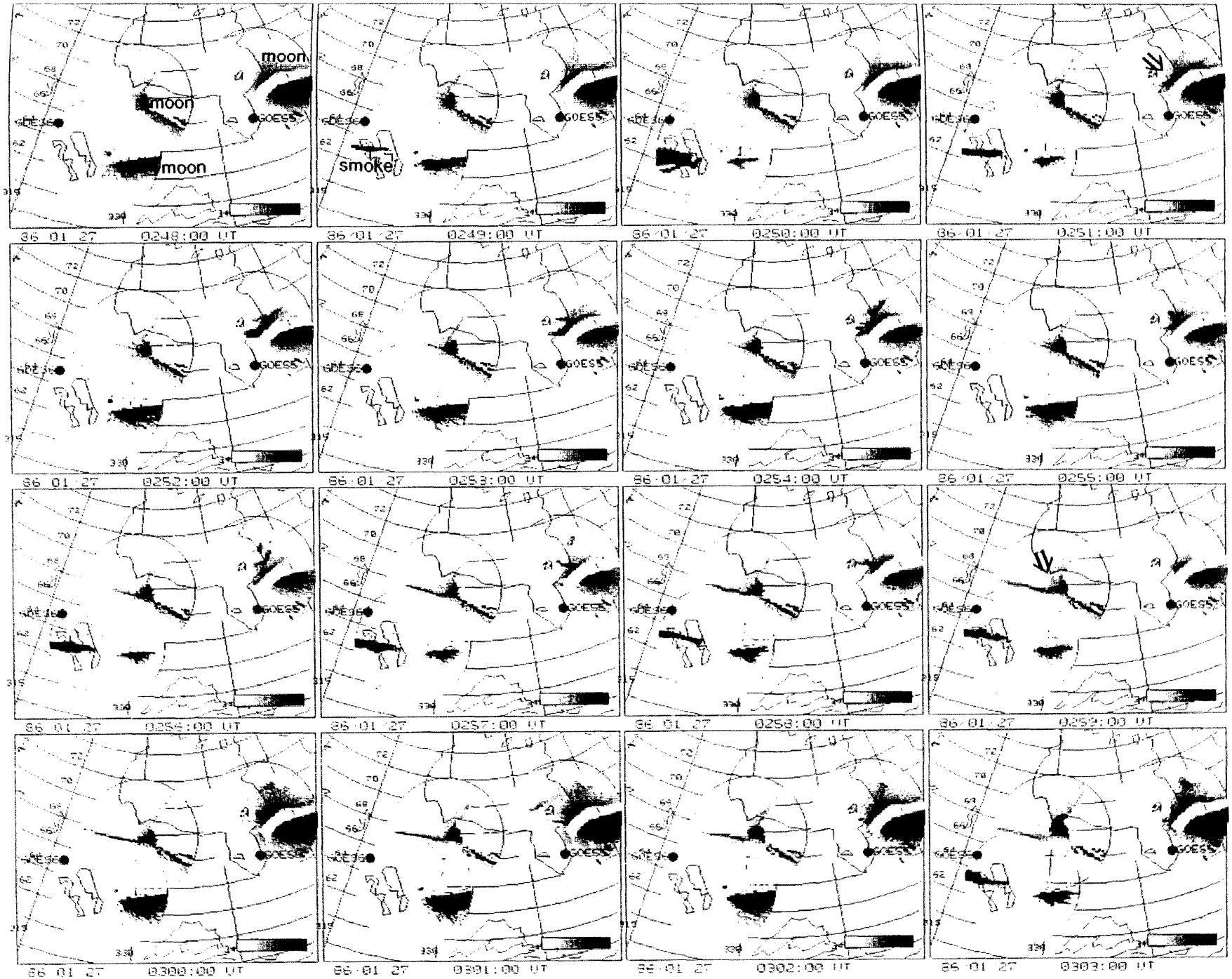

Figure 2.11(a) Spatial-temporal development of auroras from 0248 UT to 0303 UT on January 27, 1986.

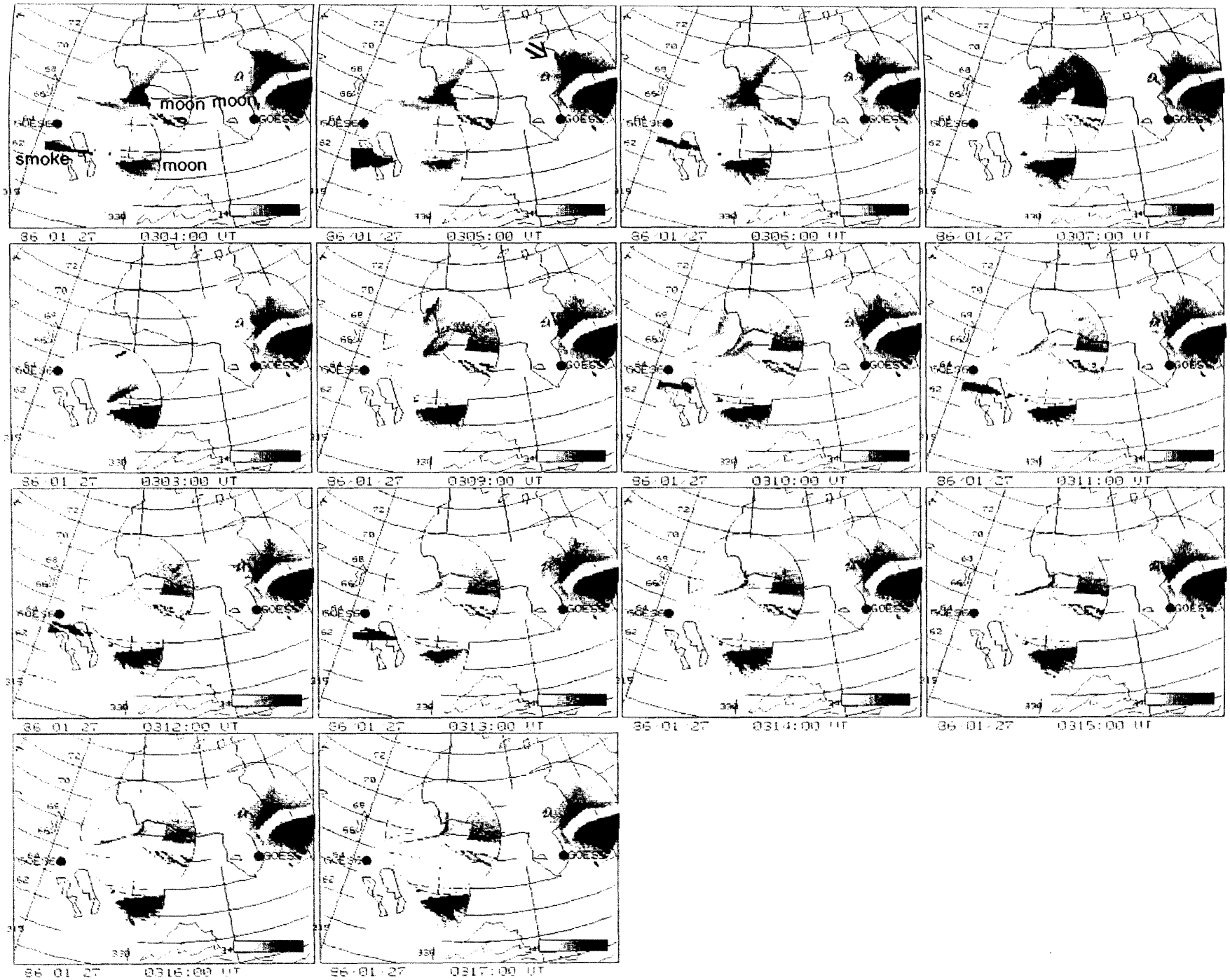

Figure 2.11(b) Spatial-temporal development of auroras from 0304 UT to 0317 UT on January 27, 1986.

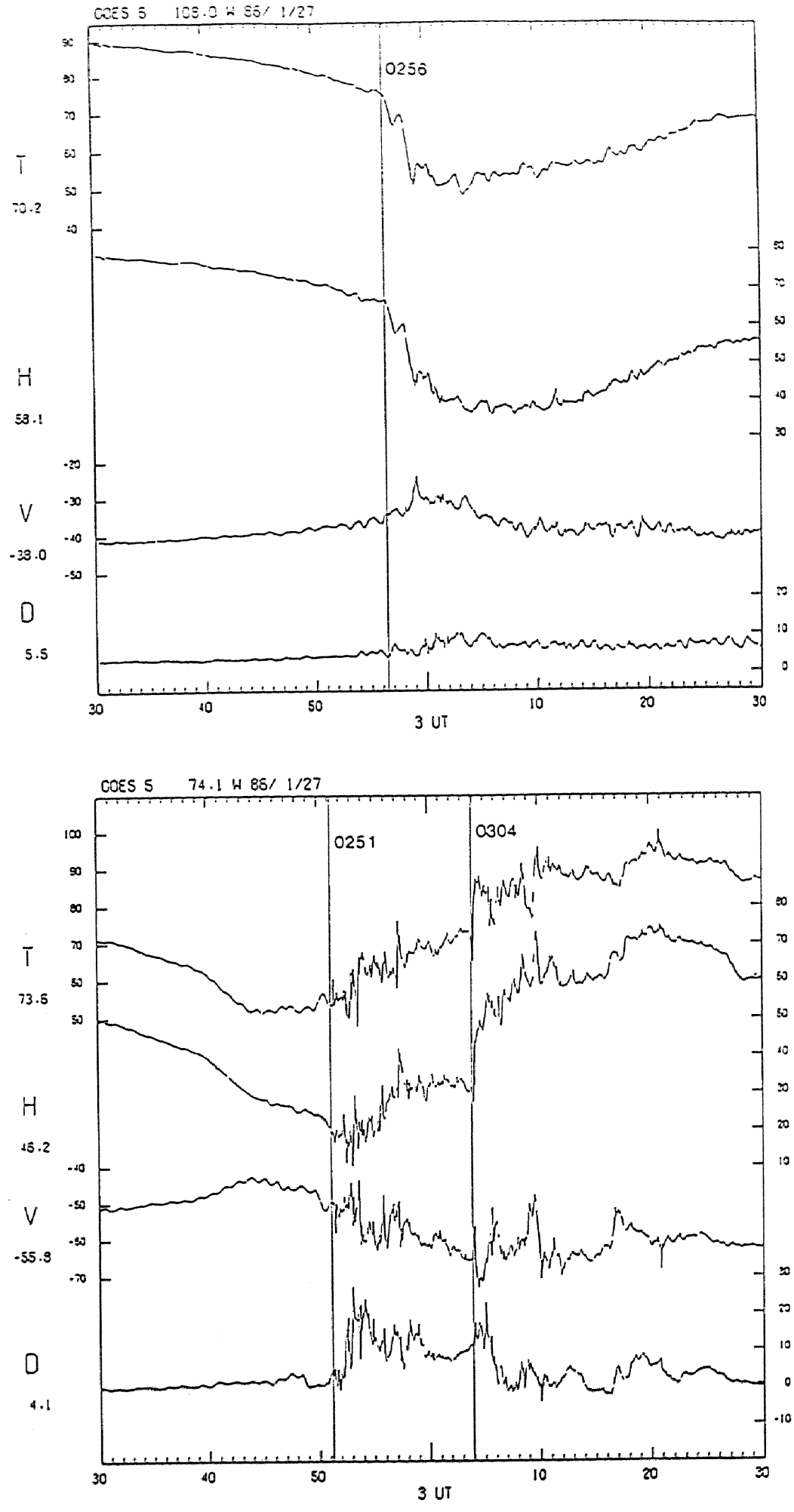

Figure 2.12 Magnetic field variations at GOES 6 and GOES 5 from 0230 UT to 0330 UT on January 27, 1986.

and from 0256 UT to 0300 UT an abrupt depression in the H component was observed. This depression appears to be correlated with the formation of an auroral surge east of SHM (Figure 2.11), about 500 km (or 15 degrees in longitude) east of the estimated foot point of GOES 6.

The Xm component magnetic field at GWR (Figure 2.8) showed a simultaneous beginning of a decrease and an irregular fluctuation at 0249 UT, together with positive Ym and negative Z perturbations, coincident with the formation of the surge above GWR shown in Figure 2.11. At SHM the Xm component began to decrease gradually at 0255 UT accompanied by simultaneous irregular fluctuations in all components. The Xm component at GWR began to decrease again at 0309 UT while at SHM and CHR the decrease began at 0313 UT.

At sub-auroral latitude stations (in Figure 2.9), Ym perturbations, positive at OTT and negative at STJ started at 0249 UT. After 10 minutes the magnetogram at VIC showed a positive Ym perturbation at 0259 UT, indicating the westward motion of the activity region.

The magnetic field variation at GOES 5 is highly correlated with the formation of an auroral surge and a N-S aligned arc just above GWR, while the variation at GOES 6 is correlated with the formation of an auroral surge slightly east of SHM, about 15 degrees east of the estimated foot point of GOES 6. This indicates that the real foot point of GOES 6, on the dusk side of the expansion onset region, was again about 15 degrees east of the estimated foot point, the same as in the previous example. On the other hand the tendency of the deviation of the real foot point was seen to be small for GOES 5, suggesting that field line deviation was not effective at the GOES 5 field line. This will be discussed in detail in Section 2.4.

2.3.1.3. Substorm at 0639 UT

SHM was located near geomagnetic midnight and GWR was located near 0200 MLT and the Kp index during this event was 5.

The auroral activity is shown in Figure 2.13. Intensification of irregular auroral forms was seen above SHM at about 0648 UT, 0704 UT, 0714 UT, and 0729 UT, and above

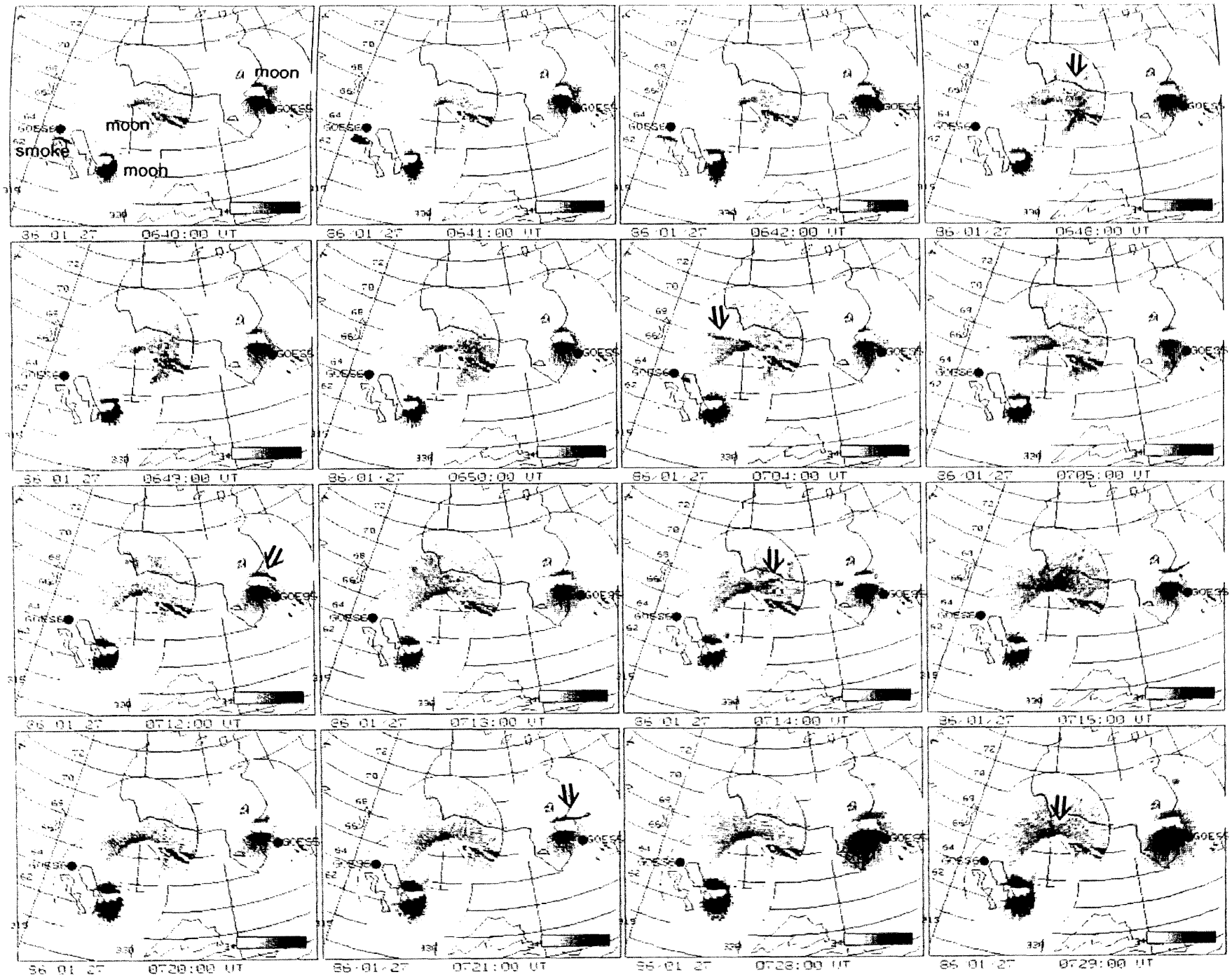

Figure 2.13 Spatial-temporal development of auroras during the substorm at 0639 UT on January 27, 1986.

GWR at about 0712 UT, and 0721 UT. Each form, indicated by the arrow, moved eastward, suggesting that the onset region of the substorm was located west of the observational region.

Figure 2.14 shows the magnetic field variations at sub-auroral latitude stations. The onset is clearly seen at 0639 UT, characterized by the Ym perturbations, negative at OTT and positive at VIC. The sign of the Ym perturbation suggests that the onset was located between the OTT and VIC meridians.

Figure 2.15 shows the magnetic field variations at auroral latitude stations. The magnetograms at LRG and LGR showed an initiation of irregular fluctuations of the Xm component at 0640 UT preceded by a gradual decrease. Simultaneously the Z component showed a sharp increase at LRG and a rather gradual decrease at LGR respectively, suggesting that the onset region is localized near LRG. Gradual decreases in the Xm component were successively observed at more eastern stations (SHM, CHR, and GWR) several minutes later, indicating eastward expansion of the substorm.

Figure 2.16 shows the magnetic field variations at the GOES satellites. A sharp increase in the H component, together with a sharp decrease in the D component and irregular fluctuations in all components, began at GOES 6 at 0640:15 UT, continuing for about 1 hour. During these fluctuations several sharp magnetic field perturbations were observed viz. an increase in the D component at 0654 UT, a sharp decrease in the H component at 0701 UT, and an increase in the D component together with irregular fluctuations in three components at 0720 UT. At GOES 5 no conspicuous variations were observed during the same period, except for the irregular fluctuations in all components from 0703 UT to 0713 UT.

At the first onset at GOES 6 (0640:15 UT) no outstanding auroral activity was seen in the field of view of SHM or LGR. From the magnetic data at LRG it is expected that auroral activity occurred above LRG, although, unfortunately, it was overcast there. It is therefore suggested that the real foot point of GOES 6 was located near LRG, 5° to 10° west of the estimated foot point. Moreover, the onsets observed by GOES 6 at 0640, 0654, 0701, and

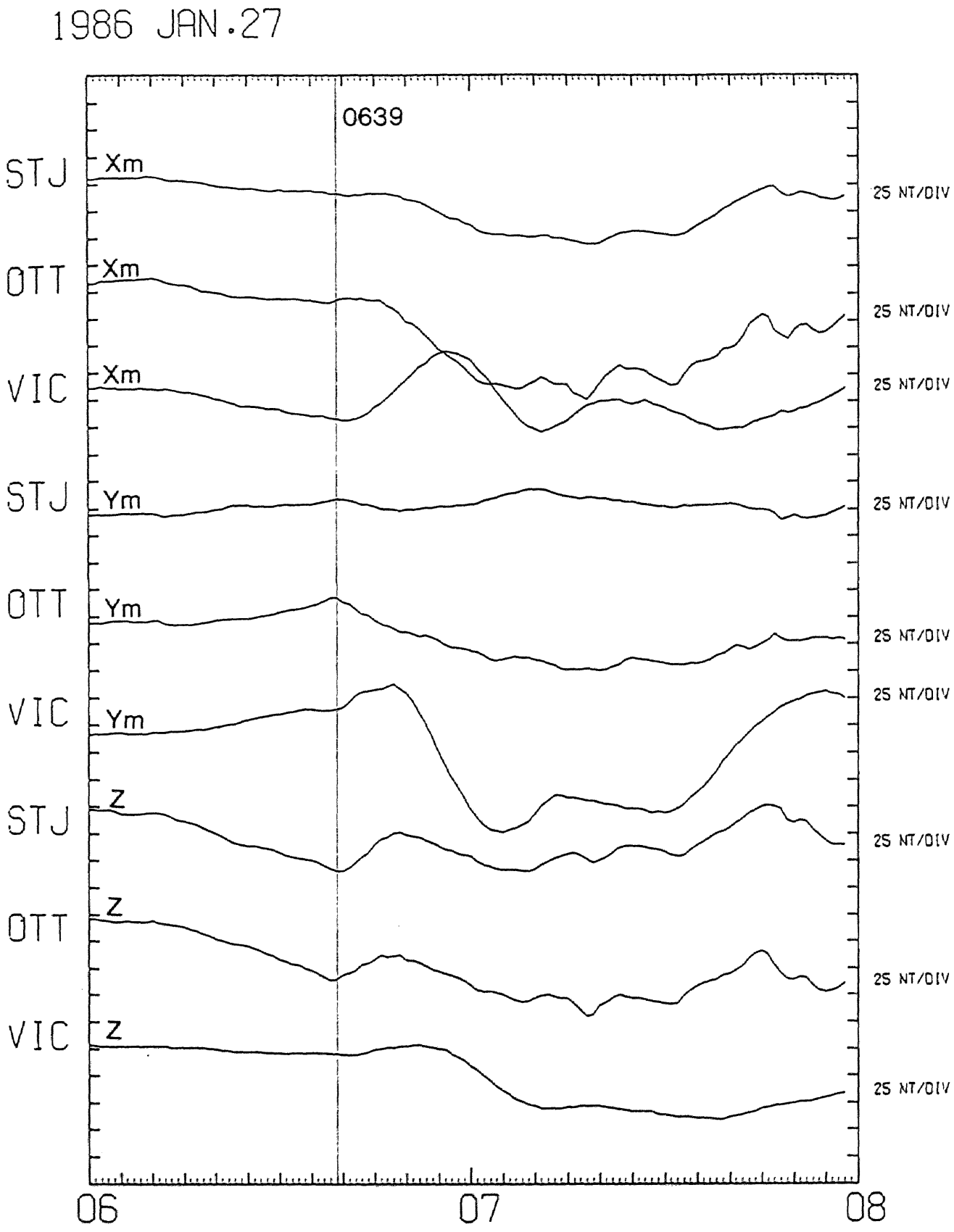

Figure 2.14 Magnetic field variations at sub-auroral zone stations from 0600 UT to 0800 UT on January 27, 1986.

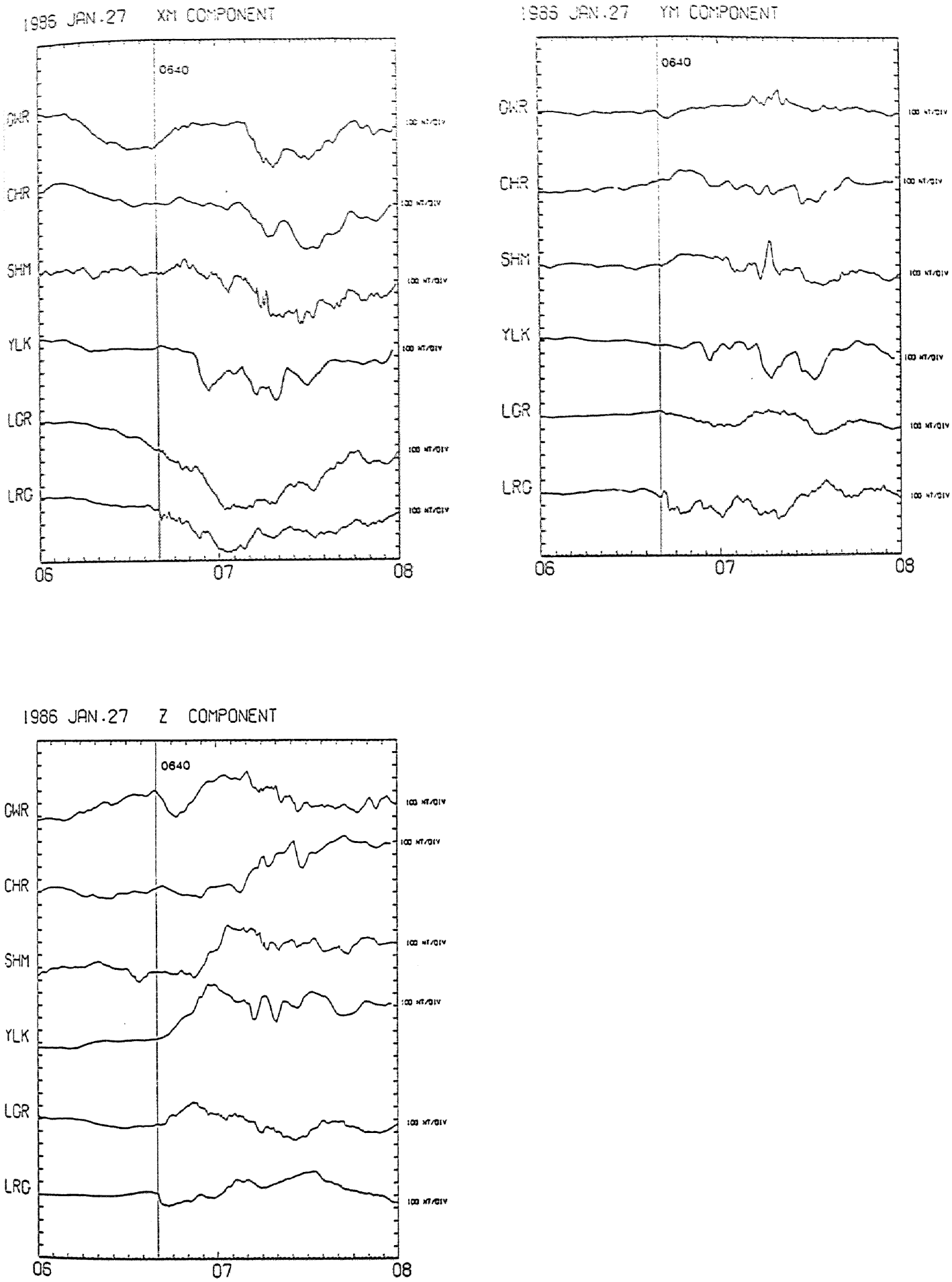

Figure 2.15 Magnetic field variations at auroral zone stations from 0600 UT to 0800 UT on January 27, 1986.

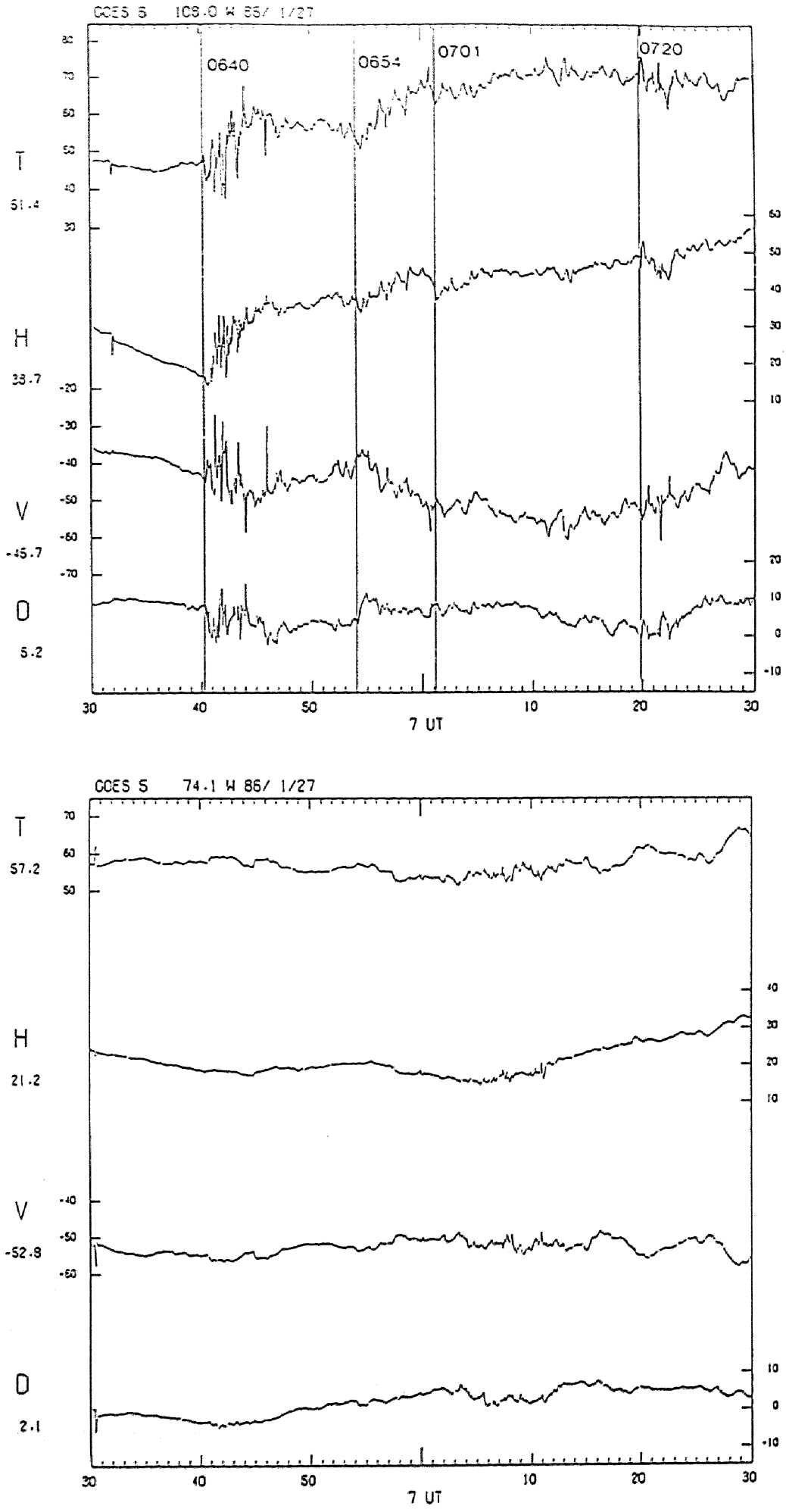

Figure 2.16 Magnetic field variations at GOES 6 and GOES 5 from 0630 UT to 0730 UT on January 27, 1986.

0720 UT seem to be associated with the auroral activities above SHM about 10 minutes later, that is, at 0648, 0704, 0714 and 0729 UT. These had presumably been above LRG about 10 minutes before, as inferred from the eastward motion of these auroras. The GOES 5 magnetic field showed no conspicuous onset, so that it is difficult to estimate the field line connection between the ionosphere and GOES 5 for these events.

2.3.2. Jan. 02, 1986

The AE index on this day is shown in Figure 2.17, in which a clear expansion occurred at about 0327 UT (indicated by the arrow). The accurate onset time is determined as 0327 UT (Figure 2.21). There is also a small localized expansion at GWR at 0252 UT, as seen in the magnetogram in Figure 2.20, although it cannot be seen in the AE index. The spatial-temporal auroral distribution, magnetic field variations at the GOES satellites, at auroral latitude stations, and at sub-auroral latitude stations are shown in Figures 2.18, 2.19, 2.20, and 2.21, respectively.

2.3.2.1. Substorm at 0252 UT

GWR was located near 2130 MLT and SHM was located near 2000 MLT. During this event the Kp value was 4–.

Figure 2.18 (a) shows the spatial-temporal distribution of auroras. There was a localized auroral expansion above (or slightly north of) GWR at 0252 UT (see the arrow). Coincident with this auroral activity, the GOES 5 magnetic field (Figure 2.19) showed a sharp increase in the D component at 0252 UT. This active auroral form became stable in a few minutes.

The magnetic field at GWR (Figure 2.20) exhibited a sharp decrease in the Z component at 0252 UT, corresponding to the auroral expansion above GWR. It is clear that the onset was highly localized because no outstanding magnetic field variations occurred at the other stations. The magnetograms at sub-auroral latitude stations (Figure 2.21) showed no prominent onset, except at OTT, where a small increase in the Ym component was observed.

Similar localized auroral activity was observed above SHM (Figure 2.18) from 0305 UT

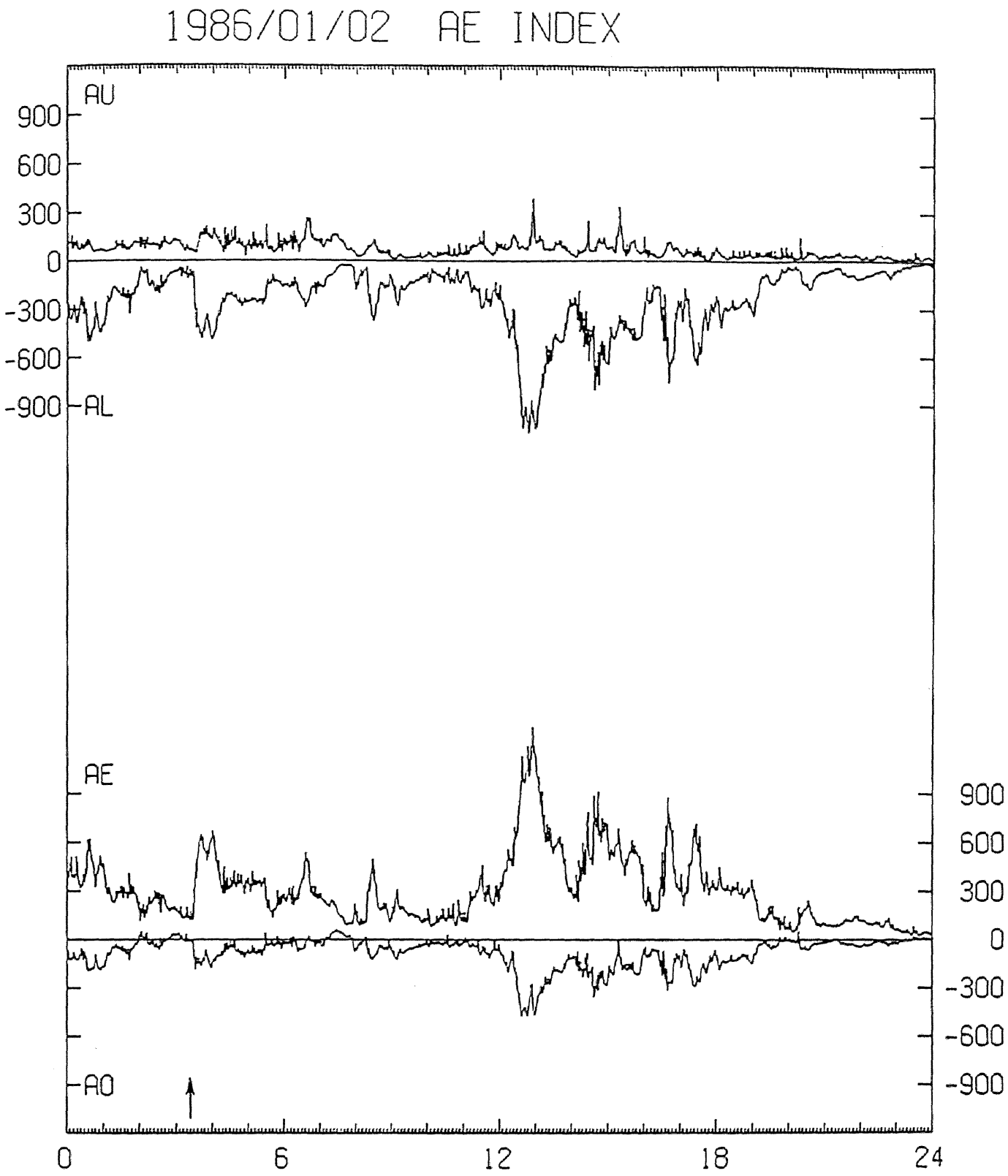

Figure 2.17 AE index on January 02, 1986.

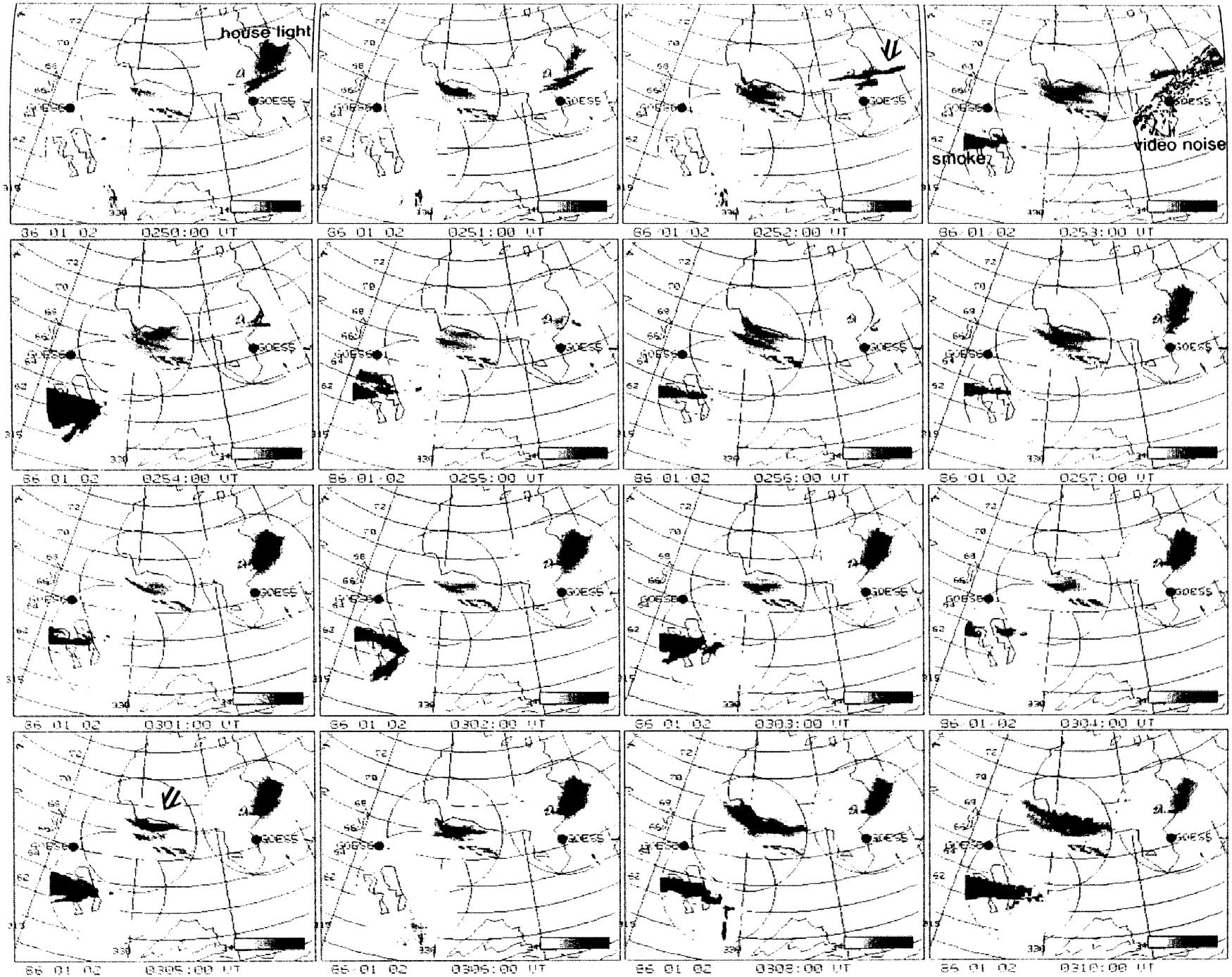

Figure 2.18(a) Spatial-temporal development of auroras from 0250 UT to 0310 UT on January 02, 1986.

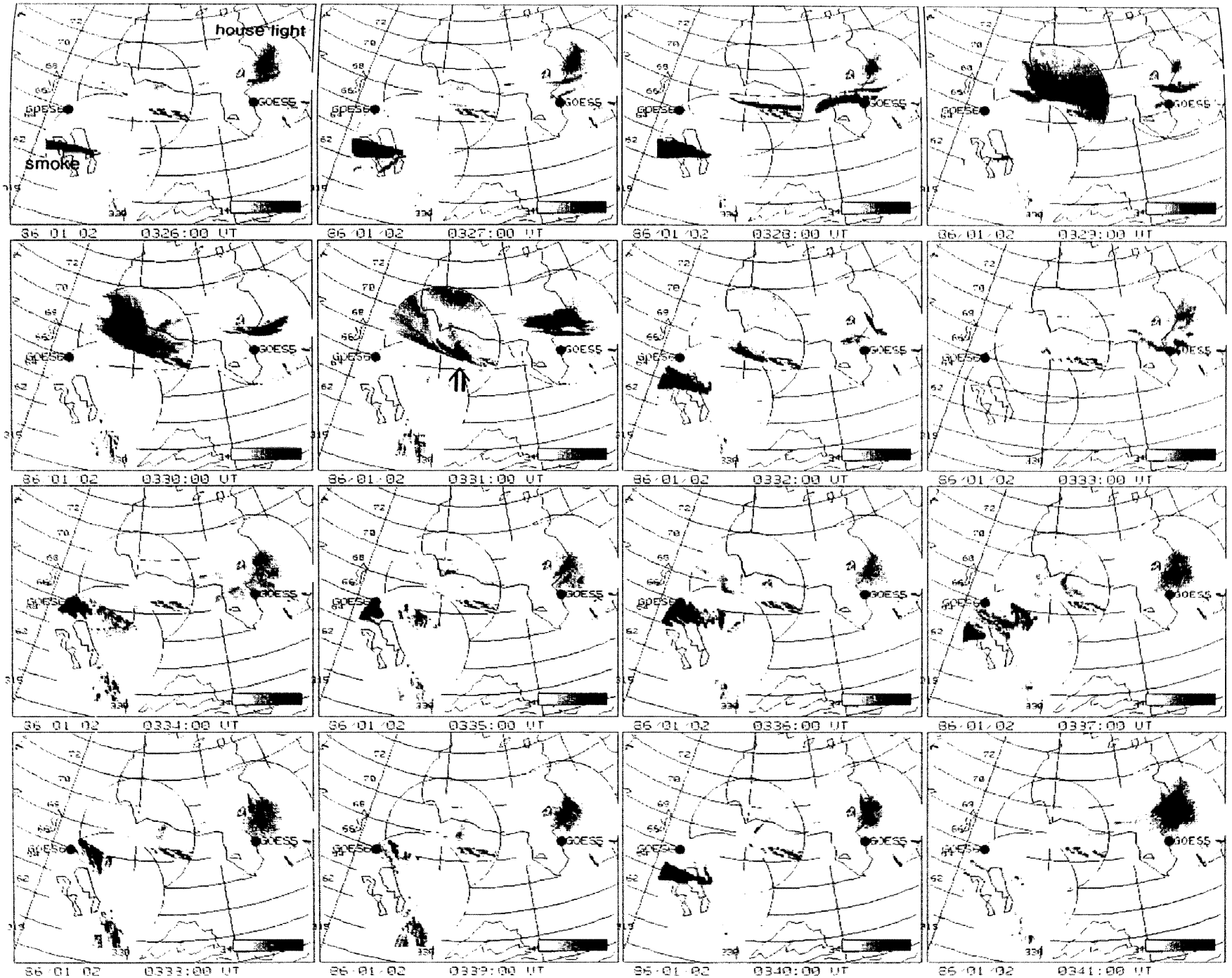

Figure 2.18(b) Spatial-temporal development of auroras from 0326 UT to 0341 UT on January 02, 1986.

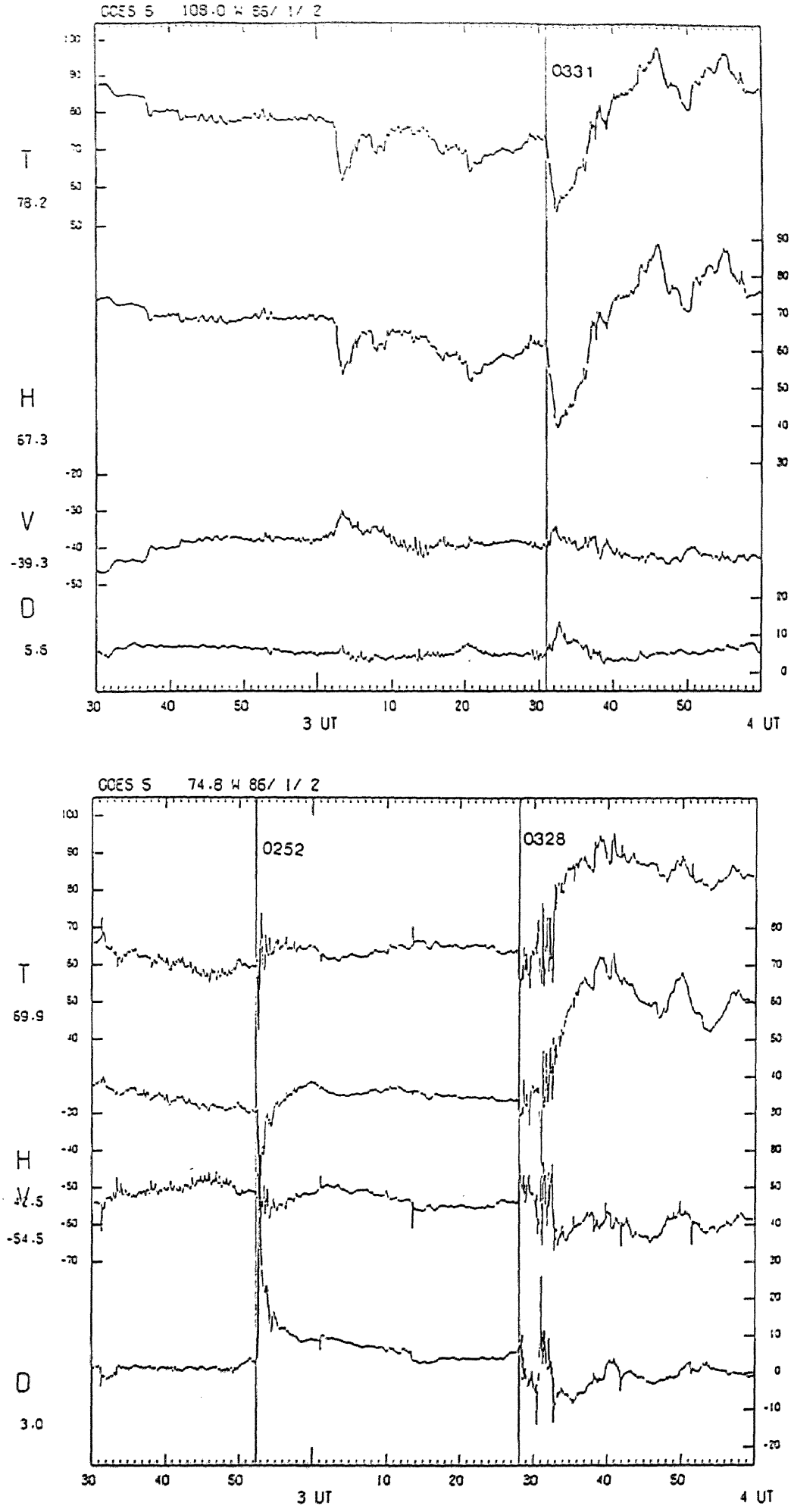

Figure 2.19 Magnetic field variations at GOES 6 and GOES 5 from 0230 UT to 0400 UT on January 02, 1986.

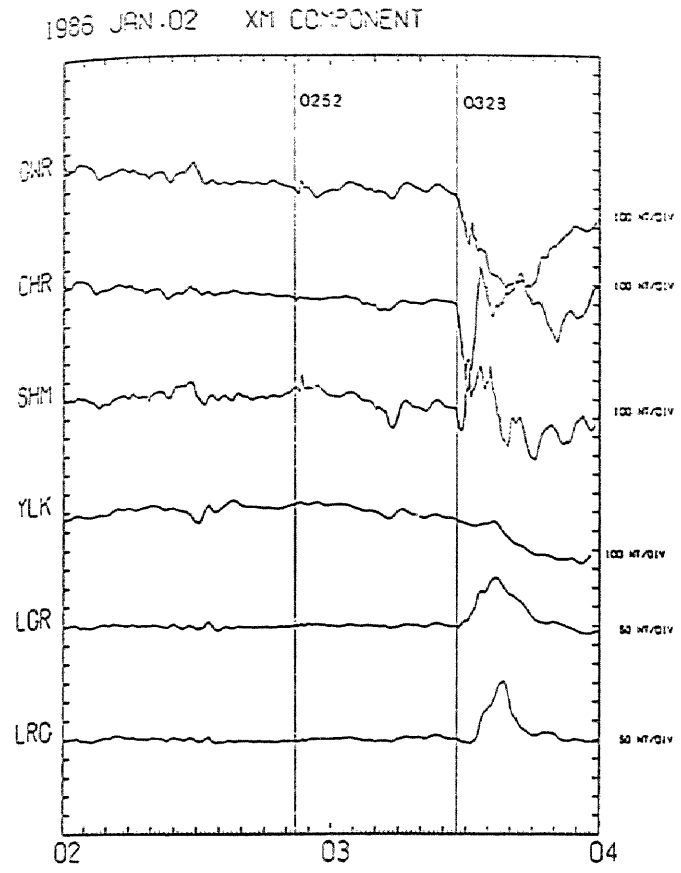

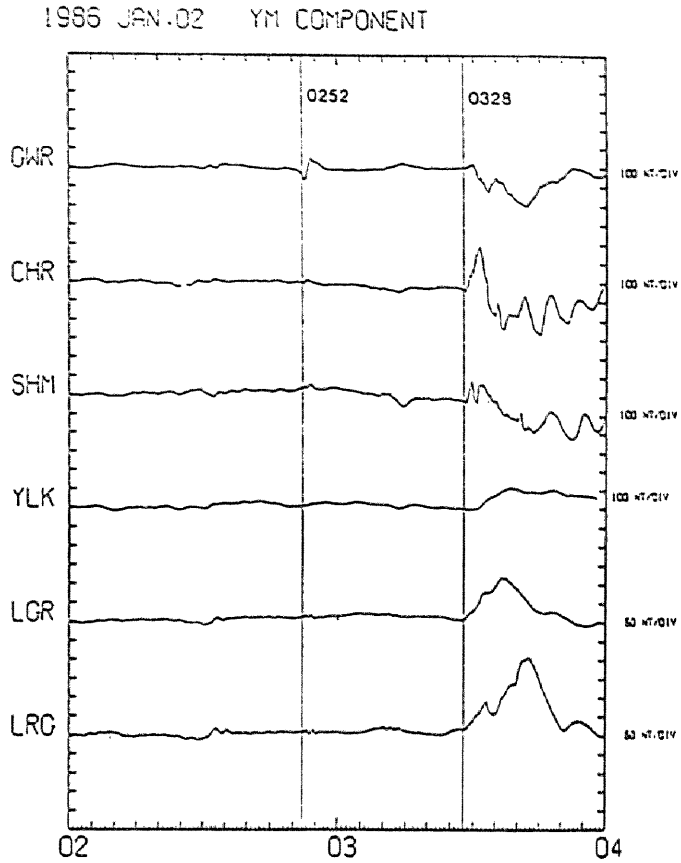

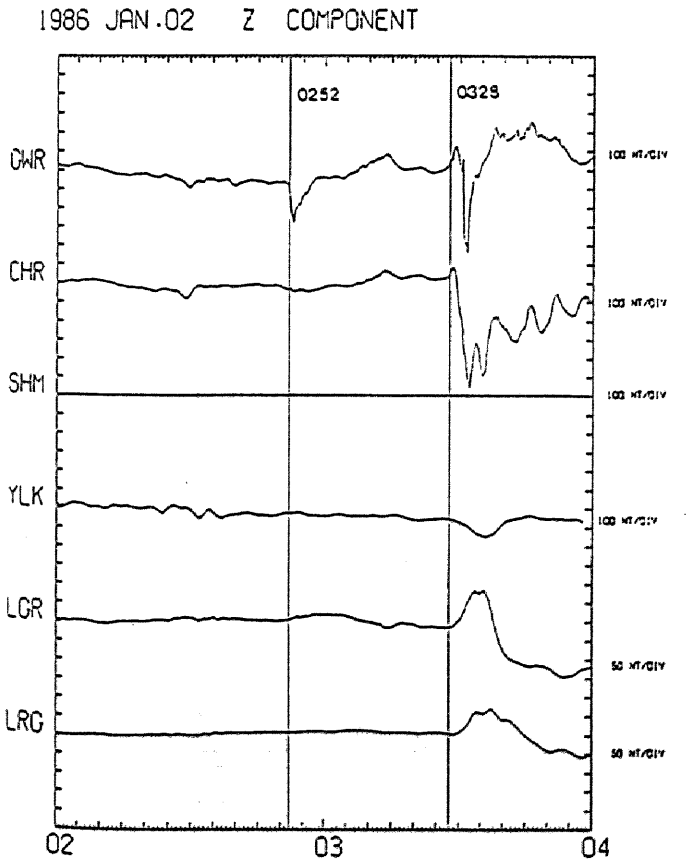

Figure 2.20 Magnetic field variations at auroral zone stations from 0200 UT to 0400 UT on January 02, 1986.

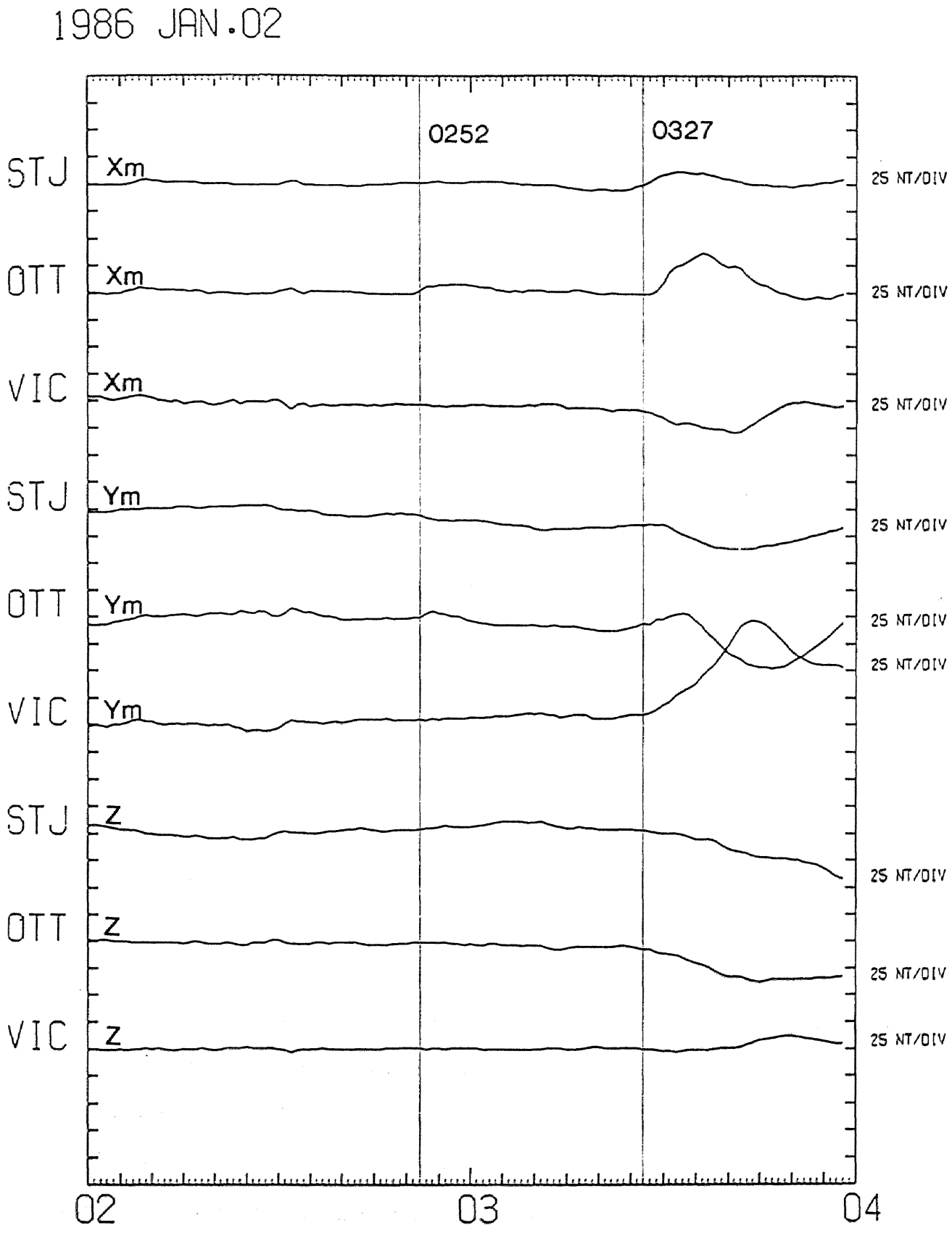

Figure 2.21 Magnetic field variations at sub-auroral zone stations from 0200 to 0400 UT on January 02, 1986

(see the arrow) to 0310 UT. The corresponding magnetic field change was observed at SHM (Figure 2.20) at 0312:30 UT, characterized by decreases in the Xm and Ym components. This activity was also localized and recovered in a few minutes. The GOES 6 magnetic field (Figure 2.19) showed a depression of the total intensity at 0302:30 UT, and there was also a small depression at 0307:20 UT. These depressions seem to be correlated with the auroral activity above SHM.

2.3.2.2. Substorm at 0327 UT

The Kp index during this event was 4. At 0328 UT an active auroral arc brightened, extending from GWR to SHM (Figure 2.18(b)). This activity moved westward, and then expanded both poleward and equatorward in the field of view of SHM to form a large vortex. At 0331 UT an equatorward moving small auroral vortex appeared (indicated by the arrow), which moved also westward, and subsequently formed into a few N-S aligned arcs a few minutes later. These moved westward as well.

The magnetograms at sub-auroral latitude stations (Figure 2.21) showed an onset at 0327 UT, characterized by an increase in the Ym component at STJ. At auroral latitudes (Figure 2.20) the onset broke out at 0328 UT almost simultaneously in the magnetograms at different stations (GWR, CHR, SHM, and LGR). Magnetic variations after the onset were very complicated, probably indicating the highly irregular structure of the ionospheric current system.

GOES 5 observed a decrease in the D component at 0328 UT (Figure 2.19), corresponding to the brightening of the auroral arc extending from GWR to SHM. At 0331 UT GOES 6 observed a sharp decrease in the H component together with an increase in the D component. The D component reached a maximum and simultaneously the H component began to recover at 0333 UT. GOES 6 showed no conspicuous magnetic field perturbation when the expansion began above SHM and GWR, that is, at 0328 UT. Instead, the magnetic field change began when an active small auroral vortex occurred equatorward of the previous activity region. This fact suggests that the magnetic field change was caused by the formation of field-aligned

currents connected to the auroral vortex nearby the real foot point of GOES 6, about 10° to 15° east of the estimated foot point, with highly localized structure in the latitudinal as well as the longitudinal direction. The details will be discussed in Section 2.4.

2.3.3. Jan. 01, 1986

The AE index is shown in Figure 2.22. On this day the activity was rather complicated. No isolated substorm was seen in the AE index, due to sequential occurrence of many substorms. Nevertheless, from the sub-auroral latitude magnetograms (Figure 2.23) three expansions can be identified: at 0226 UT, 0251 UT and 0337 UT. From the sign of the Ym component magnetic field variations the onset regions of three expansions were estimated to be located between STJ and OTT, between OTT and VIC, and between OTT and VIC meridians, respectively.

The Kp value was 3+ from 0000 UT to 0300 UT and 4- from 0300 UT to 0600 UT. The activity was located at rather high latitudes, in comparison with the examples on January 27, as seen in the sequential auroral distribution in Figure 2.25.

The magnetograms at auroral latitude stations are shown in Figure 2.24. The data from LGR were not available until 0240 UT on this day. Three onsets were observed at 0226 UT, 0250 UT, and 0338 UT.

2.3.3.1. Substorm at 0226 UT

GWR was located near 2100 MLT and SHM was located near 1930 MLT.

Figure 2.25 (a) shows the spatial-temporal distribution of auroras. A stable arc was extending in the fields of view of both GWR and SHM from about 0220 UT (not shown here). This arc (see the arrow in the upper left panel) brightened at 0225:30 UT, then expanded poleward and westward to form an auroral surge, which passed across the field of view of SHM from east to west between 0226 UT and 0230 UT. Unfortunately during the passage of the surge the southern part of the field of view of the TV camera at SHM was

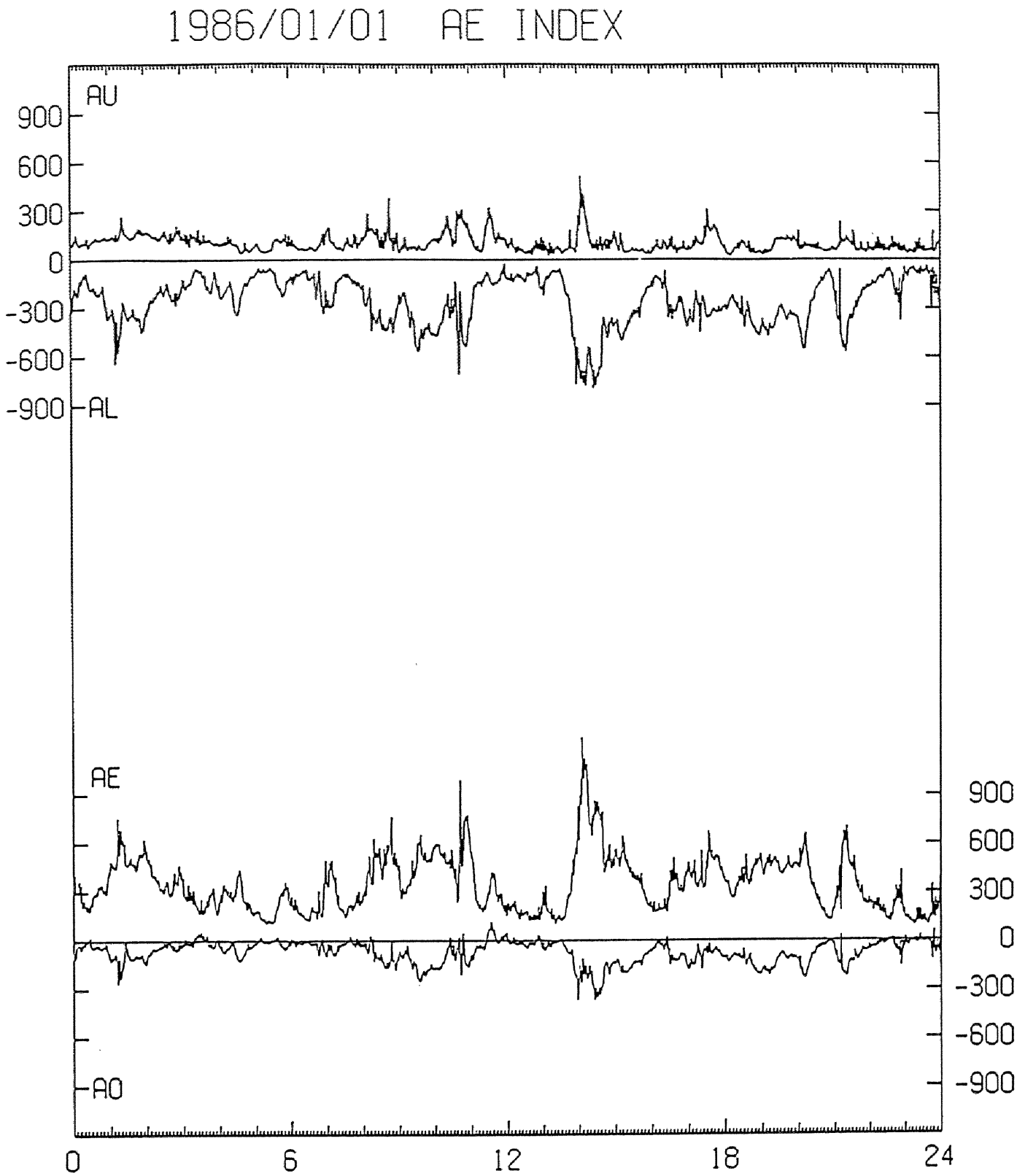

Figure 2.22 AE index on January 01, 1986.

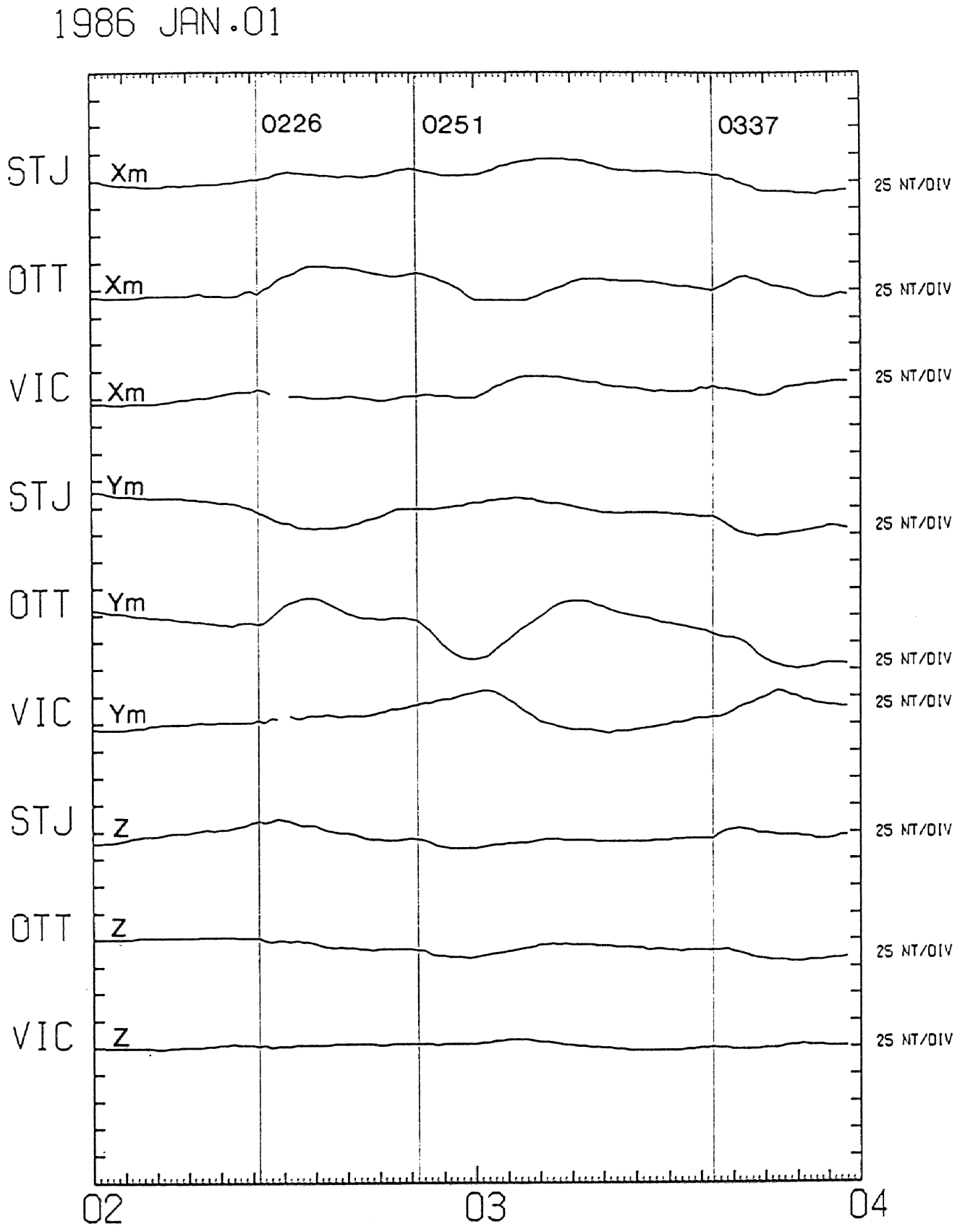

Figure 2.23 Magnetic field variations at sub-auroral zone stations from 0200 to 0400 UT on January 01, 1986.

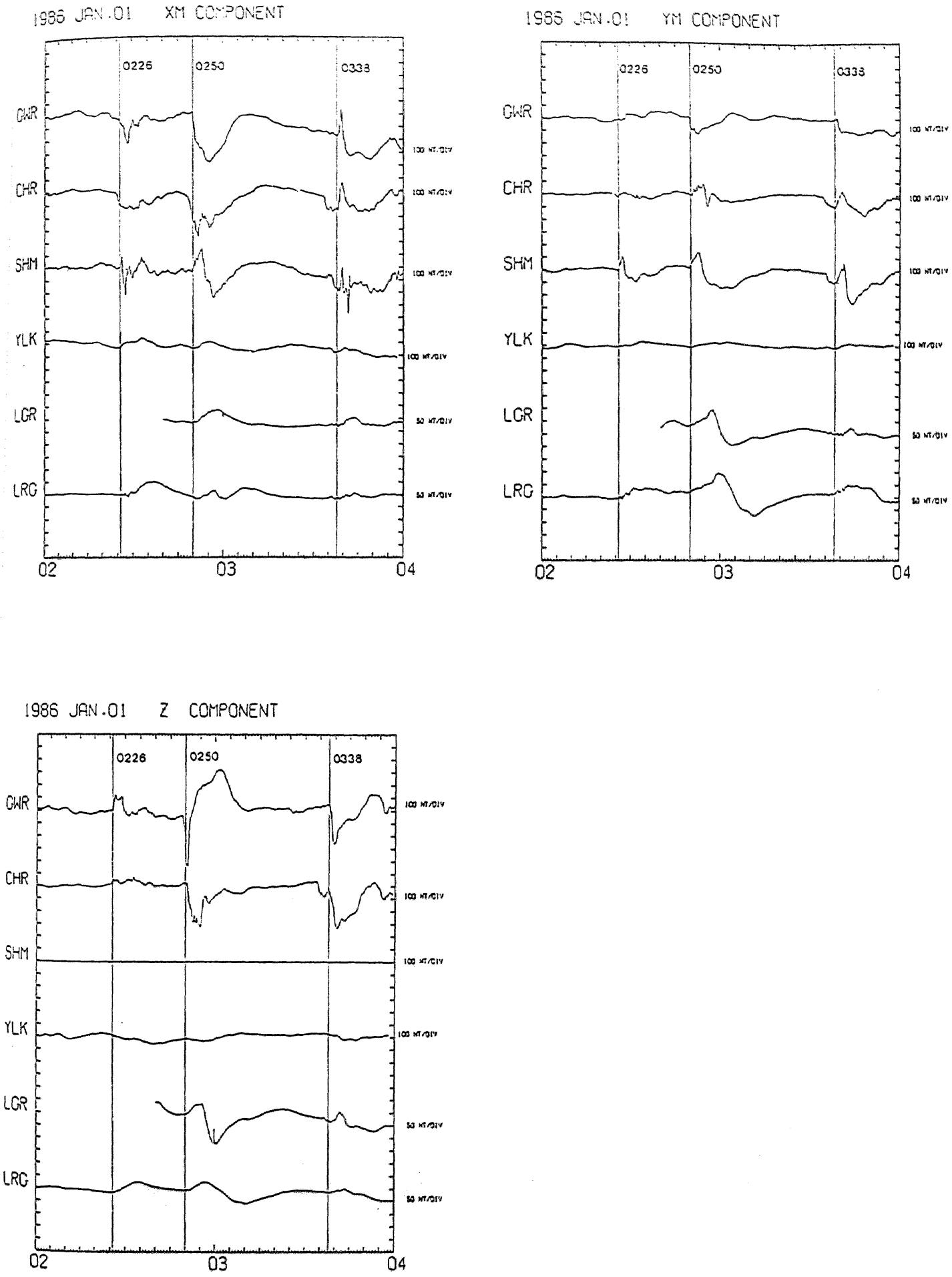

Figure 2.24 Magnetic field variations at auroral zone stations from 0200 to 0400 UT on January 01, 1986.

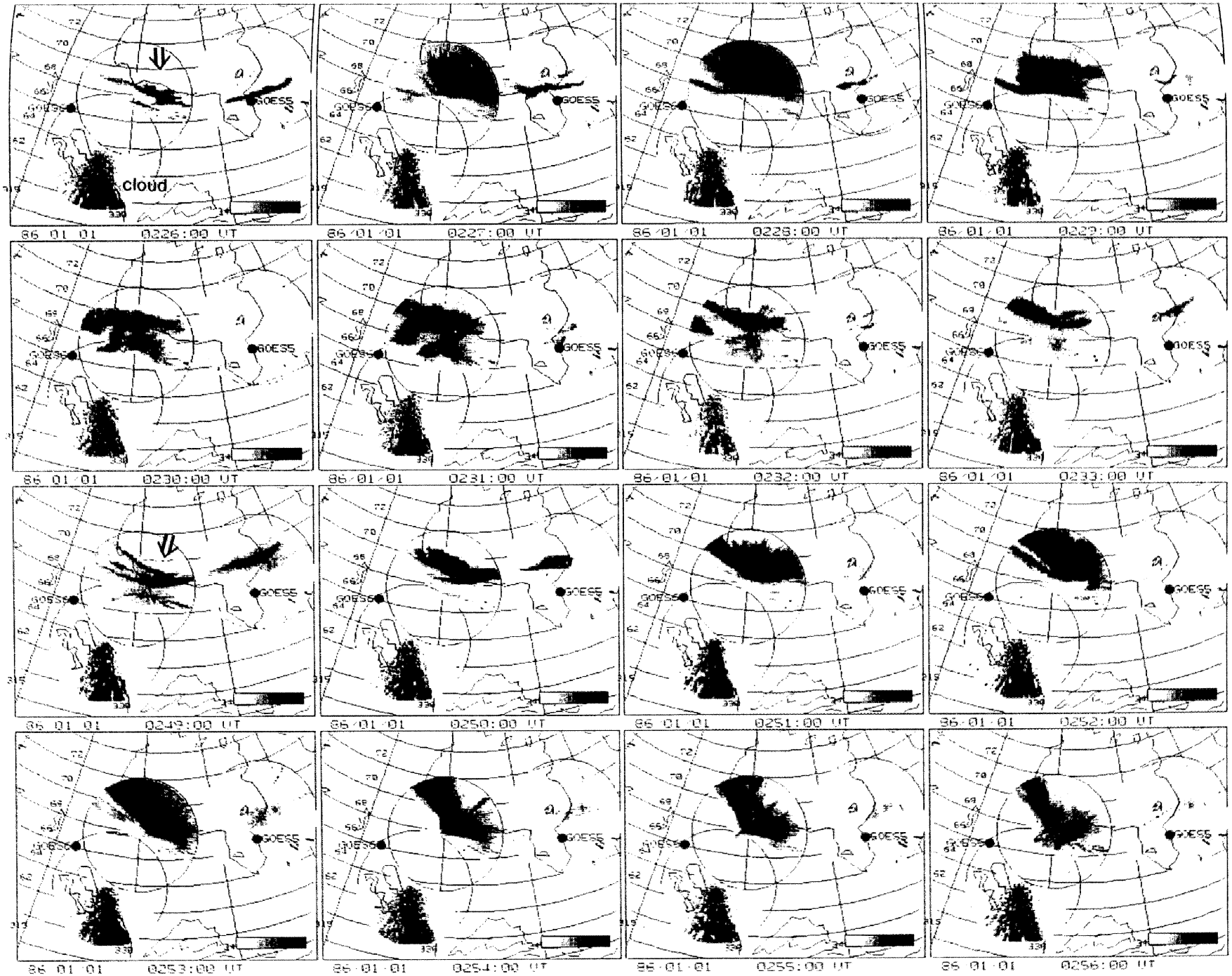

Figure 2.25(a) Spatial-temporal development of auroras during the substorms at 0226 UT and at 0251 UT on January 01, 1986.

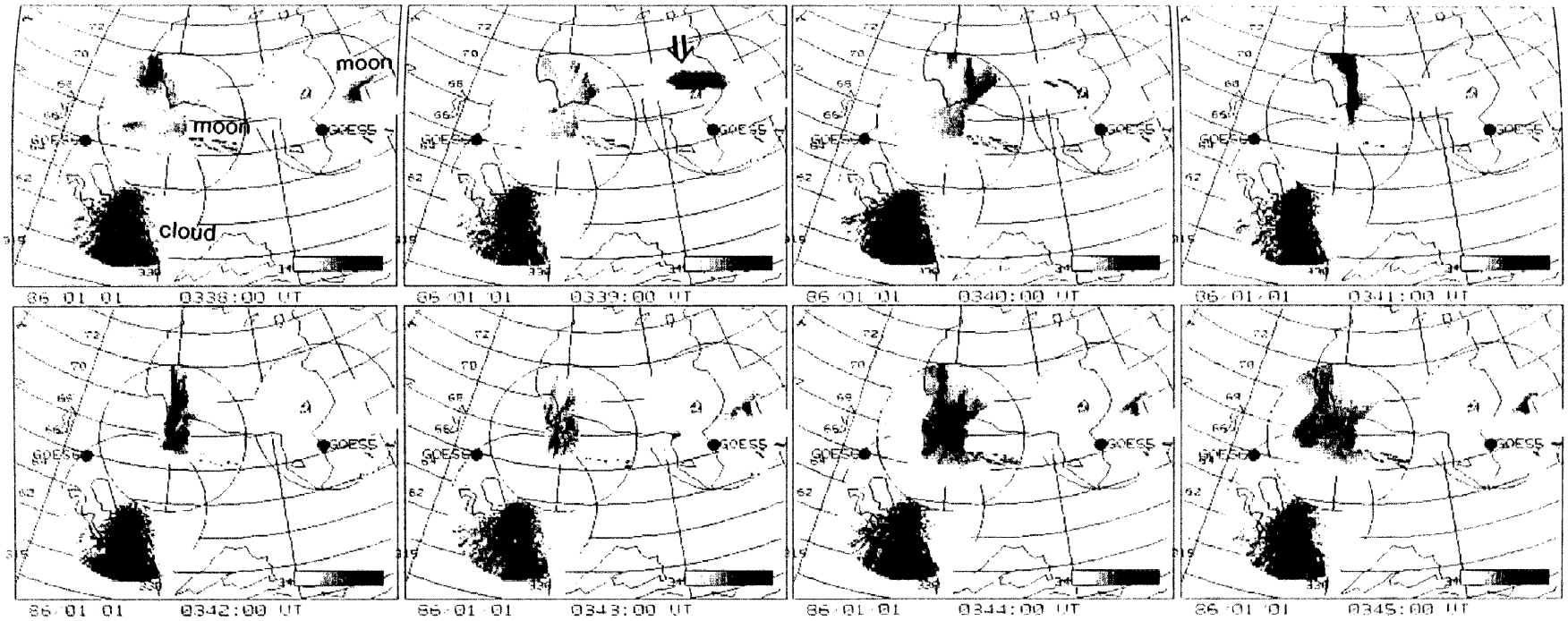

Figure 2.25(b) Spatial-temporal development of auroras during the substorm at 0337 UT, on January 01, 1986.

saturated owing to the insufficient beam intensity of the camera and hence it is difficult to examine the motion of the aurora southward of SHM.

The magnetic field variations of GOES 6 and GOES 5 are shown in Figure 2.26. GOES 5 observed a sharp decrease in the H component at 0225 UT followed by an increase, together with irregular fluctuations in all components. This H decrease is coincident with the initial brightening of the aurora above GWR, at the estimated foot point of GOES 5. GOES 6 observed irregular fluctuations in all components from 0226:30 UT. Three minutes later a sharp decrease in the H component at 0229:30 UT was observed, corresponding to the passage of a surge above SHM, about 10° to 15° east of the estimated foot point of GOES 6. There was a slight irregular fluctuation and no conspicuous net perturbation in the D component around the onset time.

2.3.3.2. Substorm at 0251 UT

The second expansion began at 0249 UT (Figure 2.25(a)), characterized by the brightening of the auroral arc extending from GWR to SHM (see the arrow in the panel of 0249 UT). The eastern part of this brightened arc, near GWR, moved equatorward and then vanished in a few minutes. Corresponding to this auroral activity, irregular fluctuations in all components of GOES 5 began at 0250 UT (Figure 2.26). About 5 minutes later, the western part of the arc above SHM rotated clockwise to form an N-S aligned arc, which traveled westward from 0254 UT to 0257 UT. At the same time GOES 6 observed a decrease in the H component at 0254 UT, together with a slight increase in the V and D components. This change is probably correlated with the passage of the N-S aligned arc about 7° to 10° east of the estimated foot point of GOES 6.

2.3.3.3. Substorm at 0337 UT

The third auroral expansion (in Figure 2.25(b)) occurred above GWR at 0338:25 UT (not shown), characterized by the brightening of an arc (see the arrow in the panel of 0339 UT). Almost simultaneously GOES 5 observed an initiation of irregular fluctuations in all

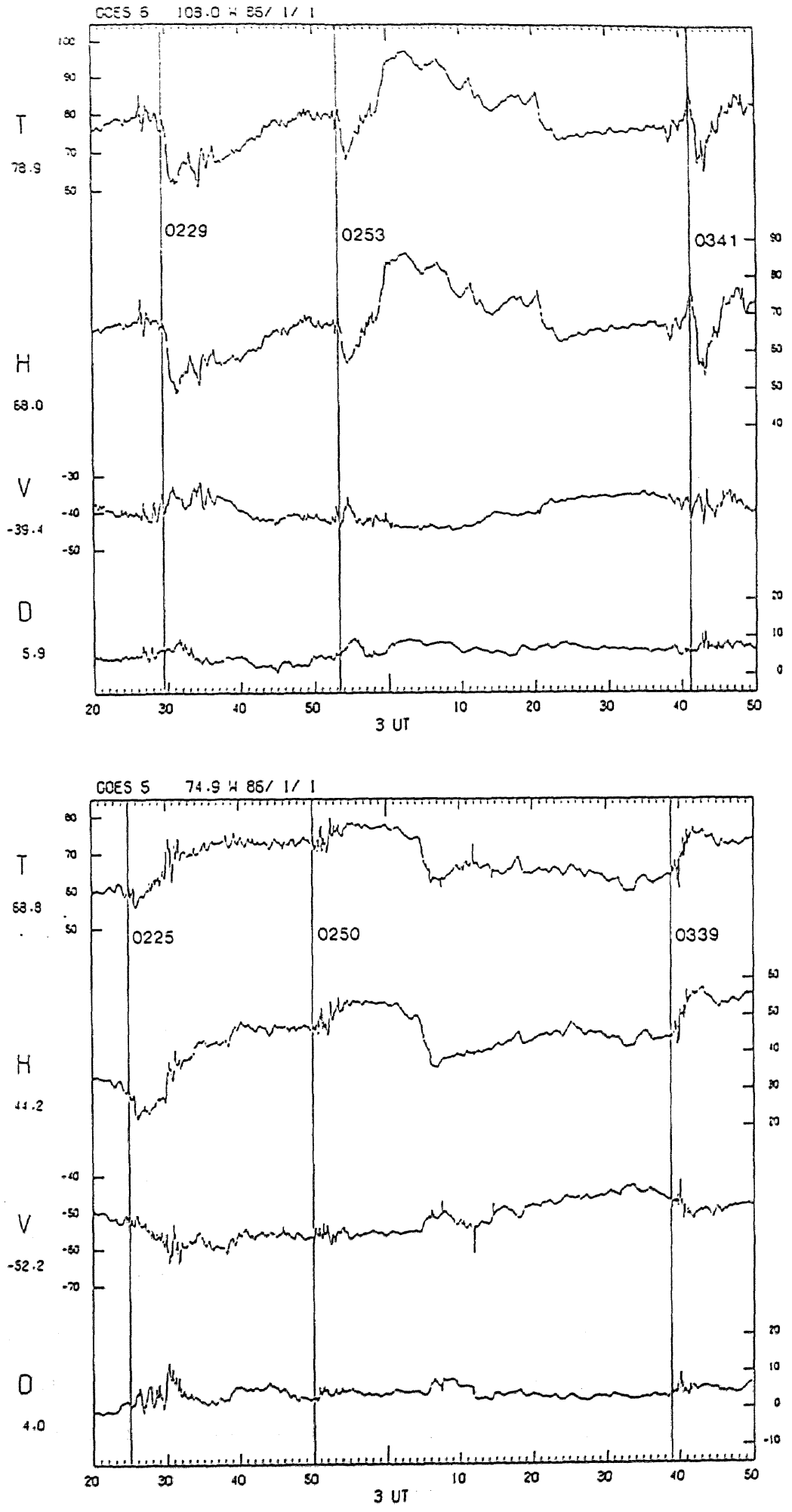

Figure 2.26 Magnetic field variations at GOES 6 and GOES 5 from 0220 UT to 0350 UT on January 01, 1986.

components at 0339 UT (Figure 2.26), together with an increase in the H component. The brightened arc moved westward and formed into an N-S aligned arc above SHM. This moved westward, passing across the field of view of SHM from 0341 UT to 0347 UT. The GOES 6 magnetic field showed an initiation of irregular fluctuations in all components at 0338 UT, accompanied by an increase and subsequent decrease in the H component. The decrease in the H component began at 0341 UT, coincident with the arrival of the N-S aligned arc above SHM, about 12° to 15° east of the estimated foot point of GOES 6.

2.3.4. Jan. 07, 1986

Figure 2.27 shows the AE index on this very disturbed day. Several expansions were observed, among them four expansions at about 0240 UT, 0540 UT, 0640 UT, and 0720 UT (see arrows) were recorded in the observational area. Accurate onset times are determined as 0239 UT, 0541 UT, 0638 UT, and 0716 UT from sub-auroral latitude magnetograms (Figures 2.29 and 2.35).

2.3.4.1. Substorm at 0239 UT

The Kp value was 6–. GWR was located near 2100 MLT and SHM was located near 1930 MLT.

Figure 2.28 shows the sequential pictures of auroral distribution. An expansion probably occurred south of GWR before 0240 UT, although the onset region was out of the field of view of three auroral observatories (GWR, SHM, and LGR). The poleward expansion front was observed in the southern sky of GWR from 0242:15 UT (not shown here). This front (indicated by the arrow of the panel of 0243 UT) moved further poleward toward the north of GWR, simultaneously a westward traveling surge was observed in the eastern field of view of LGR from 0244 UT. The head of the surge reached the zenith of LGR at 0246 UT. This surge traveled northwestward across the field of view of LGR with the speed of about 100 km/min. It also rotated clockwise as viewed parallel to the ambient magnetic field and formed into the straight arc in a few minutes, while other surges appeared east of the previous one around

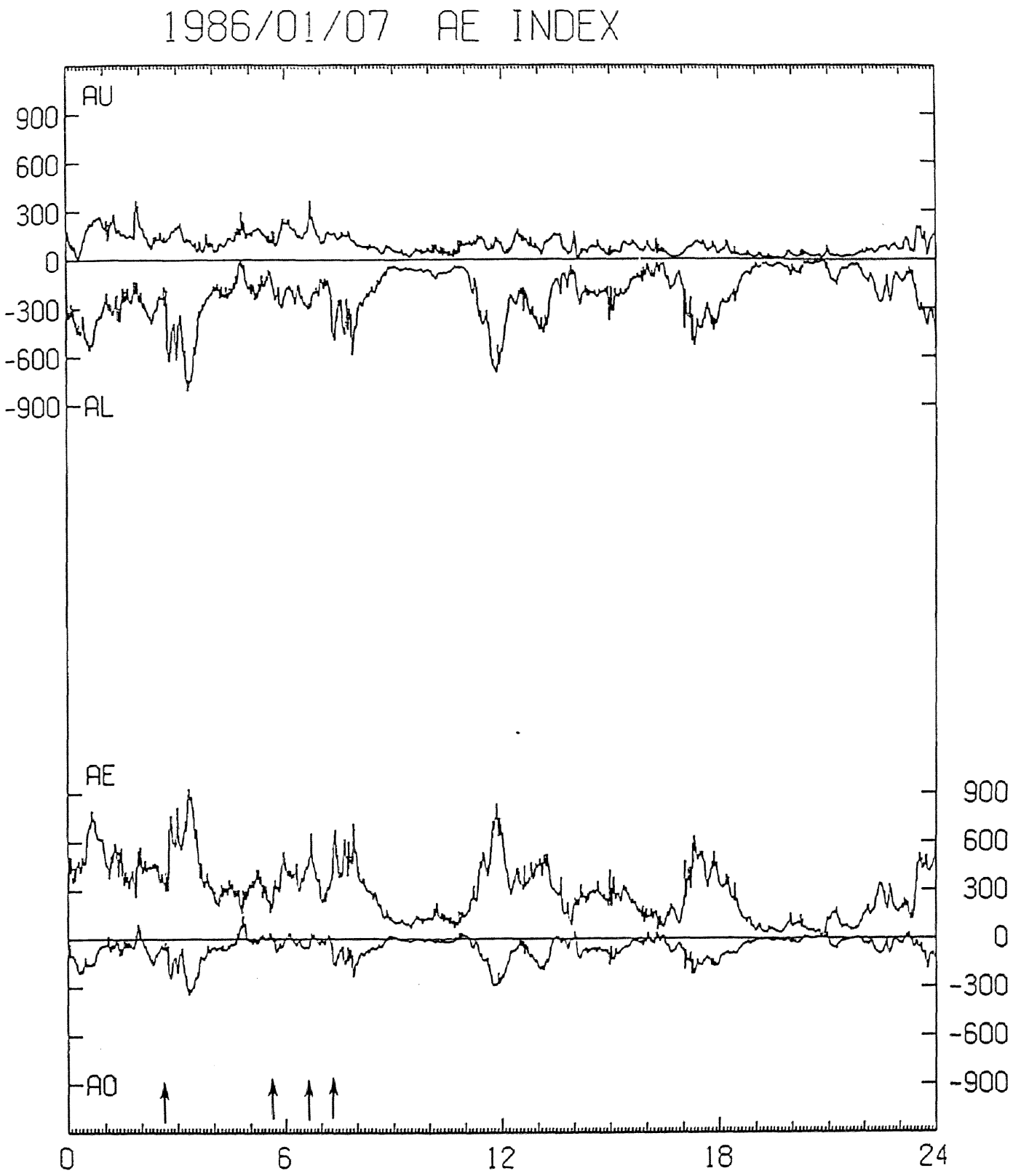

Figure 2.27 AE index on January 07, 1986.

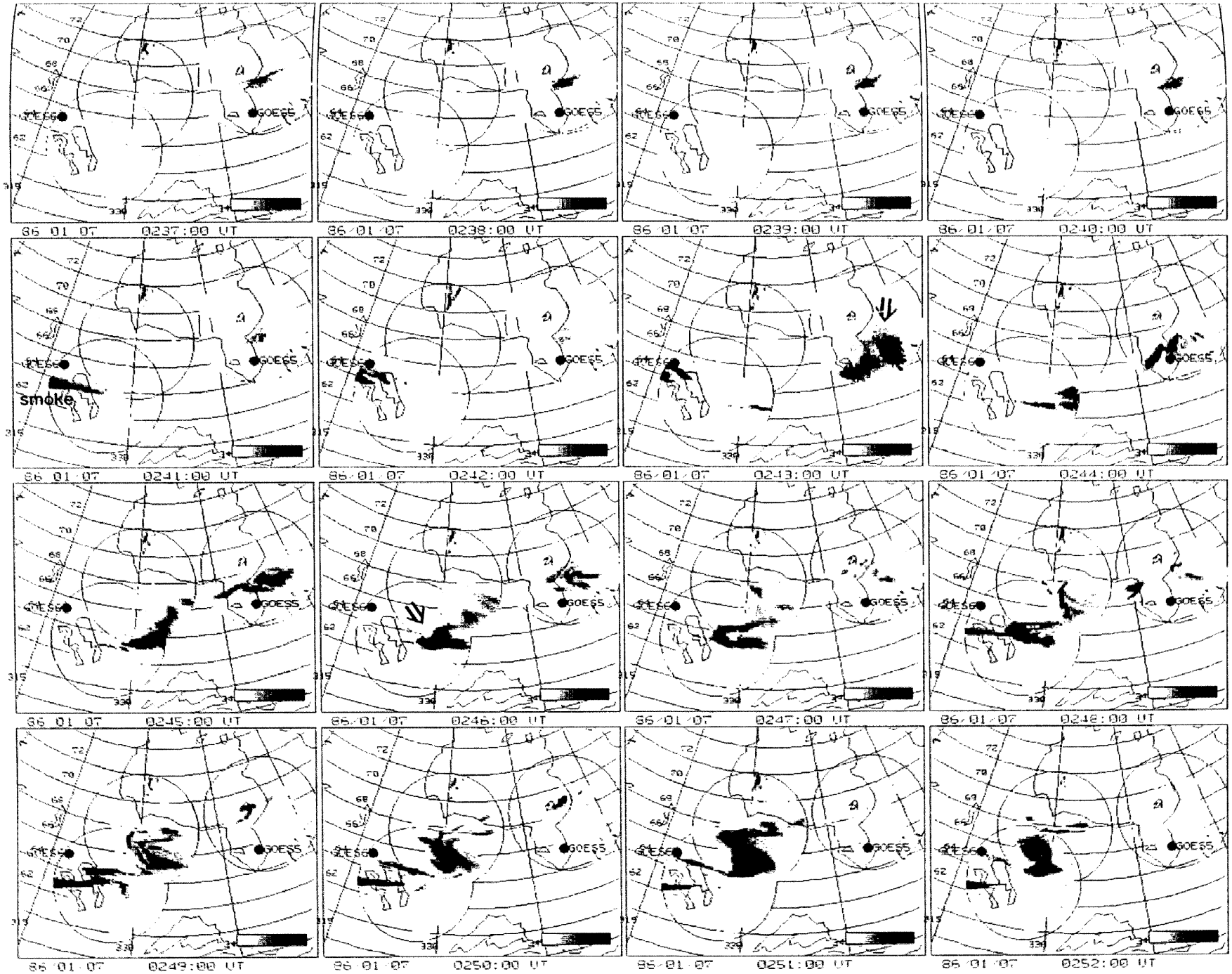

Figure 2.28 Spatial-temporal development of auroras from 0237 UT to 0252 UT on January 07, 1986.

2. Comparison of auroral activity with the magnetic field variations at geosynchronous orbit

0249 UT.

Figure 2.29 shows the magnetic field variations at sub-auroral zone stations. There was a clear onset at 0239 UT, especially in the Ym component of STJ and OTT. From this fact it is almost certain that the auroral expansion broke out at 0239 UT south beyond the field of view of GWR.

Magnetograms at auroral zone stations are shown in Figure 2.30. Unfortunately there was no magnetic data for SHM on this day because of some experiment problem. A sharp decrease in the Xm component was observed at GWR at 0242 UT. The Z component variation at GWR was first positive from about 0240 UT to 0249 UT and then negative, indicating the northward motion of a westward electrojet across the zenith of GWR. About 10 minutes later a sharp decrease in the Xm component at CHR occurred at 0253 UT. The time delay from 0242 UT, the onset time at GWR, can be explained in terms of northward and westward expansion of the electrojet. Also the magnetograms at LGR and LRG showed gradual decreases in the Xm component from about 0230 UT, and then a sharp decrease in the Z component was seen at 0242 UT at LGR.

The magnetic field variations at GOES 6 and GOES 5 are shown in Figure 2.31. GOES 5 observed sharp increases in the H and V components, together with a sharp decrease in the D component at 0238 UT. This perturbation is probably correlated with the initiation of auroral and magnetic activity south of GWR. GOES 6 observed increases in the H and D components and a decrease in the V component at 0246 UT, together with irregular fluctuations in all components.

The position of the auroral surge when GOES 6 observed a sharp increase in the D component was slightly east of LGR, about 10° to 15° east of the estimated conjugate point. Similarly as for the substorm at 0450 UT on Jan. 27, the most probable cause of this discrepancy is the effect of large-scale field aligned currents as will be discussed in Section 2.4. On the other hand, it is difficult to examine the relative location of the GOES 5 foot point to the aurora, because when GOES 5 observed the onset of magnetic field perturbations at 0238

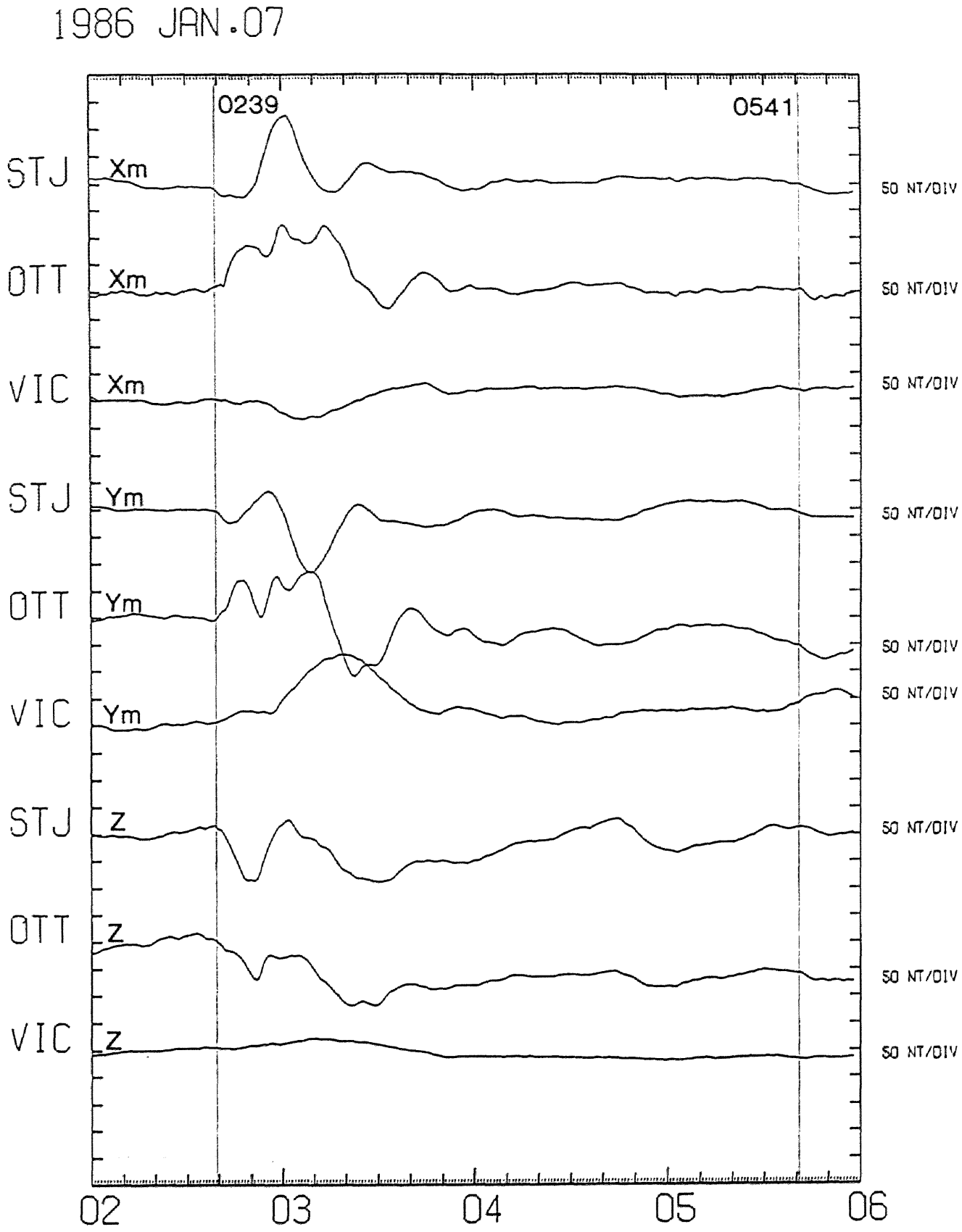

Figure 2.29 Magnetic field variations at sub-auroral zone stations from 0200 UT to 0600 UT on January 07, 1986.

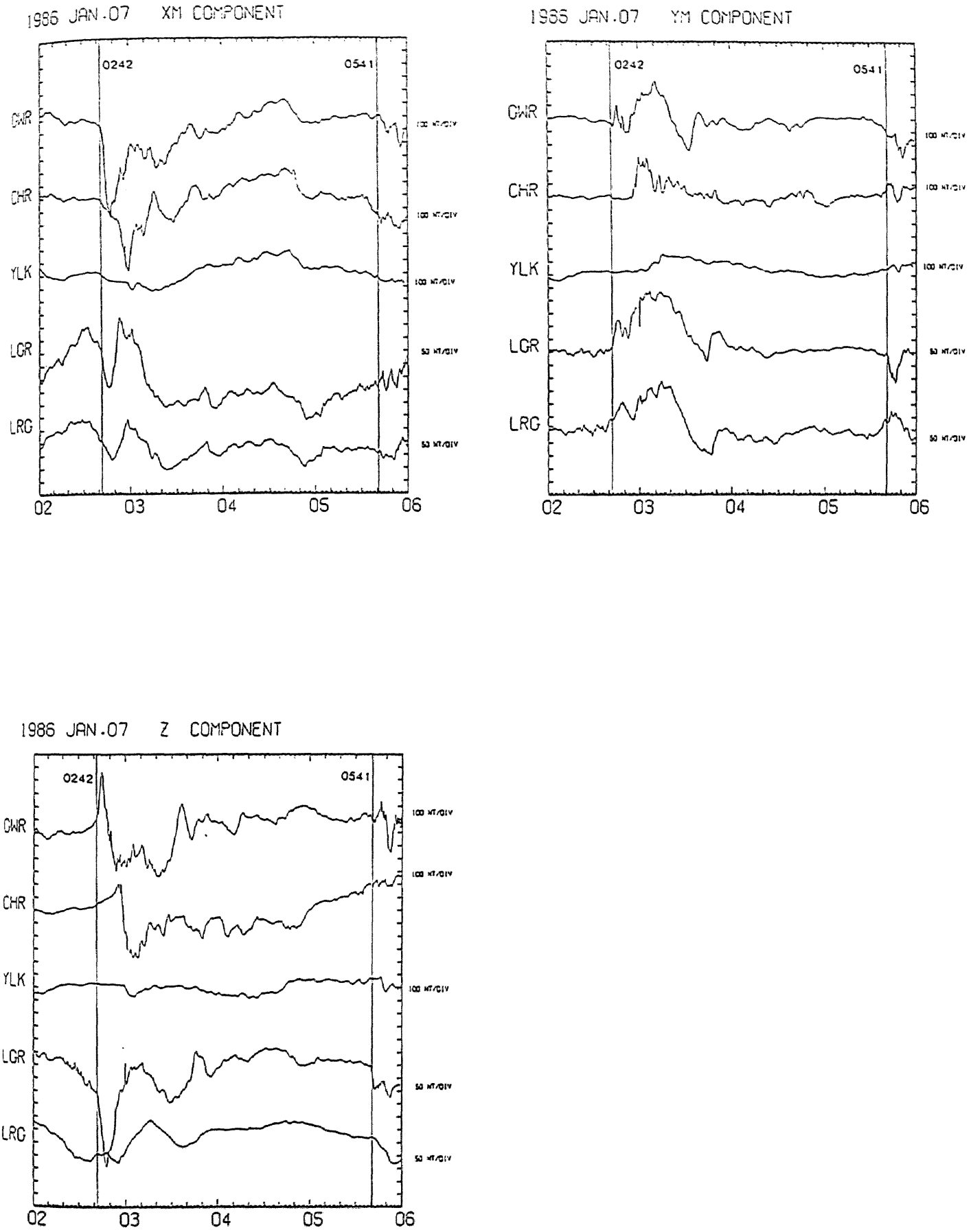

Figure 2.30 Magnetic field variations at auroral zone stations from 0200 UT to 0600 UT on January 07, 1986.

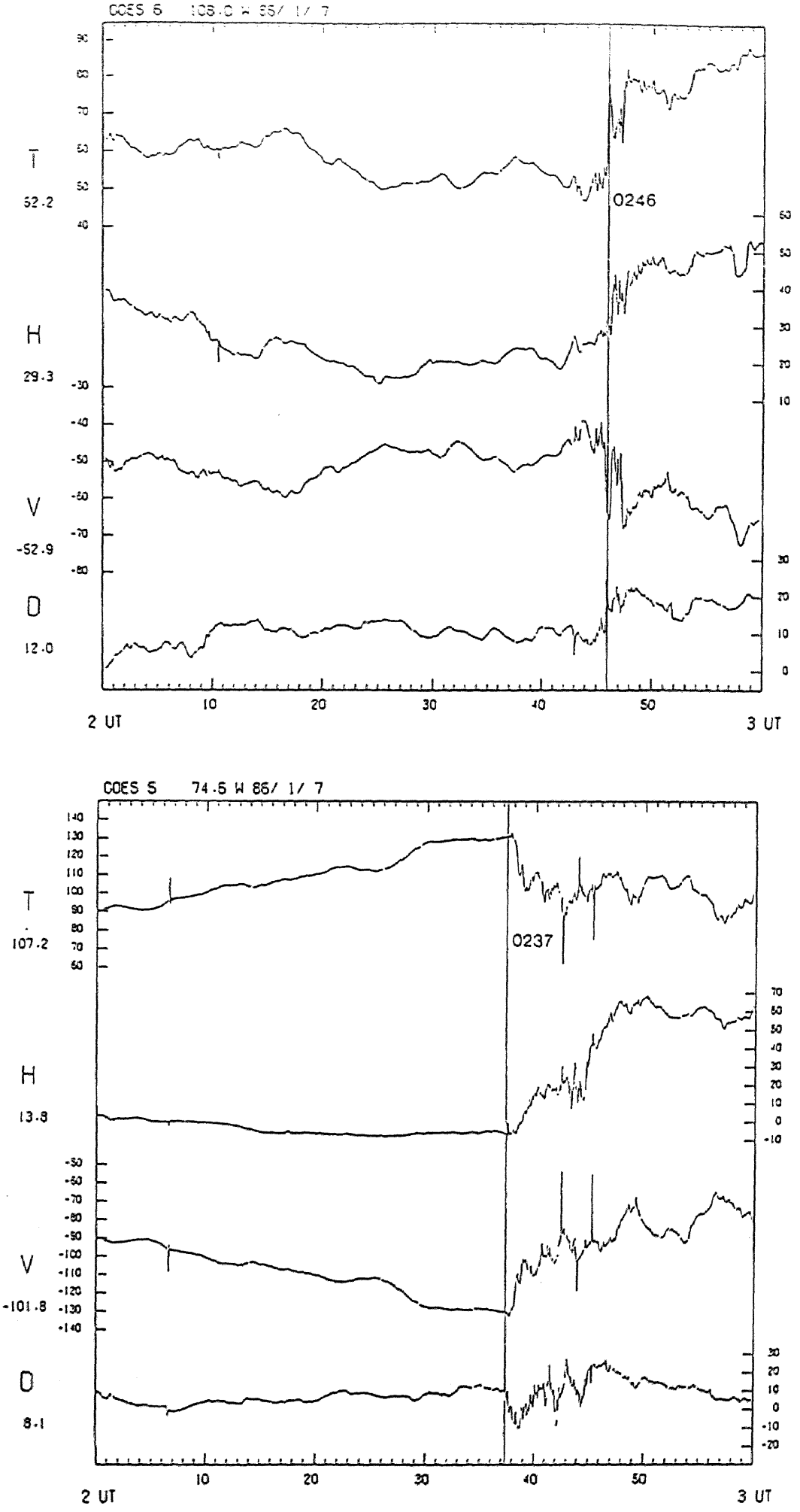

Figure 2.31 Magnetic field variations at GOES 6 and GOES 5 from 0200 UT to 0300 UT on January 07, 1986.

UT, the active aurora was beyond the field of view (about 470 km) of GWR as mentioned already.

2.3.4.2. Substorm at 0541 UT

The Kp value was 6–. GWR was located near 0030 MLT and SHM was located near 2300 MLT.

Figure 2.32 shows the spatial-temporal distribution of auroras. For this day FSM was in operation from 0139 UT, although it was overcast until 0430 UT. Several arcs were extending in the east-west direction. At 0541:30 UT a auroral surge was formed above LGR (indicated by the arrow), as a result of the deformation of the arc. This surge expanded northward and westward, and then a bright arc was left north of the original faint arc. From 0547 UT a small expansion occurred above GWR (see the arrow). Irregular and active auroral forms were deformed into loop structures. Another surge was seen (indicated by the arrow) east of SHM at 0549 UT, which moved westward toward the zenith of SHM.

The magnetic field at sub-auroral zone stations (Figure 2.29), showed an onset at 0541 UT, characterized by the Ym component perturbation, negative at STJ and positive at OTT. At auroral zone stations (Figure 2.30), a sharp decrease in the Z component occurred at 0541 UT at LGR, probably correlated with the formation and northwestward motion of the auroral surge, whereas no conspicuous change was observed in the Xm component of any station. During this event no significant change was seen in the AE index (Figure 2.27), suggesting that this activity was small and localized.

The magnetic field variations at GOES 6 and GOES 5 are shown in Figure 2.33. At 0541:30 UT a sharp increase in the D component at GOES 6 began, together with irregular fluctuations in all components. This perturbation is coincident with the development of the formation of the surge form above LGR, about 9° to 11° east of the estimated foot point of GOES 6. The D component showed a sharp increase again at 0548 UT, coincident with the formation of the surge east of SHM, about 18° to 20° east of the estimated foot point of GOES 6. The GOES 5 magnetic field showed a decrease in the D component at 0548 UT;

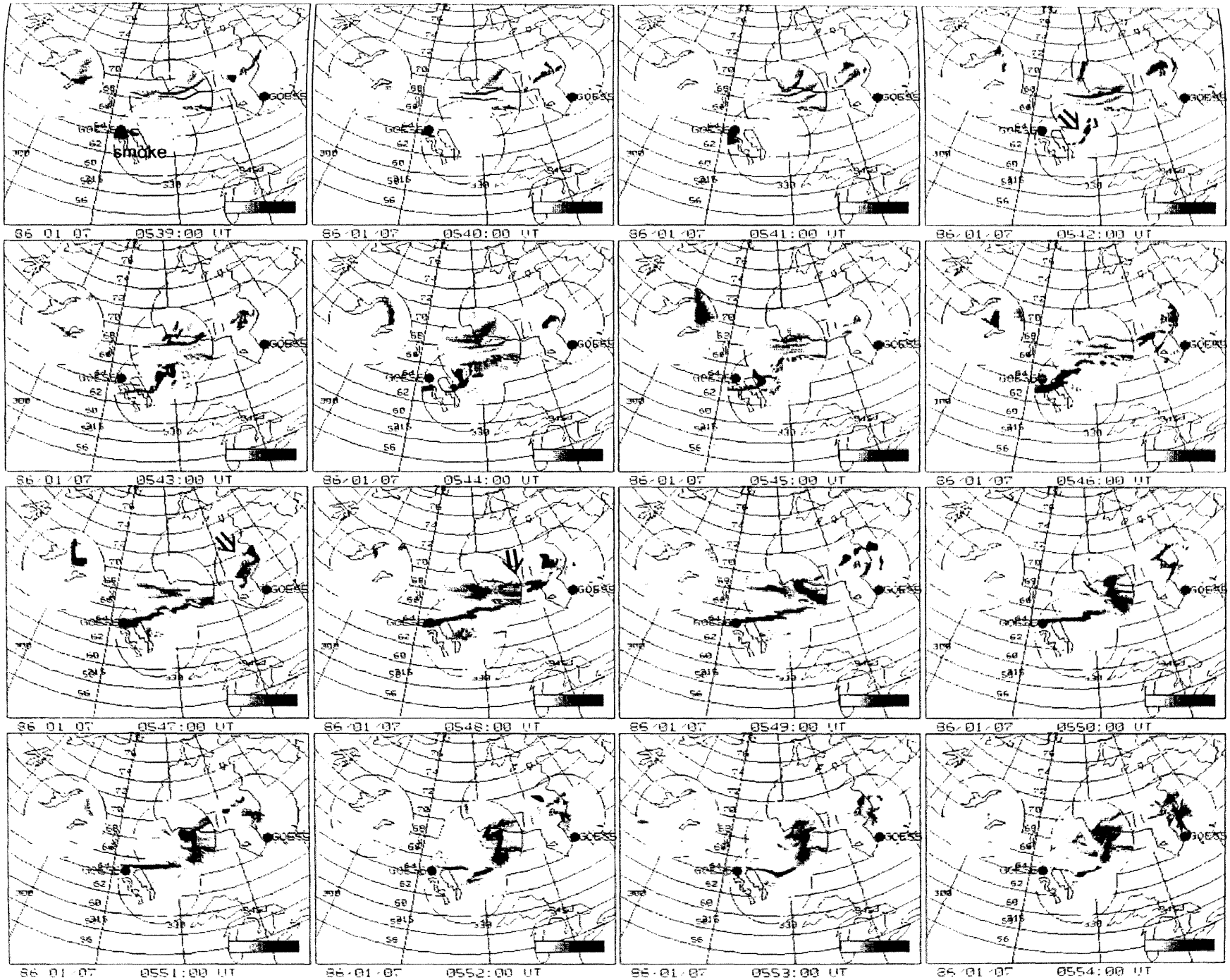

Figure 2.32 Spatial-temporal development of auroras from 0539 UT to 0554 UT on January 07, 1986.

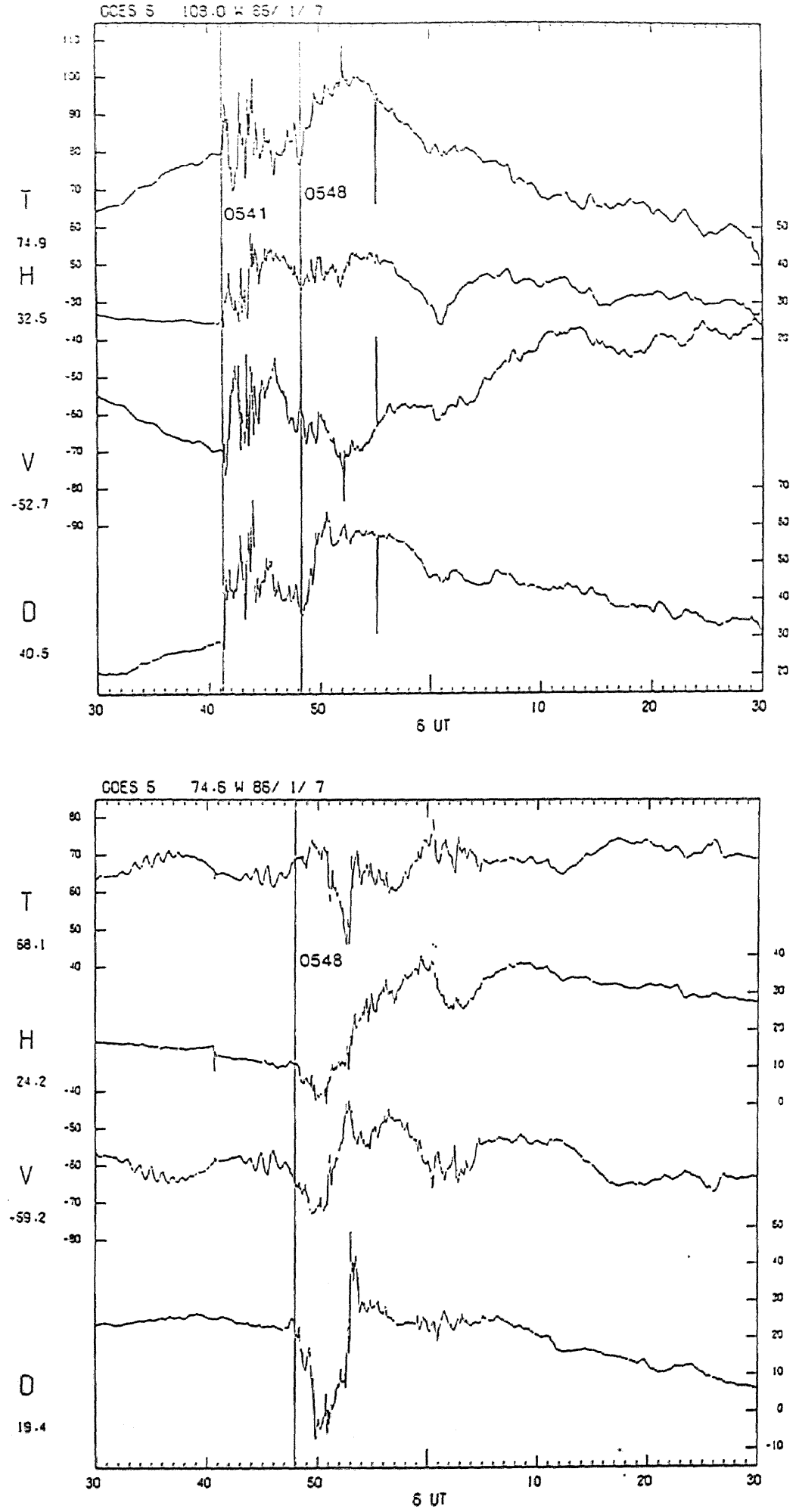

Figure 2.33 Magnetic field variations at GOES 6 and GOES 5 from 0530 UT to 0630 UT on January 07, 1986.

it is probably correlated with the small expansion of the aurora above GWR at that time.

2.3.4.3. Substorm at 0638 UT

The Kp value was 4. GWR was located near 0130 MLT and SHM was located near magnetic local midnight.

Figure 2.34 shows the sequential pictures of auroral distribution. A vortex type aurora was seen from 0636 UT between SHM and LGR, indicated by the arrow. This vortex moved northwestward, rotating clockwise. There was no conspicuous activity in the field of view of GWR at this time.

Magnetic field variations at sub-auroral zone stations are shown in Figure 2.35. The Ym components at STJ and OTT began to decrease at 0638 UT, and simultaneously the Xm components began to increase. The Xm component magnetic field at auroral zone stations LGR and LRG (Figure 2.36) showed gradual increases around 0640 UT, preceded by the gradual decreases. The Z component at LGR began to decrease at 0638 UT. From these data it is difficult to identify the expansion onset because we cannot distinguish the expansion phase from the recovery phase of the preceding event.

Magnetic field variations at GOES 6 and GOES 5 are shown in Figure 2.37. GOES 6 observed a clear onset at 0639 UT, characterized by a sharp increase in the D component. This is probably correlated with the development of the surge near LGR. As in the previous examples, the location of the surge at the onset time of GOES 6 was about 8° to 11° east of the estimated foot point of GOES 6. There was no prominent short-time scale magnetic field variation at GOES 5 at that time.

2.3.4.4. Substorm at 0716 UT

The Kp value was 4 and GWR was located near 0200 MLT, SHM was located near 0030 MLT.

Figure 2.38 shows the spatial-temporal development of auroras. An auroral vortex appeared above SHM at 0705 UT (not shown). This vortex (indicated by the arrow in the

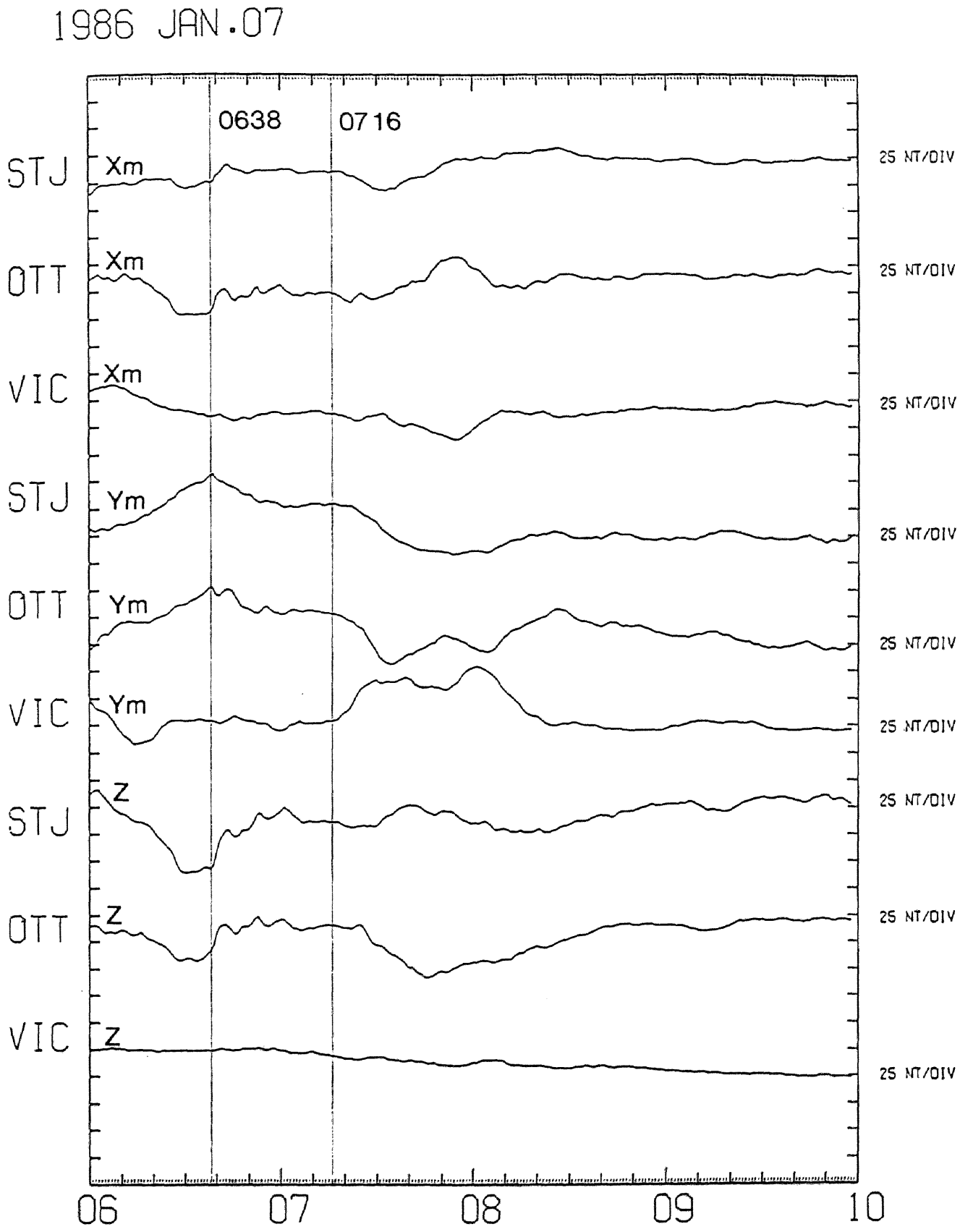

Figure 2.35 Magnetic field variations at sub-auroral zone stations from 0600 UT to 0800 UT on January 07, 1986.

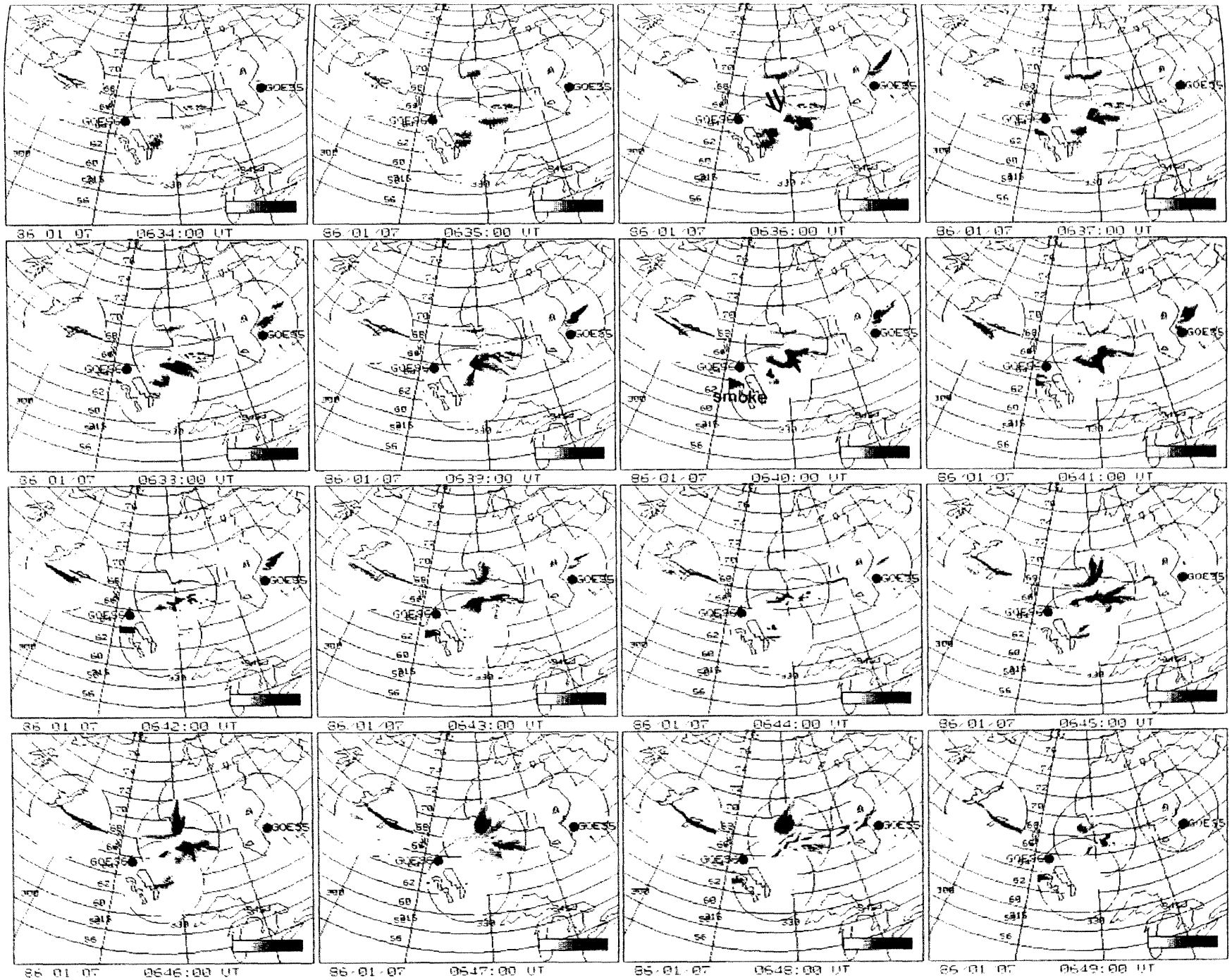

Figure 2.34 Spatial-temporal development of auroras from 0634 UT to 0649 UT on January 07, 1986.

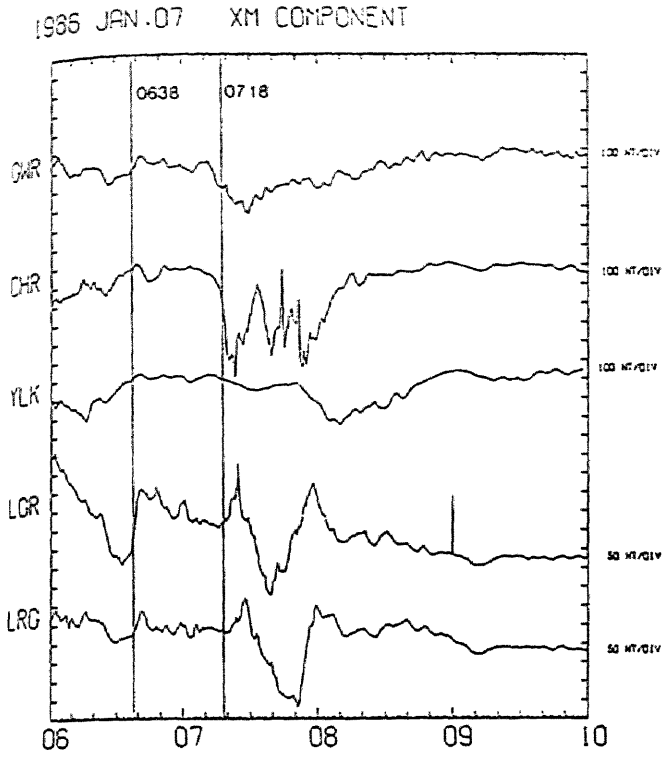

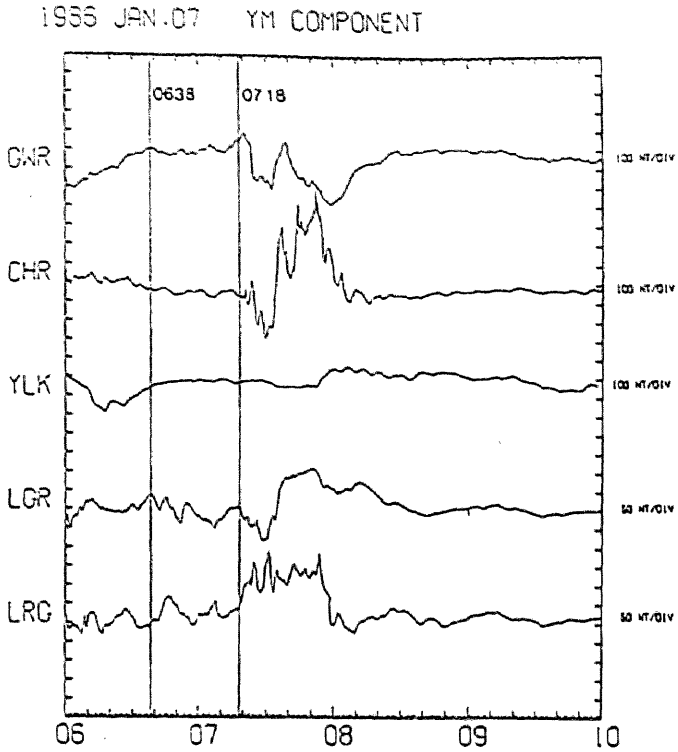

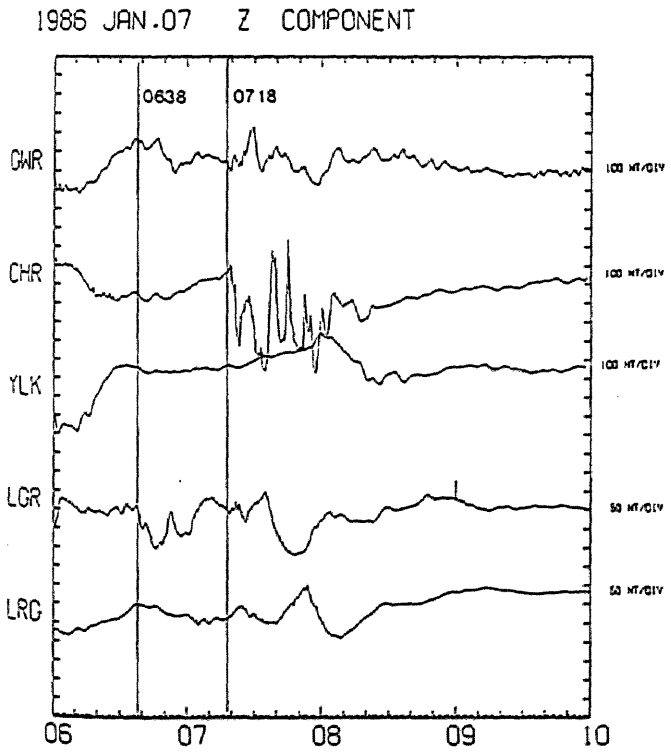

Figure 2.36 Magnetic field variations at auroral zone stations from 0600 UT to 0800 UT on January 07, 1986.

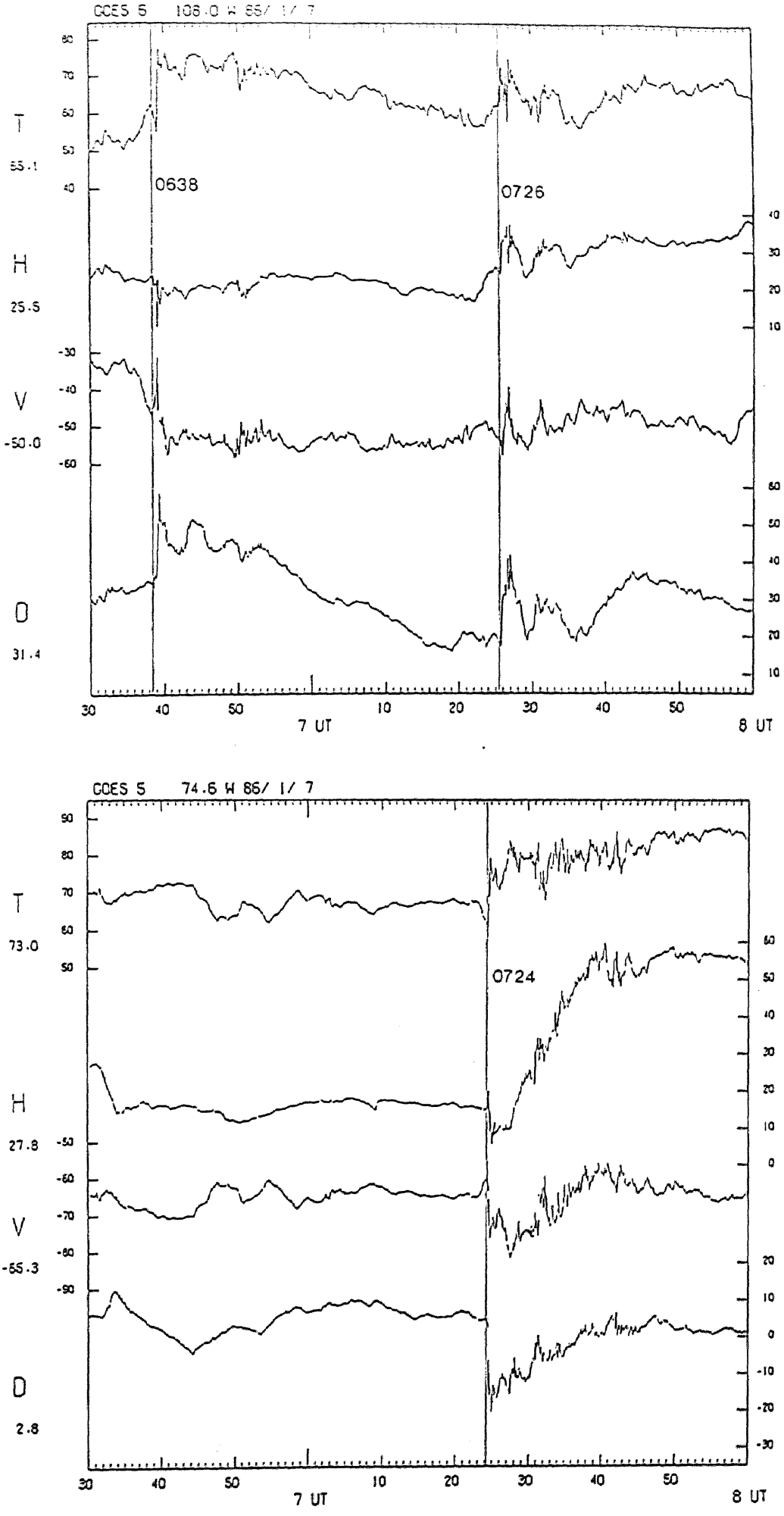

Figure 2.37 Magnetic field variations at GOES 6 and GOES 5 from 0630 UT to 0800 UT on January 07, 1986.

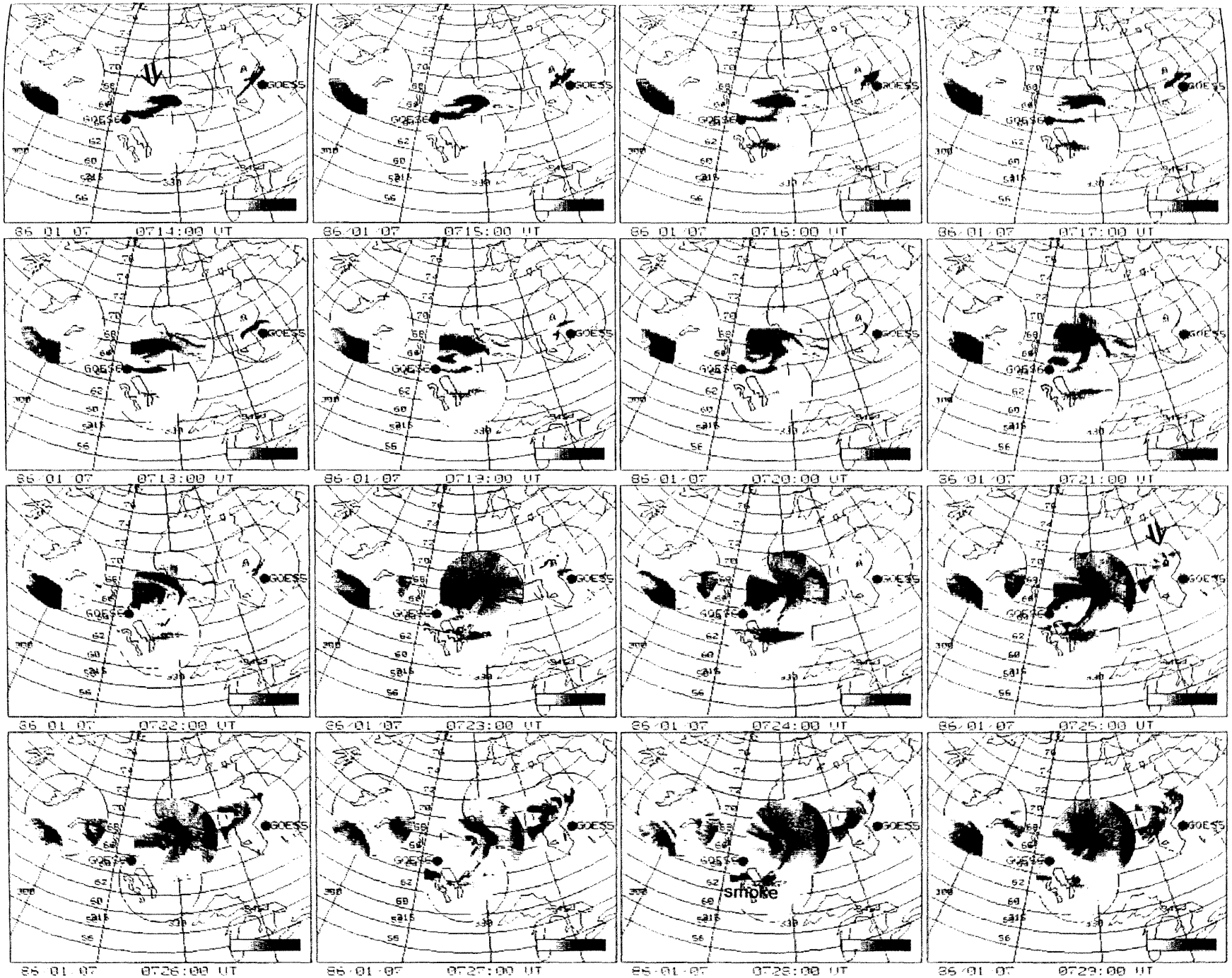

Figure 2.38 Spatial-temporal development of auroras from 0714 UT to 0729 UT on January 07, 1986.

upper left panel) stayed at almost the same position, while rotating clockwise and growing larger until the western part reached the eastern field of view of FSM around 0723 UT with a spatial extent of about 800 km. This aurora was formed into an N-S arc around 0727 UT. Another vortex appeared in the western field of view of GWR at 0725 UT (indicated by the arrow).

At sub-auroral zone stations (Figure 2.35), the Ym components of OTT and VIC began to decrease and increase respectively around 0716 UT, although these changes were rather gradual. At auroral zone stations, a decrease in the Xm component was observed at 0718 UT at CHR as shown in Figure 2.36, although this change was rather gradual, in accordance with the gradual development of the aurora. The Xm components of LGR and LRG showed increases from 0720 UT, followed by decreases a few minutes later, indicating the latitudinal motion of the ionospheric current system.

Magnetic field variations at GOES 6 and GOES 5 are shown in Figure 2.37. GOES 5 observed a very sharp decrease in the D component at 0724 UT. This change is probably associated with the development of auroral activity in the western field of view of GWR at 0725 UT (Figure 2.38). GOES 6 observed a positive perturbation of the D component at 0726 UT, coincident with the formation of the N-S aligned arc south of SHM. The auroral activity during this period was highly complicated and the determination of the part of the auroral form connected to GOES 6 is difficult. However, the magnetic variation at GOES 6 appears to be correlated with the equatorward expansion branch of the large vortex-type aurora, since the estimated foot point of GOES 6 is close to the branch.

2.4. Discussion

2.4.1. General characteristics

So far we have examined the relationship between auroral activity, magnetic field variations on the ground and those at geosynchronous altitudes. The magnetic variations at geosynchronous orbit show various features during auroral substorms such as dipolarization (increase of the H or V component), depression of total magnetic field, D component perturbations, and irregular fluctuations usually in all components. Magnetic field variations at geosynchronous orbit during substorm expansions are often explained in terms of the "current-wedge model" i.e. the collapse of the tail-current, the diversion of these currents along the magnetic field lines into and through the ionosphere, and back again to the magnetosphere along field lines (e.g. Nagai, 1982). In spite of the neglect of return currents from the ionosphere and the Region 2 currents that are actually observed, it is often claimed that this simple current system explains very well the dipolarization and large amplitude perturbation in the D component frequently observed during substorms. The real magnetic variations at geosynchronous altitudes, however, do not always show such typical features. Instead they are quite irregular, especially on a time scale of a few minutes. Short-time magnetic field variations at geosynchronous altitudes probably arise from small-scale irregularities, such as electric current and plasma injection near the satellite. They are highly localized and not always related to the global evolution of substorms. In some events the onset time at geosynchronous orbit is coincident with the onset registered by ground magnetograms, while in other events it is not. This clearly shows the magnetic variations at geosynchronous orbit are caused by a nearby current system with highly localized structure. This is supported also by the fact that GOES 5 and GOES 6, which are separated by about 35° in longitude, show quite different magnetic field variations.

The localized nature of the magnetic field variations at geosynchronous orbit indicates that we could study the field line connection between the ionosphere and the magnetosphere by examining those field-aligned currents at geosynchronous altitudes, correlated with active

auroras. In the previous section a total of 12 events were studied, and a summary is given in Table 2.2. Comparing magnetic field variations at geosynchronous orbit with auroral activity in ionospheric conjugate areas we found that the real magnetic field line deviates from Tsyganenko's model field line in many of these events. In order to see systematic change in the deviation of auroral activity from the estimated foot point of geosynchronous satellites, if any, we classify below these events described in Section 2.3 into three groups with the relative location in the center of, to the west of, and to the east of the onset region. However, it is rather difficult to locate the onset region, because auroral expansions are sometimes complicated, and because of the limited spatial extent of the ground observations the onset region is often outside the observational area. According to the original concept of the auroral substorm by Akasofu (1964), the expansion is characterized by poleward expanding bulges, westward traveling surges, and eastward moving auroral structures. Here we will classify these events according to the relative location of the active aurora to the onset region, if the onset region is within the observational area. Otherwise, we will classify them according to the direction of the auroral expansion at the observational area (poleward, eastward or westward) and the magnetic field variations at sub-auroral latitude stations (the east-west component usually shows positive perturbation to the west of the onset region and negative perturbation to the east of the onset region).

2.4.2. Center of the onset region

In the center of the onset region auroral patterns often show clear poleward and equatorward expansions. In some examples (e.g. at 0252 UT on January 2, at GOES 5) the onset time at the geosynchronous satellite is coincident with that of the auroral expansion. In other examples (e.g. at 0501 UT on January 27, at GOES 6), however, the onset time at the satellite is delayed by several minutes. This result clearly indicates that the magnetic field fluctuations at the GOES satellites are localized and they can be observed only when the localized structure pass near the satellites (Nishitani and Oguti,1988). Furthermore, the

Day	Onset time (UT)	Kp	MLT		GOES Magnetic signature and corresponding auroral activity	
			SHM	GWR	GOES 6	GOES 5
1/27	0448	5+	22	23	+D at 0452 (*dusk*) surge 66°~68°lat. 15°~20°East of FP	-D at 0449 (*dawn*) active arc ~67°lat. -5°~0°East of FP
1/27	0500	5+	22	23	irr. D at 0502 (*center*) expans. bulge ~68°lat.	no conspicuous D (?)
1/27	0249	2+	20	21	irr. D at 0256 (*dusk*) surge ~68°lat. 15°~18°East of FP	+D at 0251 (*dusk*) surge 68°~69°lat. ~0°East of FP +D at 0304 (*dusk*) N-S arc 68°~70°lat. 2°~4°East of FP
1/27	0639	5	00	02	-D at 0640 (*dawn*) no aurora around FP 5°~10°West of FP from ground magne.	no conspicuous D (?)
1/2	0252	4-	20	21	irr. D at 0302 (?) activity ~68°lat. 5°~15°East of FP	+D at 0252 (*center*) expans. bulge ~68°lat.
1/2	0327	4	21	22	+D at 0331 (*dusk*) surge ~67°lat. 10°~15°East of FP	-D at 0328 (*center*) expans. bulge ~67°lat. ~0°East of FP
1/1	0226	3+	19	21	irr. D at 0229 (*dusk*) surge 67°~70°lat. 5°~10°East of FP	irr. D at 0225 (?) active arc 67°~68°lat.
1/1	0251	3+	20	21	+D at 0253 (*dusk*) surge 68°~71°lat. 7°~10°East of FP	irr. D at 0250 (?) active arc ~69°lat. ~0°East of FP
1/1	0337	4-	21	22	irr. D at 0341 (*dusk*) N-S arc 68°~72°lat. 12°~15°East of FP	irr. D at 0339 (?) active arc 69°~70°lat. ~0°East of FP
1/7	0239	6-	20	21	+D at 0246 (*dusk*) surge 63°~65°lat. 9°~15°East of FP	-D at 0237 (*center*) no aurora yet
1/7	0541	6-	23	01	+D at 0541 (*dusk*) surge 63°~65°lat. 9°~11°East of FP +D at 0548 (*dusk*) surge 66°~70°lat. 18°~20°East of FP	-D at 0543 (*dawn*) ring arc 68°~70°lat. ~0°East of FP
1/7	0638	4	00	02	+D at 0638 (*dusk*) surge 64°~66°lat. 8°~11°East of FP	no conspicuous D (?)
1/7	0716	4	01	02	+D at 0726 (?) vortex 63°~70°lat. -13°~13°East of FP	-D at 0724 (*dawn*) vortex 68°~70°lat. -5°~0°East of FP

* FP: foot point of the satellite estimated by using the Tsyganenko's 1987 model (truncated version)
* (*dusk*), (*dawn*), (*center*), and (?) : relative location of the observation sites to the onset region.

Table 2.2 Summary of the events.

duration of the magnetic fluctuation observed at geosynchronous satellites is comparable to that of the auroral activity observed on the ground. This duration time is much smaller than that of the magnetic field variations on the ground, which represent the spatially integrated effects of field-aligned and ionospheric currents. This fact supports the idea that the magnetic fluctuations and currents are highly correlated with the small-scale auroral structures, which probably represents localized field-aligned currents flowing into or out of the ionosphere.

2.4.3. West of the onset region

Auroral dynamics to the west of the onset region are characterized by the westward motion of auroral vortices, called westward traveling surges (or auroral surges). Since the westward traveling surges are associated with strong upward field-aligned currents (e.g. Opgenoorth et al., 1983), it is reasonable to expect associated magnetic field perturbations in the azimuthal (or radial) component at the geosynchronous satellite when the aurora and the satellite are located close to a common field line.

The D component variation is probably caused by small-scale field-aligned currents near the geosynchronous satellites. This idea is supported by Fairfield and Zanetti (1989), who found similar magnetic variations in the azimuthal component between GOES 6 and AMPTE/CCE satellites when these two satellites were approximately located along the same field line. Their result supports the examination of the connection of magnetic field lines between the ionosphere and the geosynchronous altitude, by observing active auroral forms (e.g. bulges and surges) and related magnetic field variations at geosynchronous orbit.

Among the 12 events described in the previous section, GOES 6 observed positive D perturbations in 7 events and GOES 5 in 1 event when the satellites were located to the west of the onset region. Figure 2.39(a) shows the longitudinal deviation of the surges relative to the estimated foot point of GOES 6 when the satellite observed positive D perturbations. Magnetic local time ranges from ~ 1930 MLT to ~ 0030 MLT. The location of the surge when

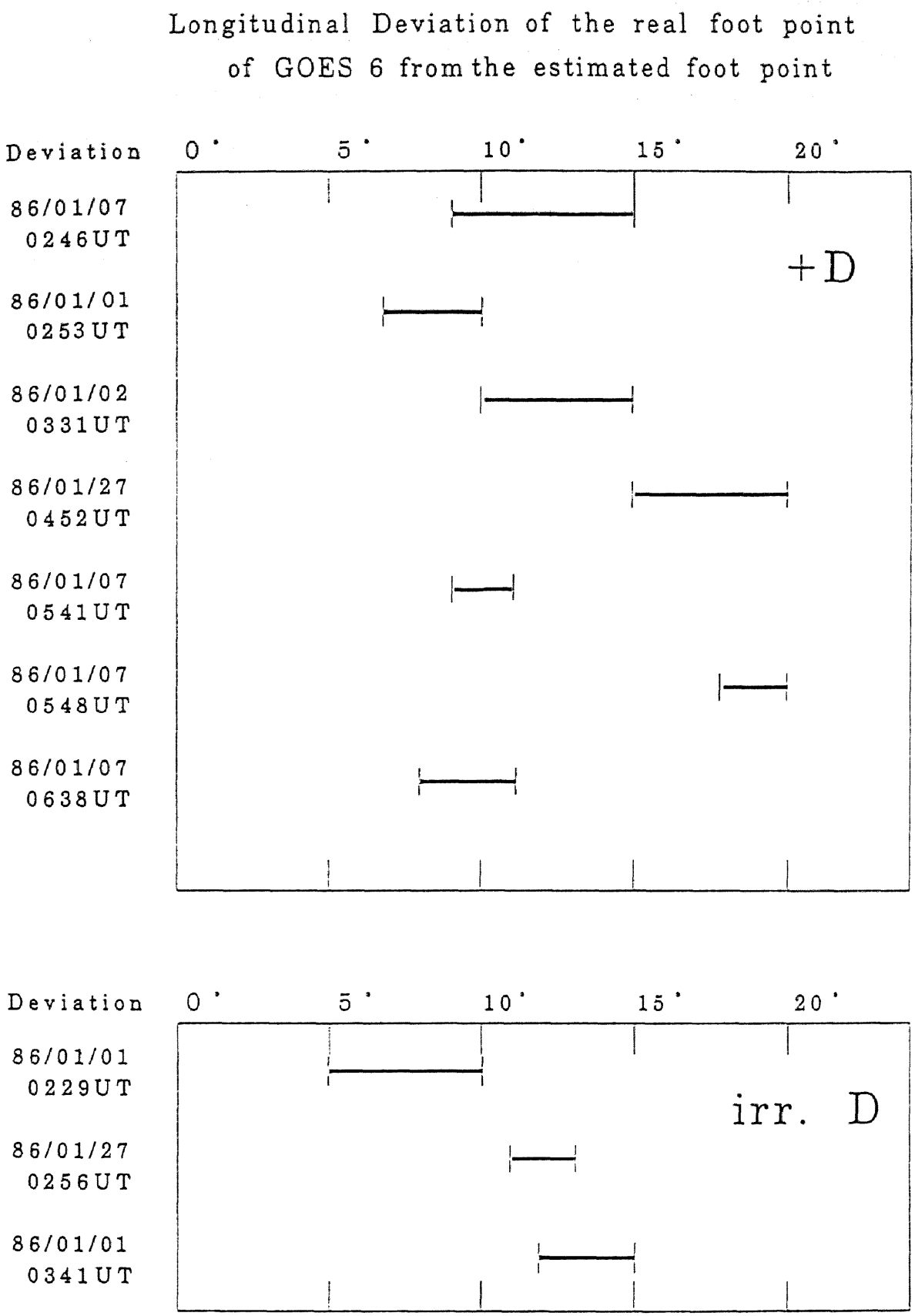

Figure 2.39 The longitudinal location of auroral surges relative to the estimated foot point of GOES 6 when the satellite observed (a) sharp positive D perturbations and (b) irregular D perturbations. The location of the surge when GOES 6 satellite observed these D perturbations is about 10° to 15° east of the estimated foot point of the satellite.

GOES 6 satellite observed a sharp positive D perturbation is about 10° to 15° east of the estimated foot point of the satellite. Therefore the field line connecting the auroral structure and the satellite must be deflected as illustrated in Figure 2.40. The relative location of the surge seems to be independent of the magnetic local time of the surges as will be discussed in detail later in this section.

The estimated foot point of GOES 6 is located near the western border of the field of view of SHM and LGR in the figures used in this study (i.e. Figure 2.5). Therefore one could ask if any other surge might be present beyond the field of view of SHM and LGR. However, we have examined the original all-sky TV images of aurora and confirmed that for all events no surge was observed within the all-sky field of view of SHM and LGR, about 1000 km in radius. Moreover, as shown in the example of Jan 27, 0452 UT, ground magnetograms and the global image taken by the DMSP satellite indicate that the surge was localized and located not near but about 15° east of the estimated foot point of the satellite. Furthermore, as shown in Figure 2.39 the surge was almost always located about 10° to 15° east of the estimated foot point. Hence it is reasonable to conclude that the real magnetic field line systematically deviates from Tsyganenko's model field line, giving the real foot point 10° to 15° east of the ionospheric conjugate point of the GOES 6 satellite estimated from Tsyganenko's model.

The most probable cause of this field line distortion is the effect of large-scale Region 1 and Region 2 field-aligned currents, because Tsyganenko's magnetic field model (1987) used in this study does not include the effect of field-aligned currents in a consistent way. As already mentioned in the general introduction, it is almost certain that the source region of the Region 1 (R1) current system is somewhere in the tail plasma sheet, and that of the Region 2 (R2) current system is in the near-earth plasma sheet and ring current region. Therefore it is reasonable to consider that the GOES 6 satellite is usually located between the two current systems R1 and R2, as illustrated in Figure 2.41.

Tsyganenko's magnetic field model (1987) used in this study includes the effect of three

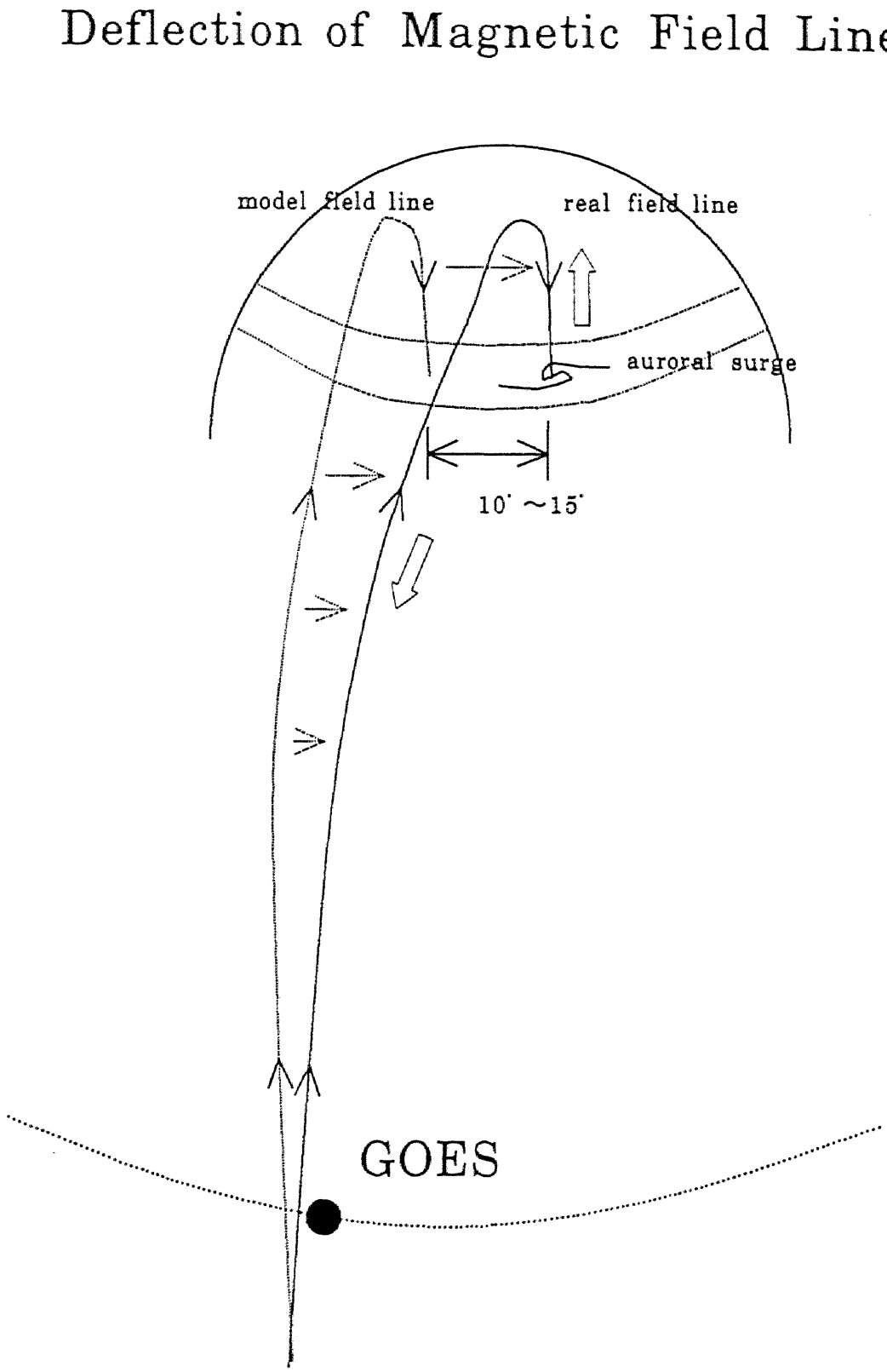

Figure 2.40 Schematic view of the distortion of the magnetic field connecting auroral surges and geosynchronous satellites from the model field line.

Region 1 and Region 2 Currents as the Cause of Field line Deflection

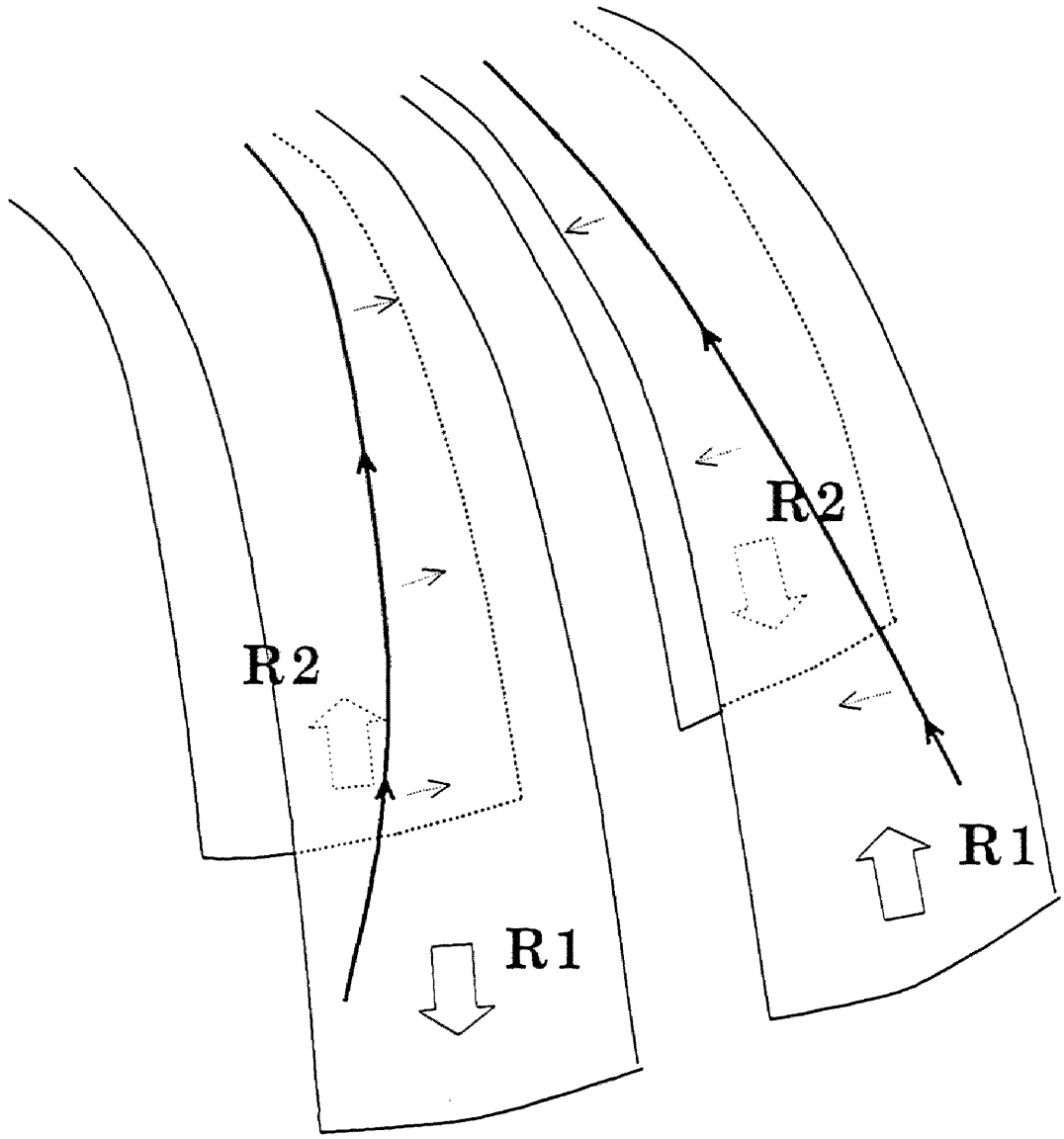

Figure 2.41 Schematic view of the Region 1 and Region 2 field-aligned currents as the cause of the distortion of the magnetic field line threading the geosynchronous satellite.

kinds of current systems: ring currents, magnetotail currents, and magnetopause currents. He claims that the model implicitly includes the effect of field-aligned currents in the magnetopause current term. However, the mathematical expression of the model cannot describe the localized currents such as field-aligned currents as will be discussed in detail in Chapter 3. Hence in order to study the magnetic field connection between the ionospheric and the magnetospheric regions, the existing magnetospheric magnetic field model (e.g. Tsyganenko, 1987) must be corrected for the effect of these large-scale field-aligned currents. The detailed estimation of this correction will be presented in Chapter 4.

The longitude of the surge relative to the estimated foot point of the GOES 6 satellite (in Figure 2.39(a)), when the satellite observed a sharp D perturbation, seems to be independent of the magnetic local time of the auroral surges as pointed out earlier. We do not know the exact distribution of Region 1 and Region 2 field-aligned currents, especially their changes through the course of magnetospheric substorms. However, we can expect that if the satellite is sandwiched between the upward Region 1 and the downward Region 2 field-aligned currents in the dusk sector, and the longitudinal width of these sheet-like field-aligned currents exceed a certain value, the foot point of the satellite will deviate eastward, with the certain magnitude of deviation independent of the magnetic local time. A detailed discussion of introducing field-aligned currents into Tsyganenko's model will be given in Chapter 4.

In 3 examples GOES 6 observed only irregular fluctuations with no net D perturbations. In addition, for these events, the surges were located 10° to 15° east of the estimated foot point of GOES 6 as shown in Figure 2.39(b). This fact suggests that, for these events as well, GOES 6 observed an irregular field-aligned current structure related to auroral surges.

There was only one event (Jan. 27, 0251 UT) in which GOES 5 observed a positive D magnetic field perturbation. The location of the surge when the positive D perturbation occurred at GOES 5 was near the estimated foot point of GOES 5, indicating that the real foot point of GOES 5 was near the foot point estimated by using Tsyganenko's model, in contrast to the GOES 6 case. GOES 5 was located at $\sim$ 2130 MLT during this event, and in

the same local time range (e.g. Jan. 27, 0448 UT) the real foot point of GOES 6 deviated from the estimated foot point. Therefore the difference in the deviation of the foot point of the satellite between GOES 5 and GOES 6 is not due to the difference in MLT. This is probably because the magnetic latitude of GOES 5 (11.3°) was higher than that of GOES 6 (9.0°). The auroral activity discussed here is involved within the whole latitudinal extent of the auroral oval. This may suggest that the localized field-aligned currents connected with the auroral activity tend to be located somewhere between large-scale Region 1 and Region 2 currents. If this is the case, GOES 6 probably observes nearby small-scale field-aligned currents usually at a lower latitude than GOES 5. As a result, it is probable that GOES 6 was located where the magnetic effect of both the Region 1 and the Region 2 currents are significant, while GOES 5 tended to be located closer to the Region 1 current, with smaller deflection of magnetic field lines by these field-aligned currents.

From one example of the positive D perturbation at 0231 UT, Jan. 02 observed by GOES 6, it is noted that the current system connected to the auroral surge has a localized structure not only in azimuthal but also in latitudinal extent. In this example the ground onset time is 0327 UT, while GOES 6 did not observe perturbations until 0331 UT when the auroral vortex moved southward. This example is good evidence for the radially localized nature of the current system connected to the auroral surge. If we assume the size of the surge on the ionosphere to be 200 x 200 km and project it onto the geomagnetic equatorial plane, taking into account the magnetic flux conservation, the spatial size of the field-aligned current associated with the surge comes to about 1 R_E (in the radial direction) x 0.5 R_E (in the azimuthal direction). We may expect that small-scale field-aligned currents at geosynchronous orbit which are associated with auroral surges are localized to this order.

The localized nature of these small-scale currents could provide a way to estimate the conjugate point of the geosynchronous satellite in the latitudinal as well as the meridional direction. Auroral surges, when GOES 6 observed sharp positive D perturbations, were located at various latitudes from 63° to about 70° as shown in Table 2.2. According to

Tsyganenko's 1987 model the latitude of the satellite foot point is expected to depend on the Kp index. However, in fact the latitude is affected more significantly by the inclination angle of the GOES 6 magnetic field vector (Figure 2.42) which probably indicates the local ring or magnetotail current intensity near the satellite, and the Dst index which indicates the effect of global ring current intensity (Figure 2.43). The Kp (Figure 2.44) and the AE (Figure 2.45) indices are of lesser importance. This indicates that the latitude of the real foot point of the GOES satellite is highly correlated with the intensity of the ring current or the magnetotail current (Kaufmann, 1987); the latitude of the real foot point decreases with increasing magnetotail current. It is difficult to say which of the global or local ring / magnetotail currents affect the latitudinal location of the satellite foot point most significantly, because of the limited number of examples used in this study.

2.4.4. East of the onset region

The auroral dynamics to the east of the onset region are rather complicated. Active forms such as bulges and surges are not found. The major prominent features of auroras after the expansion onset are eastward propagating auroral branches and eastward extending discrete arcs.

The sharp negative D perturbations observed at GOES 5 in the 4 examples (at 0329 UT on Jan. 02, at 0549 UT and 0725 UT on Jan. 07, and at 0449 UT on Jan. 27) are always accompanied by the eastward extension of arcs. This clearly indicates that small-scale magnetic field variations at the GOES 5 satellite are caused by small-scale field-aligned currents related to these eastward extending arcs, i.e. the real foot point of GOES 5 is near the estimated foot point. On the other hand, there was only one example (at 0641 UT, on Jan. 27) where GOES 6 observed sharp negative D perturbations. At the onset of this expansion, there was no conspicuous auroral activity near the estimated foot point of GOES 6. Instead a localized magnetic field perturbation was observed at LRG about 10° west of the estimated GOES 6 foot point, suggesting that the real foot point of GOES 6 was about

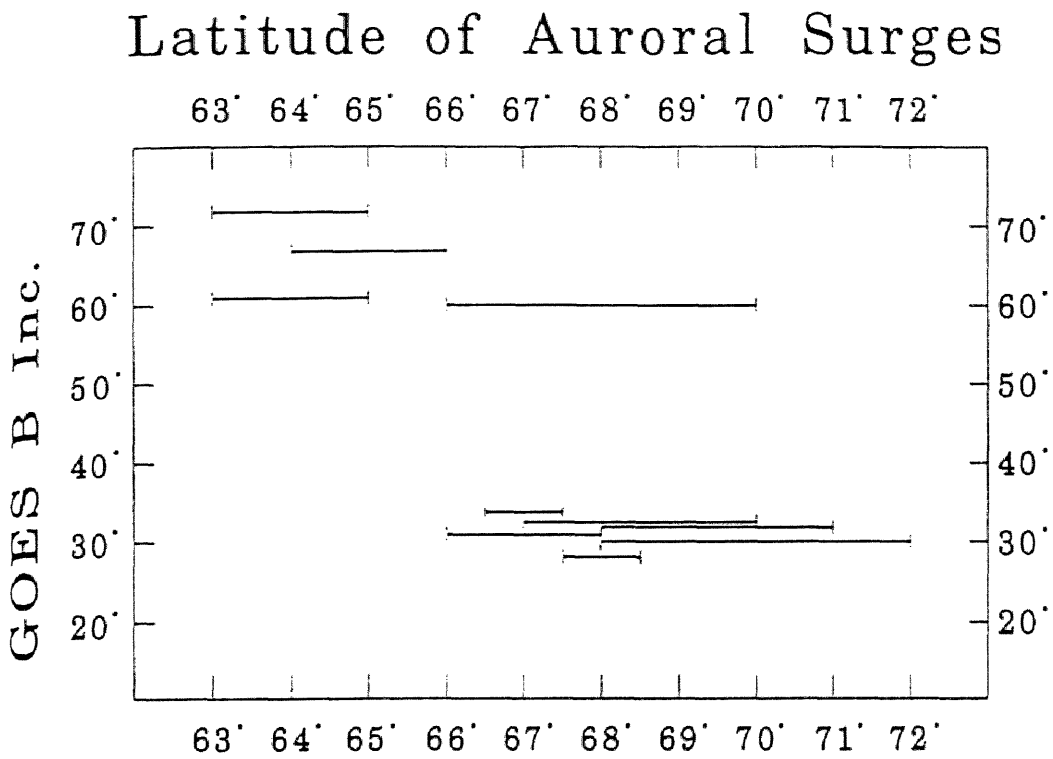

Figure 2.42 Relationship between the inclination angle of the GOES 6 satellite and the latitude of auroral surges when the satellite observed corresponding magnetic field perturbations.

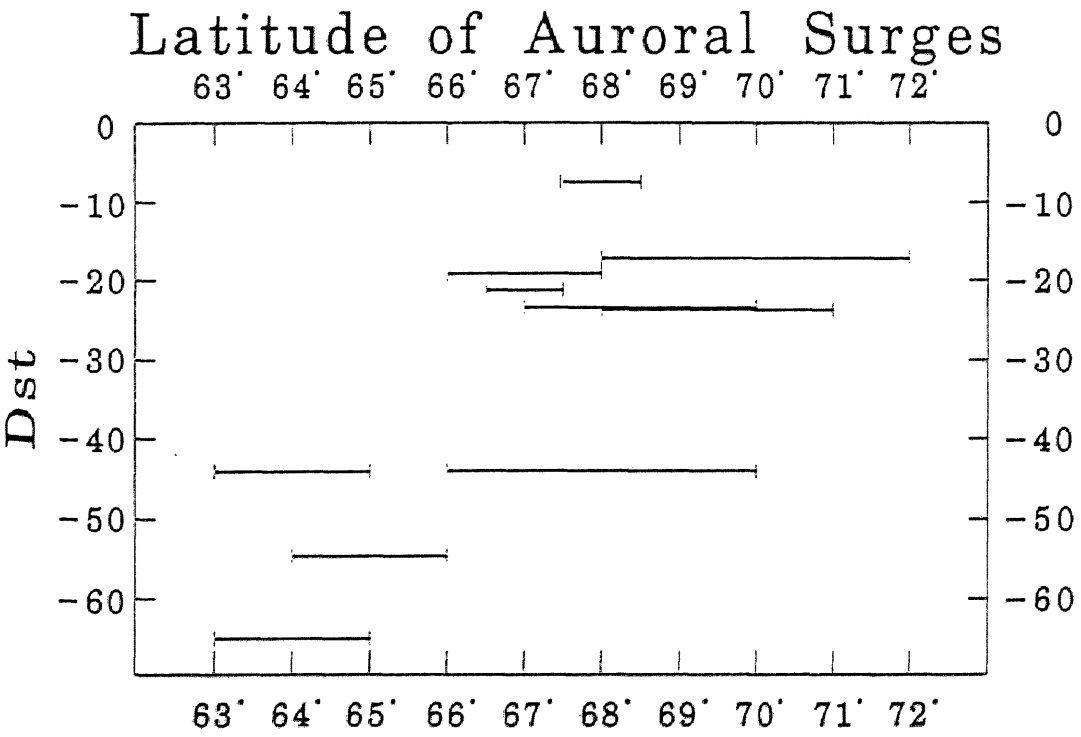

Figure 2.43 Similar to Figure 2.42 for the relationship between the Dst index and the latitude of auroral surges.

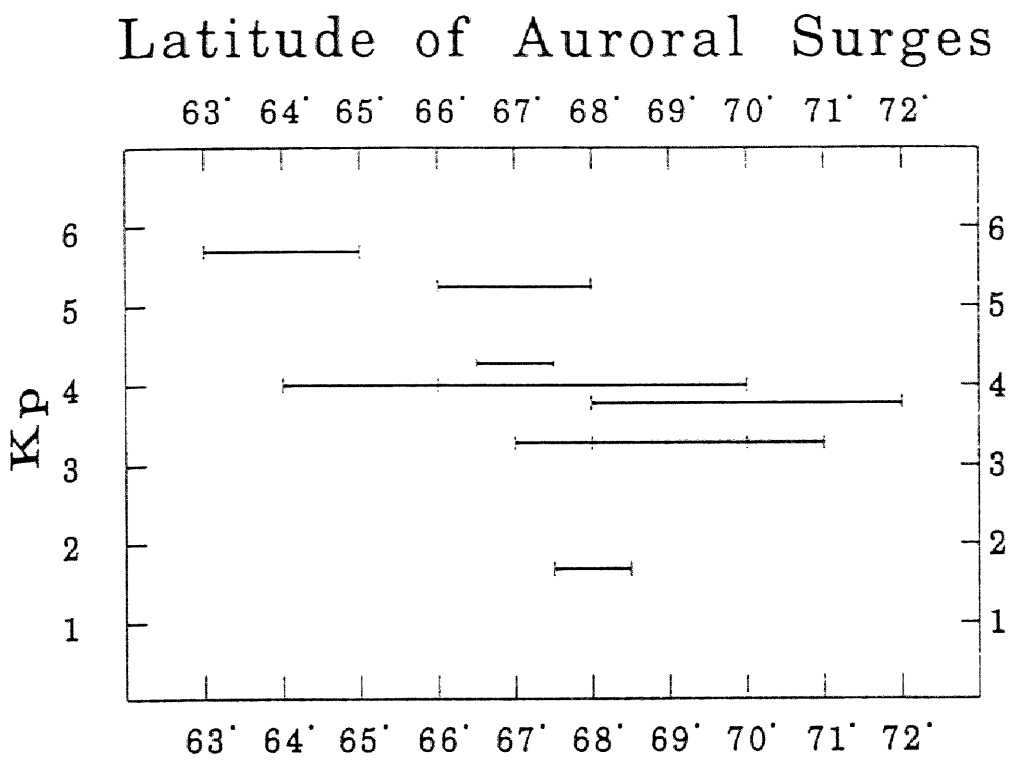

Figure 2.44 Similar to Figure 2.42 for the relationship between the Kp index and the latitude of auroral surges.

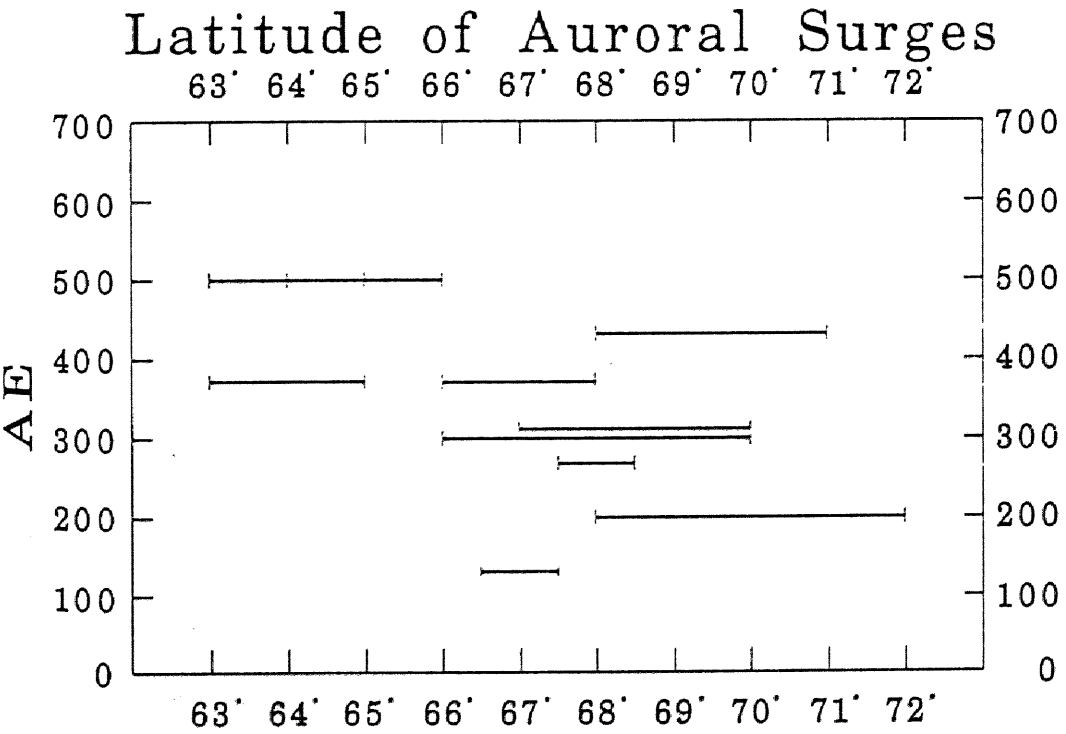

Figure 2.45 Similar to Figure 2.45 for the relationship between the AE index and the latitude of auroral surges.

10° west of the estimated foot point. The difference in the magnetic field line deviation between GOES 5 and GOES 6 is probably caused by the relative location of the field line of auroral arcs to the large-scale field-aligned current system, as in the examples duskside of the onset region described in section 2.4.2.

2.5. Summary

We have compared magnetic field variations at geosynchronous satellites GOES 5 and GOES 6 and auroral activity observed by all-sky cameras at or near the conjugate point of these satellites. We have found that the short-time scale (< 10 minutes) magnetic field variations at geosynchronous orbit are highly localized, at least in comparison with the spatial separation of GOES 5 and GOES 6 satellites (~ 35° in longitude), suggesting that these magnetic field variations are caused by nearby small-scale currents such as field-aligned currents. The localized nature of the magnetic field variations at geosynchronous orbit shows that it is possible to examine magnetic field line connection between the ionosphere and the magnetosphere at geosynchronous orbit by comparing localized auroral activity and magnetic field variations at geosynchronous orbit. This idea is supported by the fact that the duration of the short time magnetic field variations at the GOES 5 and GOES 6 satellites at expansion onset is coincident with that of the localized auroral activity near the foot point of these satellites.

On the basis of these results, we have estimated the real foot point of the geosynchronous satellites for 12 auroral expansion events. To the west of the expansion onset region we have examined the location of the auroral surge when the geosynchronous satellite observed sharp positive D magnetic field perturbations. For the GOES 6 satellite, we found that the probable ionospheric foot point of GOES 6 longitudinally deviated from the estimated foot point (obtained by using the truncated version of Tsyganenko's 1987 model) to the west of the expansion onset region. This deviation can be explained in terms of the magnetic effects of large-scale Region 1 and Region 2 field-aligned currents, because these effects are

not included in Tsyganenko's models. Although we have only 1 example in which GOES 5 observed sharp positive D perturbations, for this event we have found no deviation of the real ionospheric foot point of the satellite relative to the estimated foot point. The difference in the deviation of the real ionospheric foot point of the geosynchronous satellite is probably due to the different relative latitudinal location of the satellites to large-scale Region 1 and Region 2 field-aligned currents.

To the east of the expansion onset region, it is shown in 1 example that the real foot point of GOES 6 deviates westward, in the opposite direction to that to the west of the onset region. This is also probably caused by the downward Region 1 and the upward Region 2 field-aligned currents. For GOES 5 we have found, from 4 examples, no deviation of the real foot point of the satellite relative to the estimated foot point, suggesting a difference in latitude of GOES 5 and GOES 6 relative to the Region 1 and Region 2 currents.

It is also suggested that the small-scale field-aligned currents observed by geosynchronous satellites have localized structure not only in azimuthal but also in latitudinal extent. This means that we can estimate the latitudinal location of the real foot point of the satellite. It is found that the latitude of the real foot point of the satellite depends significantly on the Dst index or the magnetic field inclination of the geosynchronous satellite, which indicate the intensity of the ring and magnetotail currents (local or global), rather than auroral zone geomagnetic activity as indicated by Kp and AE.

In this chapter we have discussed mainly the azimuthal deviation of the ionospheric foot point of the geosynchronous satellites due to the large-scale Region 1 and Region 2 field-aligned currents, which are probably not included in Tsyganenko's magnetic field model. However, we have yet to discuss the characteristics of Tsyganenko's model and in the next chapter we will examine in detail the limit of Tsyganenko's model in representing the real magnetospheric magnetic field.

3. Examination of Tsyganenko's magnetic field models

In Chapter 2 we compared the magnetic field variations at geosynchronous orbit and the spatial-temporal development of auroras observed by ground all-sky TV cameras within the conjugate areas of the satellite. We used Tsyganenko's 1987 model (truncated version) for estimating the ionospheric foot point of the geosynchronous satellite as a reference. From the comparison of auroral activity with the magnetic field changes at the geosynchronous satellites we found that the real ionospheric foot point of the satellite often significantly deviated in the azimuthal direction from the estimated foot point. We suggest that this deviation is caused by the large-scale field-aligned currents such as those of Region 1 and Region 2, because the magnetic effects of these currents are not included, at least in a consistent way, into the model. Before discussing the introduction of field-aligned currents into the model and the estimation of the deviation of the ionospheric foot point of the satellite due to these currents in detail, it is worthwhile examining the characteristics of Tsyganenko's magnetic field models. In the following we will focus attention on mapping analysis and examination of field-aligned currents.

3.1. Mapping Analysis of the relationship between the polar ionosphere and the geomagnetic equator along magnetic field lines

In order to relate specific ionospheric phenomena to magnetospheric phenomena, a reliable magnetospheric magnetic field model is essential. The most popular models that contain the effect of geomagnetic activity and dipole tilt angle as parameters are Tsyganenko's models (Tsyganenko and Usmanov, 1982; Tsyganenko, 1987; Tsyganenko, 1989), henceforth referred to as TU82, T87 and T89, respectively. These models are given by analytical expressions of the magnetic field distribution due to ring currents, magnetotail currents, magnetopause currents, and some possible effect of field-aligned currents as proposed by the authors, fitting satellite (IMP and HEOS) observations. However, they have the following shortcomings: (1) The spatial extent of the observational data is limited, (2) the data dealt with are statisti-

cal averages whereas in fact the magnetospheric magnetic field is largely variable, and (3) the mathematical expressions for these models do not contain the term which consistently represents the effect of the large-scale field-aligned currents.

The validity of Tsyganenko's model was examined by Fairfield (1991), who compared the 0.5 R_E averaged magnetic field distribution obtained by the IMP and HEOS satellites with the TU82 and T87 (truncated version) models. He reported that the main deficiency of these models is the lack of the stretching of magnetic field lines near the ring and magnetotail current region. However, since the spatial extent of the satellite data was limited, his examination was insufficient to check quantitatively the magnetic field distribution all the way from the ionosphere to the geomagnetic equator under various geomagnetic activity levels, which is crucial for the present correlative study of auroral activity and magnetic field variations at geosynchronous orbit.

The mapping of the geomagnetic equatorial plane onto the ionosphere (and vice versa) along magnetic field lines on the basis of Tsyganenko's model should give some important information on the characteristics of the model magnetosphere. For example, the shape of the open-closed boundary (whose definition will be discussed later) on the ionosphere and the shape of the geomagnetic equatorial cross section will give a clue to checking the validity of the magnetospheric models. In addition, the magnetospheric (ionospheric) coordinates mapped onto the ionosphere (the geomagnetic equatorial plane) contain information on the distribution of magnetospheric currents. For example, field-aligned currents in the model, if they exist at all, will twist the magnetic field lines and significantly modify the projection of the coordinates.

In the following we examine the mapping characteristics between the polar ionosphere and the geomagnetic equator, on the basis of Tsyganenko's magnetic field models. All versions, that is, the TU82 model, T87 model (long version and truncated version), and T89 model are used to investigate their characteristics. In addition, we also examine the mapping characteristics of the magnetic field model based on the 3-dimensional MHD simulation of

the magnetosphere by Ogino (private communication, 1991), and compare it with those based on Tsyganenko's models. The comparison between Tsyganenko's observational models and the MHD simulation model, in terms of mapping, would be useful in examining the characteristics and limitation of each model. This is because the simulation gives not only magnetic field but also plasma pressure, plasma density, and plasma bulk flow consistently with each other, whereas Tsyganenko's models give only the magnetic field.

We show two kinds of mapping. Grid points on the geomagnetic equatorial plane, given as a function of radial distance and magnetic local time, are mapped (dotted lines) onto the ionospheric region as illustrated in Figure 3.1(a). From this type of mapping we can discuss, for example, the ionospheric projection of the open-closed boundary of magnetic fields if we set the definition of the open-closed boundary. Conversely, grid points on the polar ionosphere, given as a function of magnetic latitude and magnetic local time, are mapped (dotted lines) onto the geomagnetic equatorial plane as illustrated in Figure 3.1(b). From this type of mapping we can examine, for example, the size and the shape of the equatorial cross-section of the magnetosphere. Here, for simplicity, the dipole tilt effects are not taken into account.

First we will examine the T87 model, which is used in Chapter 2 for estimating the ionospheric foot point of the geosynchronous satellite. After that we will check the TU82 and T89 models for comparison. Finally we will examine the magnetospheric model based on the 3-dimensional MHD simulation by Ogino (private communication, 1991).

3.1.1. T87 model

The T87 model has two versions, that is, a truncated version and a long version (here referred to as T87T and T87L, respectively). The T87L model has 26 coefficients for representing the magnetic field due to three major magnetospheric currents (ring currents, magnetotail currents, and magnetopause currents) with the shape of the ring and magnetotail currents given *a priori* by analytical expression and magnetopause currents given by a series

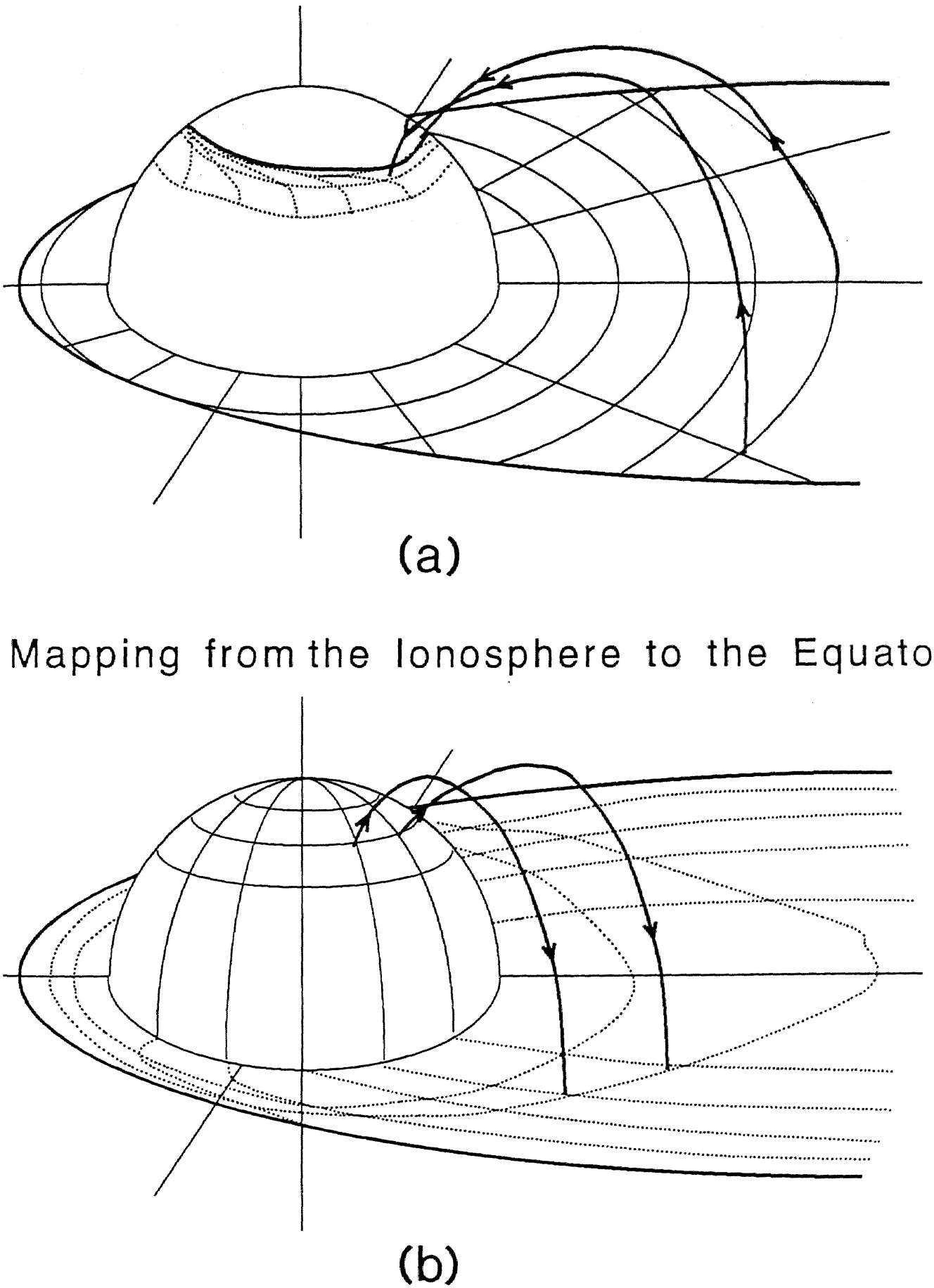

Figure 3.1 Schematic view of the mapping (a) from the geomagnetic equatorial plane onto the ionosphere and (b) from the ionosphere onto the geomagnetic equatorial plane.

of functional expansions. These coefficients are determined by fitting to the observational data set from the IMP and HEOS satellites, and this model is based on a data set covering a radial distance from about 4 R_E to 70 R_E in the magnetotail. The T87T model has 20 coefficients and can represent the magnetic field by a simpler mathematical expression with the data set covering a range in radial distance from about 4 R_E to 30 R_E.

Figure 3.2 shows the geomagnetic equatorial coordinates mapped onto the polar ionosphere by using the T87T model. The lower-left panel shows the "open-closed boundary" on the polar ionosphere. Within the egg-shaped locus the field lines pass across the plane ($\rho = \sqrt{X_{GSM}^2 + Y_{GSM}^2} = 35$ R_E or $Z_{GSM} = \pm 25$ R_E) before crossing the geomagnetic equatorial plane and are regarded as 'open', whereas outside the locus they pass the equatorial plane first and are regarded as 'closed'. We adopt this definition of the open-closed boundary because at $\rho = 35R_E$ the magnetic field strength due to the earth dipole becomes as low as 1 nT. This is comparable to the magnetic field in the solar wind, and therefore, the magnetic field lines tailward of this region can be regarded as 'open'. The shape of the open-closed boundary is approximately the same for different criteria as shown in Figure 3.3(a), $\rho = 30$ R_E, and Figure 3.3(b), $\rho = 25$ R_E, indicating that this boundary does not depend very much on the value of ρ when ρ is larger than about 30 R_E.

The upper left panel and the upper right panel in Figure 3.2 show the ionospheric projection of local time (with an interval of 15°) and radial distance (with an interval of 1 R_E from 5 R_E to 10 R_E and 5 R_E beyond 10 R_E) onto the geomagnetic equator respectively. The lower right panel shows the ionospheric projection of both local time and radial distance onto the geomagnetic equator. Obviously the equi-radial distance contour lines on the nightside become very close to each other for $R = \sqrt{X_{GSM}^2 + Y_{GSM}^2 + Z_{GSM}^2} \geq 10$ R_E and the ionospheric latitude tends to be constant as a function of the radial distance on the geomagnetic equator, indicating that the open-closed boundary is not very sensitive to the chosen parameter ρ.

All Tsyganenko's models contain a Kp-dependent parameter and accordingly the model magnetic field configuration changes with the Kp value. For low Kp (e.g. Figure 3.2, Kp

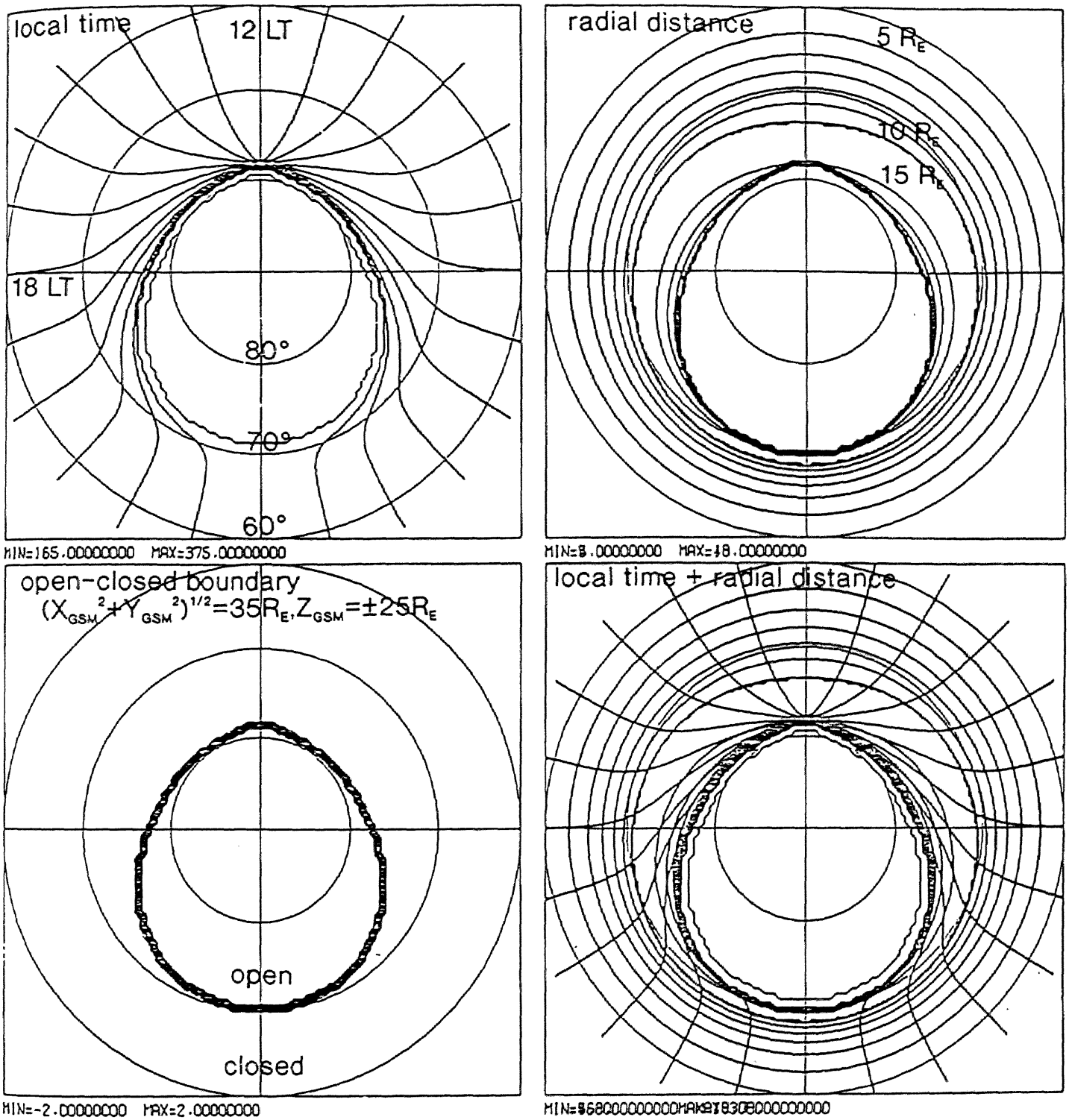

Figure 3.2 Magnetospheric equatorial coordinates mapped onto the polar ionosphere by using the T87T model (Kp = 0, 0+). The lower left panel shows the 'open-closed boundary' on the polar ionosphere, whose definition is described in the text. The upper left panel and the upper right panel show the ionospheric projection of local time and radial distance onto the geomagnetic equator respectively. The lower right panel shows the ionospheric projection of both local time and radial distance onto the geomagnetic equator.

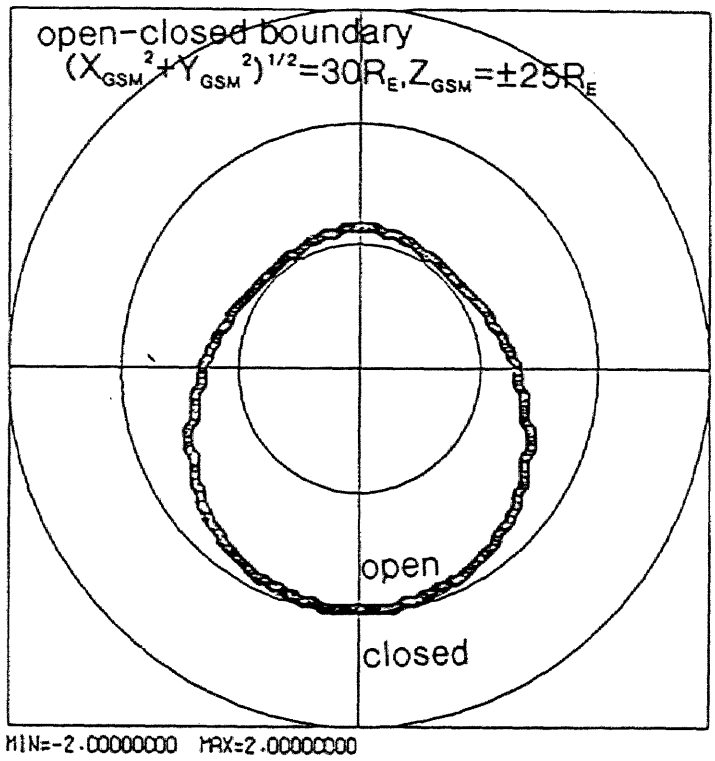

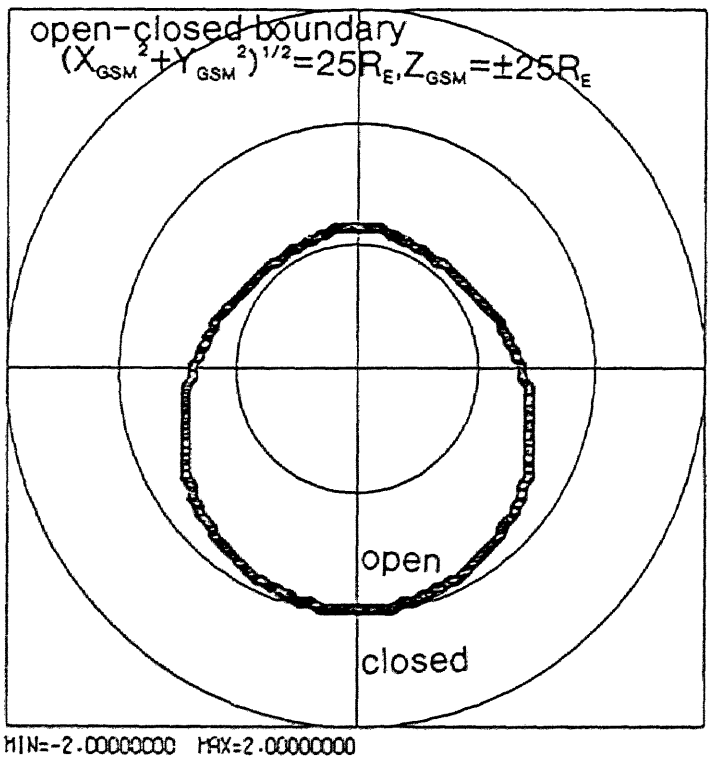

Figure 3.3 Open-closed boundary for different kinds of definition by using the T87T model (Kp = 0, 0+). This boundary is not very sensitive to the chosen parameter ρ.

= 0, 0+), the open-closed boundary is egg-shaped with the wider region located on the nightside and the center shifted antisunward. In this figure most of the area of the low latitude boundary layer is connected to the ionospheric cusp region as already pointed out by Oguti (1989); this is evident from the fact that the equi-local time contour lines converge at the cusp region as seen in Figure 3.2.

With the increase of Kp the open-closed boundary expands equatorward, changing to a more circular form as shown in Figure 3.4 (Kp $\geq$ 5+), coincident with the change of the magnetospheric magnetic field to more tail-like configuration. The converging structure of the equi-local time contour lines at the cusp region is the same as that for low Kp (= 0, 0+) in Figure 3.2.

In the T87L model, the open-closed boundary is tear-drop shaped for low Kp (e.g. Figure 3.5, Kp = 0, 0+). With the change in the definition of the open-closed boundary (change in the ρ to the smaller value) this boundary expands to a lower latitude, especially in the dayside sector (as shown in Figure 3.6). This change occurs because of the expansion of the nightside magnetotail flank, which will be considered later. With the increase of Kp the open-closed boundary expands equatorward, changing to a more circular form as shown in Figure 3.7, as is the case with the T87T model. The converging structure of the equi-local time contour lines at the cusp region is also, for all Kp, the same as that for the T87T model.

Figure 3.8 shows the polar ionospheric coordinates mapped onto the geomagnetic equator using the T87T model (Kp = 0, 0+). The upper left panel shows the projection of the polar ionospheric local time (with the interval of 15°) onto the geomagnetic equator. The upper right panel shows the projection of polar ionospheric latitude (with the interval of 1°), and the lower left panel the projection of both polar ionospheric local time and latitude. The model magnetopause can be defined as that surface of outermost magnetic field lines connected to the ionosphere. For low Kp (= 0, 0+) the shape of the magnetopause is parabolic, compressed on the dayside and stretched on the nightside, in agreement with the result based on satellite observations (Egidi et al., 1970; Fairfield, 1971). It is also seen that

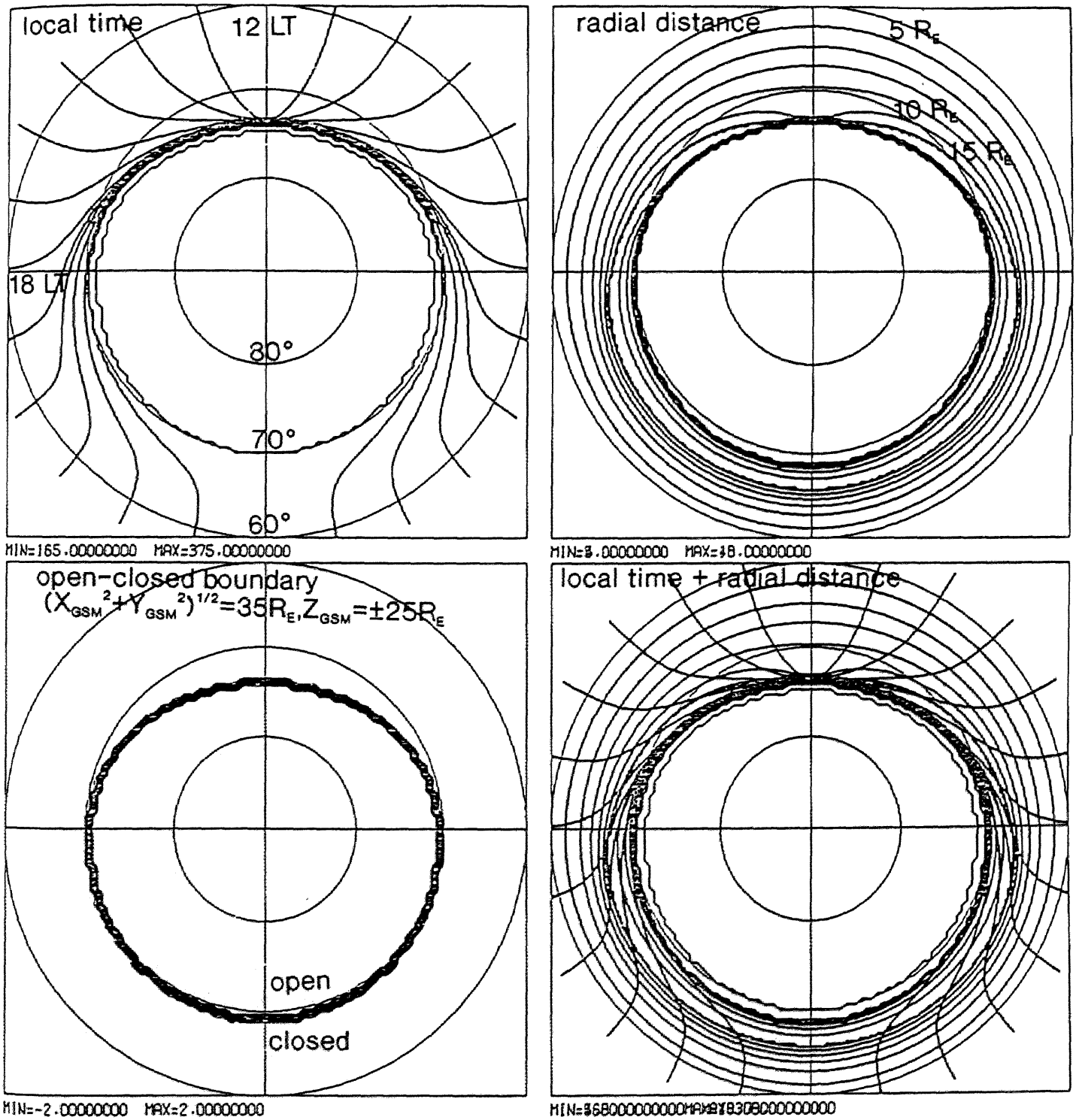

Figure 3.4 Similar to Figure 3.2 for Kp $\geq$ 5+.

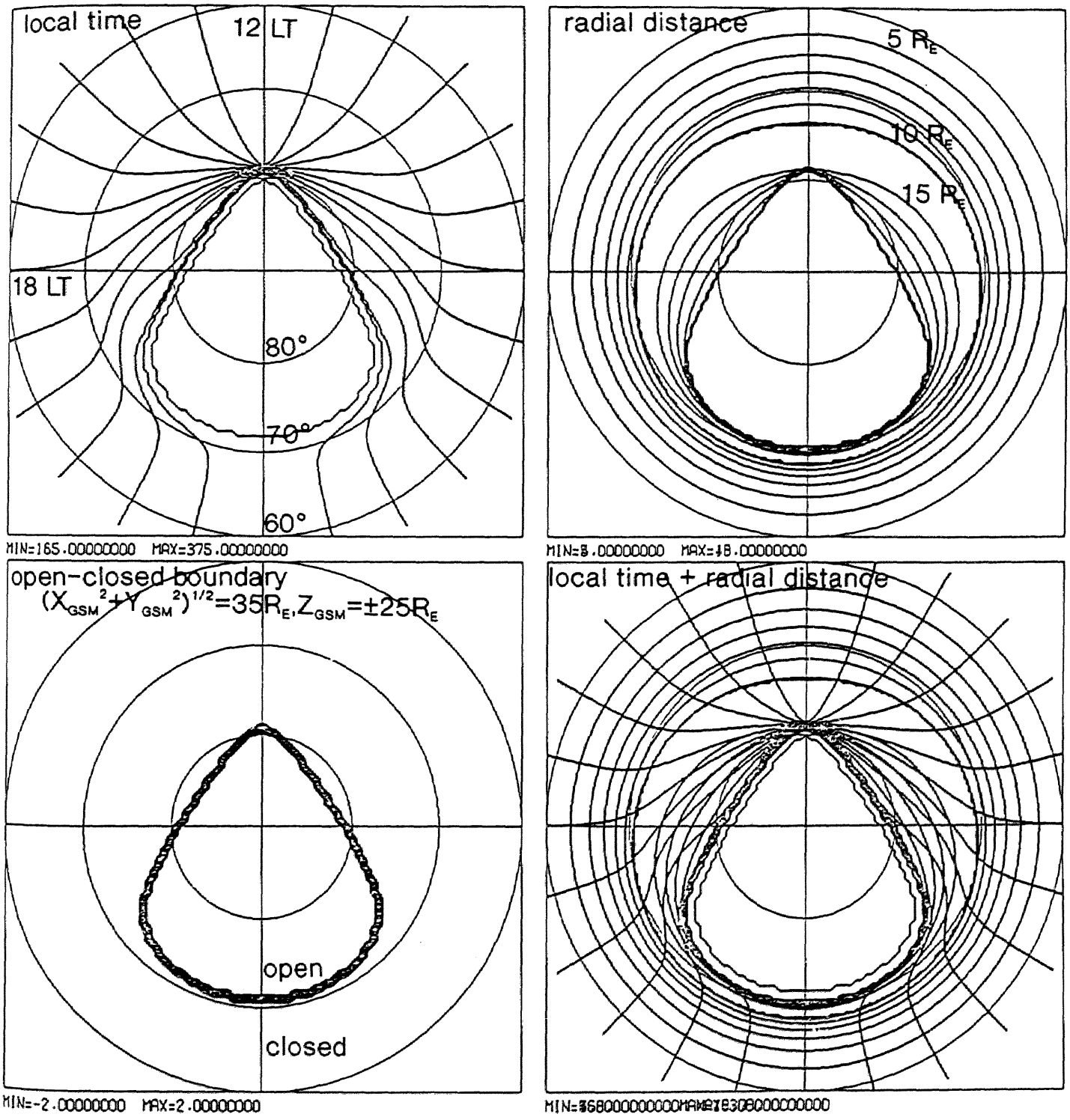

Figure 3.5 Magnetospheric equatorial coordinates mapped onto the polar ionosphere by using the T87L model (Kp = 0, 0+), in the same format as Figure 3.2.

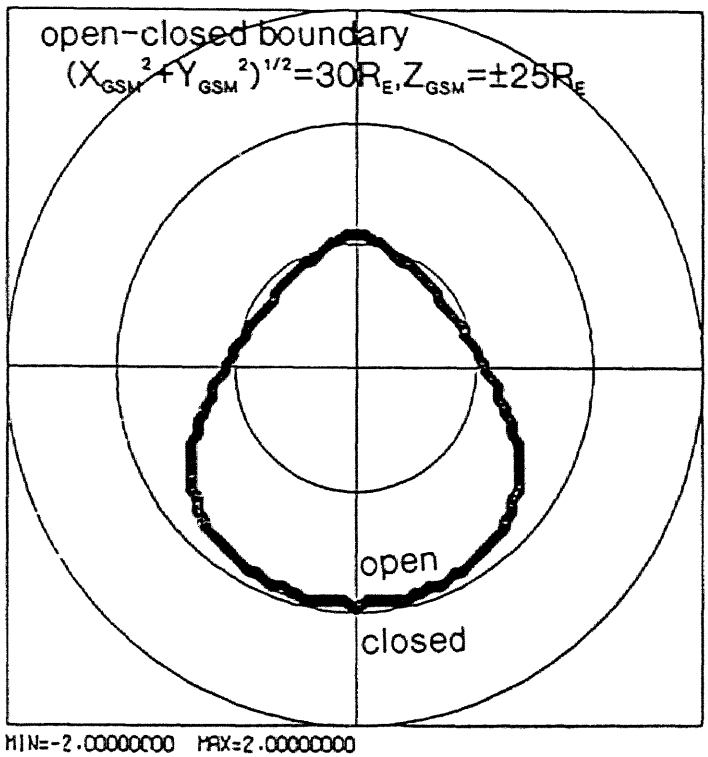

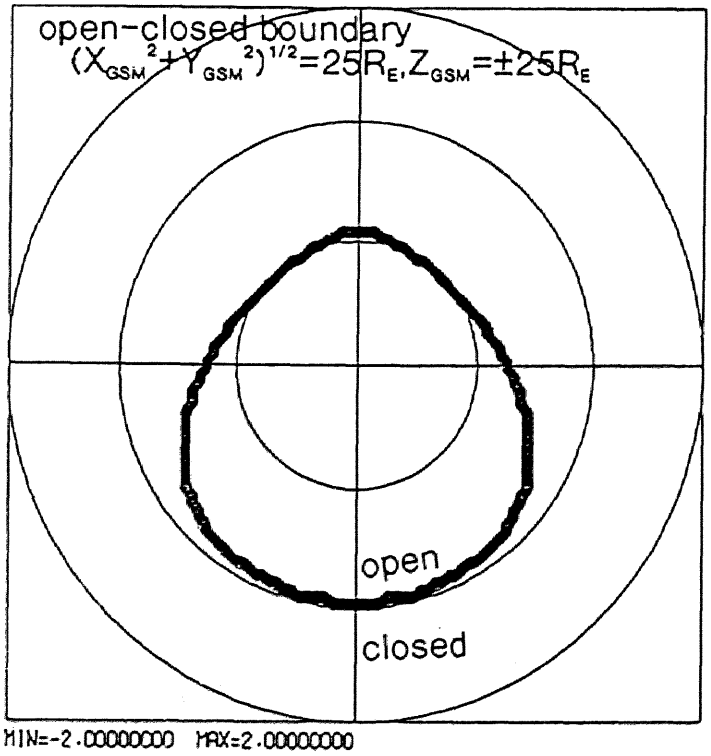

Figure 3.6 Open-closed boundary for different kinds of definition by using the T87L model (Kp = 0, 0+).

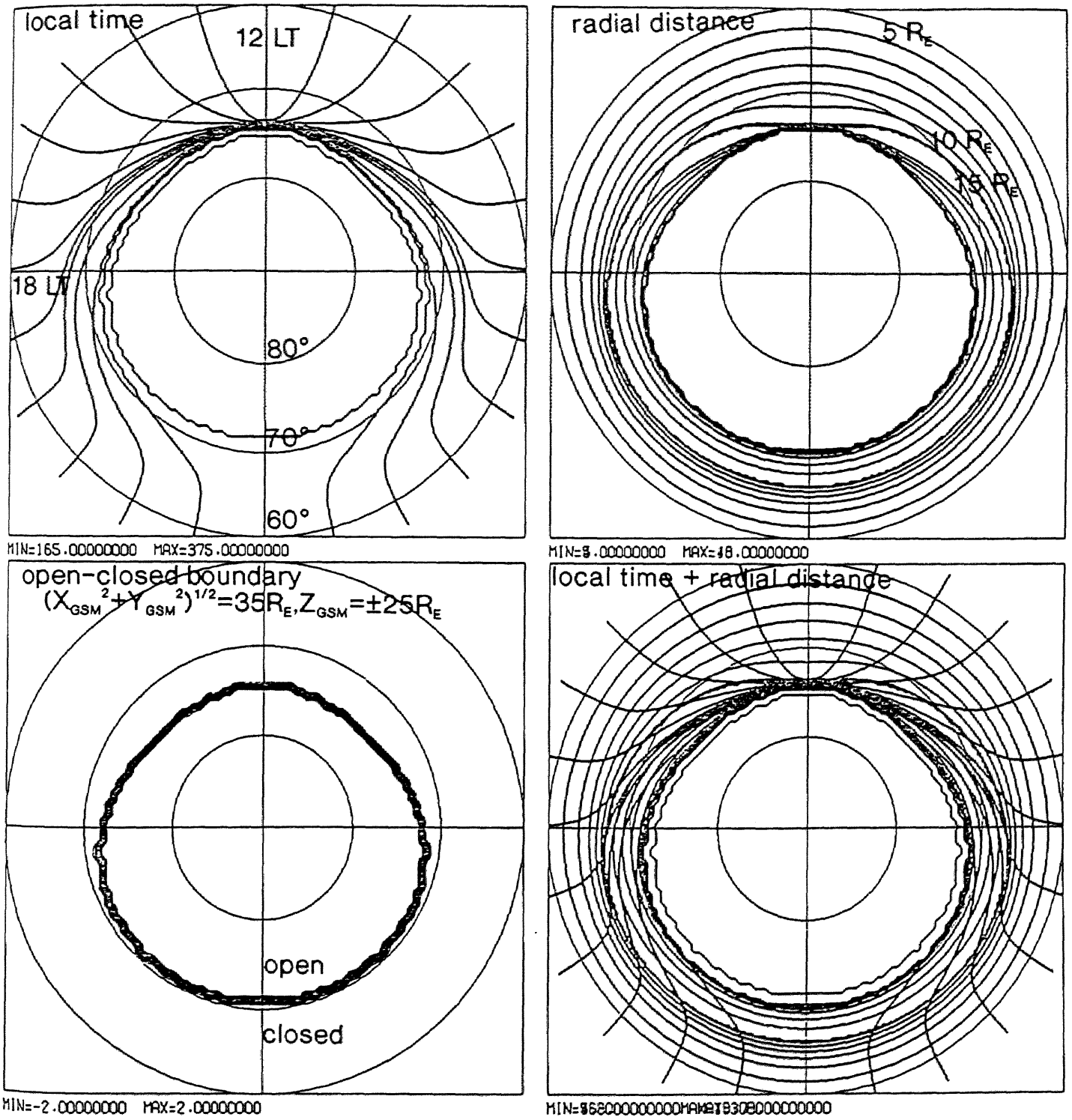

Figure 3.7 Similar to Figure 3.5 for Kp $\geq$ 5-.

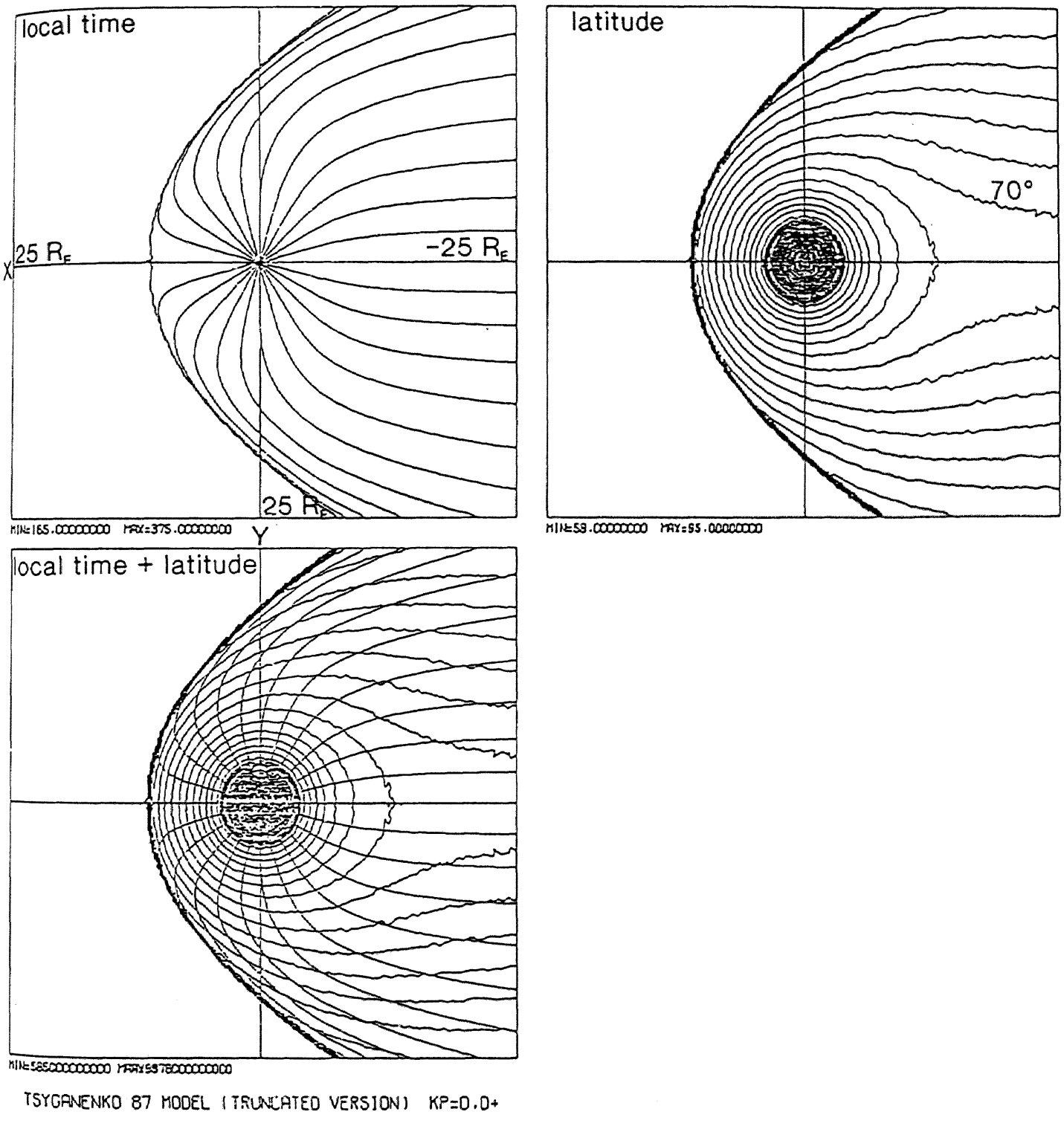

Figure 3.8 Polar ionospheric coordinates mapped onto the geomagnetic equator by using T87T model for Kp = 0, 0+. The upper left panel shows the projection of polar ionospheric local time onto the geomagnetic equator. The upper right panel shows the projection of polar ionospheric latitude, and the lower left panel shows the projection of both polar ionospheric local time and latitude.

near the midnight meridian the equi-radial distance contour lines are highly stretched in the noon-midnight direction rather than in the radial direction. This is due to the magnetotail currents flowing farther away from the earth, approximately from the dawn to the dusk.

On the other hand, for moderate to high Kp ($\geq$ 2) the shape of the model magnetopause is a peculiar, squid-shape, as shown in Figure 3.9 (Kp $\geq$ 5+). Discontinuity of the magnetopause in the magnetotail flank is evident; two hollows are seen on the dusk and dawn side. The reason why the peculiar shape of the flank occurs is seen in the schematic view of the magnetic field lines near the discontinuity in Figure 3.10. Here the field lines originating from latitude 71° and longitude 56° to 60° (long. = 0° corresponds to the local noon) on the ionosphere are given. The field line originating from latitude 71° and longitude 60° shows a quite singular nature. Starting from the ionosphere, this magnetic field line first comes near the equator and again goes away from it, and hence makes a loop-like structure. The magnetic field lines inside this loop are closed near the geomagnetic equatorial plane and are not connected to the ionosphere, thus producing the discontinuity of the magnetopause. This magnetic field line configuration is due to the inappropriate assumptions of the distribution of the model ring and magnetotail currents as well as their connection in this region of the model.

In the long version of the model (Figures 3.11, 3.12) such hollows are not found except for Kp = 4–, 4, 4+ (not shown). For low Kp the shape of the magnetopause is parabolic as shown in Figure 3.11 (Kp = 0, 0+). However, for high Kp (e.g. Figure 3.12, Kp $\geq$ 5–) the nightside magnetotail expands much greater in the dawn-dusk direction for $X_{GSM} \leq -20\ R_E$, as compared with the satellite observation (e.g. Fairfield, 1971) and 3-dimensional MHD simulation, which will be discussed in Section 3.1.4. This is because the field lines in the high-latitude magnetotail of this model expands far more in the Y_{GSM} direction than in the near-earth magnetotail as shown in Figure 3.13 (note the field lines originating from the ionosphere at lat. = 80° and long. = 30° / 330°). This unrealistic configuration of the field line is likely due to the inappropriate expression of the magnetopause current term, together

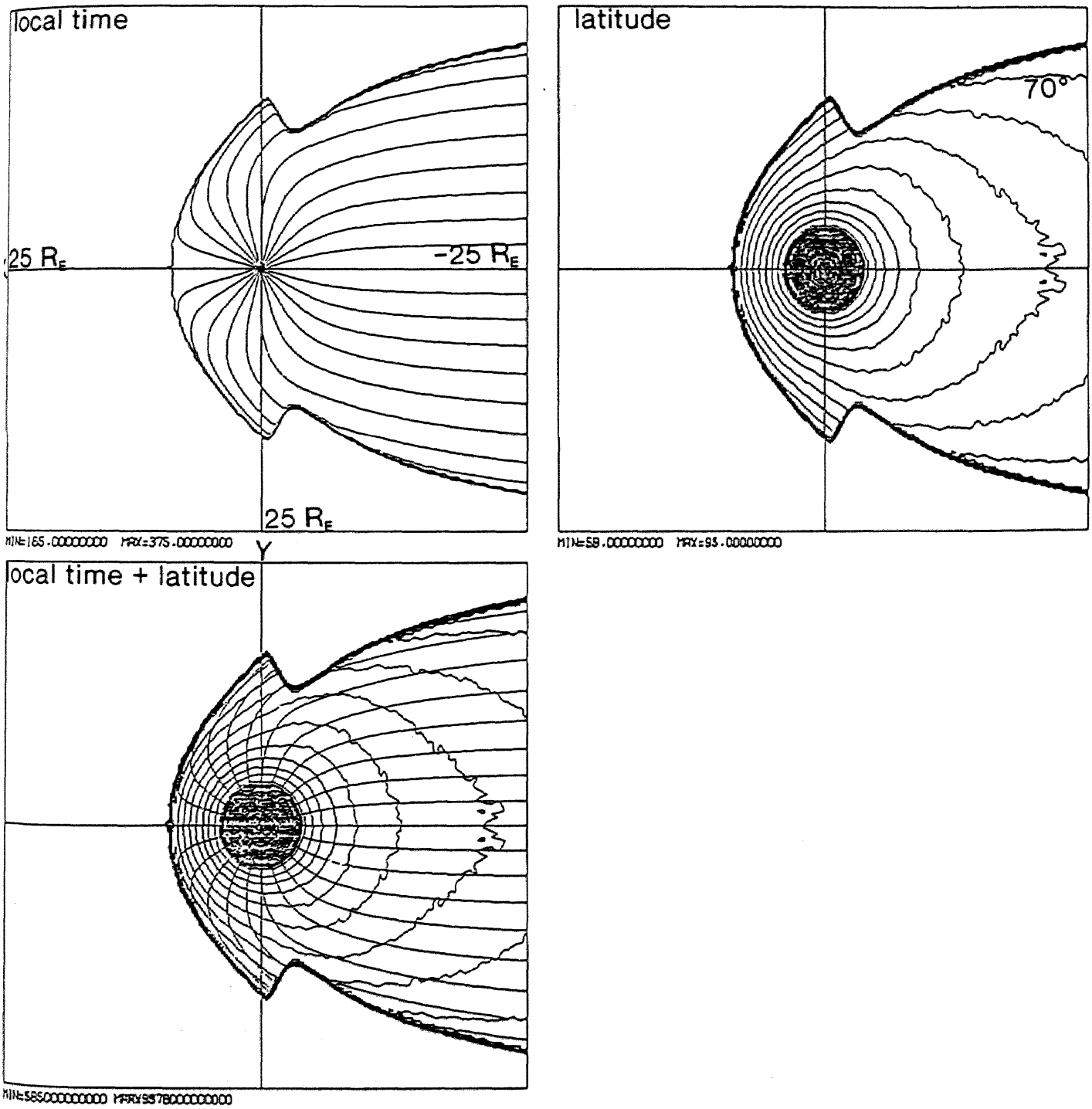

Figure 3.9 Similar to Figure 3.8 for Kp $\geq$ 5+. Discontinuity of the magnetopause in the magnetotail flank is clearly seen.

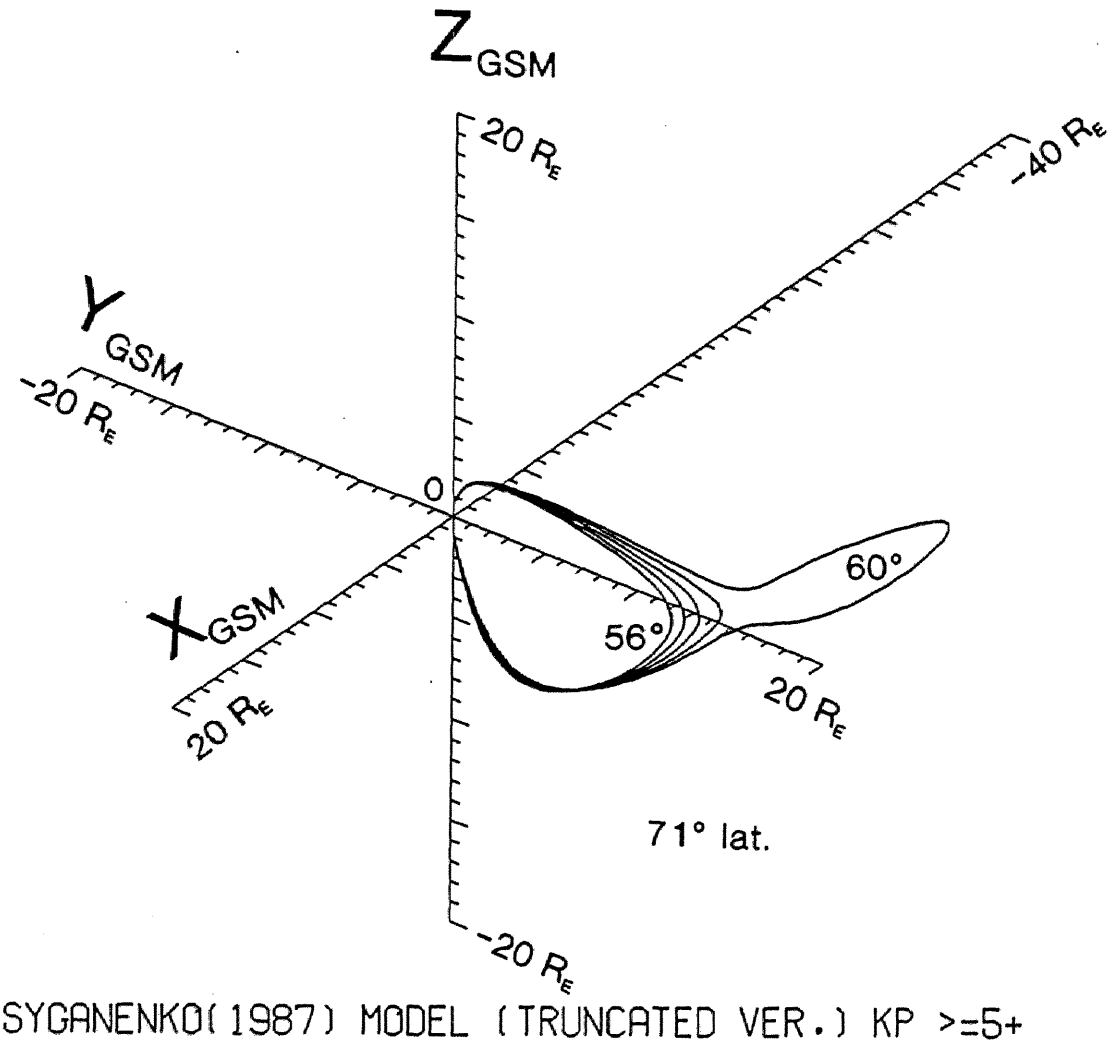

Figure 3.10 Schematic view of the magnetic field lines near the discontinuity of the magnetotail flank seen in Figure 3.9. Here the field lines originating from the ionospheric point at latitude 71° and longitude 56° to 60° (long. = 0° corresponds to the local noon) on the ionosphere are given.

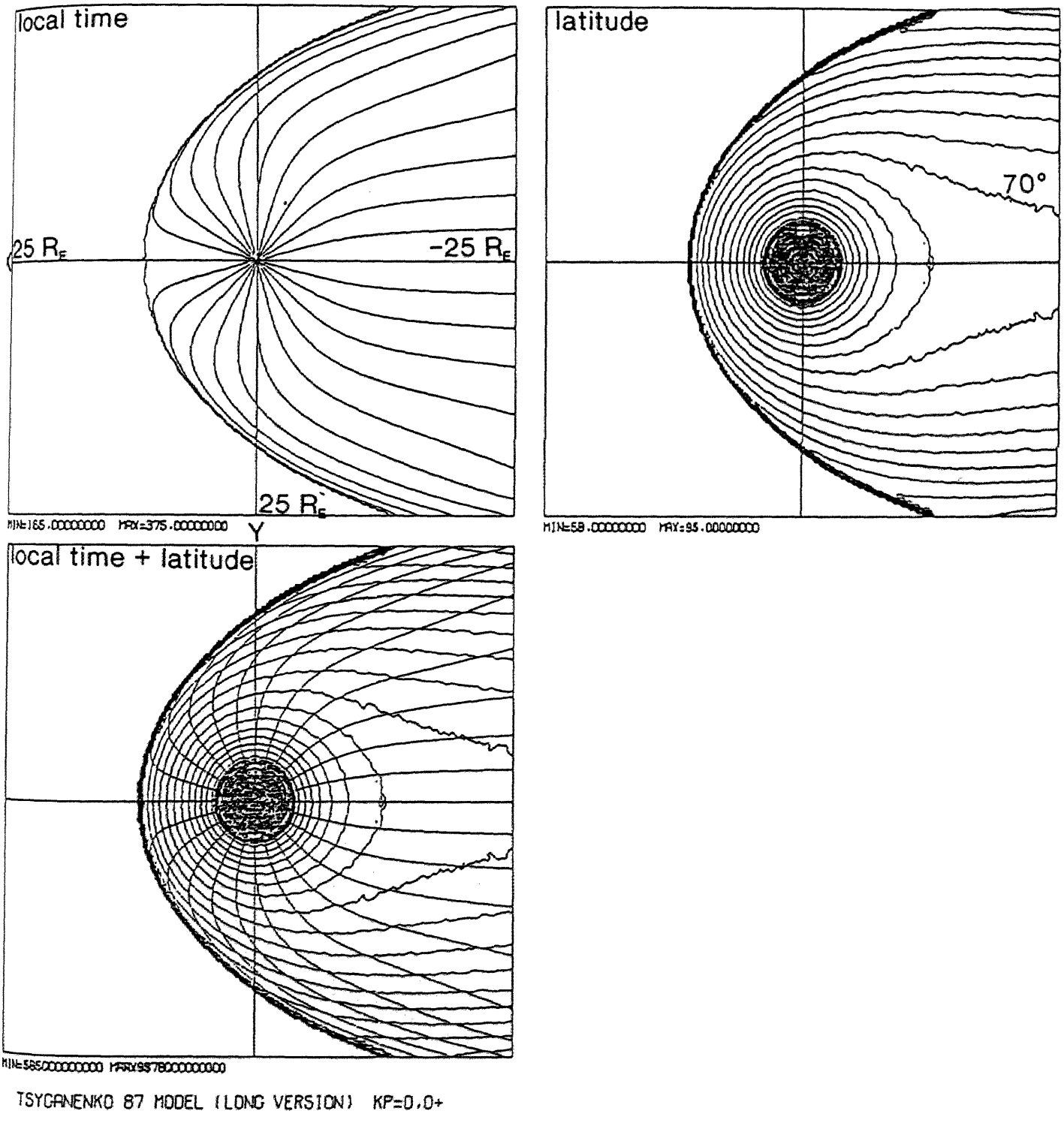

Figure 3.11 Polar ionospheric coordinates mapped onto the geomagnetic equator using T87L model for Kp = 0, 0+, in the same format as Figure 3.8.

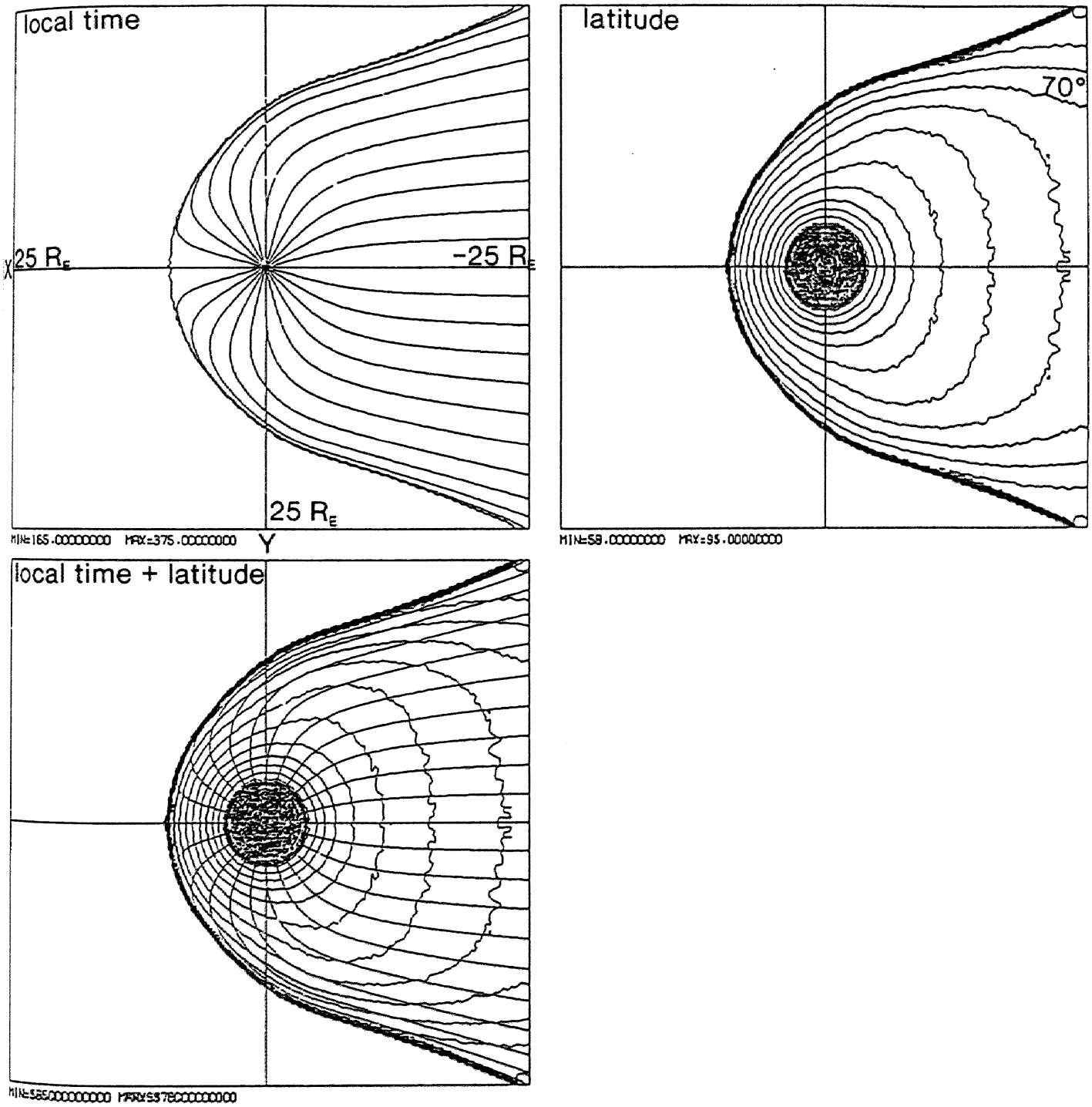

Figure 3.12 Similar to Figure 3.11 for Kp $\geq$ 5-. It is clear that the magnetotail flank expands unrealistically in the distant magnetotail.

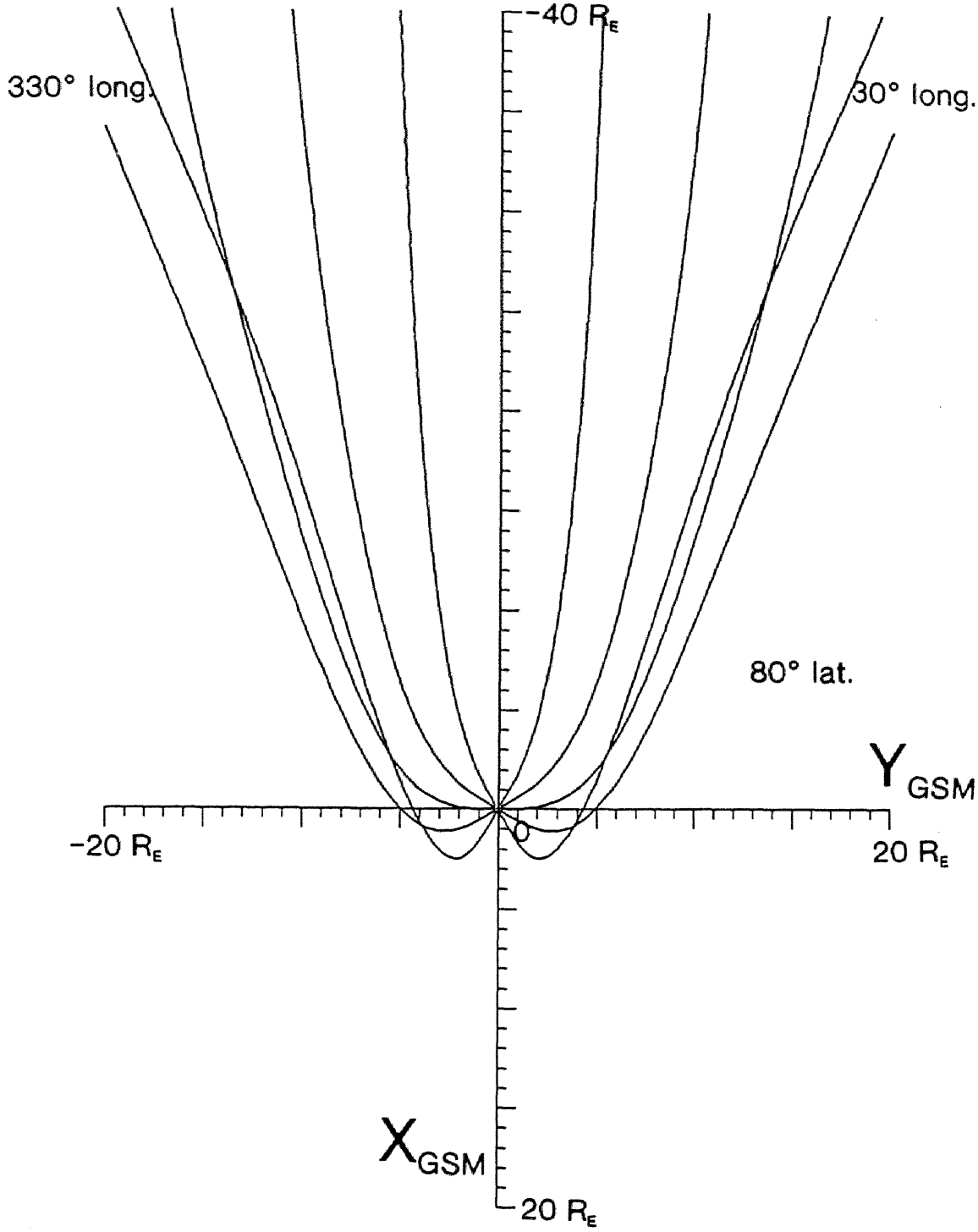

Figure 3.13 Schematic view of the field lines originating from the ionosphere at latitude 80° based on the T87L model (Kp = 4-, 4, 4+). Take notice of the field lines originating from the ionospheric point at longitude 30° or 330°. which are not aligned in the sun-earth direction in the distant magnetotail but are aligned approximately in the radial direction, which is responsible for the expanding of the distant magnetotail flank as seen in Figure 3.12.

with the magnetotail current term in the high-latitude tail region.

3.1.2. TU82 model

This model is based on the data set only for $X_{GSM} \geq -20\ R_E$. It does not include the mathematical expression of magnetotail surface currents, which in the T87 and the T89 models are introduced to flow from the dusk to dawn near the high latitude magnetopause ($Z_{GSM} = \pm 30\ R_E$) of the magnetotail.

One result of the mapping from the geomagnetic equator to the polar ionosphere using the TU82 model is shown in Figures 3.14 (Kp = 0) and 3.15 (Kp > 3+). The open-closed boundary, being defined as those 'open' field lines that pass across the plane ($\rho = \sqrt{X_{GSM}^2 + Y_{GSM}^2}$ = 35 R_E or $Z_{GSM} = \pm 25\ R_E$) before crossing the equatorial plane, changes dramatically with Kp. The nightside boundary is located at lower latitudes for low Kp, which is obviously unrealistic. This is due to the inappropriate expression of the magnetic field in the distant magnetotail as can be seen in Figure 3.16, which shows a schematic view of magnetic field lines in the distant magnetotail. The magnetosphere has a boundary on the nightside (X_{GSM} $\sim -35\ R_E$) and beyond this boundary the magnetic field lines go away from the earth and are not connected to the ionosphere. This is largely because the model is based on the data set only for $X_{GSM} \geq -20\ R_E$. Therefore for this model the definition of the open-closed boundary the same as that for the T87 model ($\rho = 35\ R_E$) is meaningless. If we define open field lines as those passing through the plane $\rho = 25\ R_E$ or $Z_{GSM} = \pm 25\ R_E$ before crossing the equatorial plane, the open-closed boundary is tear-drop shaped for low Kp (e.g. Figure 3.17, Kp = 0, 0+), which is approximately coincident with the result obtained using the T87L model. With the increase of Kp the open-closed boundary expands equatorward, changing to a more circular shape (e.g. Figure 3.18, Kp > 3+). The converging structure of the equi-local time contour lines at the cusp region is, for all Kp, the same as that for the T87T model.

Figure 3.19 shows the result of the mapping from the polar ionosphere to the geomagnetic

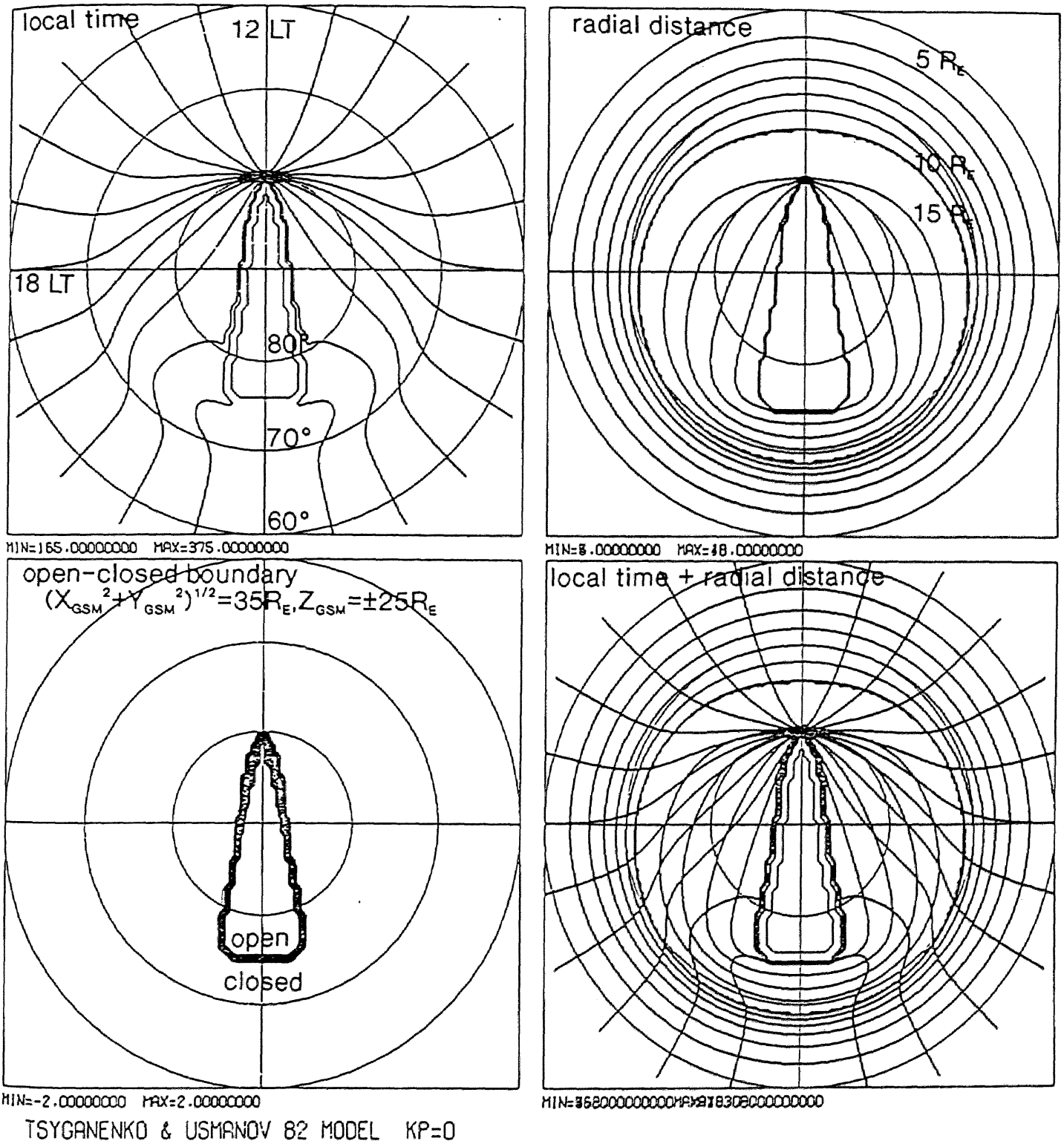

Figure 3.14 Polar ionospheric coordinates mapped onto the geomagnetic equator by using TU82 model for Kp = 0, in the same format as Figure 3.2. Here the 'open' field lines are defined as the lines passing through the plane ρ = 35 R_E or Z_{GSM} = ± 25 R_E before crossing the equatorial plane.

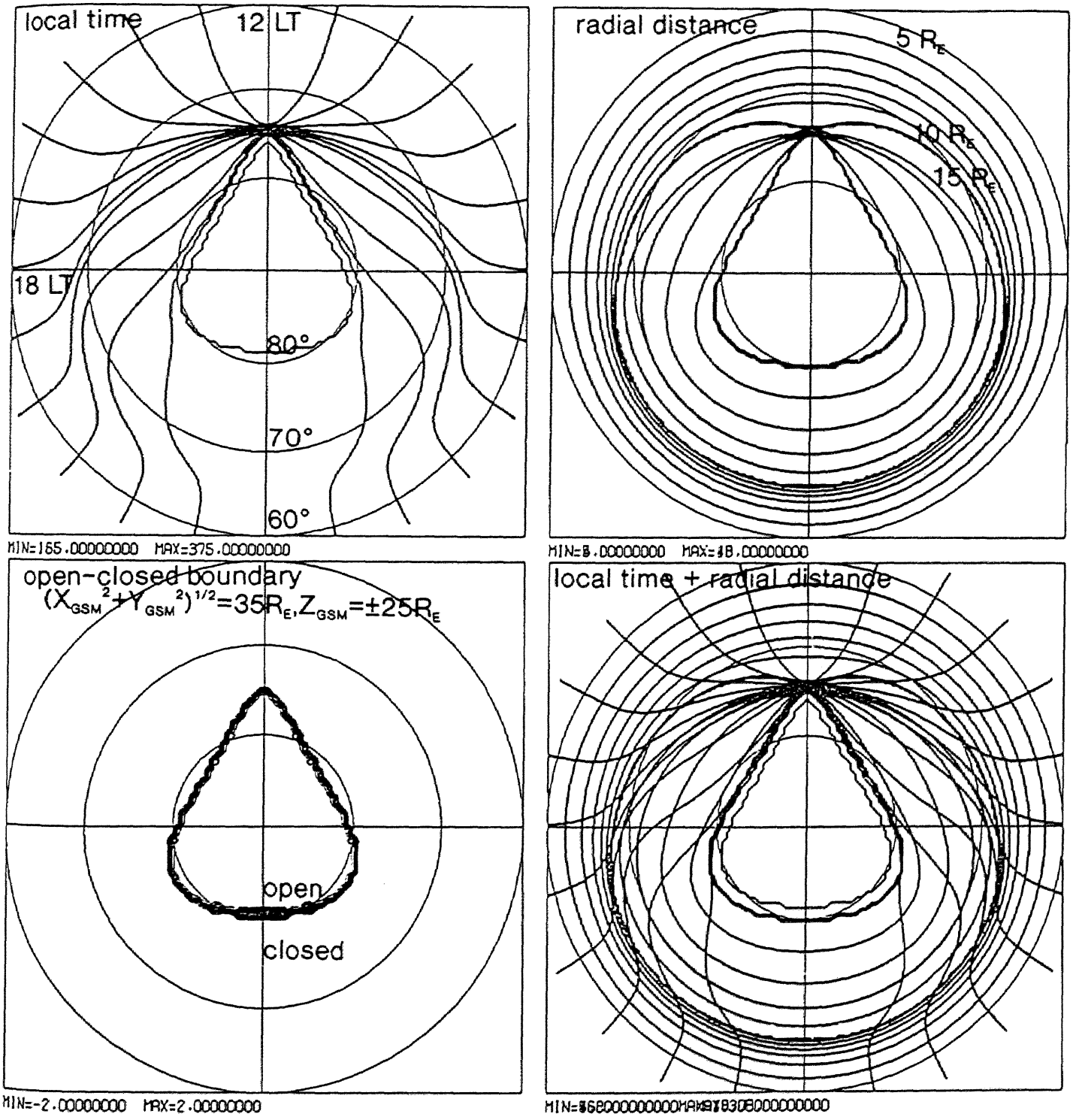

Figure 3.15 Similar to Figure 3.14 for Kp > 3+. The nightside open-closed boundary is located at higher latitude than for Kp = 0 (Figure 3.14), which is obviously unrealistic.

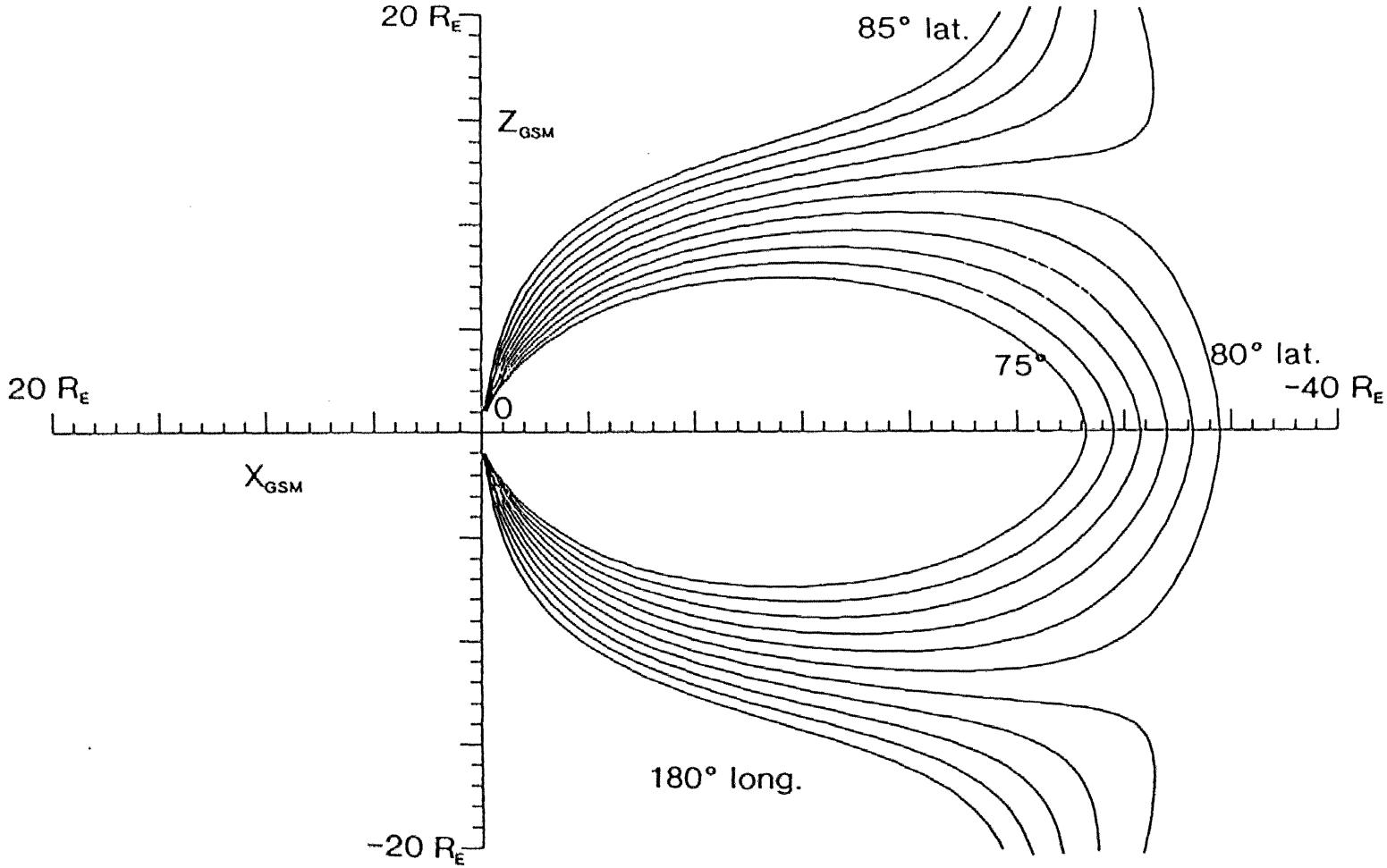

Figure 3.16 Schematic view of the magnetic field lines in the distant magnetotail based on the TU82 model (Kp $\geq$ 3+). The magnetosphere has a boundary on the nightside ($X_{GSM} \sim -35\ R_E$) and beyond this boundary the magnetic field lines go away from the earth and are not connected to the ionosphere.

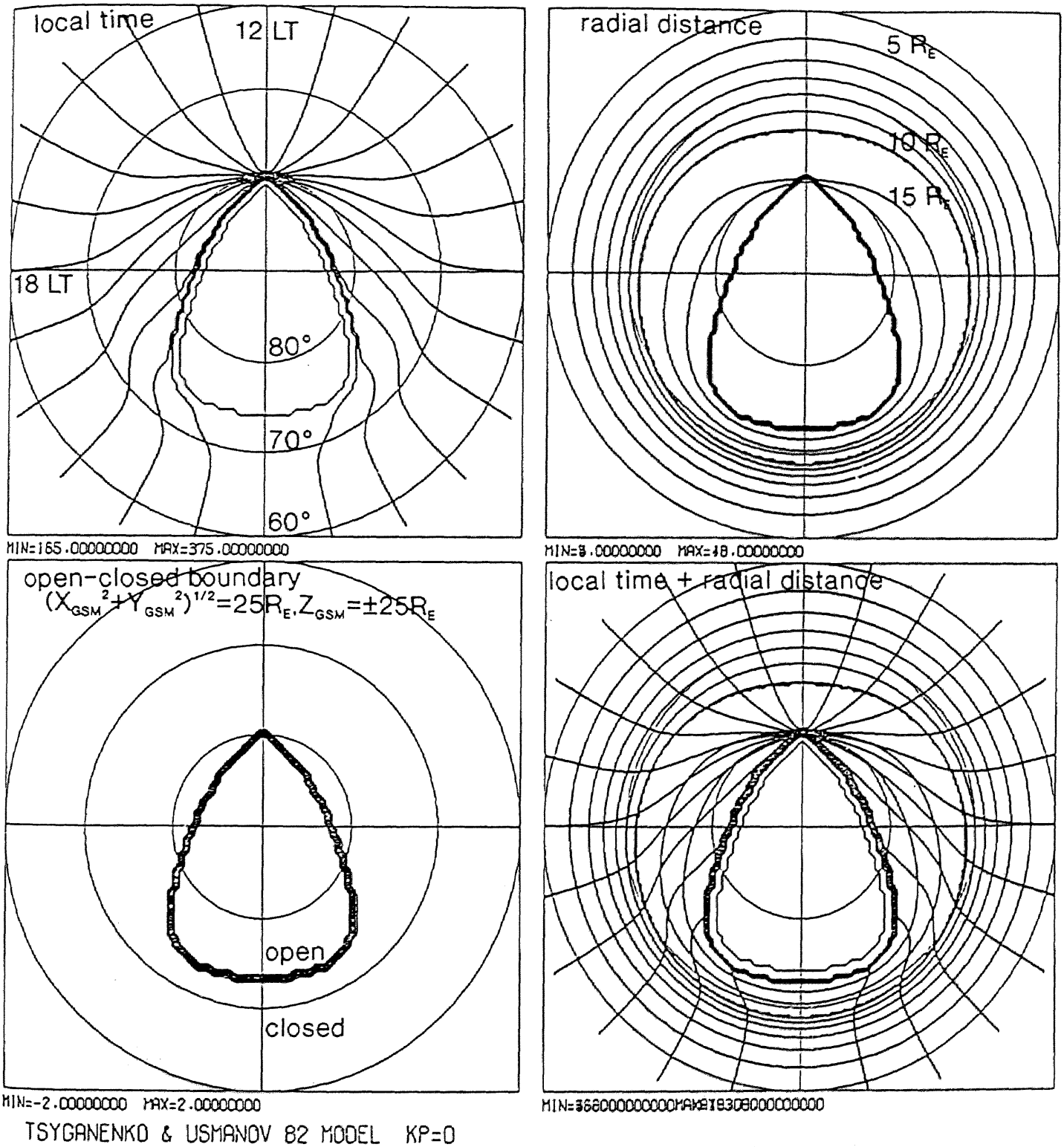

Figure 3.17 Polar ionospheric coordinates mapped onto the geomagnetic equator by using TU82 model for Kp = 0, in the same format as Figure 3.2. Here the 'open' field lines are defined as the lines passing through the plane ρ = 25 R_E or Z_{GSM} = ± 25 R_E before crossing the equatorial plane.

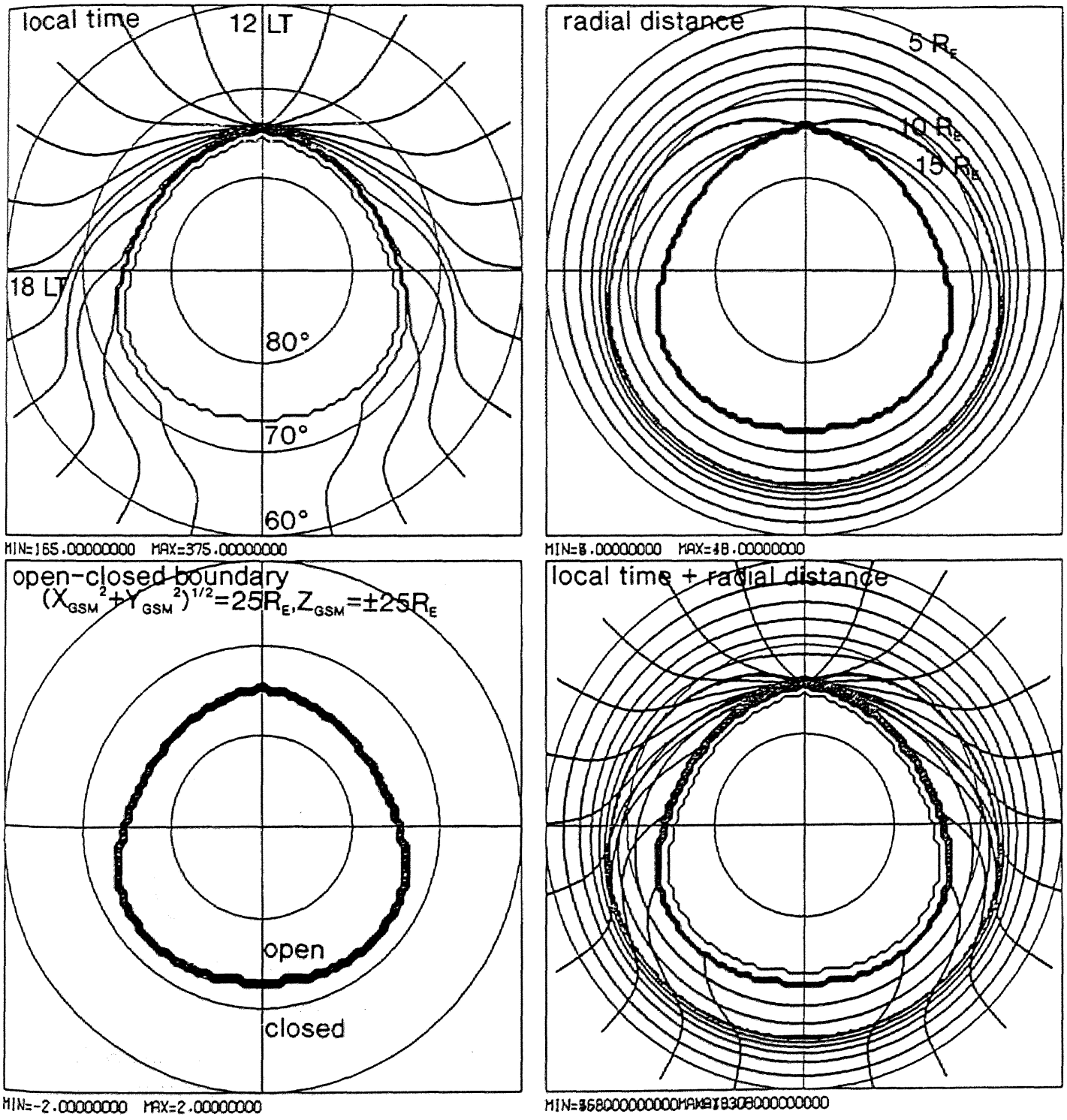

Figure 3.18 Similar to Figure 3.17 for Kp > 3+.

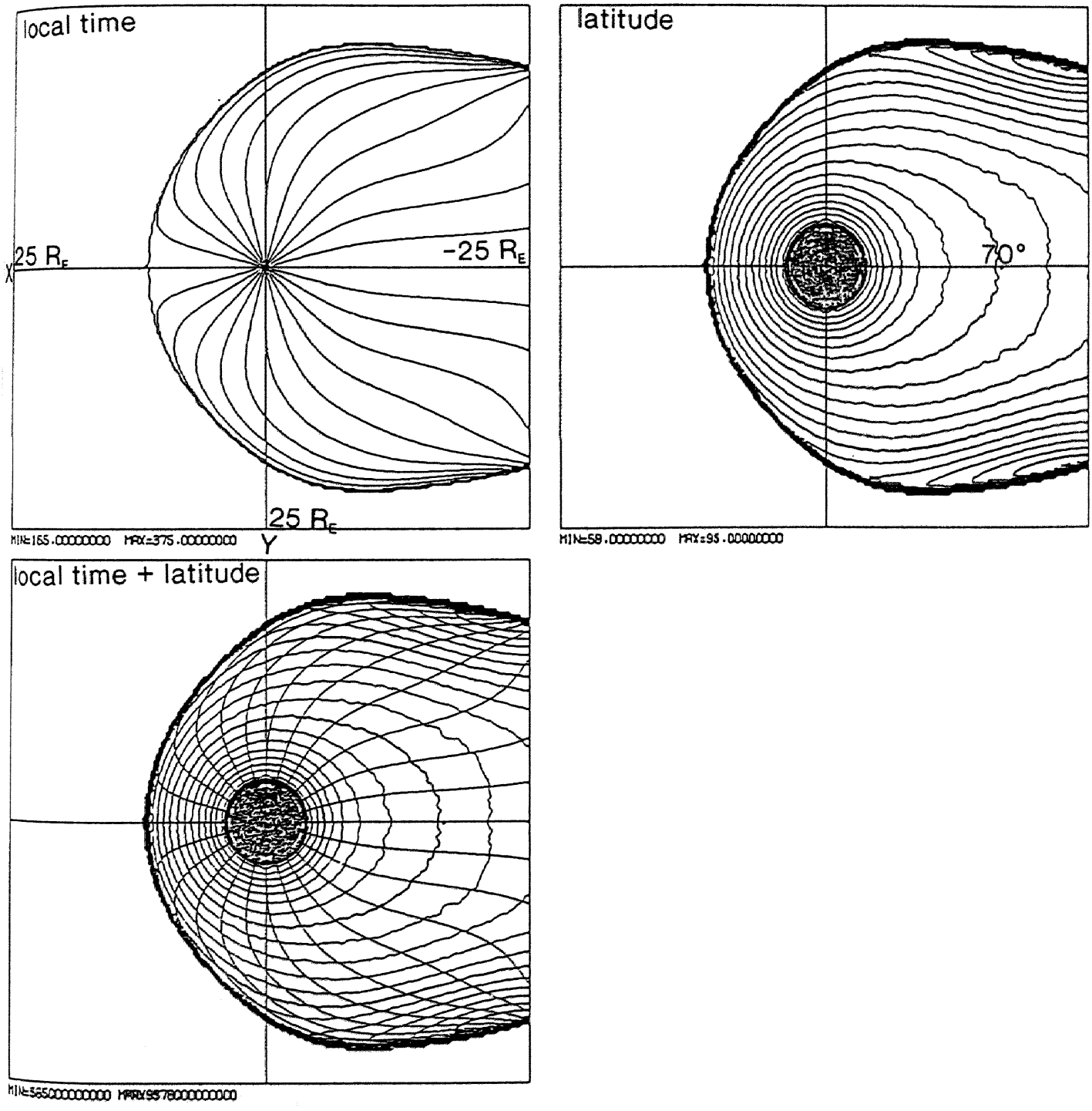

Figure 3.19 Polar ionospheric coordinates mapped onto the geomagnetic equatorial plane by using the TU82 model (Kp = 0), in the same format as Figure 3.8.

equator (Kp = 0). On the dayside the magnetopause is parabolic, while on the nightside the magnetotail flank shrinks for $X_{GSM} \leq -15$ R_E. Obviously this shrinking of the magnetotail flank is unrealistic, considering the pressure balance at the nightside magnetopause. This is probably because the spatial extent of the data is limited and the mathematical expression of this model is not considered to represent the magnetic field beyond the data coverage region. With the increase of Kp (e.g. Figure 3.20, Kp $\geq$ 3+) the dayside magnetopause becomes compressed whereas the nightside magnetotail expands in the dawn-dusk direction for -15 $R_E \leq X_{GSM} \leq 0$ R_E.

3.1.3. T89 model

The peculiarity of the T89 model is that the magnetotail currents are approximately aligned with the azimuthal direction rather than in the dawn-dusk direction. This is different from the T87 and TU82 models, in which the magnetotail currents are aligned mainly in the dawn-dusk direction rather than in the azimuthal direction. Another characteristic is the warping of the tail current sheet. Due to the dipole tilt effect the magnetotail current sheet is warped on the Y–Z plane so that it is shifted northward (southward) in GSM coordinates near the midnight meridian while it is shifted southward (northward) near the nightside magnetotail flank in the northern summer (winter). In contrast, the magnetotail current sheet is uniformly shifted northward (southward) in the T87 and TU82 models. However, since the dipole tilt angle is assumed to be 0° in this study, we do not henceforth mention this warping effect.

The result of the mapping from the geomagnetic equator to the polar ionosphere by using the T89 model is shown in Figure 3.21. For low Kp the open-closed boundary is egg-shaped with the wider end directed toward the dayside in contrast to the T87T model. This shape is approximately the same for different criteria as shown in Figure 3.22 (a), $\rho = 30$ R_E, and Figure 3.22 (b), $\rho = 25$ R_E, indicating that this boundary does not depend very much on the value of ρ when ρ is larger than about 30 R_E.

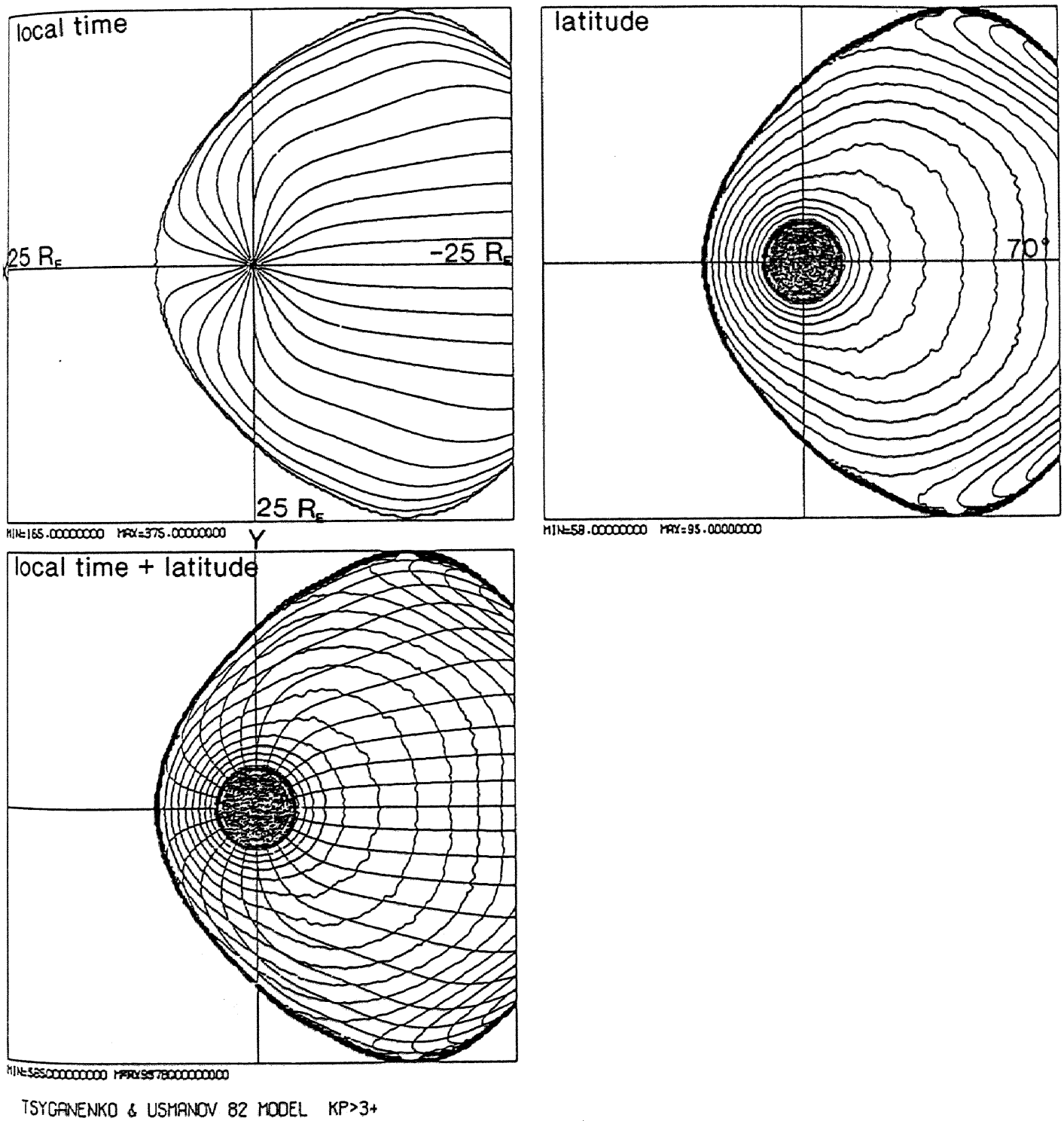

Figure 3.20 Similar to Figure 3.19 for Kp > 3+.

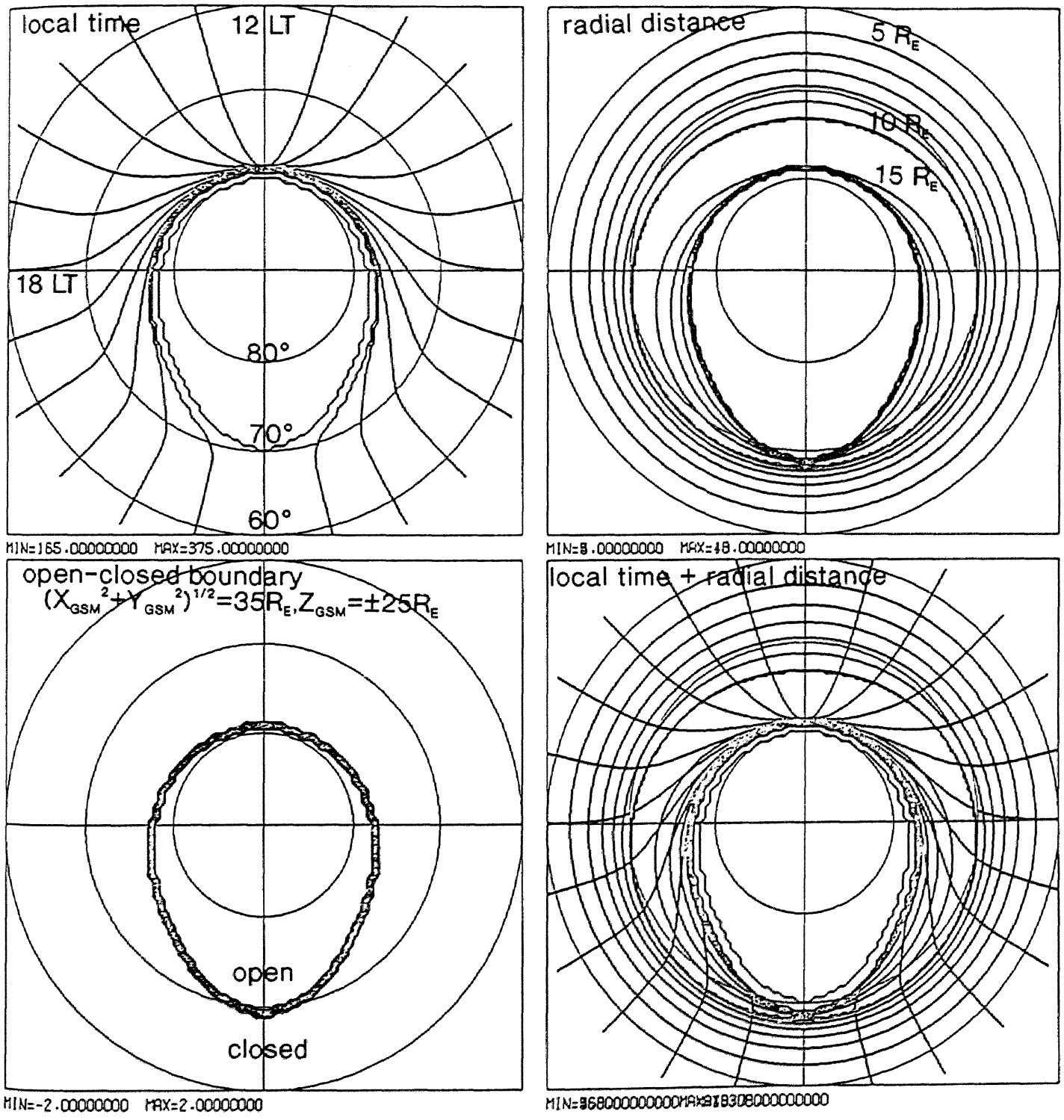

Figure 3.21 Magnetospheric equatorial coordinates mapped onto the ionosphere by using the T89 model (Kp = 0, 0+), in the same format as Figure 3.2.

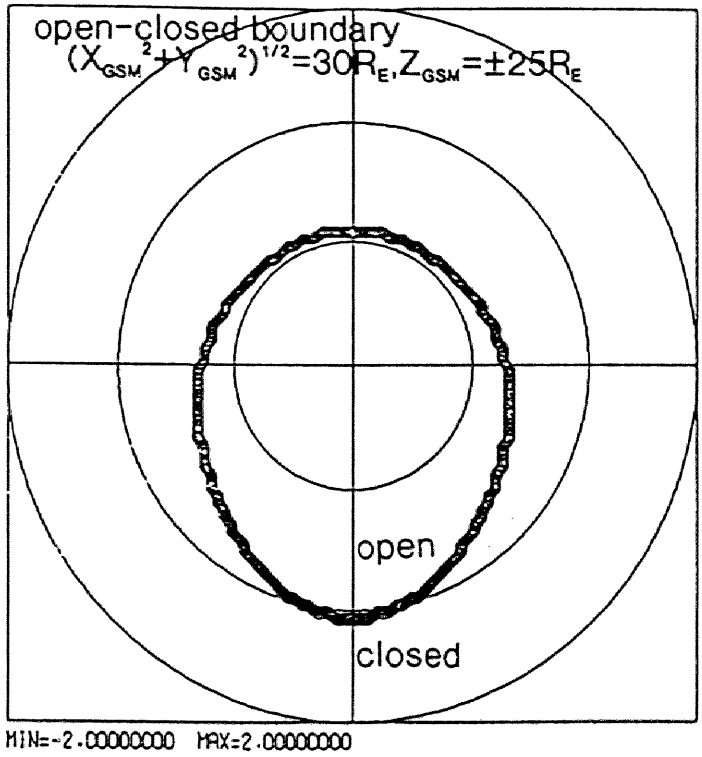

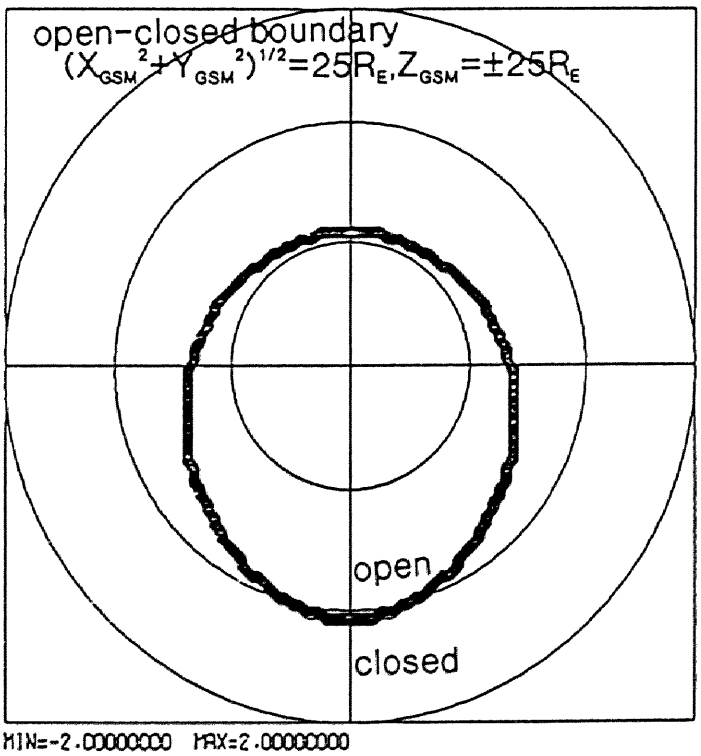

Figure 3.22 Open-closed boundary for different definitions by using the T89 model (Kp = 0, 0+). This boundary is not very sensitive to the chosen parameter ρ.

With the increase of Kp the open-closed boundary in the polar ionosphere expands equatorward (e.g. Figure 3.23, Kp $\geq$ 5–), keeping the shape of the boundary approximately the same. The converging structure of the equi-local time contour lines at the cusp region is, for all Kp, the same as that for the T87T model.

Figures 3.24 and 3.25 show the result of the mapping from the polar ionosphere to the geomagnetic equatorial plane. For all Kp the shape is parabolic and appears to be reasonable (e.g. Figures 3.24, Kp = 0, 0+ and 3.25, Kp $\geq$ 5–). Note that the pattern of equi-local time contour lines is quite different from that in the T87 model (e.g. Figure 3.8); on the nightside the contour lines are aligned in the radial direction rather than in the noon-midnight direction. This is probably because in the T89 model the magnetotail current is assumed to flow approximately in the azimuthal direction while in the T87 model it is assumed to flow approximately in the dawn-dusk direction rather than in the azimuthal direction. We cannot say which model is closer to the real magnetospheric magnetic field, because we do not know the real distribution of the current. We will discuss this matter after comparing these results with that of the model based on the 3-dimensional MHD simulation in Section 3.1.4.

3.1.4. Magnetic field model based on 3-dimensional MHD simulation of the magnetosphere

So far we have examined the characteristics of Tsyganenko's models by executing the mapping from the geomagnetic equatorial plane onto the polar ionosphere and vice versa. The most serious problem with these empirical magnetospheric magnetic field models is that they deal with only the magnetic field without any consideration of plasma parameters and hence the model magnetic field distribution is not examined in terms of the total pressure balance. This consequently indicates that the model currents, given *a priori*, are not necessarily consistent with the plasma pressure gradient which must be balanced with the magnetic field pressure.

The 3-dimensional MHD modeling of the magnetosphere by computer simulation (e.g.

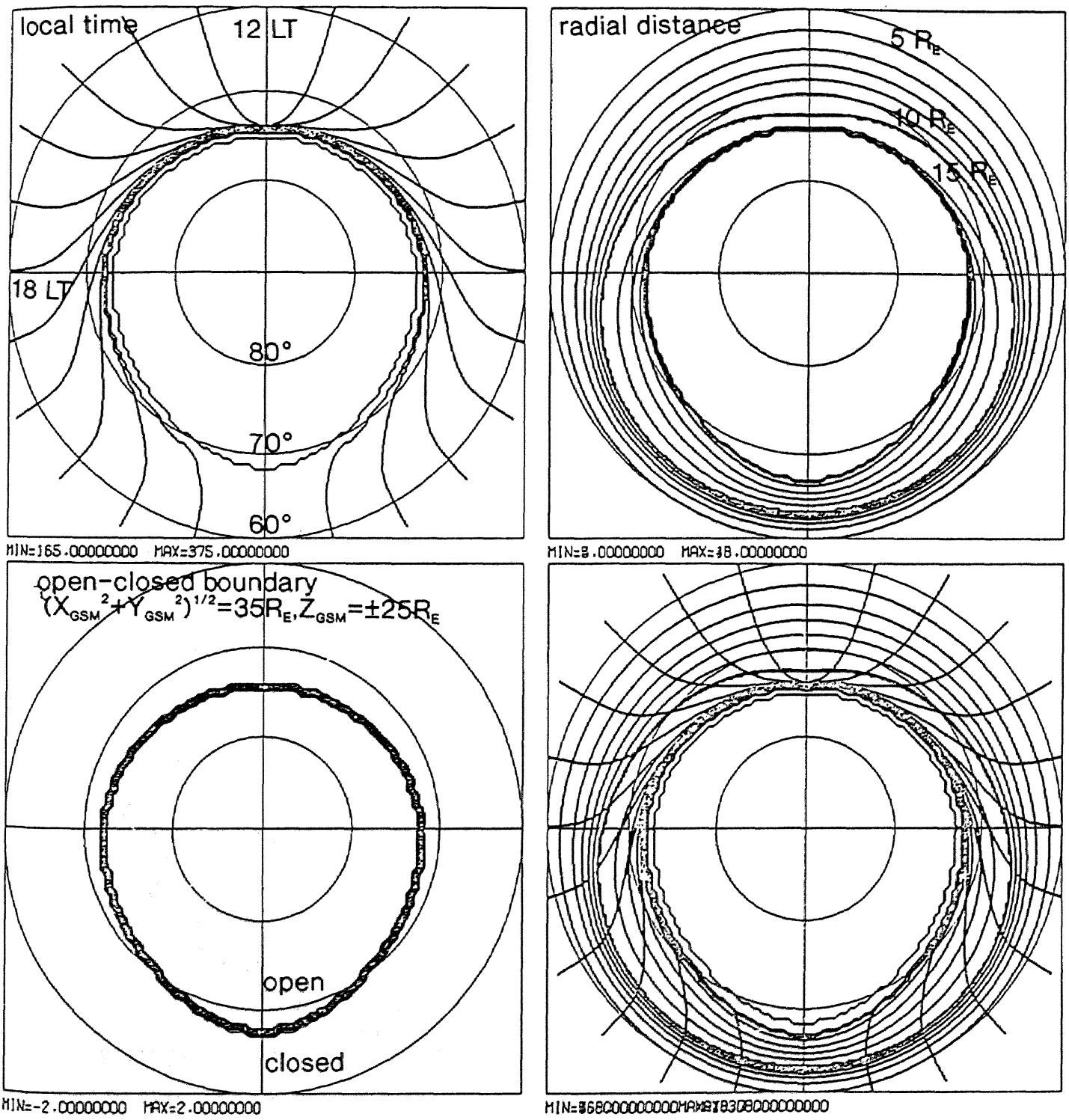

Figure 3.23 Similar to Figure 3.21 for Kp $\geq$ 5-.

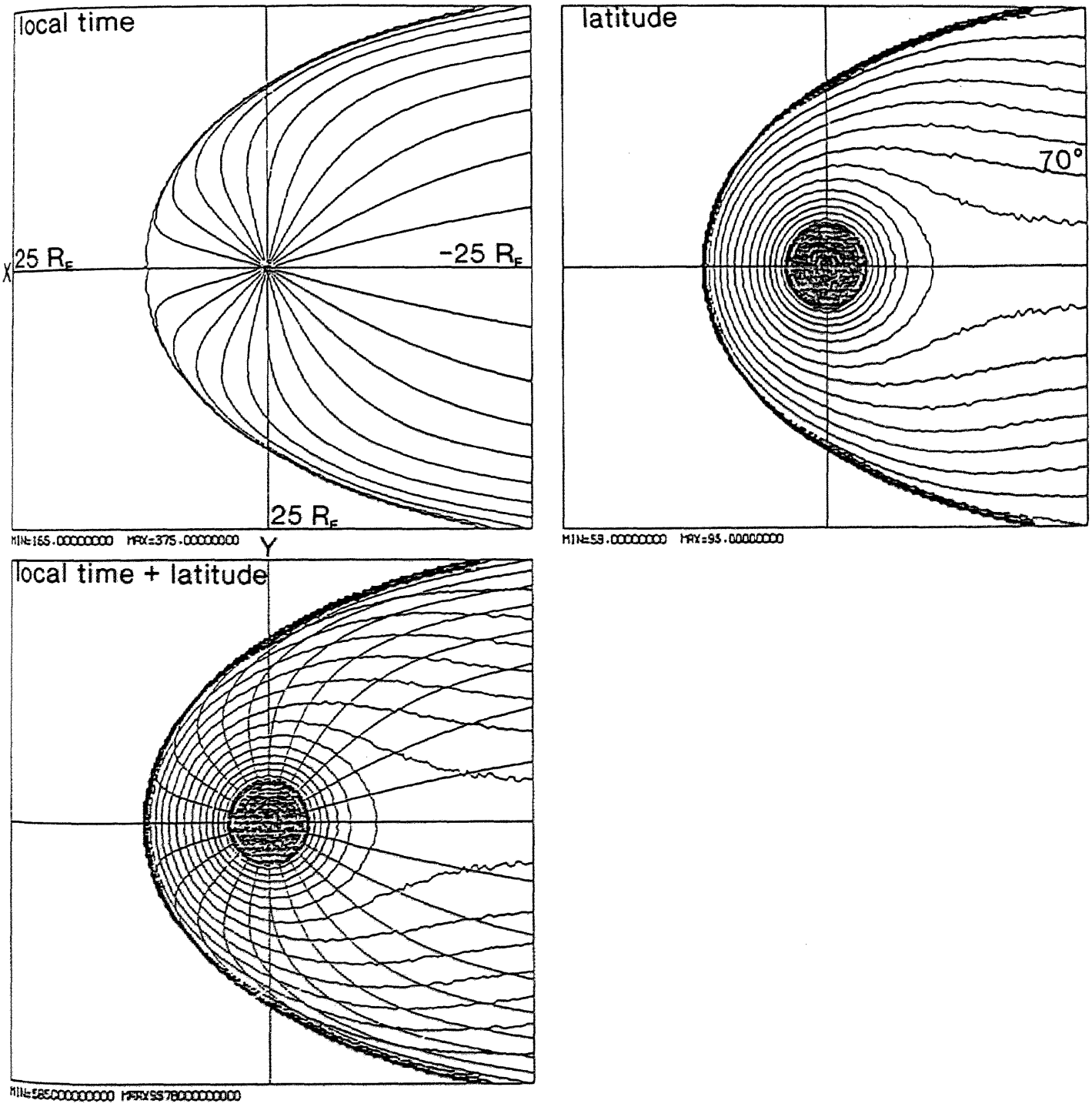

Figure 3.24 Polar ionospheric coordinates mapped onto the geomagnetic equatorial plane by using the T89 model (Kp = 0, 0+), in the same format as Figure 3.8.

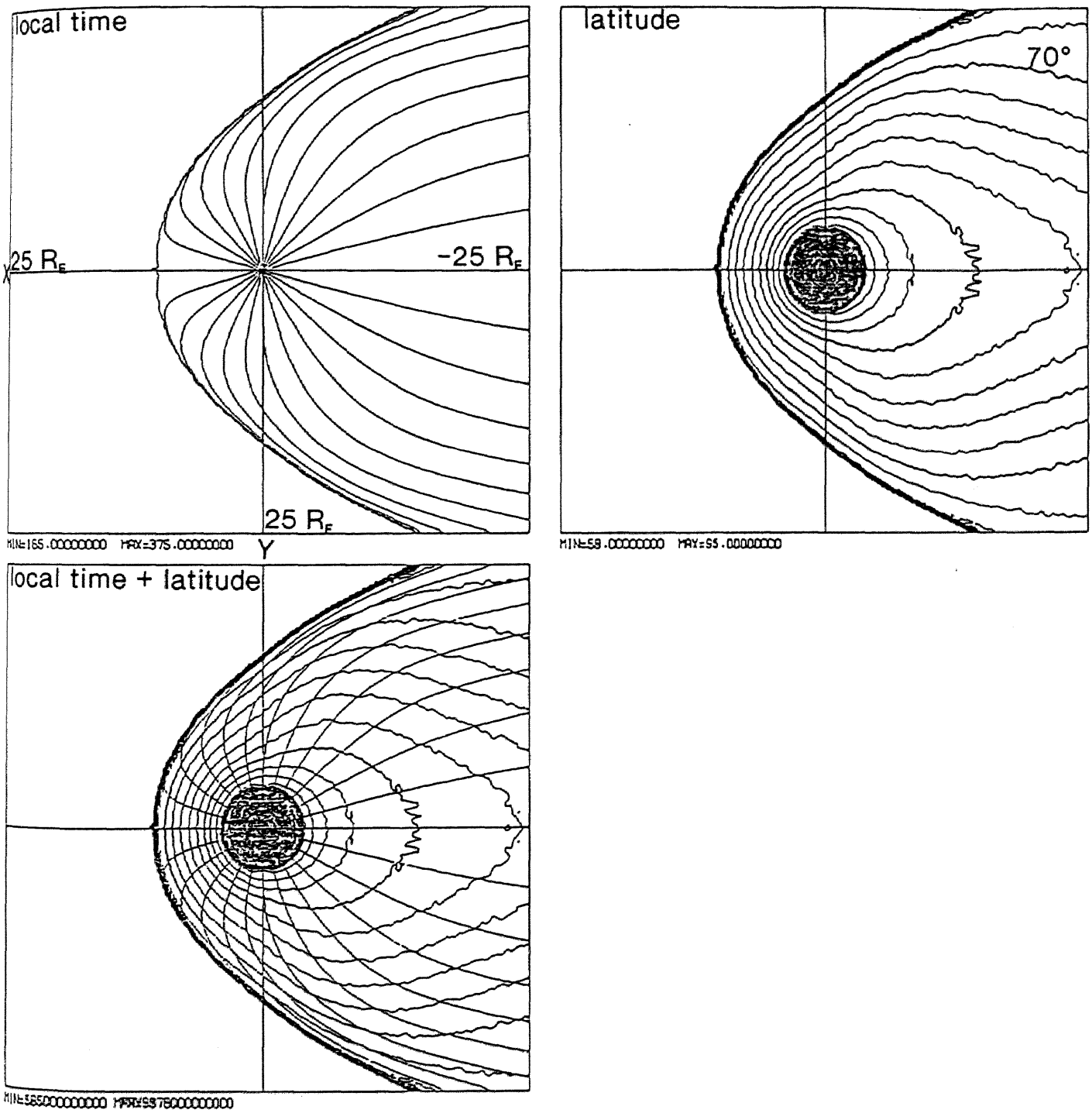

Figure 3.25 Similar to Figure 3.24 for Kp $\geq$ 5-.

Ogino, 1986) provides these parameters consistently with each other, and can be one of the most promising methods for magnetospheric magnetic field modeling, in spite of several shortcomings such as the numerical diffusion and insufficient resolution of the grid size.

Figure 3.26 shows one example of the result of mapping based on the magnetic field distribution obtained from the 3-dimensional MHD simulation by Ogino (private communication, 1991). The MHD and Maxwell's equations are solved as an initial value problem by using the two-step Lax-Wendroff scheme. The grid number of (Nx, Ny, Nz) = (240, 100, 100) and the grid spacing of $(\Delta x, \Delta y, \Delta z)$ = (0.25 R_E, 0.25 R_E, 0.25 R_E) are used. Parameters of the upstream uniform solar wind in this study are as follows: number density of 5/cc, velocity of 300 km/s and temperature of 2 x 10^5 °K. Solar wind magnetic field is assumed to be zero. Here we use the values 30 minutes after the initial state when a quasi-steady-state magnetospheric configuration was obtained. Figure 3.26 shows the mapping from the geomagnetic equator to the ionosphere, in the same format as Figure 3.2. Here the 'open' field lines are defined as the field lines passing across the plane (X_{GSM} = -35 R_E, Y_{GSM} = ± 25 R_E or Z_{GSM} = ±25 R_E), the boundaries of the simulation region, before crossing the geomagnetic equatorial plane. Since almost all the 'open' field lines pass across the plane X_{GSM} = -35 R_E first and the radial distance contour lines are very close to each other for R ≥ 20 R_E, this definition is not much different from that used in discussing the T87 and T89 models. The open-closed boundary is tear-drop shaped, although it is much smaller than that obtained by using the T87 and T89 models for the smallest Kp. One important point is that the equi-local time contour lines on the nightside have sharp bends at latitude ~ 72°. As seen in Figure 3.26, the local time contour lines are almost radially aligned for latitudes lower than 72°, whereas they turn sharply towards dawn or dusk approximately along the open-closed boundary in the latitude higher than ~ 72°, then converge at the ionospheric cusp region. This feature is not found in any of the mapping result using Tsyganenko's models; the equi-local time contour lines on the nightside turn much slower in all versions of Tsyganenko's models (e.g. Figures 3.2). These sharp bends of the local time contours in the

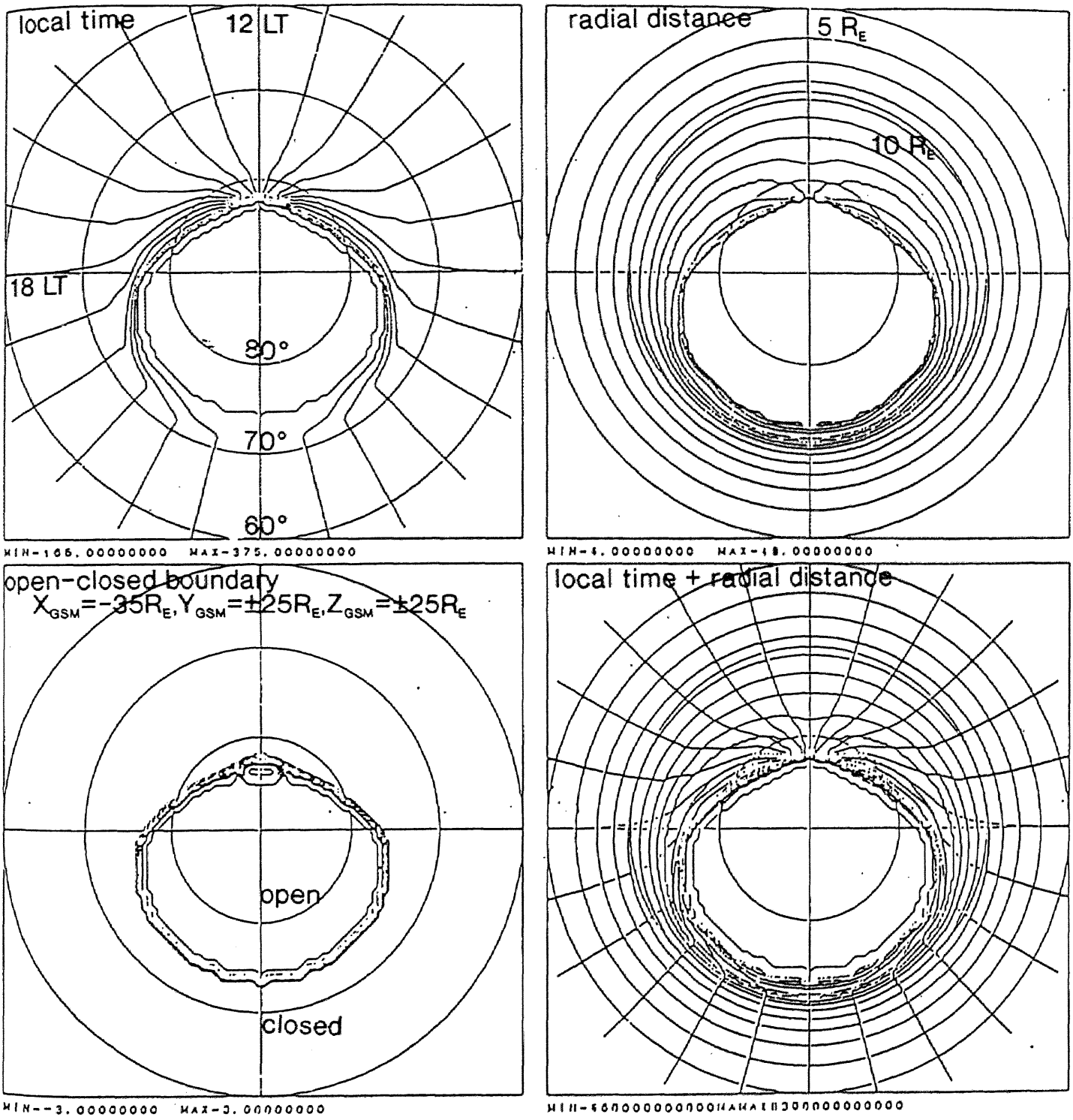

Figure 3.26 Magnetospheric equatorial coordinates mapped onto the polar ionosphere by using the model based on the 3-dimensional MHD simulation by Ogino (private communication), in the same format as Figure 3.2.

simulation indicate the presence of localized field-aligned current sheets as will be discussed later.

Figure 3.27 shows the result of mapping from the ionosphere to the geomagnetic equator by using the model based on the MHD simulation. In the near-earth magnetotail ($\rho > 13$ R_E) the contour line of the local time deviates dawnward (duskward) on the dawn (dusk) side relative to the radial direction (convex outward), indicating the presence of large-scale field-aligned currents. To explain these contour lines, this region must be sandwiched by Region 1 (earthward on the dawnside and tailward on the duskside) and Region 2 (tailward on the dawnside and earthward on the duskside) field-aligned currents and the field lines deviate duskward (dawnward) in the dusk (dawn) region in going from the ionosphere to the geomagnetic equator. On the other hand, these deviations are not conspicuous in the result by using Tsyganenko's models (e.g. Figures 3.2, 3.4). This fact shows that the effect of large-scale but localized field-aligned currents is not systematically included in Tsyganenko's model, although it may be widespread in the magnetosphere without any localized structure. The detailed discussion will be given in Section 3.2.

3.1.5. Discussion

In the above we have made a mapping analysis of the magnetosphere, by using Tsyganenko's models and a 3-dimensional MHD simulation of the magnetosphere. The characteristics of each model are summarized in Table 3.1. As a result of mapping we have found several interesting characteristics of Tsyganenko's models, together with the magnetic field model based on the MHD simulation.

Tsyganenko's models are based on satellite observations with limited spatial extent, so that these models are limited. The data coverage of the TU82 model ($X_{GSM} \gtrsim -20$ R_E) and the T87L model ($X_{GSM} \lesssim -30$ R_E) is smaller than that of the T87 and the T89 models, which is up to $X_{GSM} \sim -70$ R_E beyond the lunar orbit in the magnetotail. Beyond the data coverage region the model magnetosphere often shows unrealistic features (e.g. nightside boundary

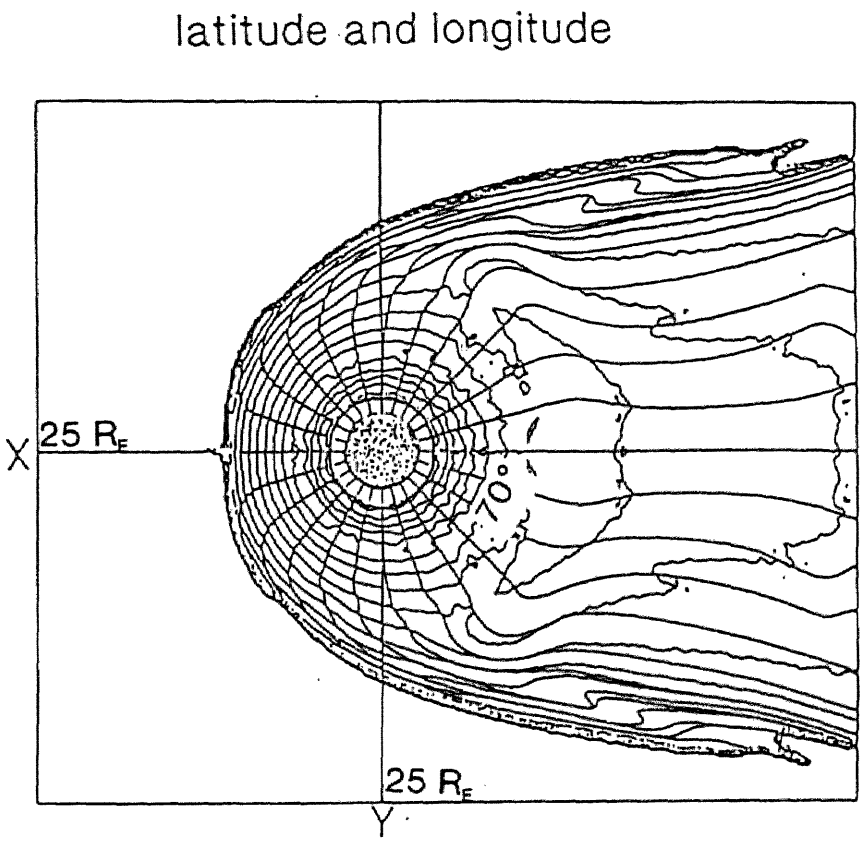

Figure 3.27 Polar ionospheric coordinates mapped onto the geomagnetic equatorial plane by using the model based on the 3-dimensional MHD simulation.

MODEL	O-C boundary	MP Boundary	contour line of LT on the magnetospheric equator	
			near tail ($X \gtrsim -10$)	distant tail ($X \lesssim -10$)
T87T	egg circular for high Kp	parabolic discon. in the flank for high Kp	stretched tailward	stretched tailward
T87L	tear-drop circular for high Kp	parabolic expans. in the dist. tail for high Kp	stretched tailward	stretched tailward
TU82	tear-drop circular for high Kp	circular (shrink in the tail)	stretched tailward	stretched tailward
T89	egg (reversed)	parabolic	radial	radial
MHD simulation	tear-drop (small)	parabolic	radial	stretched tailward

Table 3.1 Characteristics of the models, based on mapping analysis.

of the magnetosphere in the TU82 model in Figure 3.16).

Even within the data coverage region of the model, several defects due to the inadequate mathematical expression of the model are found, such as the unrealistic connection between magnetotail and ring current (the T87T model), and the inappropriate representation of the magnetic field in the high latitude magnetotail region (the T87L model). The shortcomings of these models, described above, occur because the mathematical expressions of these models are not appropriate for representing the specific region of the magnetosphere (especially the high latitude region of the magnetosphere). In other words, the simple mathematical expressions of these models are not realistic for representing the real magnetospheric magnetic field over a considerable spatial extent.

The comparison of the results obtained by using Tsyganenko's model with that of the 3-dimensional MHD simulation is one method of examining Tsyganenko's models. As a result of the examination of the projection of the ionospheric coordinates onto the geomagnetic equatorial plane, it is found that in the distant magnetotail ($X_{GSM} \leq -10\ R_E$) the T87L and the T87T models are similar to the 3-dimensional MHD simulation rather than the T89 model. The equi-local time lines are aligned with the sun-earth direction (as in the T87) rather than in the radial direction (as in the T89). On the other hand, in the near earth region ($X_{GSM} \geq -10\ R_E$) the equi-local time contour lines in the model of MHD simulation are similar to those in the T89 model rather than to the T87 model, i.e., aligned in the radial direction (as in T89) rather than stretched strongly antisunward (as in the T87). This is probably because the mathematical expression of the T87 model is suitable for representing the magnetic field in the distant magnetotail, while that of the T89 model is good for representing the magnetic field in the near earth region. Obviously, the mathematical expression of both models cannot be used to represent the real magnetic field over the whole magnetosphere.

The problem described above is partly due to the fact that Tsyganenko's models cannot represent the magnetic effect of localized currents such as field-aligned currents flowing between the ionosphere and the geomagnetic equator. This is evident from the comparison

with the mapping using the model based on 3-dimensional MHD simulation. The localized structure of the equi-local time contour lines in the near magnetotail of the model, based on the simulation, clearly indicates the presence of localized field-aligned currents while Tsyganenko's models do not show such localized features. The inability of Tsyganenko's models to represent the localized field-aligned currents is partly due to the data set dealt with here, which is comprised basically of statistical averages whereby the localized spatial structure of the real magnetosphere is smoothed. A more basic reason is that the mathematical expressions of Tsyganenko's models do not involve the magnetic effect of field-aligned currents. It is evident, as seen in the next section, that the expression cannot represent the magnetic field of the Region 1 and Region 2 currents, which are very much smaller in spatial extent near the ionosphere than near the geomagnetic equatorial plane, but are still essentially important in the large scale magnetospheric magnetic field configuration.

It must be noted that the magnetic field model based upon the simulation still contains shortcomings when used for mapping the real magnetosphere between the ionosphere and the magnetosphere. This is because of several problems such as numerical friction of the simulation which leads to a restriction on the solar wind velocity. The velocity of the solar wind in the simulation cannot be higher than a certain value ($\sim$ 300 km/s). This is much smaller than the value of 600 to 700 km/s actually observed by the satellites during the events studied in Chapter 2, when the magnetosphere is rather disturbed. Nevertheless, the MHD simulation is the only method of modeling which considers the relationship between the plasma parameters and the magnetic field, and the model based on the simulation shows many meaningful structures such as the large-scale but localized field-aligned currents. Therefore it is worth while comparing this model with Tsyganenko's empirical magnetic field models.

In this section we suggest that the shortcomings of Tsyganenko's models are largely due to the absence of field-aligned currents. Next, we will examine in detail how the magnetic effect of field-aligned currents could, or could not, be included in the models.

3.2 Examination of field-aligned currents in Tsyganenko's models

3.2.1 Introduction

In Section 3.1, we have examined the magnetic field connection between the polar ionosphere and the geomagnetic equatorial plane by using Tsyganenko's magnetic field models. We noted several shortcomings of the models from the mapping analysis, some of which are likely due to the absence of field-aligned currents in Tsyganenko's model.

In this section we will examine the basic structure of Tsyganenko's models i.e. whether these models properly represent the magnetic field due to the field-aligned currents or not. Tsyganenko claims that the effects of field-aligned currents are included implicitly in those models in the expansion coefficients which represent the magnetic field due to magnetopause currents. However, the analytical expression of the magnetospheric magnetic field in Tsyganenko's models evidently does not involve the magnetic field due to large-scale, but localized field-aligned currents, which flow along the magnetic field lines between the geomagnetic equatorial plane and the polar ionosphere.

In spite of this, there are studies in which field-aligned currents, or rather, field-aligned components of the magnetospheric currents are calculated using Tsyganenko's magnetic field model. Figure 3.28 shows one result of the calculation (Elphic et al., 1987). The rotation of the model field (current vector) is calculated, the field-aligned component of the current is averaged from the geomagnetic equatorial plane to the polar ionosphere along magnetic field lines, and then the currents are projected onto the equatorial plane. Regions of field-aligned currents flowing into the ionosphere are represented by hatched areas, and regions of currents flowing out of the ionosphere are represented by open areas. In the dayside and the near-earth nightside region, pairs of field-aligned currents with the polarity of Region 1, out of (into) the ionosphere on the duskside (dawnside), can be seen, and in the distant magnetotail a pair of field-aligned currents with the polarity of Region 2, opposite to the Region 1, are seen.

However, the field-aligned current averaged along the field lines does not necessarily

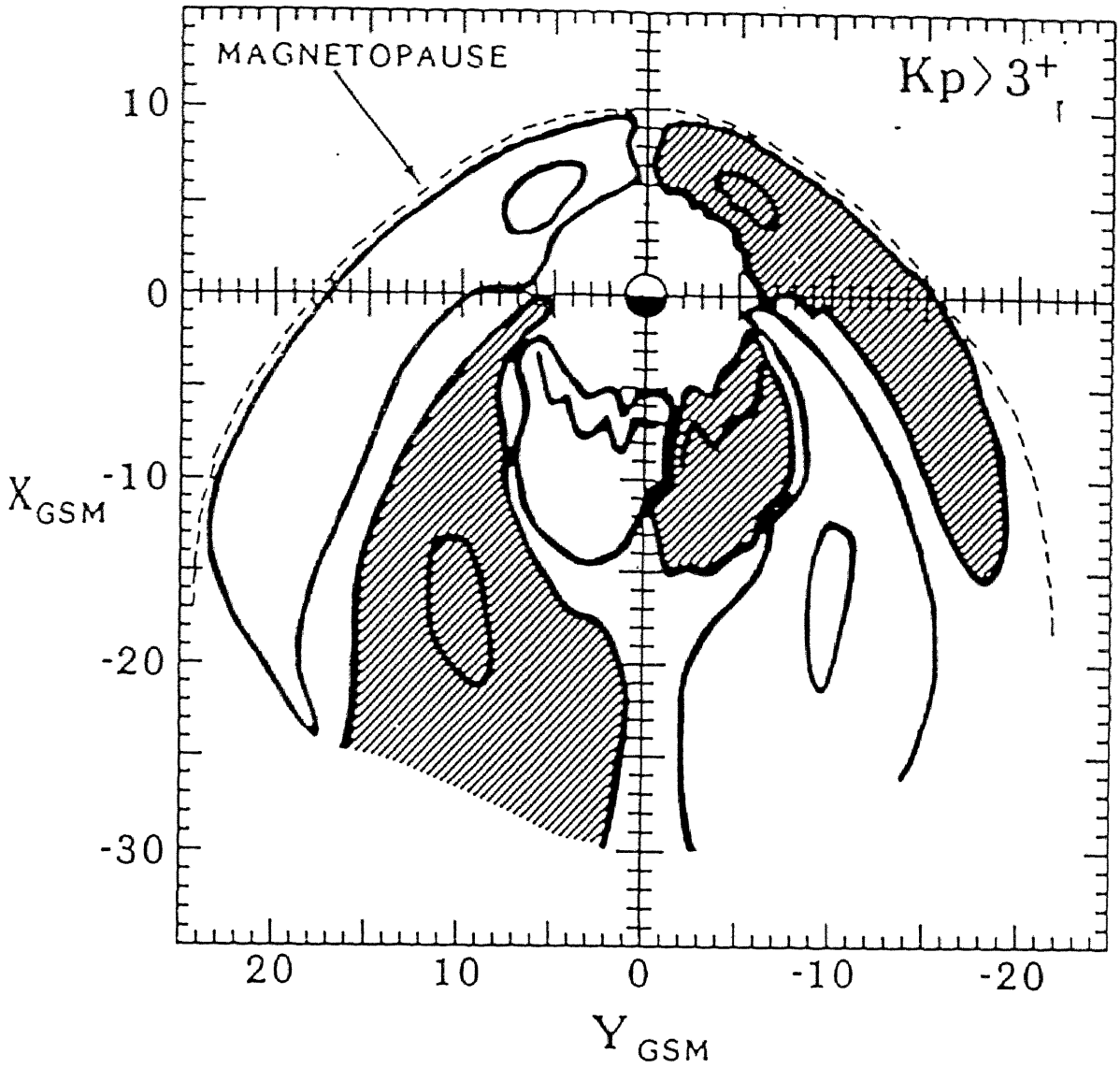

Figure 3.28 2-dimensional distribution of averaged "field-aligned currents" mapped onto the geomagnetic equatorial plane, by using the TU82 model (Elphic et al., 1988). Regions of field-aligned currents flowing into the ionosphere are represented by hatched areas, and regions of currents flowing out of the ionosphere are represented by open areas.

indicate the presence of the real field-aligned current flowing all the way between the magnetosphere and the ionosphere. Instead, this is most likely due to the field-aligned component of the model currents given *a priori*. Up to now the continuity of field-aligned currents i.e. distribution of field-aligned currents from the polar ionosphere to the geomagnetic equatorial plane along magnetic field lines of these models, have not yet been examined. Since in Tsyganenko's model no analytical expression satisfies the field-aligned current continuity near the ionosphere, all of these field-aligned components of currents must be "short-circuited" before reaching the ionosphere, and therefore could not be called field-aligned current.

In this section we examine the nature of the "field-aligned current" included in Tsyganenko's model, first by the 2-dimensional distribution of the field-aligned component of the currents averaged along the magnetic field lines, and then by the distribution of the current along the magnetic field line to see how the continuity of the current is satisfied along the field lines. We also examine which of the three terms included in the model, namely ring current, magnetotail current, and magnetopause current term, is responsible for the field-aligned component of the current, to check what meaning the "field-aligned current" has in Tsyganenko's model.

3.2.2 Calculation of field-aligned currents

Before discussing current continuity we examine the global distribution of the field-aligned component of the currents included in the models. First we calculate the 2-dimensional distribution of the currents averaged along the magnetic field lines in the same manner as the previous calculation (Elphic et al., 1987), although the "averaged field-aligned currents" here do not necessarily indicate the real field-aligned current. Figure 3.29 shows the distribution of the field-aligned component of magnetospheric currents as mapped to the northern polar ionosphere, averaged from the polar ionosphere to the geomagnetic equator using the TU82 model with Kp > 3+, with a dipole tilt angle of 0°. The magnitude of the current is normalized by the total intensity of the magnetic field B, considering the flux

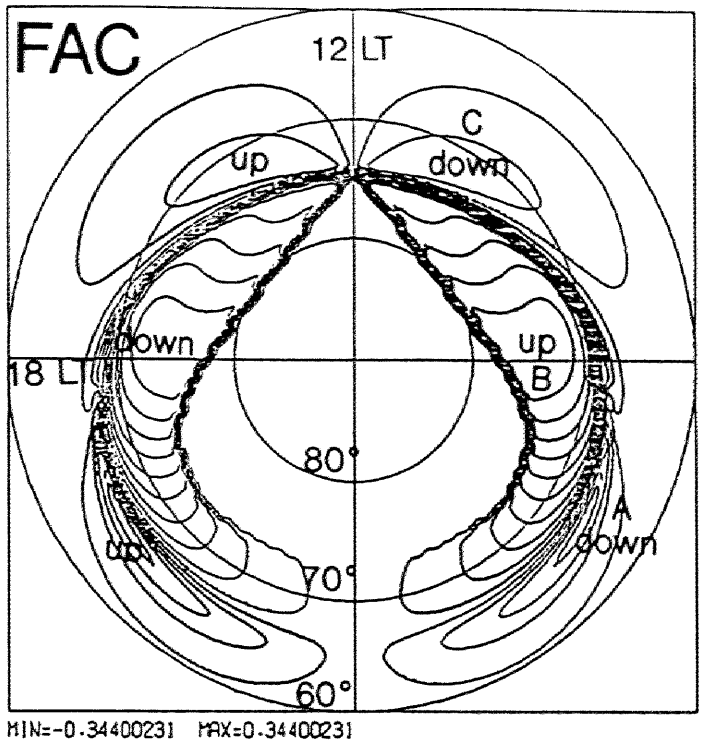

Figure 3.29 2-dimensional distribution of the field-aligned component of magnetospheric currents as mapped to the northern polar ionosphere, averaged from the polar ionosphere to the geomagnetic equator using TU82 model with Kp > 3+, with the dipole tilt angle = 0°. Thick lines indicate the upward (or tailward) field-aligned component of the current, and thin lines indicate downward (earthward) field-aligned component.

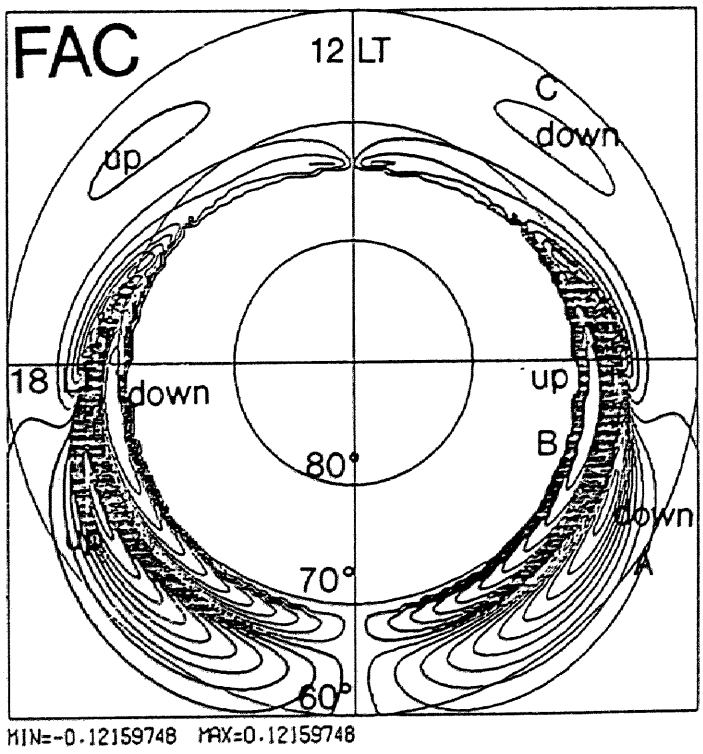

Figure 3.30 Similar to Figure 3.29 by using the T87T model (Kp $\geq$ 5+).

continuity. A pair of currents with Region 1 polarity, that is, downward (upward) on the dawnside (duskside), is seen in the nightside low-latitude (66°) region. A pair of currents with Region 2 polarity is seen in the nightside high-latitude (71°) region. A pair of currents with the Region 1 polarity is also located in the dayside low-latitude (66°) region. Naturally, the polarity of these currents is the same as that in the previous study (Elphic et al., 1987) shown in Figure 3.28. Evidently the current distribution in Figure 3.29 is inconsistent with the observation of the field-aligned currents (e.g. Figure 1.2).

We obtain almost the same result by using the T87T model with Kp $\geq$ 5+ (Figure 3.30) and the T87L model with Kp $\geq$ 5– (Figure 3.31). The dayside current system certainly exists for all the models, although for the T87L model it is too weak to be apparent in Figure 3.31. For other Kp values of these models we also obtain similar patterns (not shown).

The definite discrepancy between the pattern of the field-aligned current observed by the satellite and that estimated from these models is enough to disclaim the validity of the field-aligned currents in these models. Obviously the "field-aligned current" in Figure 3.29 is not the real field-aligned current. In order to examine where the "field-aligned currents" in Tsyganenko's models come from, we examine the distribution of the "field-aligned current" along magnetic field lines. From now on we use the T87T model (with Kp $\geq$ 5+), which was used in estimating the foot point of the geosynchronous satellite in Chapter 2. We have obtained approximately the same result by using other models (not shown here).

Here we deal with the field line originating from the ionospheric point with maximum averaged field-aligned current density of the Region 1 polarity, that is, at latitude 65° and 20 L.T. The distribution of the current density along magnetic field lines by using the T87L model is shown in Figure 3.32. The left and right limits of this figure correspond to the ionosphere and the geomagnetic equatorial plane respectively. The current is normalized by the total intensity of the magnetic field, considering the flux continuity. It is evident that the field-aligned component of the current is highly localized near the geomagnetic equatorial plane (at latitude $\sim$ 10°). This strongly suggests that the "field-aligned current" here, flowing

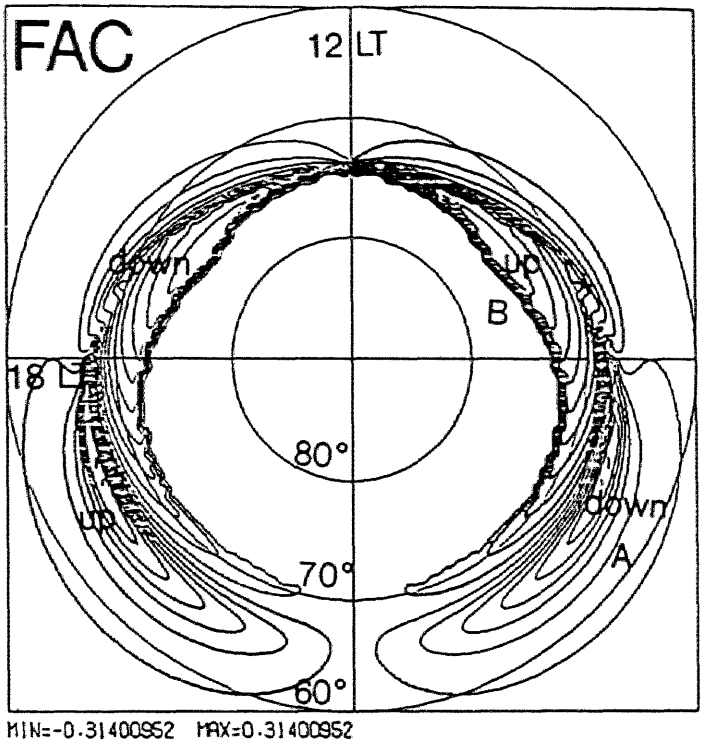

Figure 3.31 Similar to Figure 3.29 by using the T87L model (Kp $\geq$ 5-).

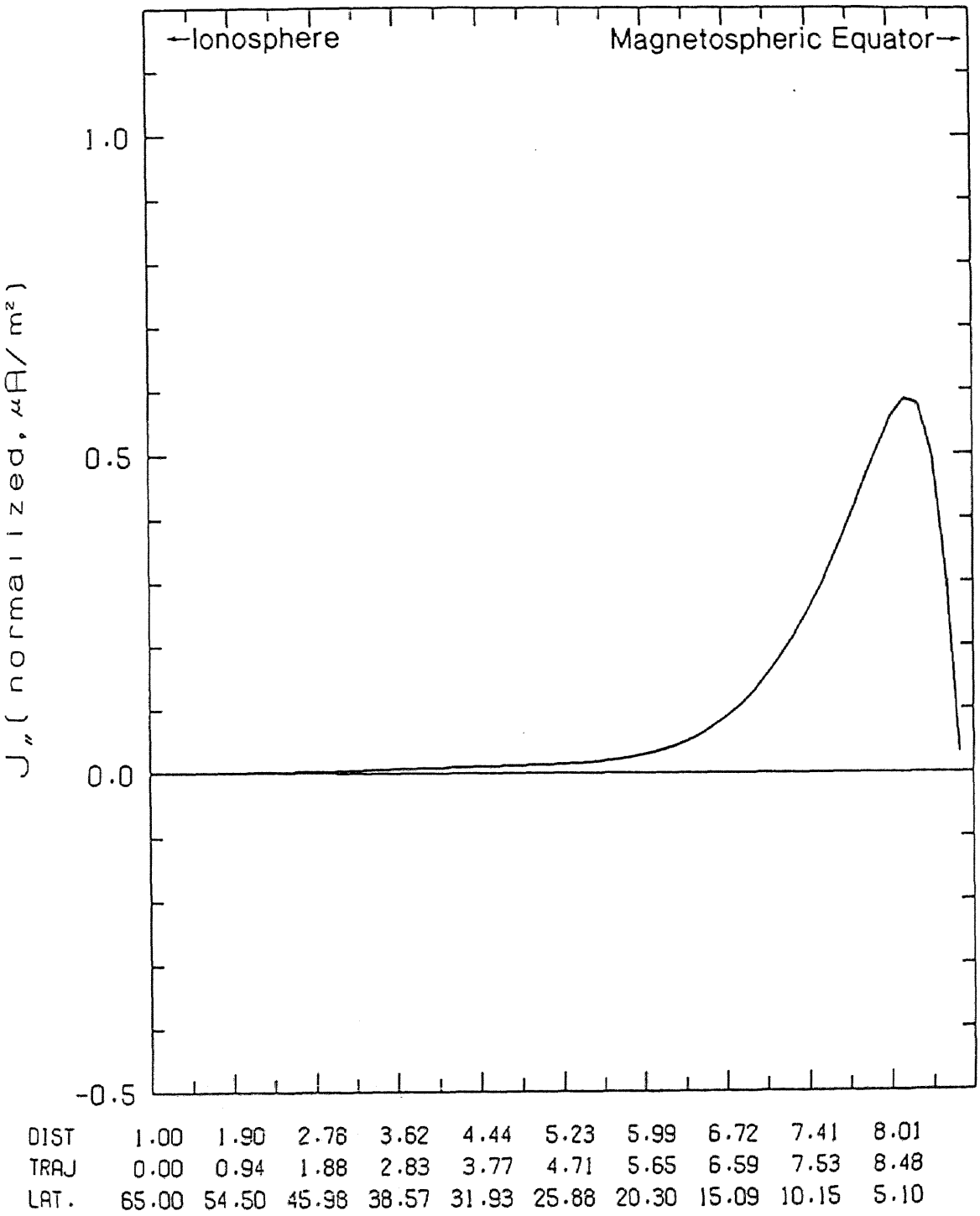

Figure 3.32 Distribution of the field-aligned current density along the magnetic field line originating from the ionospheric point at latitude 66°, and 22 L.T. by using the T87L model (Kp $\geq$ 5-). The left and right limits of this figure correspond to the ionosphere and the geomagnetic equator respectively. The current is normalized by the total intensity of the magnetic field, considering the flux continuity.

from slightly above the geomagnetic equator, is nothing more than a field-aligned component of the magnetospheric equatorial current given *a priori* in these models.

This is confirmed by examining which is responsible for the "field-aligned current" i.e. the ring, magnetotail or magnetopause currents given in these models. Figure 3.33 shows the contribution of these three terms included in the T87T model to the field-aligned component of the current along the magnetic field lines originating from the ionospheric point at latitude 60°, 20 L.T. The field-aligned components of current, due to all currents, are localized near the geomagnetic equator. It is evident that it is not the magnetopause current term but the magnetotail current term that significantly contributes to the field-aligned component of the current. This is in contrast to Tsyganenko's claim that some effects of field-aligned currents might be involved in the magnetopause current term in the form of a series expansion. The field-aligned component comes mostly from magnetotail currents given *a priori* in Tsyganenko's model.

Tsyganenko's model gives the expression of magnetotail currents *a priori*, and, therefore, the field-aligned component of magnetospheric currents essentially depends on the model expression. For the T89 model we obtain a completely different result as shown in Figure 3.34, which represents the distribution of the averaged field-aligned current in the same format as Figures 3.29, 3.30 and 3.31. On the duskside and dawnside low-latitude region a pair of currents are seen with the polarity of Region 2, and on the duskside and dawnside high-latitude region a pair of currents are seen with the polarity of Region 1. The sign of the currents is completely opposite to that for the T87L model, although these models are based on approximately the same satellite data set. This is due to the difference in the form of the magnetotail current given in the model; the magnetotail current given in the T87L model is more aligned with the dawn-dusk direction, while the current given in the T89 model is more aligned with the azimuthal direction.

From the above result, it is evident that Tsyganenko's model does not include the effect of field-aligned currents at all. That is, the calculation of "field-aligned current" (or field-

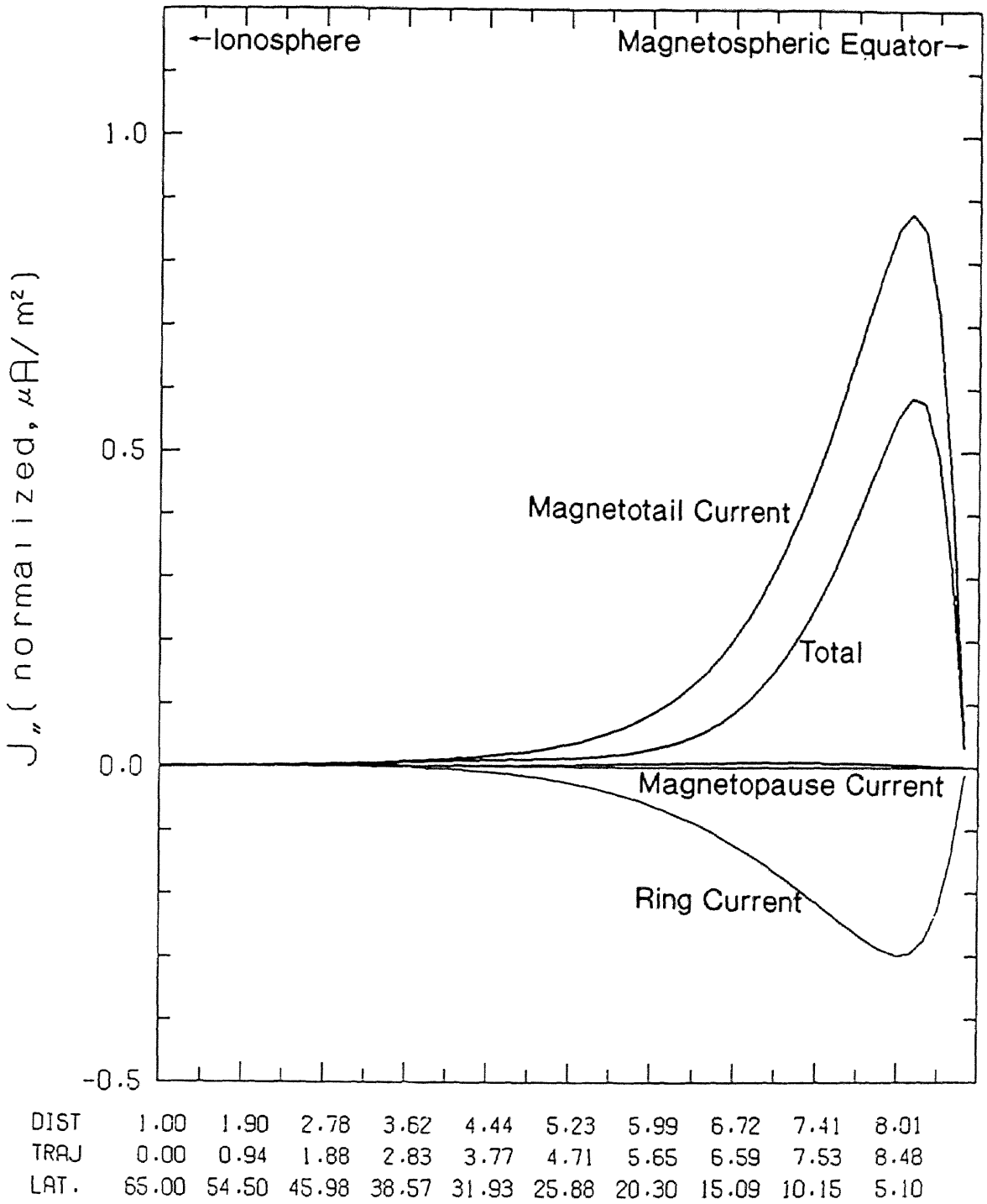

Figure 3.33 Contribution of the three terms (ring current term, magnetotail current term, and magnetopause current term) included in the T87T model to the distribution of field-aligned component of the current along the magnetic field line originating from the ionospheric point at latitude 65° and 20 L.T.

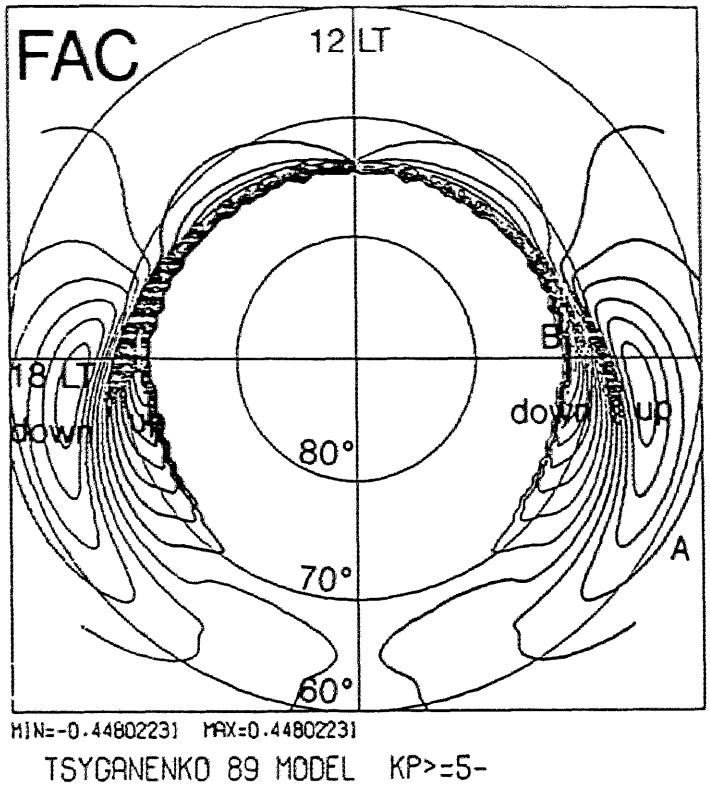

Figure 3.34 Similar to Figure 3.29 by using the T89 model (Kp $\geq$ 5-).

aligned component of the current) does not make sense in Tsyganenko's model, because the field-aligned component of the current comes from the form of the current given *a priori*, not from the parts of the series expansion determined from the fitting method.

3.3 Summary

In this chapter we have examined Tsyganenko's magnetospheric magnetic field models by using two methods, mapping analysis and examination of field-aligned currents.

As a result of mapping we have found several shortcomings of Tsyganenko's models. These defects are due partly to the limited spatial extent of the data set (e.g. the shrinking of the nightside magnetotail flank in the TU82 model), and partly to the difficulty in representing the magnetic field over the whole magnetosphere in a rather simple mathematical expression (e.g. the hollows in the magnetotail flank in T87T model and the extraordinary expansion of the nightside magnetotail flank in the T87L model).

One important problem of the model is that the mathematical expression of the model cannot represent the magnetic effect of large scale but localized currents such as field-aligned currents. This is evident also from the comparison with mapping using the 3-dimensional MHD simulation. The absence of the large scale field-aligned currents in the model could also be one important reason why the model cannot express the whole magnetosphere appropriately.

We have also examined the nature of the "field-aligned currents" in Tsyganenko's models. We have found that the field-aligned component of the current is not from the magnetopause current term in the form of a series expansion, but from the magnetotail current term. This is in contrast to Tsyganenko's claim that field-aligned currents are implicitly included in the magnetopause current term.

Tsyganenko's models do not include the magnetic effects of field-aligned currents. Therefore it is necessary to introduce field-aligned currents into Tsyganenko's models, in order to know the magnetic field connection between the ionosphere and the magnetosphere. This

is essential for comparing magnetic field variations at geosynchronous orbit with auroral activity near the conjugate areas, which was made in Chapter 2. The actual procedure to introduce the field-aligned currents into Tsyganenko's models and their effect on the magnetic field connection will be discussed in the next chapter.

4. Introduction of field-aligned currents into Tsyganenko's model

In Chapter 2 we have examined the field line connection between the ionosphere and magnetosphere at geosynchronous altitudes, by comparing the magnetic field variations at geosynchronous orbit with the spatial-temporal development of auroras near the conjugate areas estimated by using Tsyganenko's 1987 model (truncated version). We have found significant longitudinal deviation of the ionospheric foot point of the geosynchronous satellite from that estimated by using Tsyganenko's field line model. We consider that the major cause of the deviation is the magnetic effects of large-scale Region 1 and Region 2 field-aligned currents, because these effects are not included in Tsyganenko's model as already discussed in Chapter 3.

The existence of field-aligned currents has been confirmed since the the beginning of *in situ* satellite observations (e.g. Zmuda and Armstrong, 1974). These field-aligned currents must have a significant effect on the configuration of the magnetospheric magnetic field, as already discussed in Chapter 3. However, due to the localized nature of these field-aligned currents, up to now in the empirical modeling of the magnetosphere few attempts have been made to include the effect of field-aligned currents in a consistent way (Tsyganenko, 1988; Tsyganenko, 1991).

In this chapter we introduce Region 1 and Region 2 field-aligned currents into Tsyganenko's model to examine how much these currents affect the deflection of magnetic field lines threading the geosynchronous satellites. An estimate is also made of the intensity of the current which can account for the 10° azimuthal deviation of the real foot point of the geosynchronous satellite from the estimated foot point, as reported in Chapter 2.

4.1. Procedure for introducing field-aligned currents into Tsyganenko's model

The original model used in this study is the truncated version of Tsyganenko's external field model (1987) ($Kp \geq 5+$) plus the dipole field with a dipole tilt angle of 0°. We introduce

the effect of field-aligned currents into the model in the following way.

Since it is extremely laborious and requires enormous amount of CPU time to calculate the magnetic effect of field-aligned currents with continuous distribution, we approximate these currents by a number of line currents flowing from the ionosphere to the geomagnetic equatorial plane (and vice versa). One curved line current is approximated by a series of straight line currents, each of which produces a magnetic field $\mathbf{B}$ at an arbitrary observation point as follows:

$$\mathbf{B} = \sum \frac{\mu_0}{4\pi} \frac{I d\mathbf{s} \times \mathbf{r}}{(d\mathbf{s} \times \mathbf{r})^2} \left\{ \frac{(d\mathbf{s} - \mathbf{r}) \cdot d\mathbf{s}}{|\mathbf{r} - d\mathbf{s}|} + \frac{\mathbf{r} \cdot d\mathbf{s}}{|\mathbf{r}|} \right\} \qquad (4-1)$$

where $\mathbf{r}$ is the vector from the starting point of one vector current to the observation point, $d\mathbf{s}$ is the current vector, and I is the current intensity. For example, in order to introduce the sheet current with the density of 1 μ A/m^2 and the latitudinal width of 5° on the ionosphere, which corresponds to the latitudinally integrated current intensity of 0.555 A/m, we consider line currents, each having the total current of 0.555 A/m × 1° longitude, if the longitudinal separation between these currents is 1°.

This line current approximation is valid if the observation point is located at a distance to any line current which is large compared to the separation between neighboring line currents. This might not be valid near the ionosphere where the observation point comes much closer to the nearest field-aligned line current. However, the magnitude of the magnetic field deflection is expected to be very small in this region because the ambient magnetic field is much larger than the magnetic field produced by these currents. We confirmed the validity of this approximation by considering simple axisymmetric sheet-structured field-aligned currents in the magnetic dipole field, that is, the Region 1 upward field-aligned sheet current flowing out of the ionosphere at latitude 66°, and the Region 2 downward sheet current flowing into the ionosphere at latitude 62°. Both are considered symmetric with respect to the earth's magnetic dipole axis as illustrated in Figure 4.1, and closed with equatorial radial sheet currents. Integrating the magnetic field around the dipole axis and applying Ampére's law

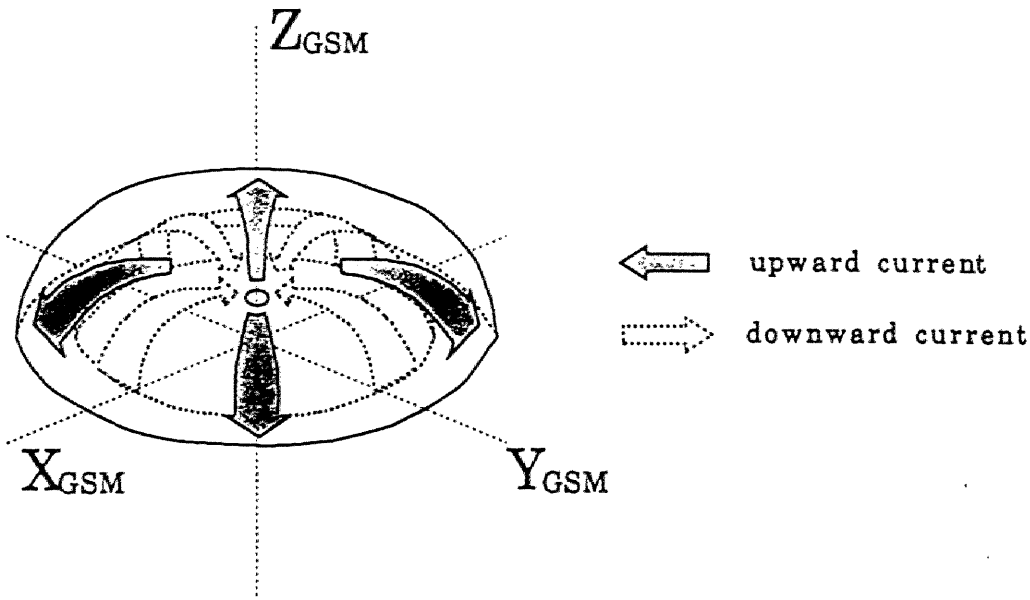

Figure 4.1 Schematic view of the axisymmetric sheet-structured field-aligned currents in the magnetic dipole field. The Region 1 upward field-aligned sheet current flows out of the ionosphere at latitude 66°, and the Region 2 downward sheet current flows into the ionosphere at latitude 62°. Both are symmetric with respect to the earth dipole axis.

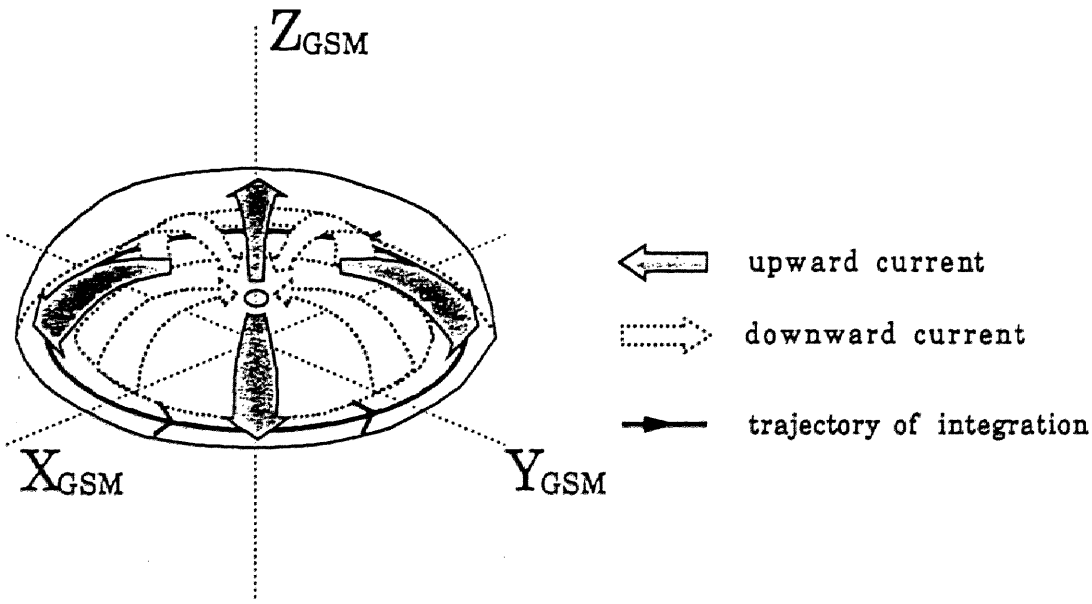

Figure 4.2 Trajectory of the integration made in deducing the equation (4–2).

as illustrated in Figure 4.2, we get the equation

$$2\pi\rho \cdot \mathbf{B} = \mu_0 I_{circ}, \tag{4-2}$$

where I_{circ} is the total Region 1 and total Region 2 currents flowing out of and into the ionosphere and ρ is the radial distance from the dipole axis in the cylindrical coordinates. Then the exact solution of the magnetic field produced by these field-aligned sheet currents can be obtained as,

$$\mathbf{B} = \frac{\mu_0 I_{circ}}{2\pi\rho}. \tag{4-3}$$

We also consider a number of field-aligned line currents flowing in the same way as the sheet currents, as shown in Figure 4.3. Although in these figures only field-aligned currents in one hemisphere are drawn, actually we calculate the effect of field-aligned currents in both hemispheres and that of equatorial radial currents. Figure 4.4 shows the azimuthal deviation of the magnetic field line originating from the ionosphere at latitude 64°, obtained for both sheet and line currents (with a separation of 1° and 10°), plotted against the distance along the magnetic field line from the ionosphere to the geomagnetic equator. The latitudinally integrated intensity is 0.555 A/m for both sheet and line currents. It is evident that the azimuthal deviation of the magnetic field line is almost the same all the way along the magnetic field line from the ionosphere to the geomagnetic equator for sheet and line currents.

When these field-aligned line currents are introduced, they of course modify the magnetic field and, as a result, these currents deviate from the original modeled magnetic field lines. Accordingly we must change the distribution of field-aligned currents until the flow direction of these currents becomes parallel to the magnetic field lines by using the iteration method. The major change of field-aligned current distribution caused by the currents themselves is, however, the azimuthal deflection of current flow lines from the original location. If the currents have a sheet structure in the azimuthal direction, this change does not affect the longitudinal deflection of the magnetic field line threading a geosynchronous satellite

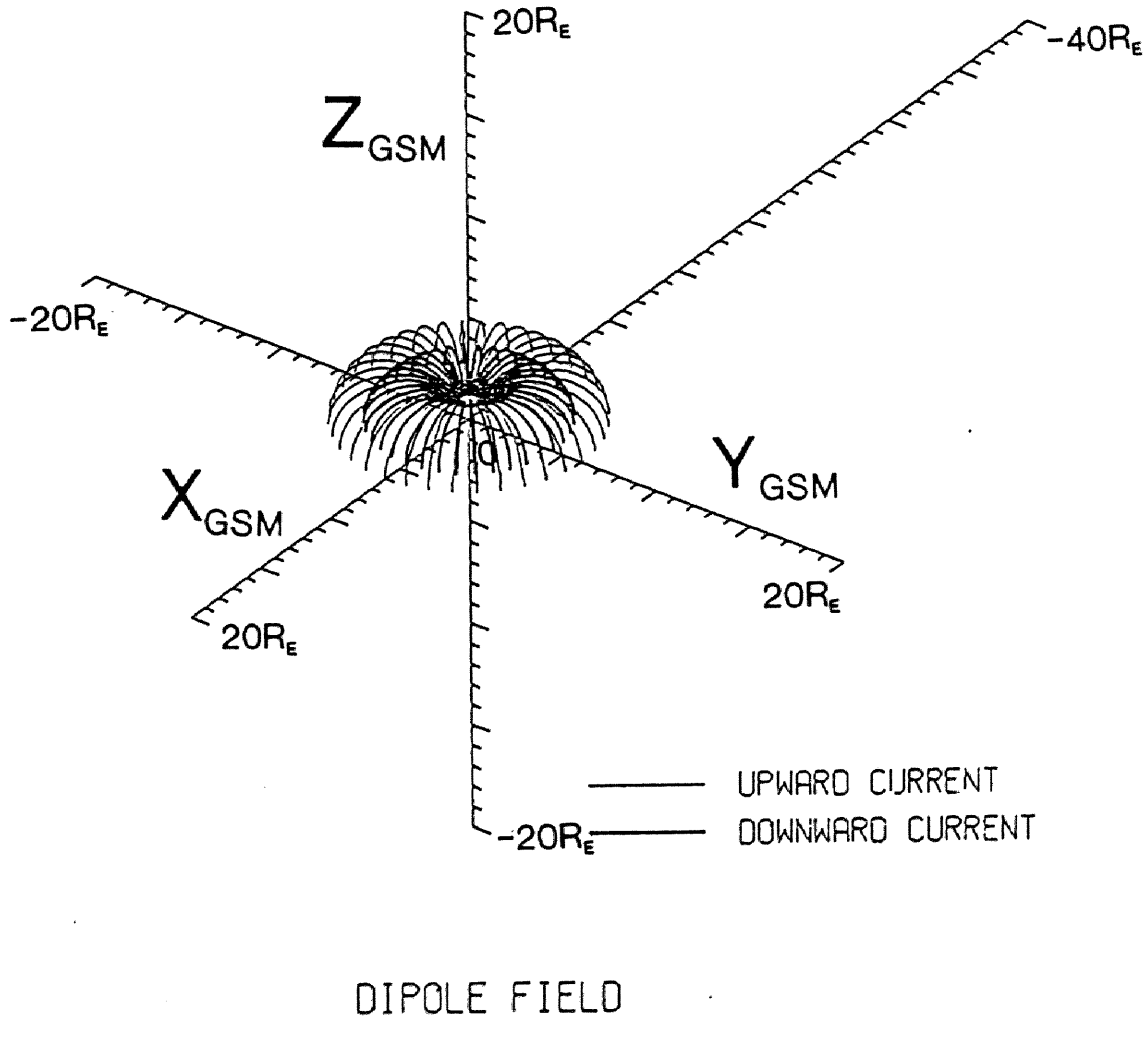

Figure 4.3 Schematic view of the field-aligned line currents flowing in the same way as the sheet-structured field-aligned currents illustrated in Figure 4.1.

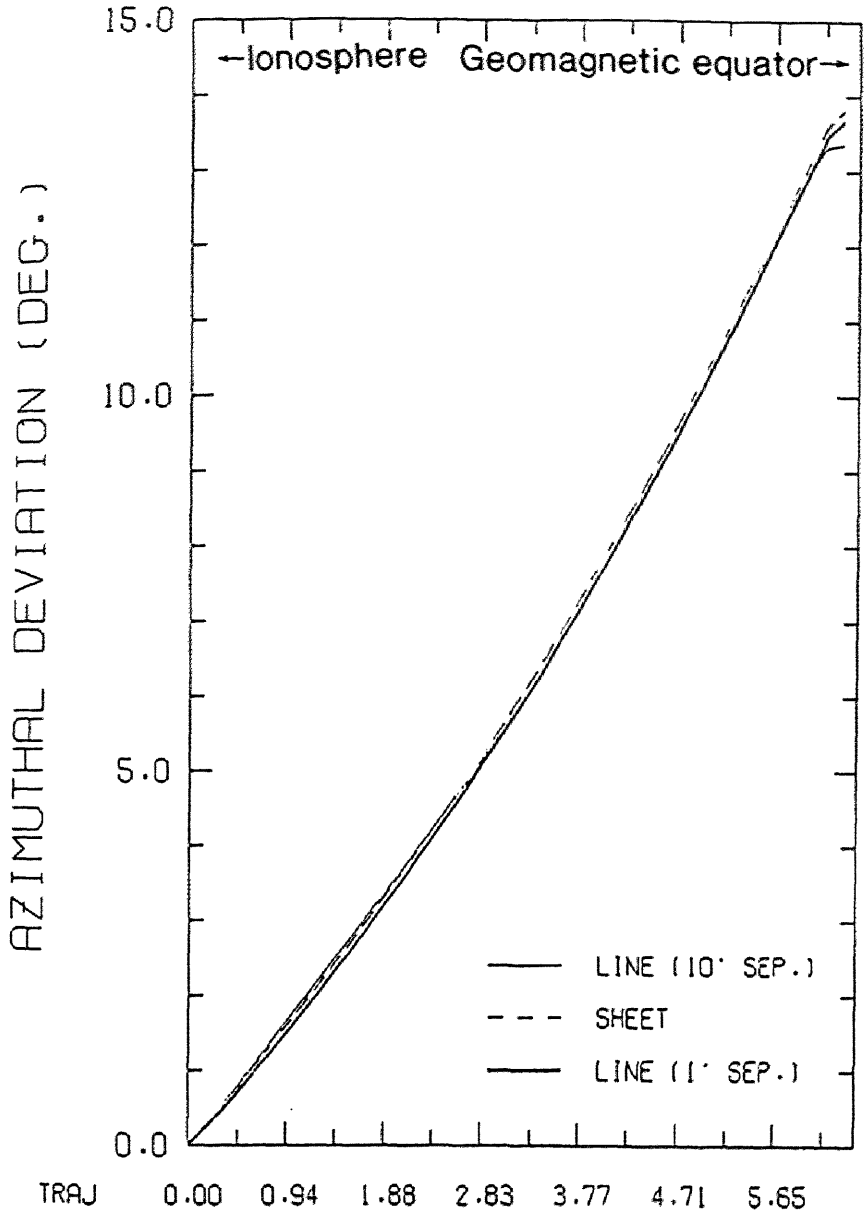

Figure 4.4 The azimuthal deviation of the magnetic field line originating from the ionosphere at latitude 64°, obtained by using sheet current and line currents with the separation of 1° and 10°, as a function of the distance along the magnetic field line from the ionosphere to the geomagnetic equator. The latitudinally integrated intensity is 0.555 A/m for both sheet and line currents.

surrounded by the Region 1 and Region 2 currents. This is indicated in Figure 4.5, where axisymmetric field-aligned line currents are introduced into the dipole magnetic field with the upward current flowing from the ionosphere at 66° lat. and the downward current flowing into the ionosphere at 62° lat., with longitudinal interval of 10°. This figure shows the geomagnetic equatorial end point of the magnetic field line originating from the ionosphere at latitude 64° and longitude 0°, together with the geomagnetic equatorial end point of the field-aligned line currents. The changes of these positions with the increasing step of iteration are marked by the numbers 1,2,...5. The intensity of the current used in this iteration is 0.277 A/m for the first step (to avoid the unrealistic deflection of the magnetic field line caused by approaching the neighboring line current), and 0.555 A/m for the second and the latter steps. The equatorial end points of the field-aligned current flow lines move westward by about 5° in longitude, for both upward and downward currents. However, the equatorial end point of the field line surrounded by upward and downward field-aligned currents, with the ionospheric end points fixed, hardly changes with the increasing step of iteration. Hence from now on we consider only the first-order approximation, that is, Region 1 and Region 2 field-aligned currents flow along the original model field lines.

On the basis of the line current approximation, as described above, we introduce field-aligned currents into Tsyganenko's 1987 model (truncated version). First we examine the spatial distribution of field-aligned currents. The 2-dimensional distribution of field-aligned currents on the ionosphere is obtained statistically by Iijima and Potemra (1976, 1978) from the TRIAD satellite data. Under quiet condition (Figure 4.6(a), Iijima and Potemra, 1978), Region 1 and Region 2 are located at 68° to 76° lat. and 64° to 74° lat. respectively. They are located at a lower latitude on the nightside than on the dayside. Around magnetic midnight the duskside and dawnside currents overlap each other with duskside Region 1 current connected to the dawnside Region 2 current. However, these field-aligned currents shift equatorward with increasing geomagnetic activity (Figure 4.6(b)). Under highly disturbed geomagnetic conditions, the latitude of the equatorward edge of the Region 1 current near

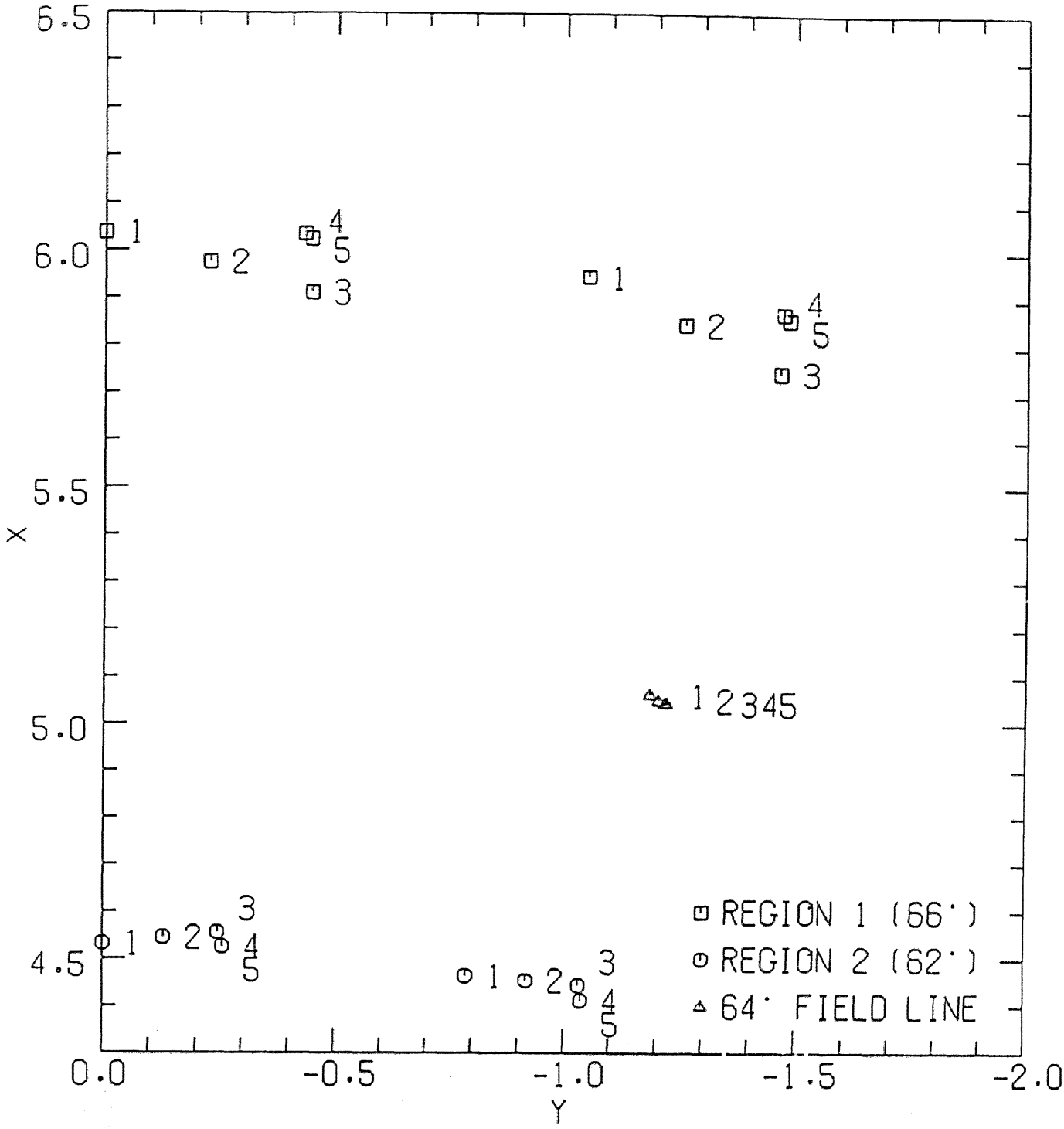

Figure 4.5 The change of the geomagnetic equatorial end point of the magnetic field line originating from the ionosphere at latitude 64° and longitude 0°, with the increasing step of the iteration of "field-aligned" currents, together with the geomagnetic equatorial end point of the field-aligned line currents. Here axisymmetric field-aligned line currents with the upward current flowing from the ionosphere at 66° lat. and the downward current flowing into the ionosphere at 62° lat., with the longitudinal interval of 10° are introduced into the dipole magnetic field.

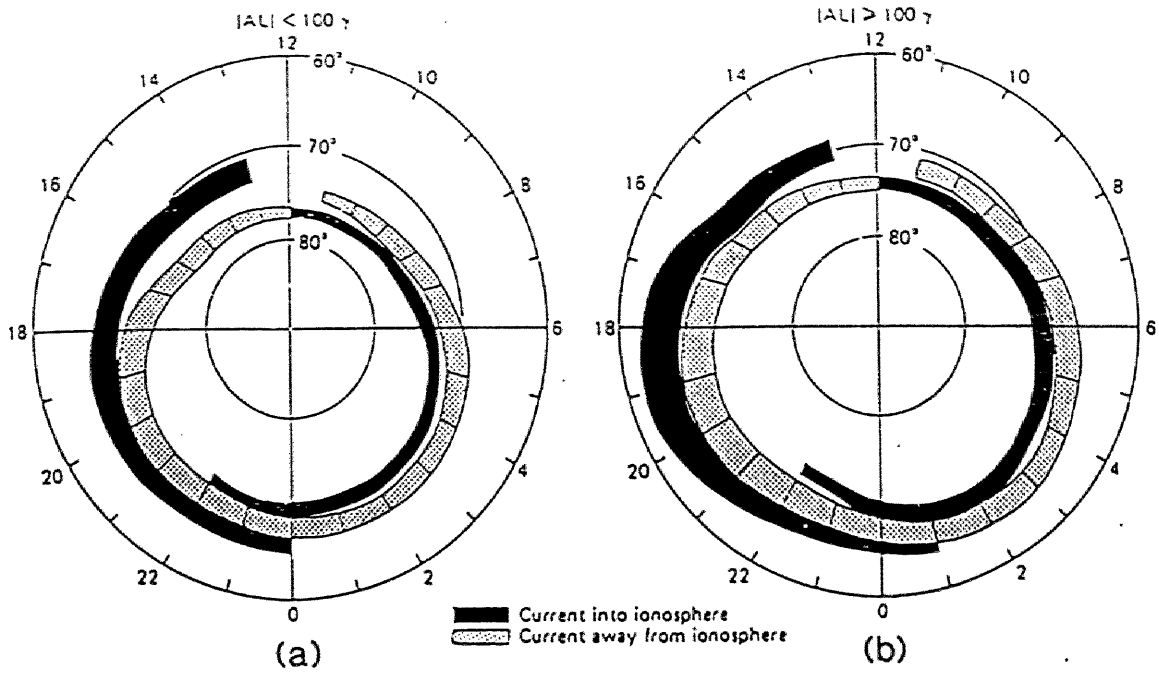

Figure 4.6 Two-dimensional distribution of field-aligned currents (a) for $|AE| < 100\ \gamma$ and (b) for $|AE| \geq 100\ \gamma$ (Iijima and Potemra, 1978).

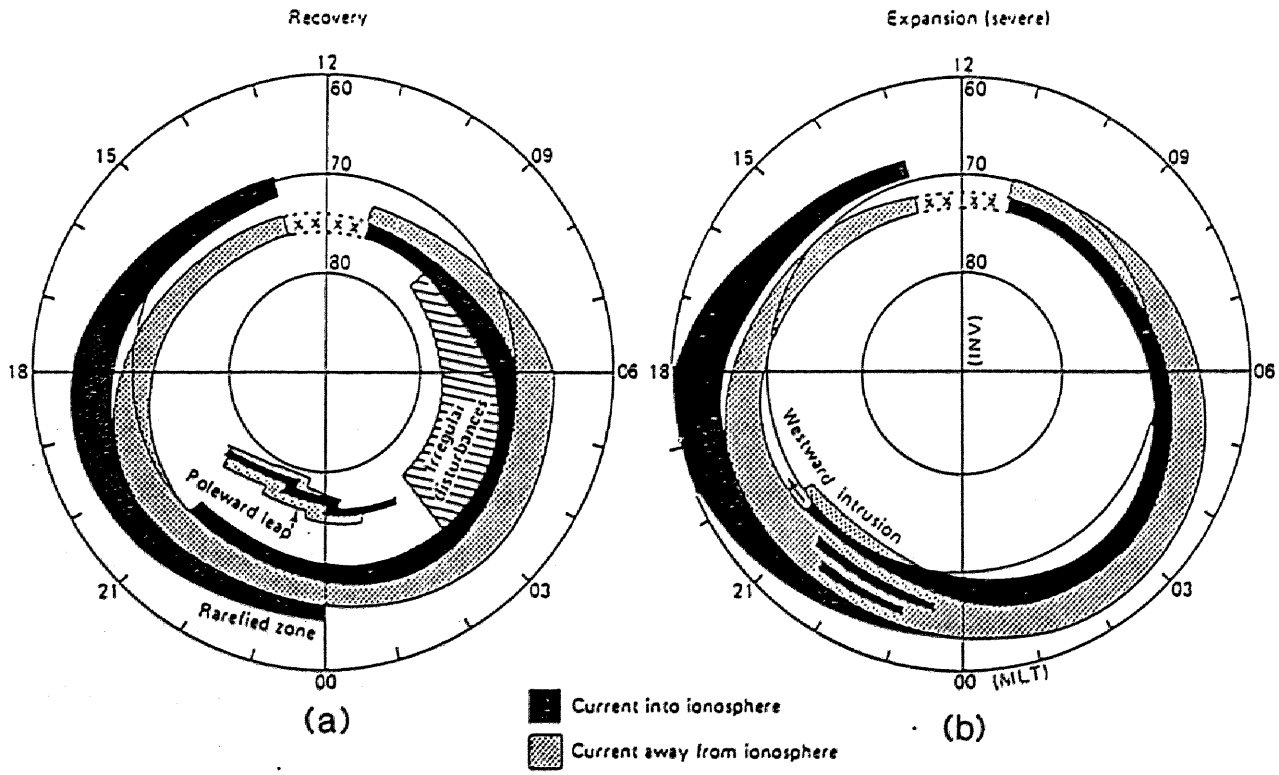

Figure 4.7 Two-dimensional distribution of field-aligned currents (a) for the recovery phase and (b) for the expansion phase of substorms (Iijima and Potemra, 1978).

midnight can be as low as 64° as shown in Figure 4.7. Moreover, the distribution of field-aligned currents changes drastically throughout the course of magnetospheric substorms, as shown in this figure, and is time-dependent.

We are interested in the magnetic effect of the Region 1 and Region 2 field-aligned currents on the azimuthal deviation of the ionospheric foot point of the geosynchronous satellite on the nightside under disturbed geomagnetic conditions. Therefore we assume for simplicity that the Region 1 and Region 2 currents are distributed only on the nightside and are centered at constant geomagnetic latitudes 66° and 62° respectively on the ionosphere. They surround the magnetic field lines originating from the ionosphere at latitude 64°, which are connected to geosynchronous altitudes. That is, upward field-aligned currents are located at 66° lat. in the ionosphere from 1800 MLT to 0000 MLT and at 62° lat. from 0000 MLT to 0600 MLT, while downward field-aligned currents are located at 62° lat. from 1800 MLT to 0000 MLT and at 66° lat. from 0000 MLT to 0600 MLT. The distribution of these currents is indicated by the projection onto the polar ionosphere in Figure 4.8(a) and the schematic view in Figure 4.8(b). The consideration of only nightside field-aligned currents seems reasonable, because the dayside field-aligned sheet currents do not affect the deflection of the magnetic field lines near magnetic midnight very much. This will be shown in the next section.

Next we consider the intensity of the Region 1 and Region 2 field-aligned currents, which have been measured statistically in many studies (e.g. Iijima and Potemra, 1978). One example of the result is shown in Figure 4.9. On average the Region 1 current is more intense than the Region 2, whereas near midnight the intensity of the Region 1 and Region 2 field-aligned currents are approximately the same. Since we are dealing with magnetospheric and ionospheric phenomena near magnetic midnight, we assume that the intensity of the Region 1 and Region 2 currents is the same. Of course the intensity of these currents depends on the geomagnetic activity level (Iijima and Potemra, 1976), although we do not know the precise temporal variation of the intensity of the field-aligned currents during the course of magnetospheric substorms. First we use a sheet current intensity of 0.3 A/m as the average

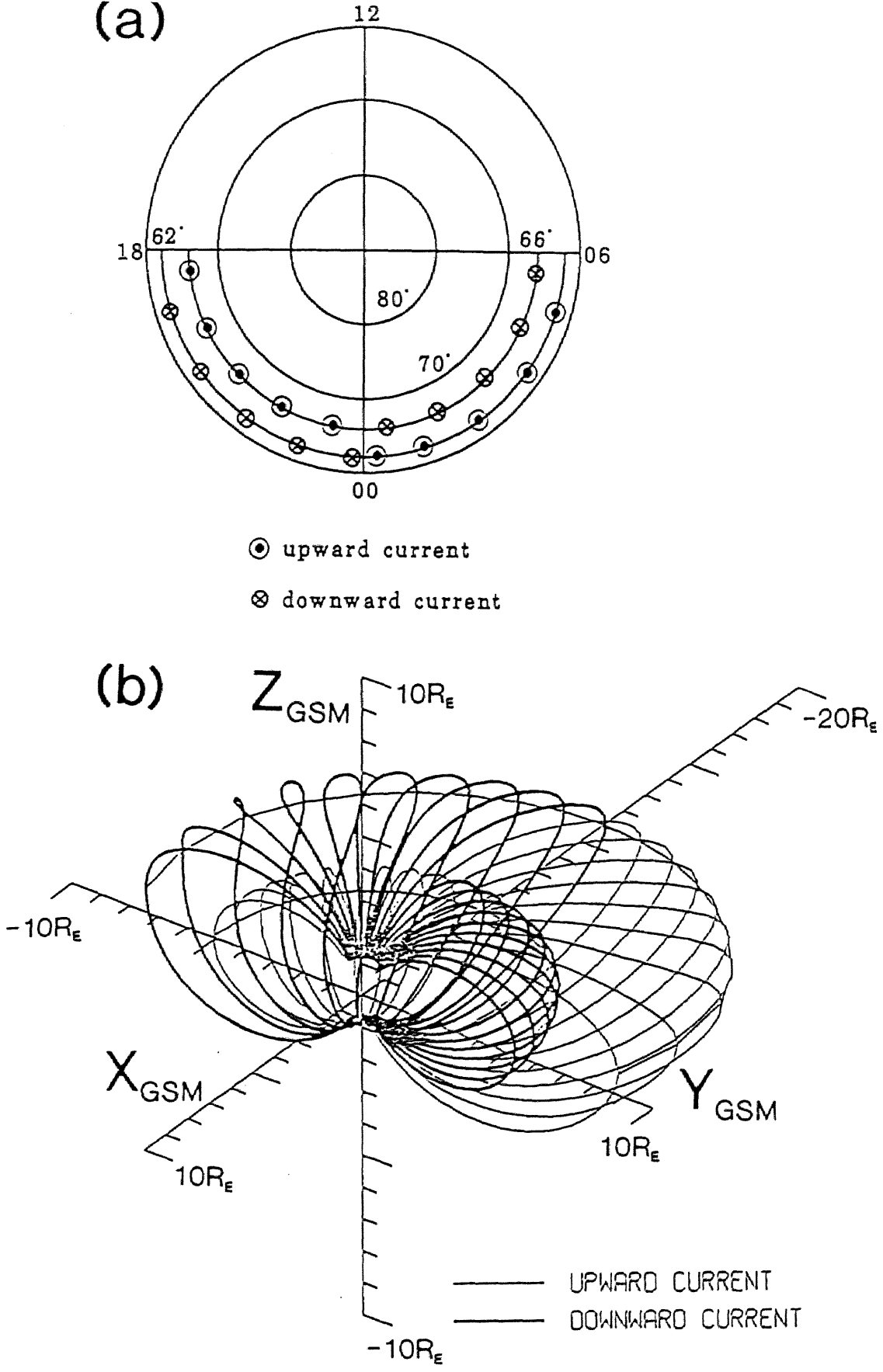

Figure 4.8 Ionospheric projection (a) and schematic view (b) of model field-aligned currents used in this study. Upward field-aligned currents are located at 66° lat. on the ionosphere from 1800 MLT to 0000 MLT and at 62° lat. from 0000 MLT to 0600 MLT, while downward field-aligned currents are located at 62° lat. from 1800 MLT to 0000 MLT and at 66° lat. from 0000 MLT to 0600 MLT.

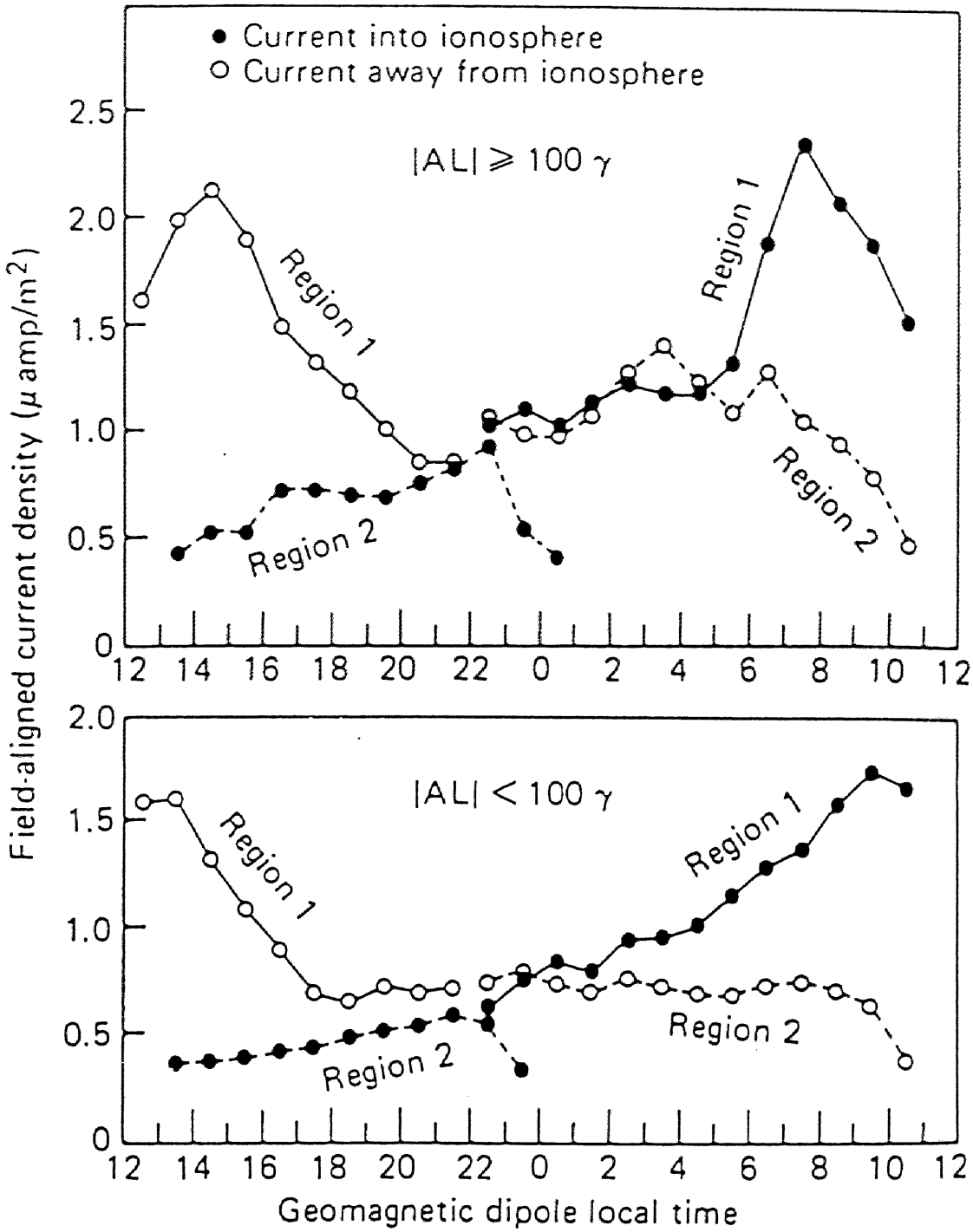

Figure 4.9 Diurnal distribution of field-aligned current densities (a) during active periods ($|AL| \geq 100\ \gamma$) and (b) during weakly disturbed periods ($|AL| < 100\ \gamma$) (Iijima and Potemra, 1978).

value and then we use an intensity of 0.45 A/m as the intensified value under disturbed geomagnetic conditions, which is frequently observed by polar-orbiting satellites (e.g. Iijima and Potemra, 1976).

The magnitude of the deflection depends also on the relative location of the field line of interest to the large-scale current system. We assume, for simplicity, that the field line threading the auroral surge is located just between the Region 1 and Region 2 currents. This assumption is reasonable, because in the examples used in this thesis auroral surges usually occur just after the expansion onset. It is well known that the expansion onset usually starts near the equatorial boundary of the preexisting discrete auroral arcs (Rostoker et al., 1980), that is, the equatorward edge of the Region 1 current.

It is also an important factor as to whether the Region 1 and Region 2 currents are closed through the equatorial azimuthal current (Type I current system after Boström et al., 1964) or through the radial current (Type II current) as shown in Figure 4.10. First we assume that the Region 1 and Region 2 currents are closed with Type I azimuthal equatorial currents. Then we discuss how much the change of the closure currents to the Type II affects the magnitude of magnetic field deflection. We do not consider the effects of ionospheric closure currents. This is due to the fact that the magnetic field caused by these ionospheric currents is significantly weaker than the ambient magnetic field because the current intensity increases with decreasing radial distance as $1/r$ whereas the magnetic field strength varies approximately as $1/r^3$. Hence the ionospheric currents hardly deflect the magnetic field line, even near the ionosphere.

We will also discuss the dependence of the magnitude of magnetic field line deflection on other parameters such as the separation of the Region 1 and Region 2 field-aligned currents, and the magnetic local time of the field line of interest.

4.2. Estimation of the magnitude of magnetic field line deflection caused by field-aligned currents

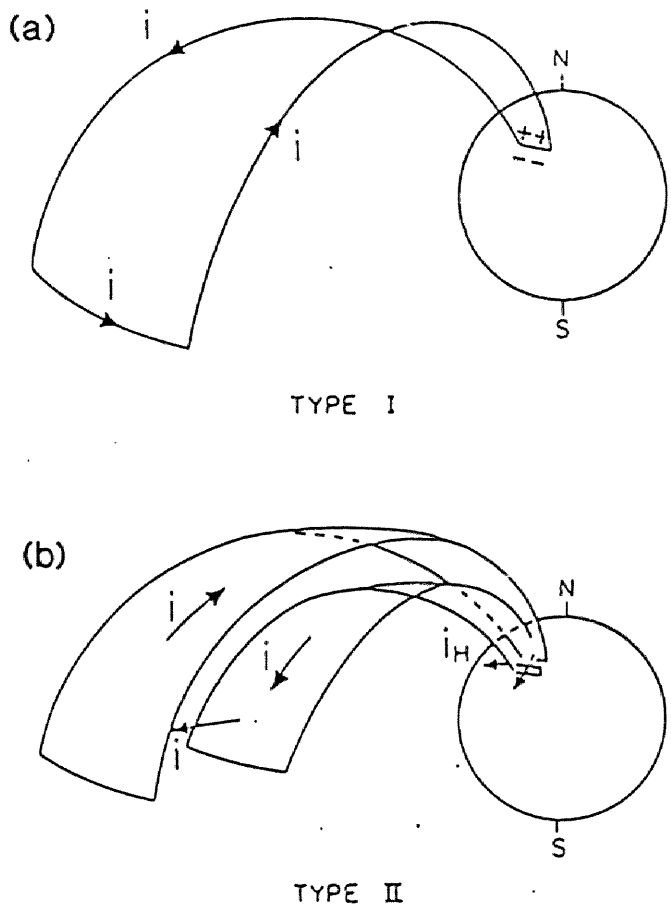

Figure 4.10 Schematic view of the (a) Type I and (b) Type II current systems (Boström et al., 1964).

Figure 4.11 is a plot of magnetic field lines onto the X-Y plane (in GSM coordinates) as viewed along the Z axis, with and without the field-aligned currents. The current intensity is 0.3 A/m, and the azimuthal interval of line currents is 1°. Here we consider Type I azimuthal closure current. It is clearly seen that the magnetic field lines originating from the ionosphere at latitude 64°, surrounded by the Region 1 and Region 2 currents, are deflected by about 6° to 7° in longitude from the earth to the geomagnetic equator, westward (eastward) in the dusk (dawn) sector in comparison the original model field lines, indicating that the ionospheric foot point of the geosynchronous satellite deviates eastward (westward) in the dusk (dawn) sector. The 6° to 7° deflection is about 70 % of the value obtained from the comparison between the temporal location of auroral surges and related magnetic field changes at geosynchronous orbit, as reported in Chapter 2.

If we assume the current intensity as 0.45 A/m, we get deflection of the magnetic field line of about 10° to 11° as shown in Figure 4.12. This value is approximately the same as that obtained from the observations described in Chapter 2. This suggests that field-aligned currents of the intensity appropriate to disturbed conditions of the magnetosphere can account for the deviation of the ionospheric foot point of the geosynchronous satellite of about 10° reported in Chapter 2.

Since the field-aligned currents introduced here have a sheet structure, the magnitude of the azimuthal deflection of magnetic field lines surrounded by these field-aligned currents is not expected to be affected very much by other parameters such as the magnetic local time of the field line of interest and the spatial separation of Region 1 and Region 2 currents. We will now confirm this.

Figure 4.13 shows the azimuthal deviation of the foot point of the satellite plotted against the magnetic local time. It is obvious that the magnitude of the deviation is practically independent of the magnetic local time except very near magnetic local midnight. This is reasonable because of the sheet-like structure of the Region 1 and Region 2 currents, as already mentioned. Although we do not know the precise distribution of the field-aligned

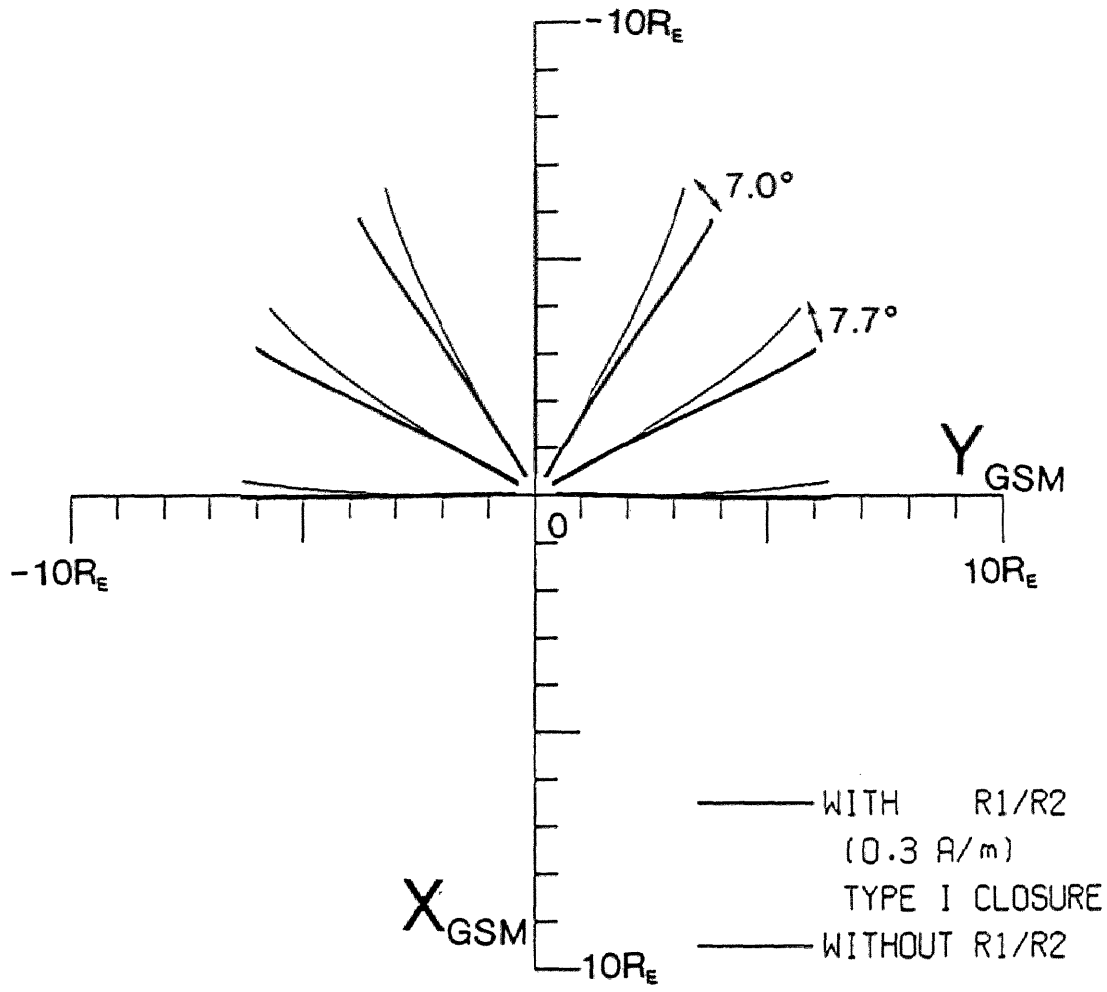

Figure 4.11 Plot of magnetic field lines onto the X-Y plane in GSM coordinates as viewed along the Z axis, with (thick lines) and without (thin lines) the field-aligned currents. The current intensity is 0.3 A/m, and the azimuthal interval of line currents is 1°. Here we consider Type I azimuthal closure currents.

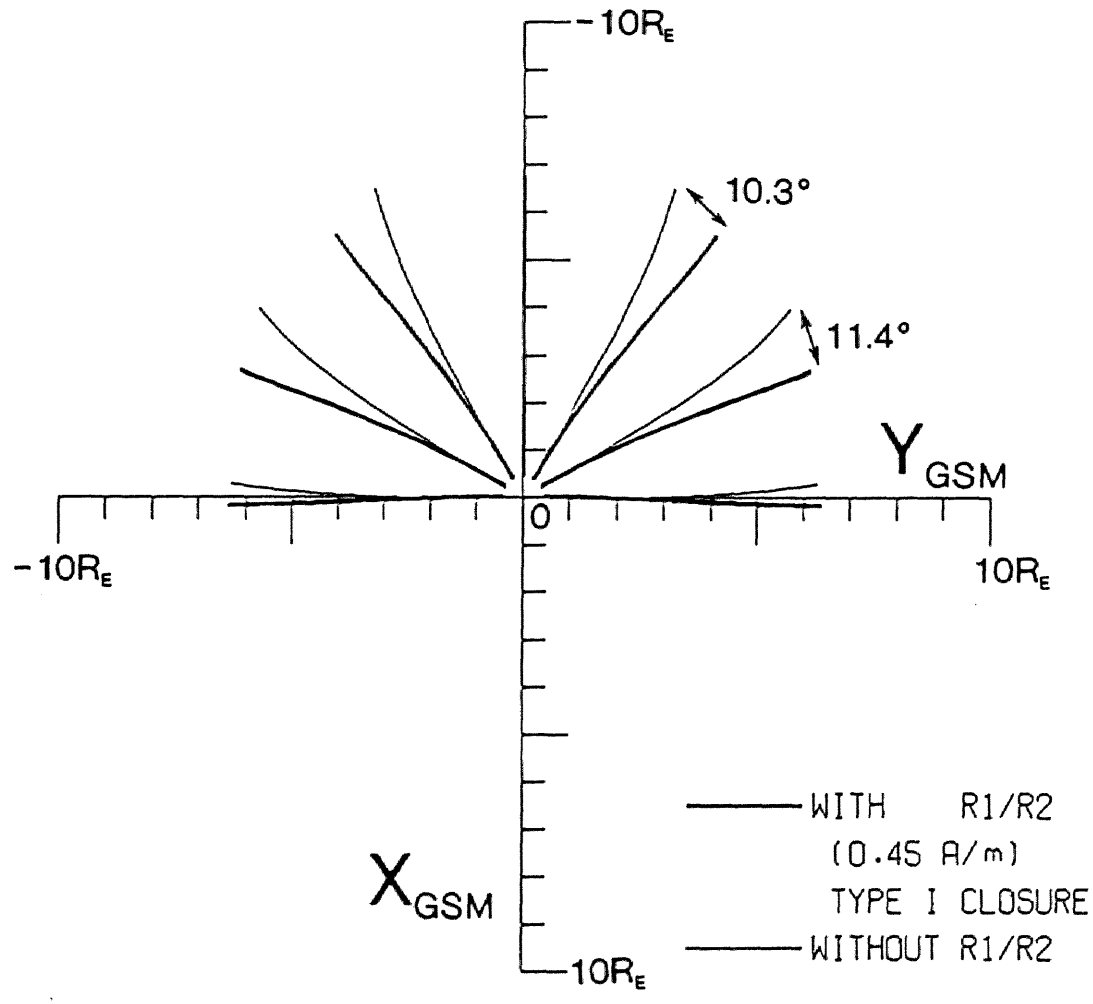

Figure 4.12 Same as Figure 4.11, except for the current intensity of 0.45 A/m.

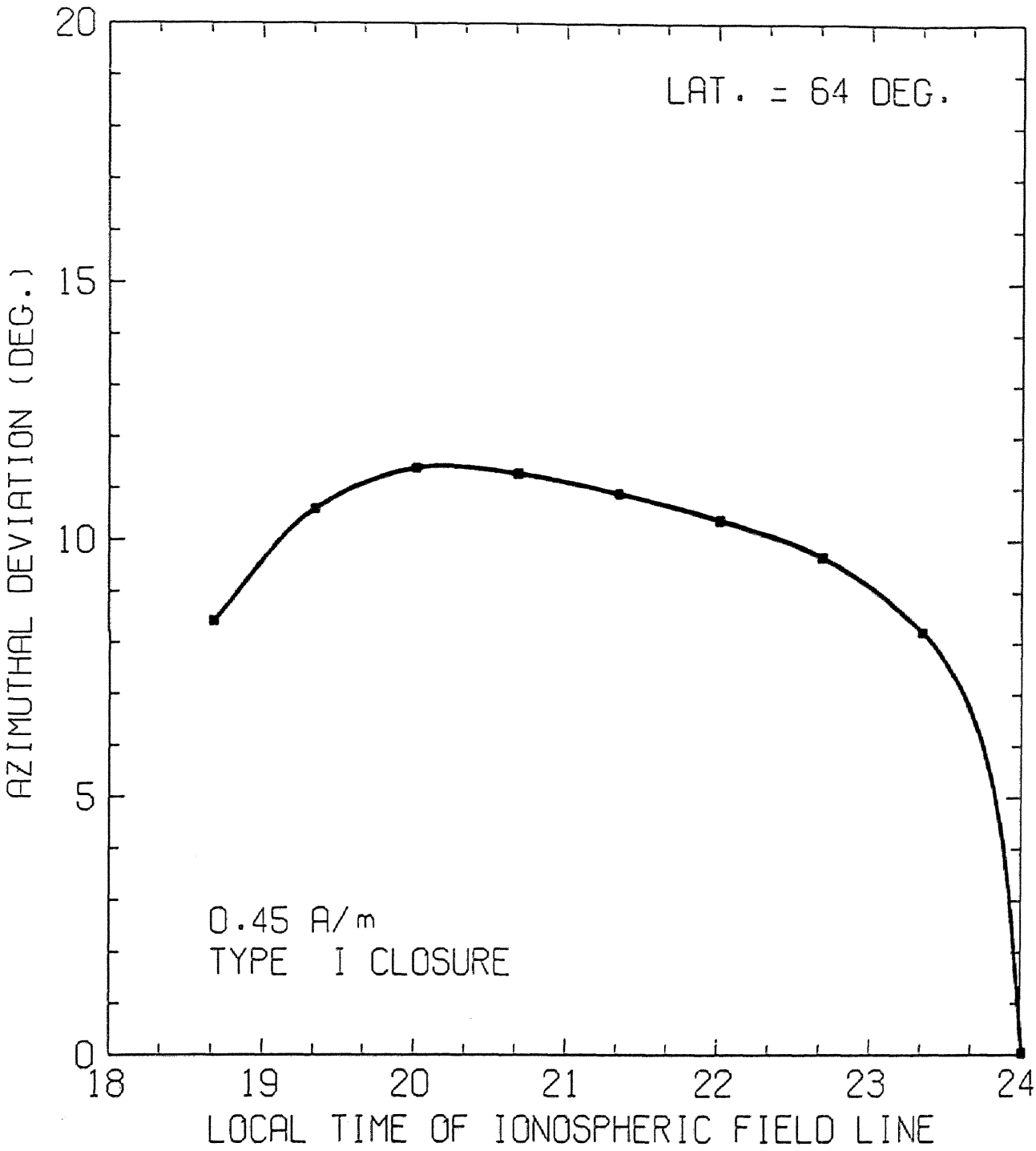

Figure 4.13 Azimuthal deviation of the foot point of the geosynchronous satellite plotted against the magnetic local time.

currents during the disturbed period, we can at least say that the magnitude of the magnetic field deflection is constant, if the longitudinal extent of the Region 1 and Region 2 currents surrounding the field line of interest exceeds a certain value (about 15°). This is clearly indicated also in Figure 4.14, where the azimuthal deviation of the foot point of the satellite is plotted against the magnetic local time for two values of the longitudinal extent of the large-scale field-aligned currents (thick line for the current distribution of 1800 MLT to 0600 MLT and thin line for the current distribution of 1600 MLT to 0800 MLT). Obviously the presence of the dayside field-aligned currents hardly affects the magnitude of the magnetic field deflection near magnetic midnight.

The magnitude of deflection does not depend very much on any change of the separation of Region 1 and Region 2 field-aligned currents either, as shown in Figure 4.15. This is not surprising, given the conservation of the total magnetic flux between a pair of Region 1 and Region 2 sheet currents. Here we assume that the field line threading the auroral surge is located in between the Region 1 and Region 2 currents, as already mentioned earlier.

In contrast, the change of the distribution of equatorial closure currents may have considerable effect on the azimuthal magnetic field deflection, especially near the geomagnetic equatorial plane. When we add Type II radial closure currents as shown in Figure 4.10(b) instead of Type I azimuthal closure currents (Figure 4.10(a)), the azimuthal deviation of the ionospheric foot point of the satellite becomes about 1.5 times the value for Type I azimuthal closure currents, as shown in Figure 4.16. This fact suggests that the equatorial radial current can have a significant influence in distorting magnetic field lines. However, the magnetic field deflection depends on how much the Region 1 and Region 2 currents are actually closed with radial currents and azimuthal currents respectively. In addition, since the actual equatorial radial current has finite thickness, the azimuthal deflection of the magnetic field becomes small inside the equatorial volume current layer. Consequently the integrated azimuthal deflection of the magnetic field line from the ionosphere to the geomagnetic equator is expected to become smaller. This will be discussed further in the

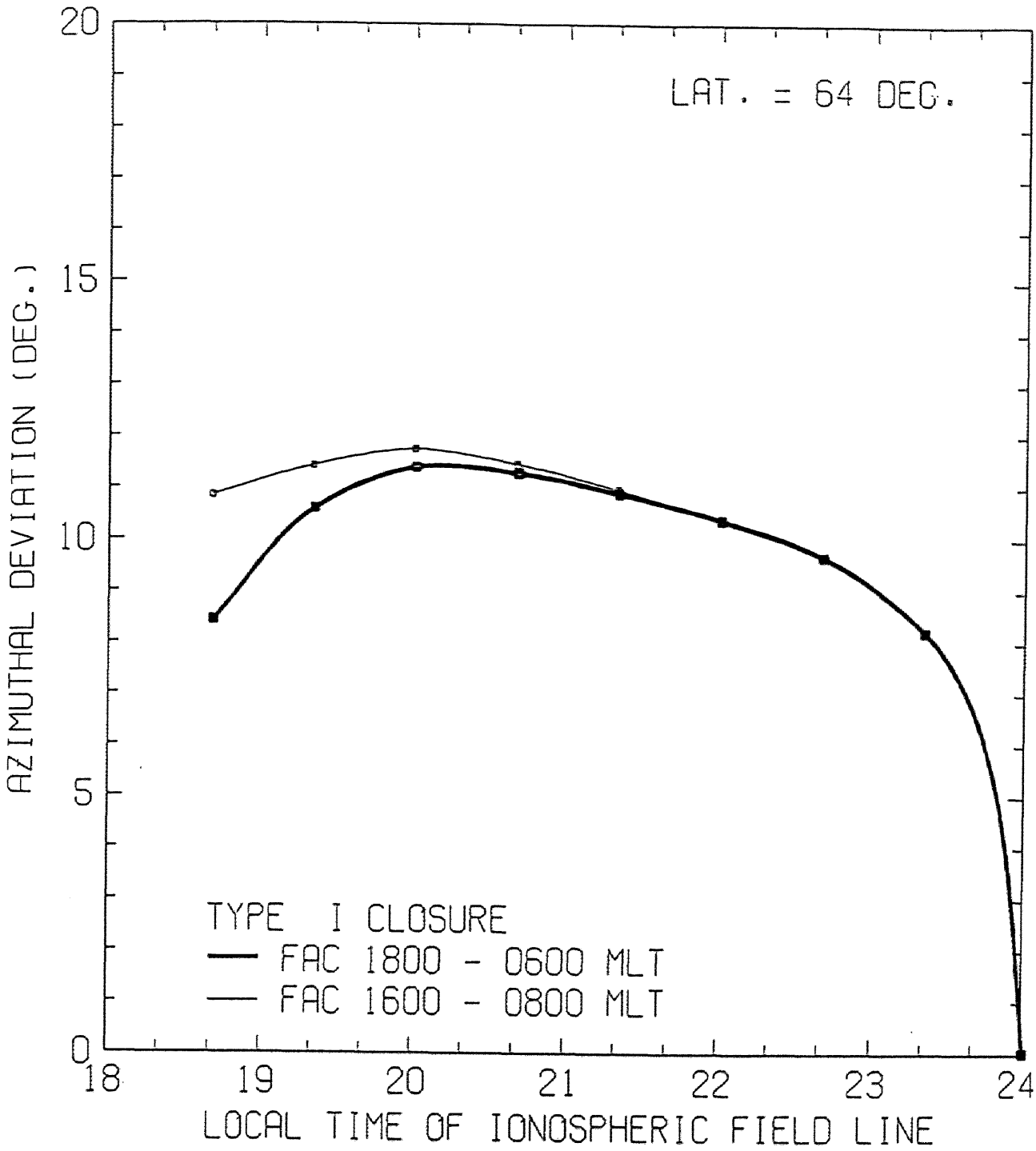

Figure 4.14 Azimuthal deviation of the foot point of the satellite plotted against the magnetic local time for two values of longitudinal extent of the large-scale field-aligned currents (thick line for the current distribution of 1800 MLT to 0600 MLT and thin line for the current distribution of 1600 MLT to 0800 MLT).

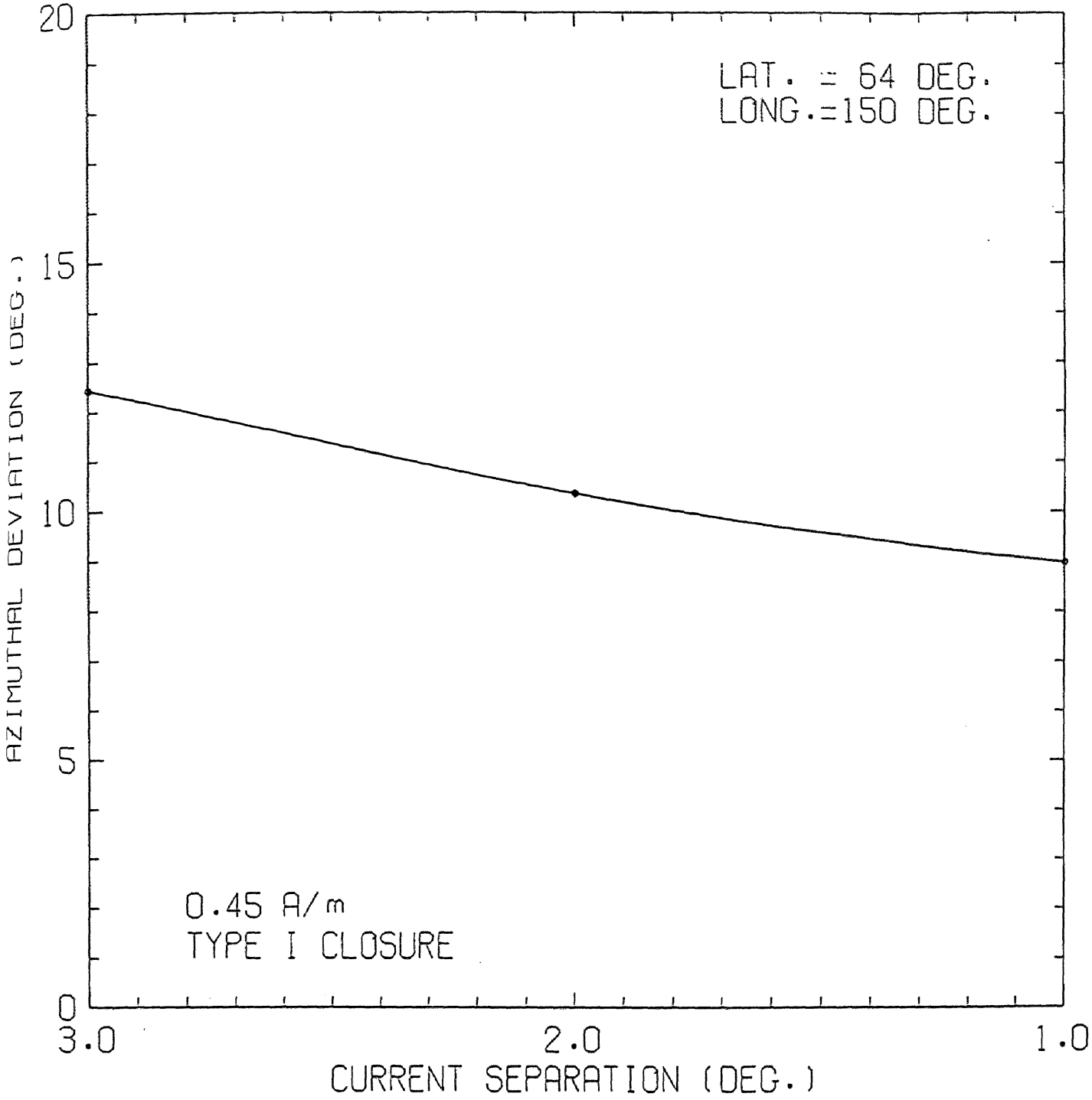

Figure 4.15 Azimuthal deviation of the foot point of the satellite plotted against the latitudinal separation of Region 1 and Region 2 field-aligned currents.

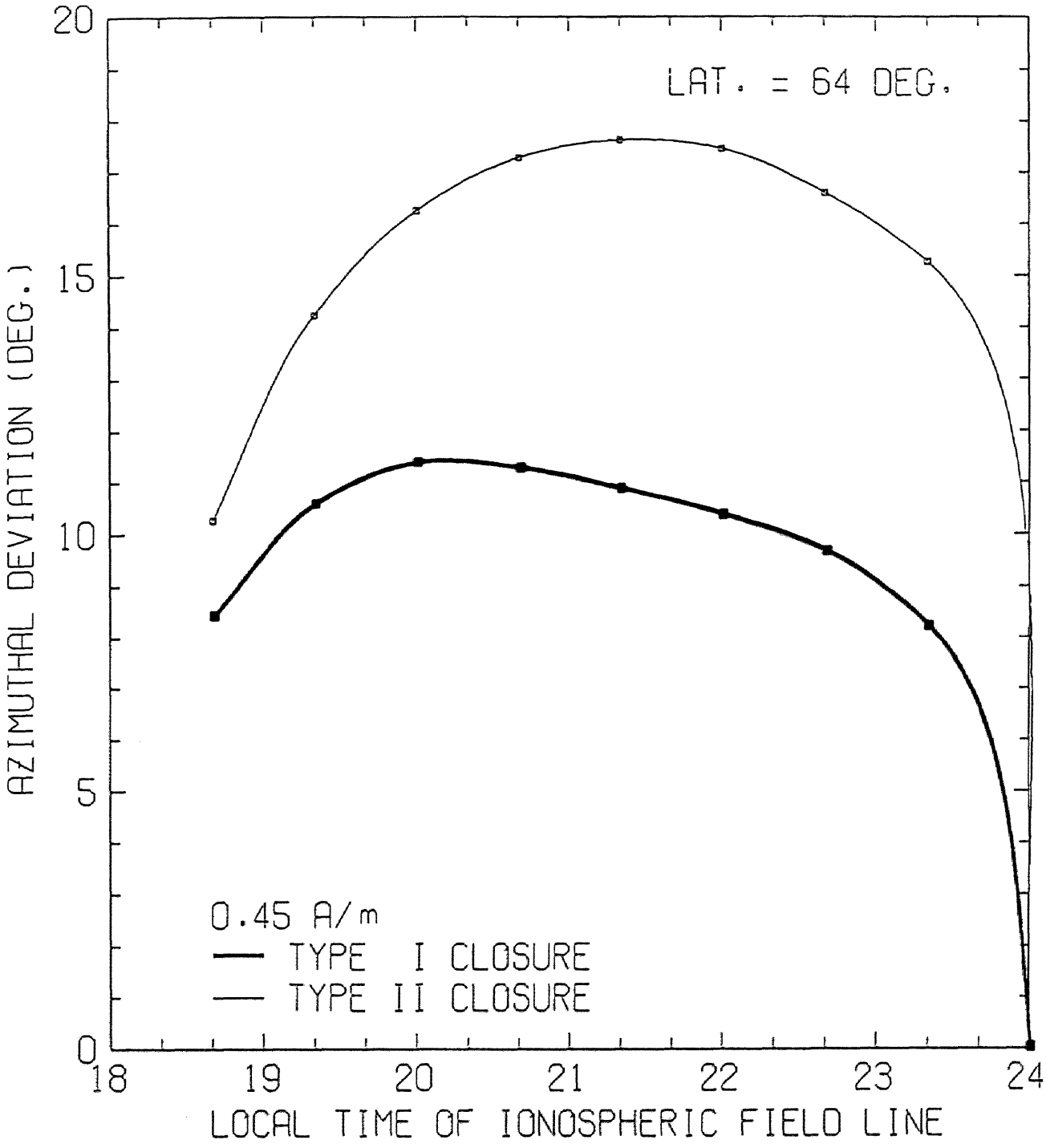

Figure 4.16 Azimuthal deviation of the foot point of the satellite plotted against the magnetic local time for the Type I closure currents (thick line) and for the Type II closure currents (thin line).

next section.

4.3 Discussion

So far we have introduced Region 1 and Region 2 field-aligned currents into Tsyganenko's model and examined how much these currents modify the magnetic field lines in going from the ionosphere to geosynchronous altitudes.

Since the large-scale field-aligned currents usually have a sheet structure, naturally the magnitude of the deflection does not depend very much on the degree of separation of Region 1 and Region 2 currents. In addition, it does not depend on the magnetic local time very much either, if the longitudinal extent of the large-scale field aligned currents surrounding the field line of interest exceeds a certain value (about 15°).

On the other hand, the equatorial current closure can considerably affect the magnitude of magnetic field line deflection, as shown in Section 4.2. However, we do not know exactly how much the Region 1 and Region 2 currents are actually closed with radial currents and azimuthal currents respectively. Iijima et al. (1990) used AMPTE/CCE magnetic field data to obtain the statistical distribution of equatorial currents and showed that the intensity of the azimuthal equatorial current is about three times as large as that of the radial current. However, we have little information on the temporal variation of the current closure especially during the course of substorms. Moreover, as already mentioned in the previous section, if the equatorial radial current has finite thickness, the azimuthal deflection of the magnetic field becomes small inside the equatorial volume current layer and accordingly the integrated deflection of the magnetic field is reduced. If we take the value of the current thickness as 2 R_E, which is equal to the thickness of the magnetotail current used in Tsyganenko's model, the magnitude of magnetic field line deflection which is caused by the equatorial radial current is reduced by about 50 %. Therefore the effect of magnetospheric equatorial closure currents is expected to be small in comparison with that of field-aligned currents themselves.

Now we can conclude that it is the intensity of Region 1 and Region 2 field-aligned

currents, together with the relative location of the field line of interest to the large-scale field-aligned currents, which affects the magnitude of the magnetic field deflection most significantly. The next problem is how intense the actual field-aligned currents are and where the auroral surges are located, relative to these Region 1 and Region 2 field-aligned currents, for the examples used in this paper. These problems will be discussed in Chapter 5 by using the DMSP-F7 polar-orbiting satellite data.

Figure 4.17 shows the result of the magnetic field mapping from the geomagnetic equatorial plane to the polar ionosphere, based on this modified Tsyganenko's model ($Kp \geq 5-$) which includes the large-scale field-aligned currents with the latitudinally integrated intensity of 0.45 A/m. Sharp bends of equi-local time contour lines found at latitudes 66° and 62°, are the result of the field-aligned currents in these regions, similar to the mapping result based on the 3-dimensional MHD simulation. This fact indicates that the introduction of field-aligned currents could much improve the validity of Tsyganenko's model. In addition, this also suggests the usefulness of the MHD simulation for the study of magnetospheric magnetic field distribution.

These large-scale field-aligned currents modify the magnetic field (especially the azimuthal component) at the geosynchronous satellite. It is worth while examining whether the magnitude of the magnetic field produced by these currents is reasonable or not, in order to confirm the validity of the introduction of these field-aligned currents. The distribution of the azimuthal component magnetic field from the ionosphere to the geomagnetic equator along the magnetic field line threading the geosynchronous satellite is shown in Figure 4.18. For the Type I azimuthal closure currents (thick line), the azimuthal component is 0 nT on the equator because of the symmetry of the current system between the northern and the southern hemisphere (not shown in this figure) and it becomes larger as the observation point goes away from the equator toward the ionosphere. There is a slight decrease of the D component magnetic field near the ionosphere. However, this is due to the invalidity of the line current approximation in this region, and the magnetic field line deflection in this

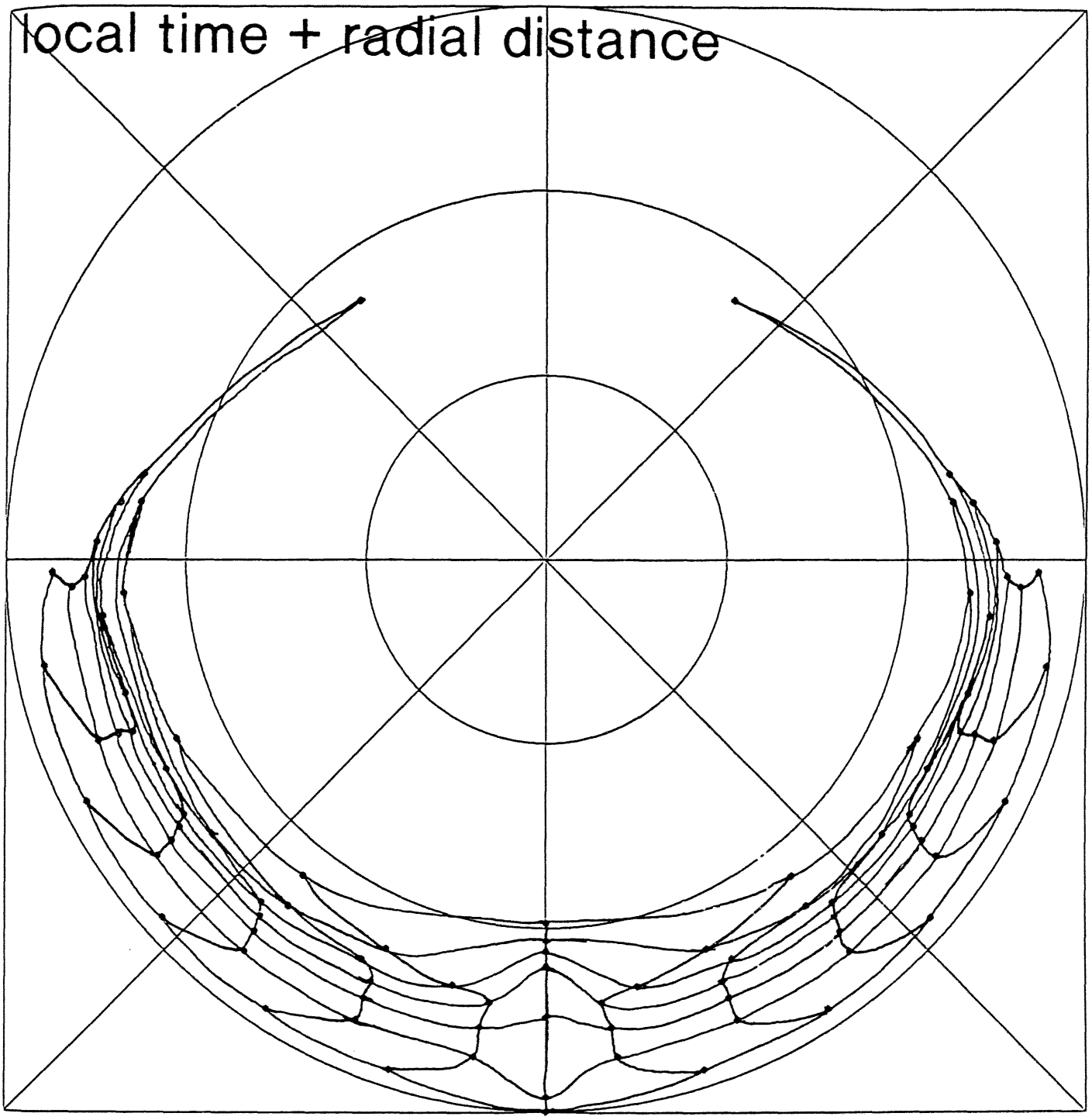

Figure 4.17 Result of the magnetic field mapping from the geomagnetic equatorial plane to the polar ionosphere, based on this modified Tsyganenko's model (Kp $\geq$ 5–) which includes the large-scale Region 1 and Region 2 field-aligned currents with the latitudinally integrated intensity of 0.45 A/m. The format of the figure is the same as Figure 3.7.

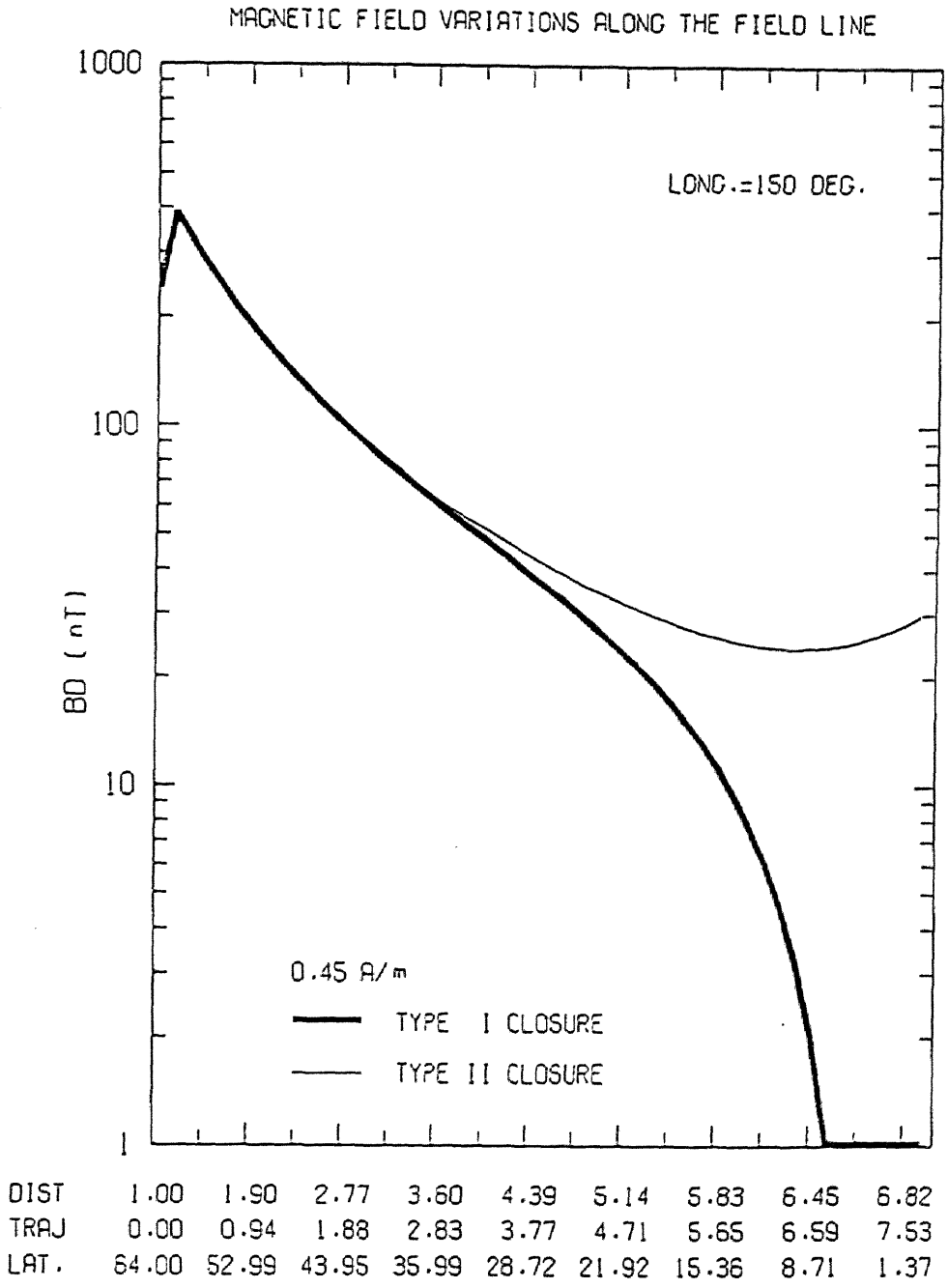

Figure 4.18 Distribution of azimuthal component magnetic field from the ionosphere to the geomagnetic equator along the magnetic field line threading the geosynchronous satellite, for the Type I closure currents (thick line) and for the Type II closure currents (thin line).

region does not contribute significantly to the integrated deflection because of the comparatively large ambient magnetic field as already mentioned. Most importantly, the azimuthal component becomes 7 nT at latitude 10°, a value which is consistent with observations at GOES 6, which is located at 9.0° geomagnetic latitude.

It should be noted, however, that Type II radial equatorial closure currents would modify the azimuthal magnetic field component near the geomagnetic equatorial plane to some extent, although we do not know exactly how much the Region 1 and Region 2 currents are actually closed with radial currents and azimuthal currents respectively. If we consider Type II radial closure currents (Figure 4.18, thin line) the azimuthal component magnetic field appears to be approximately constant (about 30 nT) for lat. $\leq 20°$. This is due to the inappropriate line (or sheet) current assumption of the equatorial current. For the volume current with the finite thickness, the azimuthal component magnetic field should decrease gradually within the current sheet and become 0 nT on the geomagnetic equator.

As already mentioned, the magnitude of the azimuthal component magnetic field perturbation depends significantly on the relative location of the observation point to the geomagnetic equatorial plane if the dipole tilt angle is 0° or, for any other angle, to the equatorial current sheet where field-aligned currents in the northern and southern hemisphere are closed via equatorial currents. On the other hand, the location of the equatorial current sheet of the real magnetosphere is quite variable, especially during disturbed periods, because of the hinging and warping of the neutral sheet (Fairfield, 1980) caused by the dipole tilt effect. Furthermore, since the real equatorial current and field-aligned currents have continuous distribution and cannot be approximated by the sheet or line currents, the magnetic field depends significantly on the relative location of the field line of interest to the large-scale currents with finite thickness. We can also say that the azimuthal component magnetic field at geosynchronous orbit has little information on the intensity of Region 1 and Region 2 field-aligned currents.

4.4. Conclusion

In this chapter we have introduced Region 1 and Region 2 field-aligned currents into Tsyganenko's model to examine how much these field-aligned currents modify the magnetic field configuration. When we introduce Region 1 and Region 2 currents appropriate to average conditions of the magnetosphere (= 0.3 A/m), we obtain the azimuthal deviation of the ionospheric foot point of the geosynchronous satellite of about 7°. If the current intensity is 0.45 A/m, a characteristic value during a geomagnetically disturbed period, the azimuthal deviation becomes about 10°, which is approximately the same as the observed value obtained from the comparison of magnetic field changes at geosynchronous orbit and auroral activity made in Chapter 2. This deviation does not depend very much on other parameters such as the separation of Region 1 and Region 2 field-aligned currents, magnetic local time (if the longitudinal extent of the large-scale sheet currents surrounding the field line of interest exceeds a certain value of about 15°), or the current closure on the geomagnetic equatorial plane.

We have made a mapping analysis based on the modified T87T model which includes the effects of field-aligned currents. Sharp bends of the equi-local time contour lines are found, which is similar to the mapping result based on the MHD simulation model. This fact supports the usefulness of the MHD simulation for the study of magnetospheric magnetic field distribution.

We have examined the effect of the large-scale field aligned currents on the magnetic field changes at the geosynchronous satellite. Although the magnitude of the D component perturbation seems to be consistent with the observations, it depends significantly on the relative location of the satellite to the equatorial current sheet. However, the location of the equatorial current sheet is highly variable, and since this current sheet has finite thickness the magnetic effect of the current system at geosynchronous orbit is difficult to determine. In addition, the magnetic field at the geosynchronous satellite has little information on the intensity of the Region 1 and Region 2 field-aligned currents.

In the next chapter we will examine the actual intensity of the large-scale Region 1 and Region 2 field-aligned currents for some specific examples, by using the data obtained by the polar-orbiting satellite DMSP-F7. We will also examine the relative location of small-scale field-aligned currents, connected to auroral surges, to the Region 1 and Region 2 currents.

5. Estimation of the intensity of Region 1 and Region 2 currents using the DMSP-F7 satellite

In the preceding chapters we have shown that the real ionospheric foot point of the geosynchronous satellite deviates frequently from the foot point estimated by Tsyganenko's magnetic field model (1987) by about 10° to 15° in longitude and that this deviation can be explained in terms of large-scale Region 1 and Region 2 currents. We have also added the effects of these field-aligned currents into Tsyganenko's model and shown that the field-aligned currents, with current intensity typical of the disturbed period of the magnetosphere, is consistent with this foot point deviation. However, we have not yet confirmed whether such currents actually flow or not, for the specific events studied in this thesis. In this chapter we compare the intensity of Region 1 and Region 2 currents introduced into Tsyganenko's model for explaining the 10° deviation of the foot point of the satellite in Chapter 4, with the observation of the field-aligned current intensity by the polar-orbiting satellite DMSP-F7 for some events. We will also check the relative location of auroral surges to the large-scale field-aligned currents, to see whether the auroral surge is located at the position where the significant deflection of the magnetic field line by Region 1 and Region 2 currents is expected.

5.1. DMSP-F7 Data

The passes of the polar-orbiting satellite DMSP-F7 are in the 0830 – 2030 geographic local time meridian plane. The instruments used in the present study are: the standard DMSP high-resolution visible wavelength line scanning imager (Eather, 1979), the triaxial fluxgate magnetometer (Rich, 1984), and a pair of zenith-looking ion and electron particle spectrometers (Hardy et al., 1984). Among the data obtained with these instruments, the image data has already been referred to in Chapter 2 (Figure 2.6).

Among all the events described in Chapter 2, there were fortunately two examples where the DMSP-F7 satellite passed near the ground observation site near the foot point of the GOES 5 and GOES 6 satellites (GWR, SHM and LGR) shortly after the expansion onset;

the onsets at 0452 UT, Jan. 27 and at 0639 UT, Jan. 07. We now describe these two examples separately in the following section.

5.2. Observations of field-aligned currents

5.2.1. Substorm at 0448 UT on January 27

Figure 5.1 shows the ionospheric foot point trajectory of the DMSP satellite. DMSP passed 50 km east of SHM at 0458:00 UT from geomagnetic north towards the south. Unfortunately, the passage time was between two events at 0448 UT and at 0500 UT, so that the satellite did not measure the intensified field-aligned currents just during the expansion. The auroral configuration in this figure is the same as that observed by the scanning imager onboard the DMSP satellite (Figure 2.6), as already mentioned in Chapter 2. Above GWR there were a few faint arcs. Above SHM there was an S-shaped band, extending from about 200 km east of SHM toward the far west. The ionospheric foot point of DMSP-F7 passed near the eastern edge of this S-shaped band from north to south. This S-shaped band was formed as a result of the deformation of an auroral surge which appeared at 0451 UT. From the comparison of the motion of this surge and the magnetic field variations at the geosynchronous satellite GOES 6, we have found an azimuthal deviation of the real foot point of GOES 6 of about 15° from the foot point estimated by using Tsyganenko's 1987 model (truncated version), as already mentioned in Chapter 2.

Figure 5.2 shows the magnetic field variations observed by DMSP-F7. The X is positive downward, the Y is positive forward and the Z is maintained in the horizontal, cross-track direction, to complete the right-handed orthogonal set. Since the satellite passes approximately along the geomagnetic meridian line for geomagnetic latitudes smaller than about 70°, the time (spatial) derivative of the Z component magnetic field indicates the density of field-aligned currents, if the current is distributed in a long slab extending in the longitudinal direction. During the period shown in this figure, the satellite passed the whole northern polar region from ~ 0900 MLT toward ~ 2200 MLT. On the night side the satellite observed

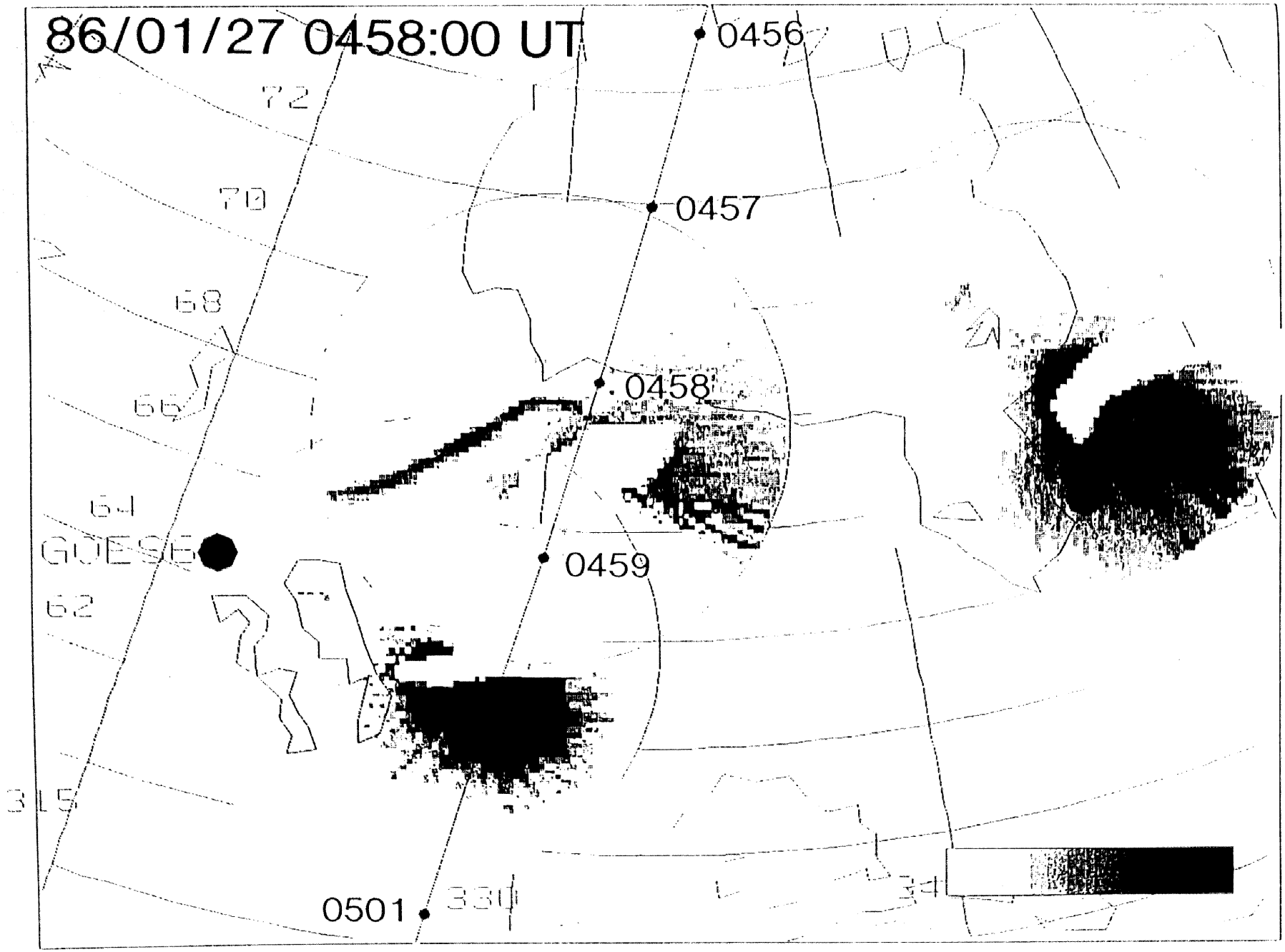

Figure 5.1 Ionospheric foot point trajectory of the DMSP-F7 satellite during the expansion at 0448 UT on January 27, 1986.

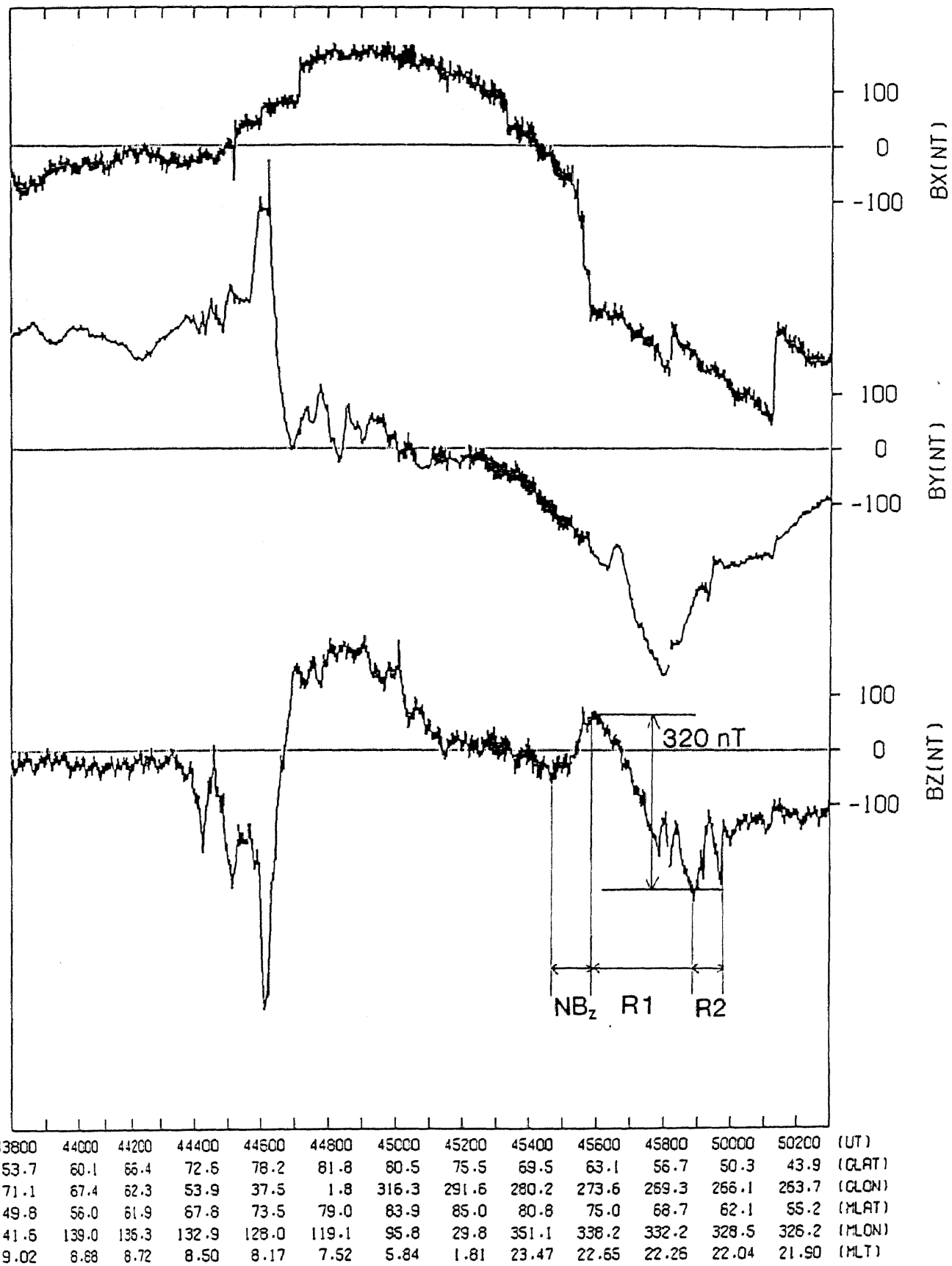

Figure 5.2 Magnetic field variations at DMSP-F7 from 0438 UT to 0503 UT on January 27, 1986. The X is positive downward, the Y is positive forward and the Z is maintained in the horizontal, cross-track direction, to complete the right-handed orthogonal set.

a pair of duskside Region 1 (upward) and Region 2 (downward) currents accompanied by the downward current (NB_Z current) to the north of the Region 1 current.

Figure 5.3 shows the magnetic field variations at DMSP-F7 with higher time resolution than Figure 5.2. In the Region 1 current zone several pairs of small-scale field-aligned currents are observed. These small-scale currents are associated with auroral arcs. For example, the upward field-aligned current observed at 68° geomagnetic latitude is collocated with the eastern part of the S-shaped arc observed both on the ground and by the DMSP-F7 satellite. For the other small-scale currents we cannot find a specific auroral structure. However, these currents are probably associated with faint auroras with luminosity below the threshold level of the TV cameras. The energy-time spectrum of the downgoing electrons and ions is shown in Figure 5.4. In this figure, a sharp inverted-V type structure was observed, coincident with the upward current around 0458 UT (at 68° lat.) identified from the magnetic field variation in Figure 5.3. Poleward of the currents described above there are less sharp inverted-V's extending from 69° to 71° lat. and a broad electron precipitation region from 71° to 74° lat.

In Chapter 4 we introduced Region 1 and Region 2 field-aligned currents into Tsyganenko's model. Assuming the latitudinally integrated current intensity to be 0.45 A/m, we have obtained the deviation of the ionospheric foot point of the geosynchronous satellite of about 10° in longitude. Since the magnitude of the magnetic field deflection is proportional to the intensity of the Region 1 and Region 2 currents, the intensity of these currents which cause the 15° azimuthal deviation of the foot point of the geosynchronous satellite is about 0.68 A/m. The field-aligned currents with this intensity would produce the Z component magnetic field perturbation at the DMSP-F7 satellite of 840 nT in amplitude. The actual amplitude of the Z component magnetic field variation during the passage of the Region 1 current is 320 nT, and 150 nT during the passage of the Region 2 current. These values are less that half the value (840 nT) needed to account for the azimuthal deviation of ionospheric foot point of the satellite of about 15°.

It should be emphasized, however, that the current intensity was measured after the

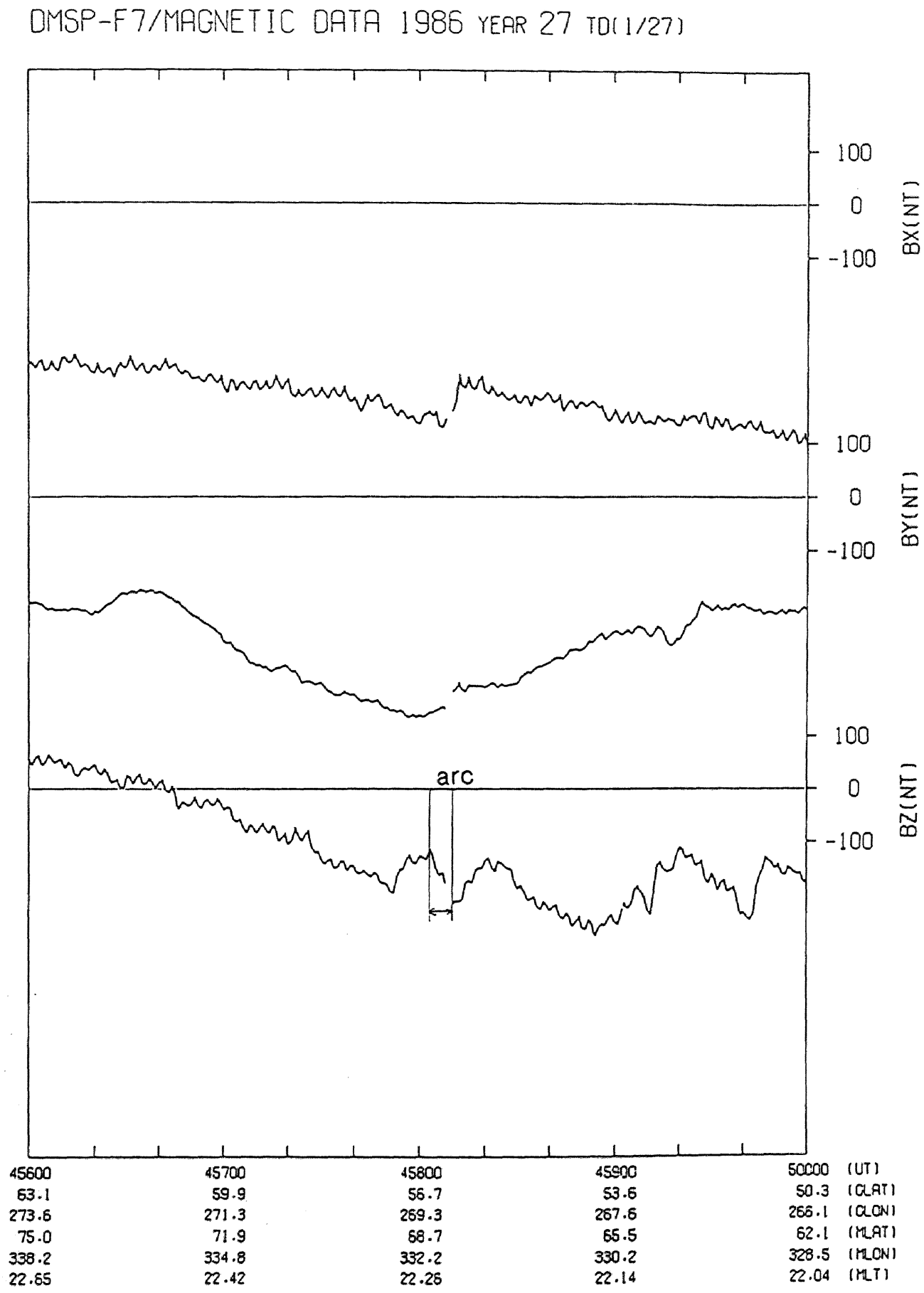

Figure 5.3 Similar to Figure 5.2 for the higher time resolution, from 0456 UT to 0500 UT.

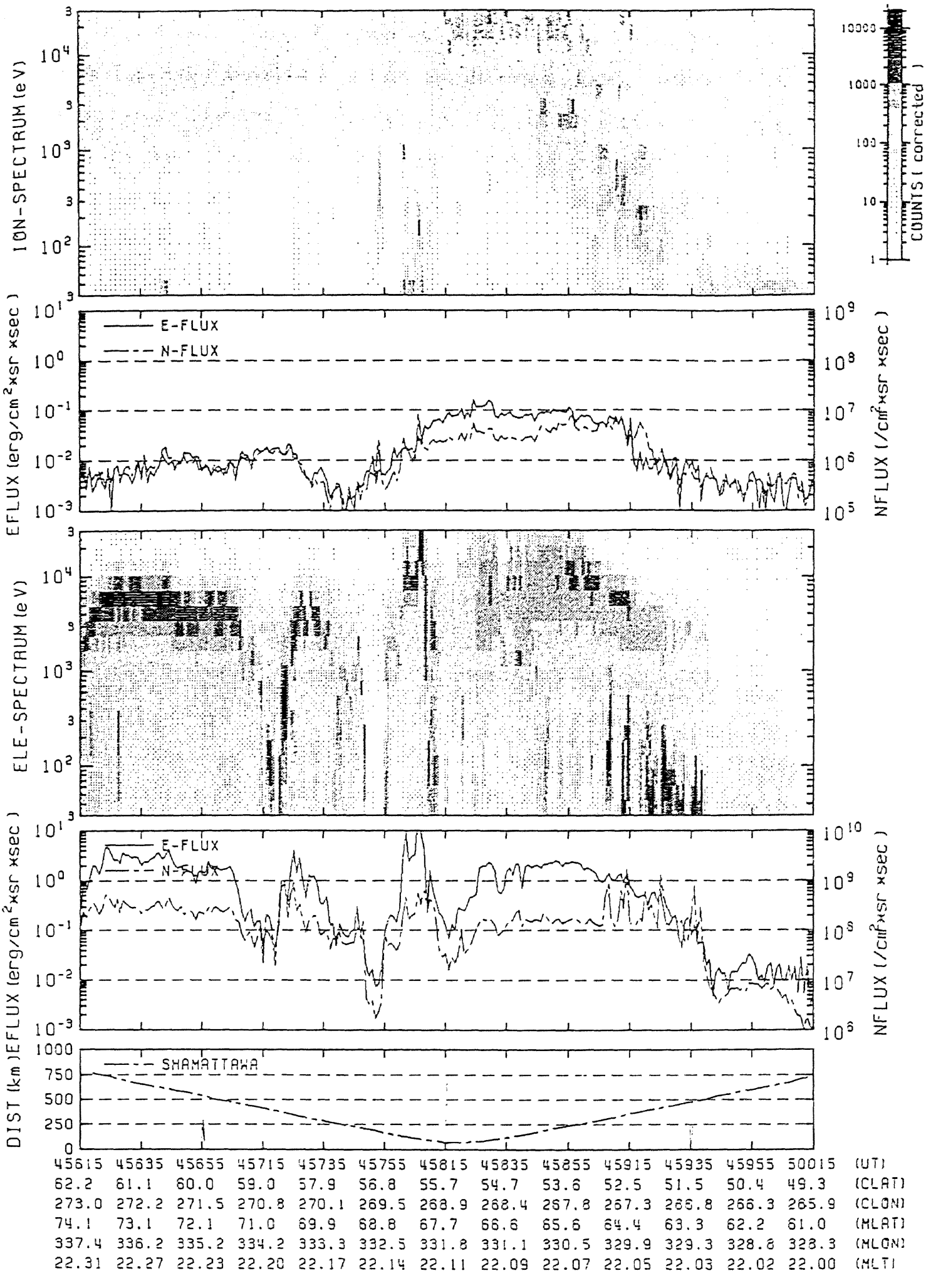

Figure 5.4 Energy-time spectrum of the downgoing electrons and ions observed by DMSP-F7 from 0456:15 UT to 0500:15 UT on January 27, 1986.

peak of the first expansion at 0448 UT, during the recovery phase and before the onset of the second expansion at 0500 UT. Considering the statistical relationships between the intensity of Region 1 and Region 2 field-aligned currents and the geomagnetic activity reported by many studies (e.g. Iijima and Potemra, 1976), it is reasonable to infer that the Region 1 and Region 2 currents could become as intense as 840 nT. This is sufficient to explain the deflection of field lines of about 15° in longitude at 0453 UT, when GOES 6 observed small-scale field-aligned current connected to the auroral surge. On the other hand, the current intensity was probably reduced when the DMSP-F7 satellite passed the large-scale field-aligned current region at about 0458 UT.

It is also important to know where the auroral surge was located relative to the Region 1 and Region 2 field-aligned currents. This will be discussed in detail in Section 5.3.

5.2.2. Substorm at Jan. 07, 0639 UT.

The foot point trajectory of the DMSP-F7 is shown in Figure 5.5. This satellite passed above FSM at 0640 UT from geomagnetic north towards the south, across two discrete auroral arcs. An auroral surge was seen about 200 km north of LGR, 30° east of the trajectory of the satellite. From the comparison of the motion of this surge and the magnetic field variation at the GOES 6 satellite which began at 0638 UT, we found an eastward deviation of the real foot point of the satellite of about 10° in longitude from the foot point estimated by using Tsyganenko's 1987 model (as already discussed in Chapter 2). Although this satellite passed 30° west of the auroral surge of interest, it observed Region 1 and Region 2 currents just after the expansion onset, hence the intensity of large-scale field-aligned currents during the expansion was observed. Unfortunately there were no data from the scanning imager onboard the DMSP-F7 satellite during this period.

Figure 5.6 shows the magnetic field variation at DMSP-F7. During the period the satellite passed the whole northern polar region from ~ 0930 MLT toward ~ 2200 MLT. On the midnight side a pair of duskside Region 1 and Region 2 currents were observed

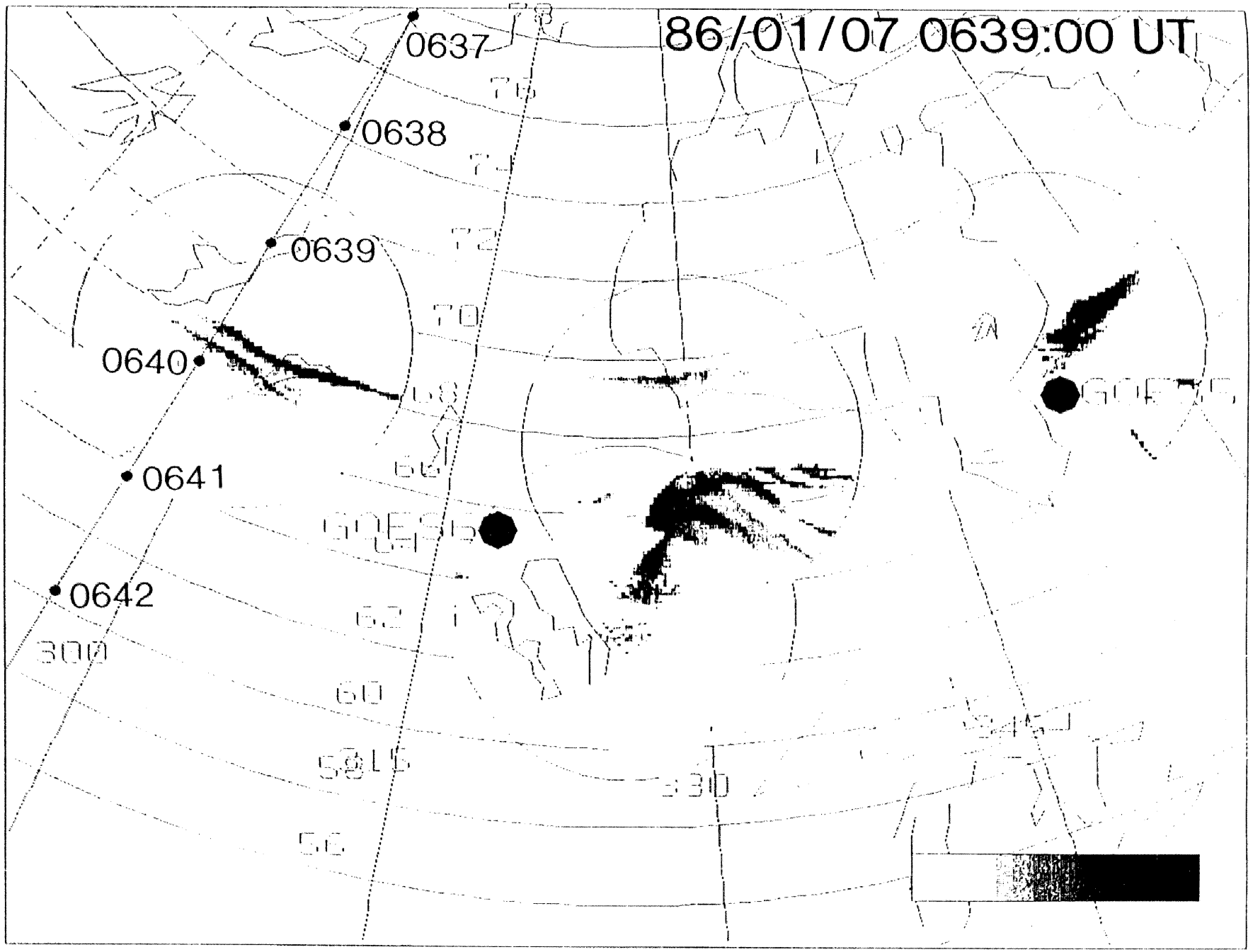

Figure 5.5 Ionospheric foot point trajectory of the DMSP-F7 satellite during the expansion at 0639 UT on January 07, 1986.

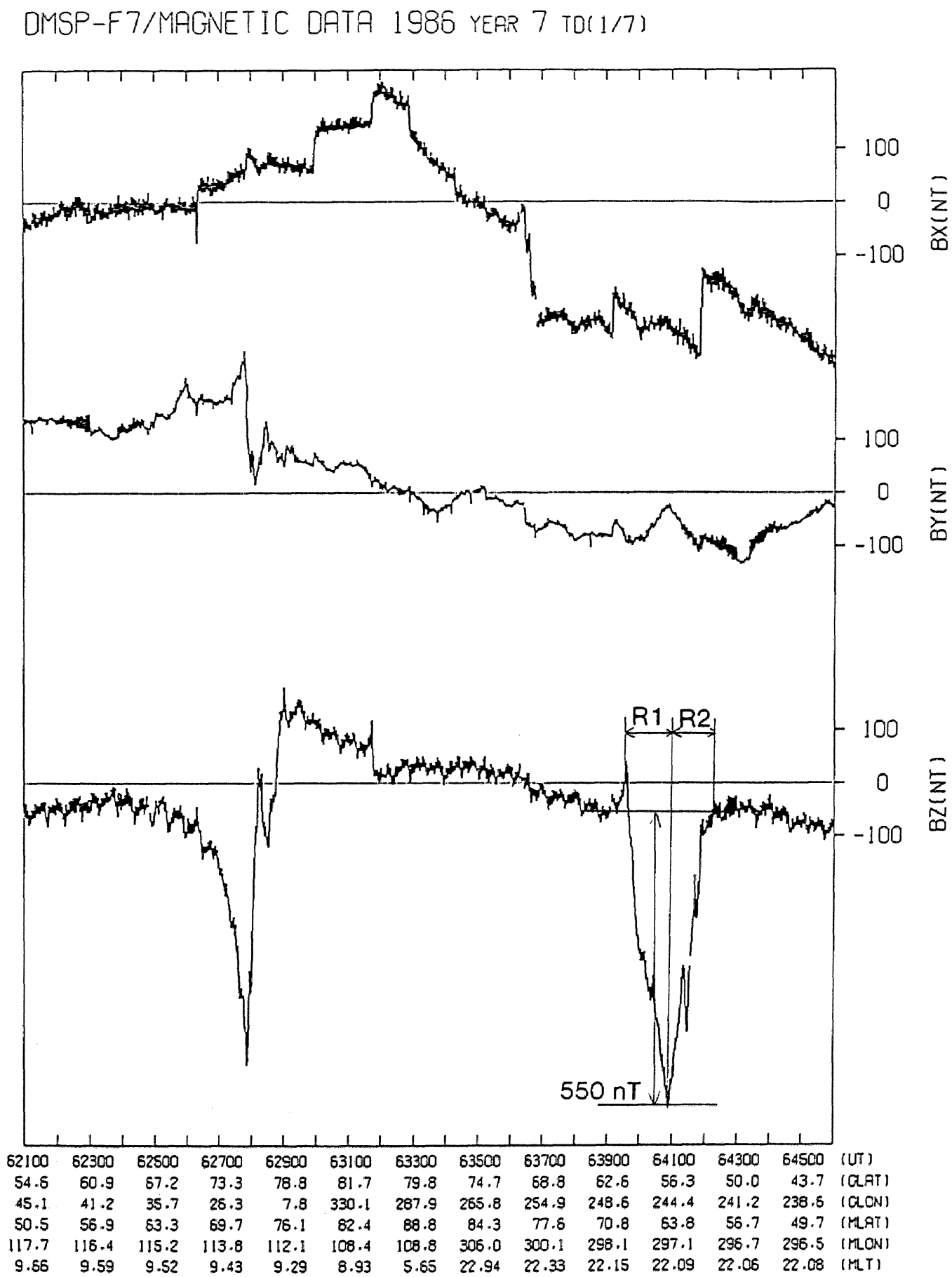

Figure 5.6 Magnetic field variations at DMSP-F7 from 0621 UT to 0646 UT on January 07, 1986.

from 0639:40 UT (~ 68.5° magnetic lat.) to 0641:00 UT (~ 65.0° magnetic lat.), and from 0641:00 UT to 0642:00 UT (~ 60.0° magnetic lat.), respectively. At the poleward edge of the Region 1 current there were two steep negative slopes in the Z component as can be clearly seen in Figure 5.7, which shows the magnetic field variation with higher time resolution. These slopes, which indicate the presence of small-scale upward field-aligned currents, are collocated with the two discrete arcs observed by the ground TV camera and crossed by the DMSP-F7 satellite as shown in Figure 5.5. They are collocated also with the particle precipitation region as shown in Figure 5.8; two sharp inverted-V's were seen in the electron energy-time spectrum. The relative location of the auroral surge to the Region 1 and Region 2 field-aligned currents will be discussed in Section 5.3.

The intensity of the Region 1 and Region 2 currents which cause the 10° azimuthal deviation of the foot point of the geosynchronous satellite is about 0.45 A/m. The field-aligned currents with this intensity would produce a Z component magnetic field perturbation at the DMSP-F7 satellite of 560 nT in amplitude. The actual amplitude of the Z component magnetic field variations at DMSP-F7 across the Region 1 and Region 2 currents is 550 nT for both. This value is sufficiently large to produce the deviation of the foot point of the geosynchronous satellite of about 10° in longitude. If we assume that the intensity of the Region 1 and Region 2 field-aligned currents was constant over the longitudinal extent of 30°, we can say that during this event the intensity of the Region 1 and Region 2 currents surrounding the auroral surge of interest was of the sufficient magnitude to produce the deviation of the ionospheric foot point of the geosynchronous satellite of about 10° in longitude.

5.3. Discussion

We have examined two available examples of approximately simultaneous observation of ground TV camera, GOES satellites, and DMSP satellite to estimate the intensity of the Region 1 and Region 2 field-aligned currents. For the first event on January 27 the Region 1

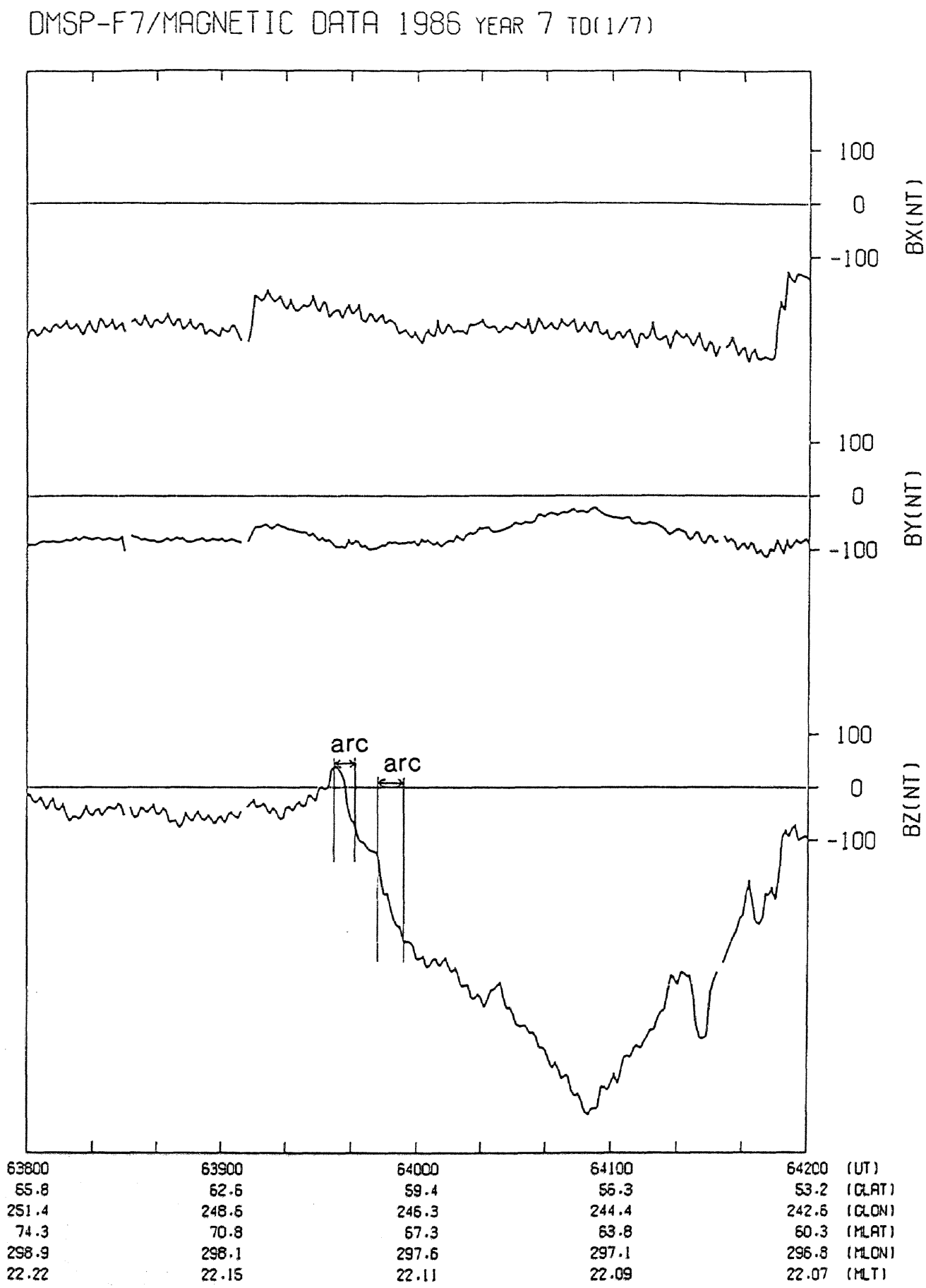

Figure 5.7 Similar to Figure 5.6 for the higher time resolution, from 0638 UT to 0642 UT.

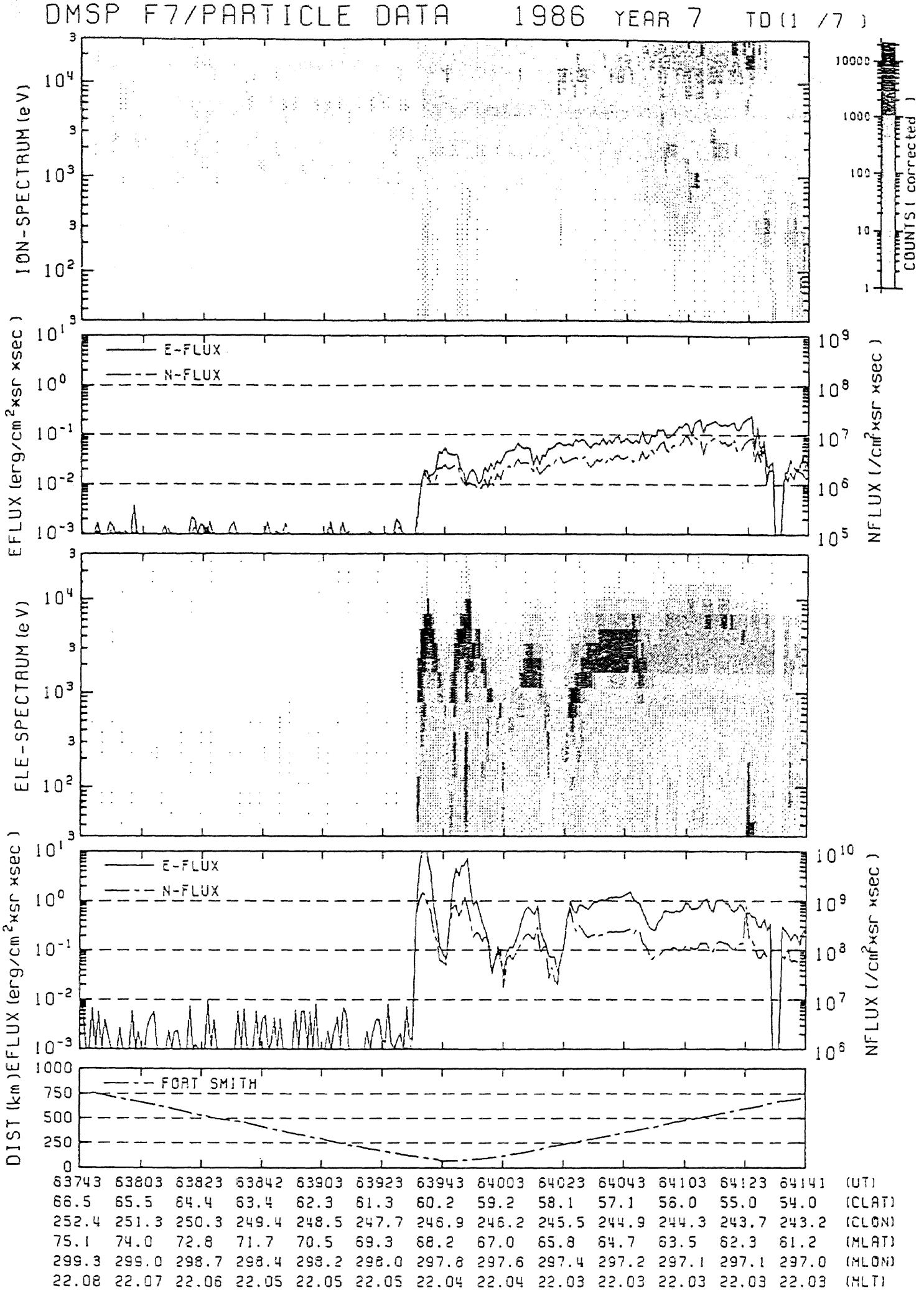

Figure 5.8 Energy-time spectrum of the downgoing electrons and ions observed by DMSP-F7 from 0637:43 UT to 0641:41 UT on January 07, 1986.

and Region 2 currents showed the intensity to be much less than the value needed to cause the 15° azimuthal deviation of the ionospheric foot point of the satellite. On the other hand, for the second event on January 07 the field-aligned current intensity was large enough to cause the azimuthal field line deflection of about 10°. This is probably due to the difference in the substorm phase. For the first event the observation was made during the recovery phase and for the second event during the auroral expansion, which is confirmed from the magnetograms at auroral zone stations (Figure 2.8 and 2.36).

For the second event the AE value (Figure 2.27) showed a sharp peak of 620 nT with AU 340 nT and AL 280 nT. On the other hand, for the first event the AE value (Figure 2.4) was 360 nT with AU 150 nT and AL 210 nT at 0458 UT when DMSP passed across the large-scale field-aligned currents. During the expansion which began at 0448 UT, the AE index had no prominent sharp peak. However, the expansion at 0448 UT was rather localized near SHM, where a decrease in the Xm component of about 400 nT was observed. The activity did not reach the AE station CHR, about 250 km north of SHM, and as a result AE had no outstanding peak for this expansion. If we tentatively add the magnetogram at SHM to redefine the AE index, the AE would be 550 nT with AU 150 nT and AL 400 nT, which is approximately the same as that for the second event (620 nT). Furthermore, the geomagnetic activity level around the auroral observation sites (GWR, SHM, and LGR) was higher for the first example, as can be clearly seen in Figures 2.8 and 2.36. In the first example, on January 27, a sharp negative Xm perturbation of about 400 nT was observed at SHM. In the second example on January 07 the most outstanding change was the rather gradual positive Xm perturbation of about 200 nT at LGR. Hence it is suggested that when GOES 6 observed a sharp positive D perturbation at 0452 UT during the first event, the intensity of the Region 1 and Region 2 currents was large enough to produce the 15° longitudinal deviation of the foot point of GOES 6.

As already mentioned in the previous chapters, the magnitude of the deviation of the foot point of the satellite depends not only on the intensity of large-scale field-aligned currents

but also on the relative location of the field lines threading auroral surges to these currents. Auroral surges are observed frequently in the polar boundary of the Region 1 currents (e.g. Bythrow and Potemra, 1987). However, in this study we are dealing with the surge only a few minutes after the expansion onset. Since the expansion onsets occur usually near the equatorward boundary of the discrete auroral region (Rostoker et al., 1980), we can therefore expect that auroral surges in the examples discussed in this study are located near the equatorward boundary of the Region 1 current.

We can examine this relative location by using the ground TV images and the DMSP magnetic field data for the two examples described above. For the first example on January 27, the surge was located at 66° to 68° geomagnetic latitude at 0453 UT. The equatorward boundary of the Region 1 current was at about 65° at 0459 UT as seen in Figure 5.3. Although these two were observed within a 6 minutes interval, they are observed almost at the same longitude. Hence it seems certain that the surge was located at the equatorward boundary of the Region 1 current within a range of 1°, equatorward of the center of the Region 1 current ($\sim$ 69°). For the second example on January 07, the surge was located at 64° to 66° geomagnetic latitude at 0639 UT and the equatorward boundary of the Region 1 current was located at about 64° at 0641 UT (Figure 5.7). While these two observations were made with a longitudinal difference of about 30°, these two values were obtained almost simultaneously. If we assume that the geomagnetic latitude of the Region 1 and Region 2 field-aligned current was constant over the longitudinal area of 30°, we may expect that the surge was located near the equatorward boundary of the Region 1 current within a range of 2°, equatorward of the center of the Region 1 current ($\sim$ 66°). We can therefore conclude that for these two events the auroral surges were located at the position where the significant deflection of the magnetic field line by large-scale field-aligned current can be expected.

5.4 Summary

We have used the DMSP-F7 magnetic field data to examine the intensity of the Region

1 and Region 2 field-aligned currents, together with the location of auroral surges relative to these currents for the two expansions: at 0448 UT on January 27 and at 0639 UT on January 07.

For the first example on January 27, the DMSP passed across the Region 1 and Region 2 currents at about 0458 UT. The intensity of the Region 1 and Region 2 currents was much less than the value obtained from the model calculation made in Chapter 4, to account for the 15° azimuthal deviation of the ionospheric foot point of the geosynchronous satellite. On the other hand, for the second example on January 07, the satellite passed across the Region 1 and Region 2 currents at about 0640 UT and the current intensity was large enough to cause the measured 10° longitudinal deviation of the foot point. From the magnetograms at auroral-zone stations and the AE index, we conclude that for the first example DMSP passed the current region during the recovery phase whereas, for the second example, the satellite passed the region during the expansion. Therefore the difference in the intensity of the Region 1 and Region 2 currents between these two examples can be ascribed to the difference in the substorm phase as well as the activity level around the observation sites. In addition, it is suggested that the Region 1 and Region 2 field-aligned currents develop and decay within a considerably short time scale of several minutes.

We have also examined the relative location of the auroral surges to the large-scale field-aligned currents for these two examples. For both examples the auroral surge was located near the equatorward edge of the Region 1 field-aligned currents within a range of 1° to 2°, equatorward of the center of the Region 1 current. Hence we can conclude that for the two examples the surge was located at the position where a significant deflection of the magnetic field line is expected by large-scale field-aligned currents.

6. Conclusions

6.1 Summary

The short time scale magnetic field variations at the geosynchronous satellite are caused by small-scale field-aligned currents nearby the satellite. These currents have spatially localized structures in both azimuthal and radial extent. These currents are highly correlated with active auroral forms such as surges and bulges in the vicinity of conjugate areas. Hence it is possible to estimate the ionospheric foot point of the geosynchronous satellite from the comparison of magnetic field variations at geosynchronous orbit and auroral activity at ionospheric altitudes.

The latitude of the ionospheric foot point of the geosynchronous satellite depends on the intensity of magnetospheric equatorial ring and/or magnetotail currents. This is quite reasonable because these currents stretch the earth's geomagnetic field lines to the more taillike configuration. The longitude of the foot point of the geosynchronous satellite is much affected by the presence of large-scale Region 1 and Region 2 field-aligned currents, which are not included into Tsyganenko's model.

The absence of field-aligned currents in Tsyganenko's model is apparent also from the direct examination of the model by two kinds of approach, i.e., mapping analysis and examination of field-aligned currents. Obviously Tsyganenko's model does not correctly represent large-scale but localized structures such as Region 1 and Region 2 field-aligned currents. This is evident from the comparison of Tsyganenko's model with the model based on a 3-dimensional MHD simulation, where a highly localized magnetic field line distortion is found in the near magnetotail, indicating the presence of field-aligned currents. In addition, several unrealistic characteristics are present in Tsyganenko's model especially in the high latitude magnetotail region, because of the limited spatial extent of the magnetospheric observational data set utilized in establishing the model and, more basically, due to the inappropriate mathematical expression of the model.

Thus the introduction of the effect of field-aligned currents into Tsyganenko's model is an

essential requirement to examine the magnetic field line connection between the ionosphere and the geomagnetic equatorial plane. As a result of the introduction of Region 1 and Region 2 field-aligned currents into the model, with the current intensity typical of the disturbed period of the magnetosphere, the ionospheric foot point of the geosynchronous satellite deviates about 10° in longitude. This value is consistent with that obtained from the simultaneous observations at geosynchronous orbit and on the ionosphere.

Of course, the magnitude of the azimuthal deviation of the field line is much affected by the actual intensity of the Region 1 and Region 2 currents. Among two examples of the almost simultaneous observation of field-aligned currents by the DMSP-F7 satellite during substorm expansion, the current intensity was, for one event, large enough to cause the observed deviation of the foot point of the geosynchronous satellite. For the other event, the current intensity was less than half the required value, but this can be attributed to the difference in the substorm phase. The relative location of the field line of interest to these currents is also an important factor. For the above examples the auroral surge of interest was located at the position where the significant deflection of the magnetic field line by large-scale field-aligned current was expected. The deflection of the magnetic field obtained by the comparison of auroras and magnetic field variations at geosynchronous orbit can therefore be explained consistently in terms of Region 1 and Region 2 field-aligned currents actually observed.

The comparative study of magnetospheric and ionospheric phenomena is thus very useful for the examination of the magnetic field connection between the polar ionosphere and the geomagnetic equatorial region. This method affords great possibility for checking existing magnetic field models and would be a great help in establishing a new magnetospheric magnetic field model.

Tsyganenko's magnetic field model of the magnetosphere, although broadly referred to as a good statistical model, has a systematic error in the region surrounded by the Region 1 and Region 2 field-aligned currents. The introduction of these currents could much improve

which represents the real magnetosphere well. MHD simulation, although at present it has several shortcomings, could be one of the most useful methods of quantitatively modeling the magnetosphere. This kind of approach also has the great possibilities for modeling the time-dependent magnetosphere, for example, during substorms. The detailed study of the magnetic field model using MHD simulation, especially its transient characteristics, is highly desirable.

References

Akasofu, S.-I., The Development of the auroral substorm, *Planet. Space Sci., 12*, 273–282, 1964.

Akasofu, S.-I., Polar and magnetospheric substorms, D. Reidel, Publ. Co., Dordrecht, Holland, 1968.

Akasofu, S.-I., The roles of the north-south component of the interplanetary magnetic field on large-scale auroral dynamics observed by the DMSP satellite, *Planet. Space Sci., 23*, 1349–1454, 1975.

Akasofu, S.-I., Physics of magnetospheric substorms, D. Reidel, Publ. Co., Dordrecht, Holland, 1977.

Akasofu, S.-I., and S. Chapman, The ring current geomagnetic disturbances and the Van Allen radiation belt, *J. Geophys. Res., 66*, 1321–1350, 1961.

Akasofu, S.-I., D.S. Kimball, and C.-I. Meng, The dynamics of the aurora – II : Westward traveling surges, *J. Atmos. Terres. Phys., 27*, 173–187, 1965.

Akasofu, S.-I., S. DeForest, and C. McIlwain, Auroral displays near the foot of the field line of the ATS-5 satellite, *Planet. Space Sci., 22*, 25–40, 1974.

Armstrong, J.C., S.-I. Akasofu, and G. Rostoker, A comparison of satellite observations of Birkeland currents with ground observations of visible aurora and ionospheric currents, *J. Geophys. Res., 80*, 575–586, 1975.

Baker, D.N., and R.L. McPherron, Extreme energetic particle decreases near geostationary orbit: A manifestation of current diversion within the inner plasma sheet, *J. Geophys. Res., 95*, 6591–6599, 1990.

Barfield, J.N., C.S. Lin, and R.L. McPherron, Observations of magnetic field perturbations at GOES 2 and GOES 3 during the March 22, 1979, substorms : CDAW 6 analysis, *J. Geophys. Res., 90*, 1289–1295, 1985.

Barfield, J.N., N.A. Saflekos, R.E. Sheehan, R.L. Carovillano, T.A. Potemra, and D. Knecht, Three-dimensional observations of Birkeland currents, *J. Geophys. Res., 91*, 4393–4403, 1986.

Baumjohann, W., R.J. Pellinen, H.J. Opgenoorth, and E. Nielsen, Joint two-dimensional observations of ground magnetic and ionospheric electric fields associated with auroral zone currents: Current systems associated with local auroral breakup, *Planet. Space Sci., 20*, 431–447, 1981.

Boström, R., A model of the auroral electrojets, *J. Geophys. Res., 69*, 4983–4999, 1964.

Bythrow, P.F., and T.A. Potemra, Birkeland currents and energetic particles associated with optical auroral signatures of a westward traveling surge, *J. Geophys. Res., 92*, 8691–8699, 1987.

Chapman, S., and V.C.A. Ferraro, A new theory of magnetic storms. Part 1. The initial phase, *Terr. Mag. Atmosph. Elect., 36*, 77, 1931.

Clauer, C.R., and R.L. McPherron, Mapping the local time-universal time development of magnetospheric substorms using mid-latitude magnetic observations, *J. Geophys. Res., 79*, 2811–2820, 1974.

Craven, J.D. and L.A. Frank, The temporal evolution of a small auroral substorm as viewed from high altitudes with Dynamic Explorer 1, *Geophys. Res. Let., 7*, 465–468, 1985.

Davis, T.N. and M. Sugiura, Auroral electrojet activity index AE and its universal time variations, *J. Geophys. Res., 71*, 785–801, 1966.

DeForest, S.E., and C.E. McIlwain, Plasma clouds in the magnetosphere, *J. Geophys. Res.*, *76*, 3587–3611, 1971.

Eather, R.H., S.B. Mende, and R.J.R. Judge, Plasma injection at synchronous orbit and spatial and temporal auroral morphology, *J. Geophys. Res.*, *81*, 2805–2824, 1976.

Eather, R.H., DMSP calibrations, *J. Geophys. Res.*, *854*, 4134–4144, 1979.

Egidi, A., V. Formisano, F. Palmiotto, P. Saraceno, and G. Moreno, Solar wind and location of shock front and magnetopause at the 1969 solar maximum, *J. Geophys. Res.*, *75*, 6999–7006, 1970.

Elphic, R.C., T.J. Kelly, H.E. Spence, R.J. Walker, C.T. Russell, and M. Sugiura, Auroral zone field-aligned currents observed in the magnetotail and at intermediate altitudes: at ISEE perspective, Magnetotail Physics, Edited by A.T.Y. Lui, The Johns Hopkins Univ. Press, 1987.

Elphinstone, R.D. D. Hearn, J.S. Murphree, and L.L. Cogger, Mapping using the Tsyganenko long magnetospheric model and its relationship to Viking auroral images, *J. Geophys. Res.*, *96*, 1467–1480, 1991.

Fairfield, D.H., Average and unusual locations of the earth's magnetopause and bow shock, *J. Geophys. Res.*, *76*, 6700–6716, 1971.

Fairfield, D.H., A statistical determination of the shape and position of the geomagnetic neutral sheet, *J. Geophys. Res.*, *85*, 775–780, 1980.

Fairfield, D.H., An evaluation of the Tsyganenko magnetic field model, *J. Geophys. Res.*, *96*, 1481–1494, 1991.

Fairfield, D.H., and L.J. Zanetti, Three-point magnetic field observations of substorms in the inner magnetotail, *J. Geophys. Res.*, *94*, 3565–3578, 1989.

Feldstein, Y.I., and G.V. Starkov, Dynamics of auroral belt and polar geomagnetic disturbances, *Planet. Space Sci.*, *15*, 209–229, 1967.

Frank, L.A., and J.D. Craven, Imaging results from Dynamics Explorer 1, *Rev. Geophys.*, *26*, 249-283, 1988.

Gelpi, C., H.J. Singer, and W.J. Hughes, A comparison of magnetic signatures and DMSP auroral images at substorm onset: Three case studies, *J. Geophys. Res.*, *92*, 2447–2460, 1987.

Hardy, D.A., L.K. Schmitt, M.S. Gussenhoven, F.J. Marshall, H.C. Yeh, T.L. Schumaker, A. Huber, and J. Pantazis, Precipitating electron and ion detectors (SSJ/4) for the block 5D/flight 6-10 DMSP satellites: calibration and data presentation, AFGL-TR-84-0314, Air Force Geophys. Lab., Hanscom Air Force Base, MA, 1984.

Iijima, T., Field-aligned currents during northward IMF, Geophysical Monograph 28: Magnetospheric Currents, edited by T.A. Potemra, AGU, Washington, D.C., 1984.

Iijima, T. and T. Nagata, Signatures for substorm development of the growth phase and expansion phase, *Planet. Space Sci.*, *20*, 1095–1112, 1972.

Iijima, T. and T.A. Potemra, The amplitude distribution of field-aligned currents at northern high latitudes observed by Triad, *J. Geophys. Res.*, *81*, 2165–2174, 1976.

Iijima, T., and T.A. Potemra, Large-scale characteristics of field-aligned currents associated with substorms, *J. Geophys. Res.*, *83*, 599–615, 1978.

Iijima, T., and T. Shibaji, Global characteristics of northward IMF-associated (NB_Z) field-aligned currents, *J. Geophys. Res.*, *92*, 2408–2424, 1987.

Iijima, T., T.A. Potemra, and L.J. Zanetti, Large-scale characteristics of magnetospheric equatorial currents, *J. Geophys. Res.*, *95*, 991–999, 1990.

Kamide, Y., and S.-I. Akasofu, The location of the field-aligned currents with respect to discrete auroral arcs, *J. Geophys. Res.*, *81*, 3999–4003, 1976.

Kamide, Y., and G. Rostoker, The spatial relationship of field-aligned currents and auroral electrojets to the distribution of nightside auroras, *J. Geophys. Res.*, *82*, 5589–5608, 1977.

Kamide, Y., J.S. Murphree, C.D. Anger, F.T. Berkey, and T.A. Potemra, Nearly simultaneous observations of field-aligned currents and visible auroras by the Triad and ISIS 2 satellites, *J. Geophys. Res.*, *84*, 4425–4431, 1979.

Kamide, Y., A.D. Richmond, and S. Matsushita, Estimation of ionospheric electric fields, ionospheric currents, and field-aligned currents from ground magnetic records, *J. Geophys. Res.*, *86*, 801–813, 1981.

Kamide, Y., and W. Baumjohann, Estimation of electric fields and currents from International Magnetospheric Study magnetometer data for the CDAW 6 intervals: Implications for substorm dynamics, *J. Geophys. Res.*, *90*, 1305–1317, 1985.

Kamide, Y., and S.-I. Akasofu, The auroral electrojet and global auroral features, *J. Geophys. Res.*, *80*, 3585–3602, 1975.

Kaufmann, R.L., Substorm currents: Growth phase and onset, *J. Geophys. Res.*, *92*, 7471–7486, 1987.

Kisabeth, J.L., and G. Rostoker, Current flow in auroral loops and surges inferred from ground-based magnetic observations, *J. Geophys. Res.*, *78*, 5573–5584, 1973.

Kokubun, S., and R.L. McPherron, Substorm signatures at synchronous altitude, *J. Geophys. Res.*, *86*, 11265–11277, 1981.

Lopez, R.E., D.G. Sibeck, A.T.Y. Lui, K. Takahashi, R.W. McEntire, T.A. Potemra, and D. Klum, Substorm variations in the magnitude of the magnetic field: AMPTE/CCE observations, *J. Geophys. Res.*, *93*, 14444–14452, 1988.

Lui, A.T.Y., R.W. McEntire, and S.M. Krimigis, Evolution of the ring current during two magnetic storms, *J. Geophys. Res.*, *92*, 7459–7470, 1987.

Lundin, R., L.R. Lyons, and N. Pissarenko, Observations of the ring current composition at $L < 4$, *Geophys. Res. Let.*, *7*, 425–428, 1980.

McPherron, R.L., C.T. Russell, and M.P. Aubry, Satellite studies of magnetospheric substorms on August 15, 1968 : 9. Phenomenological model for substorms, *J. Geophys. Res.*, *78*, 3131–3149, 1973.

McPherron, R.L. and J.N. Barfield, A seasonal change in the effect of field-aligned currents at synchronous orbit, *J. Geophys. Res.*, *85*, 6743–6746, 1980.

Mead, G.D. and D.H. Fairfield, A quantitative magnetospheric model derived from spacecraft magnetometer data, *J. Geophys. Res.*, *80*, 523–534, 1975.

Mead, G.D., and D.B. Beard, Shape of the geomagnetic field solar wind boundary, *J. Geophys. Res.*, *69*, 1169–1179, 1964.

Mende, S.B., and E.G. Shelley, Coordinated ATS 5 electron flux and simultaneous auroral observations, *J. Geophys. Res.*, *81*, 97–110, 1976.

Nagai, T., Observed magnetic substorm signatures at synchronous altitude, *J. Geophys. Res.*, *87*, 4405–4417, 1982.

Nagai, T., Field-aligned currents associated with substorms in the vicinity of synchronous orbit 2. GOES 2 and GOES 3 observations, *J. Geophys. Res.*, *92*, 2432–2446, 1987.

Nagai, T., H.J. Singer, B.G. Ledley, and R.C. Olsen, Field-aligned currents associated with substorms in the vicinity of synchronous orbit 1. The July 5, 1979, substorm observed by SCATHA, GOES 3, and GOES 2, *J. Geophys. Res.*, *92*, 2425–2531, 1987.

Nishitani, N., and T. Oguti, Auroral activity and corresponding magnetic signatures at synchronous orbit, *J. Geomag. Geoelectr.*, *40*, 423–445, 1988.

Ogino, T., A three-dimensional MHD simulation of the interaction of the solar wind with the earth's magnetosphere: The generation of field-aligned currents, *J. Geophys. Res.*, *91*, 6791–6806, 1986.

Oguti, T., Metamorphoses of aurora, Memoirs of National Institute of Polar Research: Series A Aeronomy, *12*, 1–101, 1975.

Oguti, T., Questions on the dayside reconnection in connection with magnetospheric convection and open-closed boundary, *J. Geomag. Geoelectr.*, *41*, 879–915, 1989.

Oguti, T., T. Kitamura, and T. Watanabe, Global aurora dynamics campaign, 1985–1986, *J. Geomag. Geoelectr.*, *40*, 485–504, 1988a.

Oguti, T., T. Yamamoto, K. Hayashi, S. Kokubun, T. Ogawa, N. Iwagami, T. Kitamura, O. Saka, T. Araki, K. Makita, N. Sato, T. Watanabe, R.E. Horita, and J.S. Kim, Fast auroral evolution and related magnetic field changes on the ground and at conjugate satellites, *J. Geomag. Geoelectr.*, *40*, 505–536, 1988b.

Ohtani, S., S. Kokubun, R.C. Elphic, and C.T. Russell, Field-aligned current signatures in the near-tail region 1. ISEE observation in the plasma sheet boundary layer, *J. Geophys. Res.*, *93*, 9709–9720, 1988.

Olson, W.P., and K.A. Pfitzer, Magnetospheric magnetic field modeling, McDonnell Douglas Astronautics Co., preprint, 1977.

Opgenoorth, H.J., R.J. Pellinen, W. Baumjohann, E. Nielsen, G. Marklund, and L. Eliasson, Three-dimensional current flow and particle precipitation in a westward travelling surge (observed during the Barium-GEOS Rocket Experiment), *J. Geophys. Res.*, *88*, 3138–3152, 1983.

Pytte, T., R.L. McPherron, and S. Kokubun, The ground signatures of the expansion phase during multiple onset substorms, *Planet. Space Sci.*, *24*, 1115–1132, 1976a.

Pytte, T., R.L. McPherron, M.G. Kivelson, H.I. West, Jr., and E.W. Hones, Jr., Multiple-satellite studies of magnetospheric substorms: Radial dynamics of the plasma sheet, *J. Geophys. Res.*, *81*, 5921–5933, 1976b.

Rich, F.J., Fluxgate magnetometer (SSM) for the Defense Meteorological Satellite Program (DMSP) Block 5D-2, Flight 7, Tech. Rep. AFGL-TR-84-0225, Air Force Geophys. Lab., Hanscom Air Force Base, Mass., 1984.

Rosenbauer, H., H. Grünwaldt, M.D. Montgomery, G. Paschmann, and N. Scopke, HEOS 2 plasma observations in the distant polar magnetosphere: The plasma mantle, *J. Geophys. Res.*, *80*, 2723–2737, 1975.

Rostoker, G., S.-I. Akasofu, J. Foster, R.A. Greenwald, Y. Kamide, K. Kawasaki, A.T.Y. Lui, R.L. McPherron, and C.T. Russell, Magnetospheric substorms–definition and signatures, *J. Geophys. Res.*, *85*, 1663–1668, 1980.

Rostoker, G., A. Vallance Jones, R.L. Gattinger, C.D. Anger, and J.S. Murphree, The development of the substorm expansive phase: the "eye" of the substorm, *Geophys. Res. Let.*, *14*, 399–402, 1987.

Sauvaud, J.-A. and J.R. Winckler, Dynamics of plasma, energetic particles, and fields near synchronous orbit in the nighttime sector during magnetospheric substorms, *J. Geophys. Res.*, *85*, 2043–2056, 1980.

Singer, H.J., W.J. Hughes, C. Gelpi, and B.G. Ledley, Magnetic disturbances in the vicinity of synchronous orbit and the substorm current wedge: A case study, *J. Geophys. Res.*, *90*, 9583–9589, 1985.

Snyder, A.L., and S.-I. Akasofu, Observations of the auroral oval by the Alaskan meridian chain, *J. Geophys. Res.*, 77, 3419–3430, 1972.

Steen, Å., and P.N. Collis, High time-resolution imaging of auroral arc deformation at substorm onset, *Planet. Space Sci.*, *36*, 715–732, 1988.

Stern, D.P., *Solar Terrestrial Programs, A Five-Year Plan*, Solar Terrestrial Program Office, Office of Space Sciences, NASA, 1978.

Stüdemann, W., B. Wilken, G. Kremser, A. Korth, J.F. Fennell, B. Blake, R. Koga, D. Hall, The May 2–3, 1986 magnetic storm: First energetic ion composition observations with the MICS instrument on Viking, *Geophys. Res. Let.*, *14*, 455–458, 1987.

Sugiura, M. and D.J. Poros, A magnetospheric field model incorporating the OGO 3 and 5 magnetic field observations, *Planet. Space Sci.*, *21*, 1763–1773, 1973.

Terasawa, T. and A. Nishida, Simultaneous observations of relativistic electron bursts and neutral-line signatures in the magnetotail, *Planet. Space Sci.*, *24*, 855–866, 1976.

Tsyganenko, N.A., and A.V. Usmanov, Determination of the magnetospheric current system parameters and development of experimental geomagnetic field models based on data from IMP and HEOS satellites, *Planet. Space Sci.*, *30*, 985–998, 1982.

Tsyganenko, N.A., Global quantitative models of the geomagnetic field in the cislunar magnetosphere for different disturbance levels, *Planet. Space Sci.*, *35*, 1347–1358, 1987.

Tsyganenko, N.A., Quantitative model of the system of longitudinal magnetosphere currents, *Geomag. Aero.*, *28*, 331–335, 1988.

Tsyganenko, N.A., A magnetospheric magnetic field model with a warped tail current sheet, *Planet. Space Sci.*, *37*, 5–20, 1989.

Tsyganenko, N.A., Methods for quantitative modeling of the magnetic field from Birkeland currents, *Planet. Space Sci.*, *39*, 641–654, 1991.

Wiens, R.G., and G. Rostoker, Characteristics of the development of the westward electrojet during the expansive phase of magnetospheric substorms, *J. Geophys. Res.*, *80*, 2109–2127, 1975.

Zmuda, A.J., and J.C. Armstrong, The diurnal flow pattern of field-aligned currents, *J. Geophys. Res.*, *79*, 4611-4619, 1974.

Appendix: Video Image Data Processing System

We have constructed a video image data processing system, which is very useful in processing and analyzing multi-station auroral TV images.

Figure A.1 shows the block diagram of the system. First, the TV analog video images recorded in the video tape are converted into 512×480pixels × 8bits digital data by TV image processor AVIO-EXCEL. This digital data can be sent to the graphics superworkstation TITAN via Ethernet with the minimum sampling interval of 11 seconds, while for lower resolution data (256×240pixels × 8 bits) images can be sent with the minimum interval of 4 seconds. With the TITAN workstation we can process multi-station 2-dimensional auroral image to construct composite auroral images on the map over a very wide region. Although the average time to make one picture is about 30 seconds, these images created on the TITAN can be stored into the U-matic video recorder in units of one frame, so that we can make a video movie of multi-station auroral images with arbitrary frame intervals.

The digital image data can also be sent to NEC ACOS-930/10 via Ethernet, which can execute computation which requires much CPU time and a large amount of main memory. In addition, this is the only system which is equipped with an image hard copy color printer.

One example of the images, obtained using this image processing system, is shown in Figure A.2. This figure demonstrates the rotation of the auroral vortex structure. The internal motion of this auroral vortex is clockwise, as viewed parallel to the magnetic field, consistent with the result by Oguti (1975) and Steen et al. (1988).

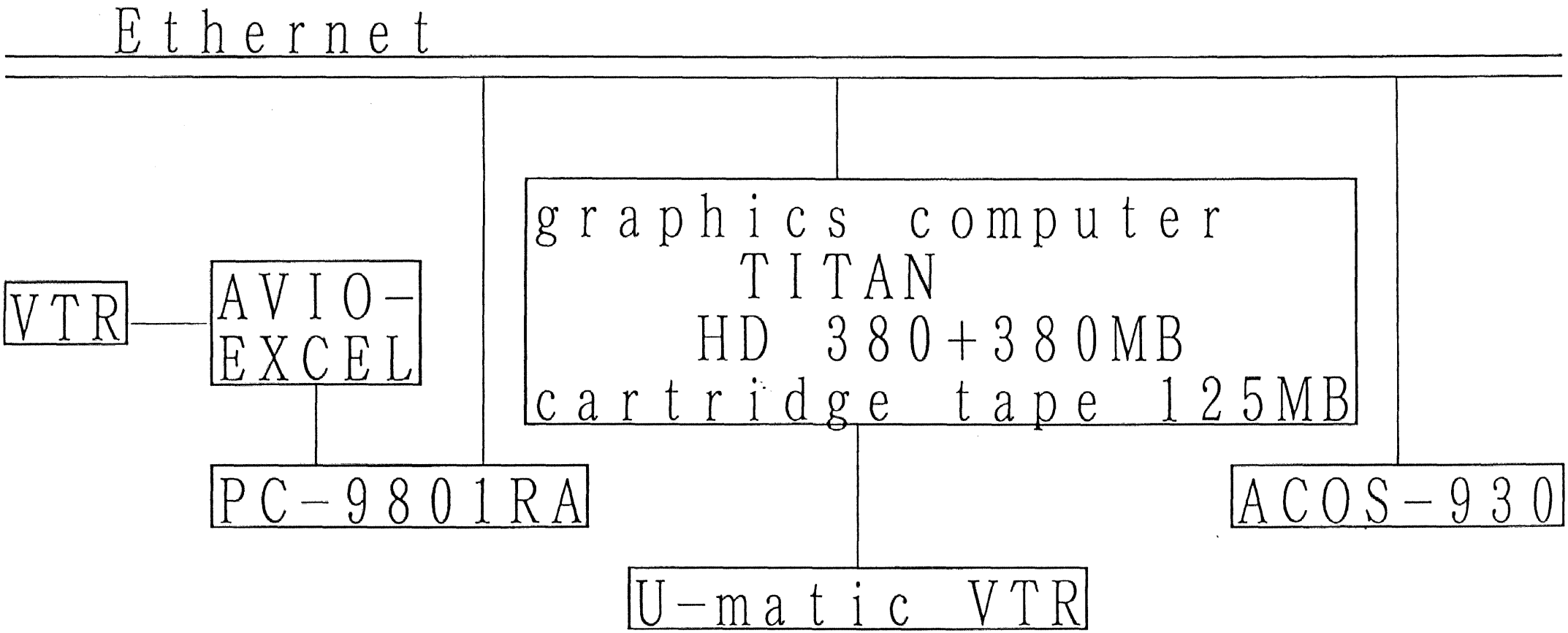

Figure A.1 Block diagram of the image processing system.

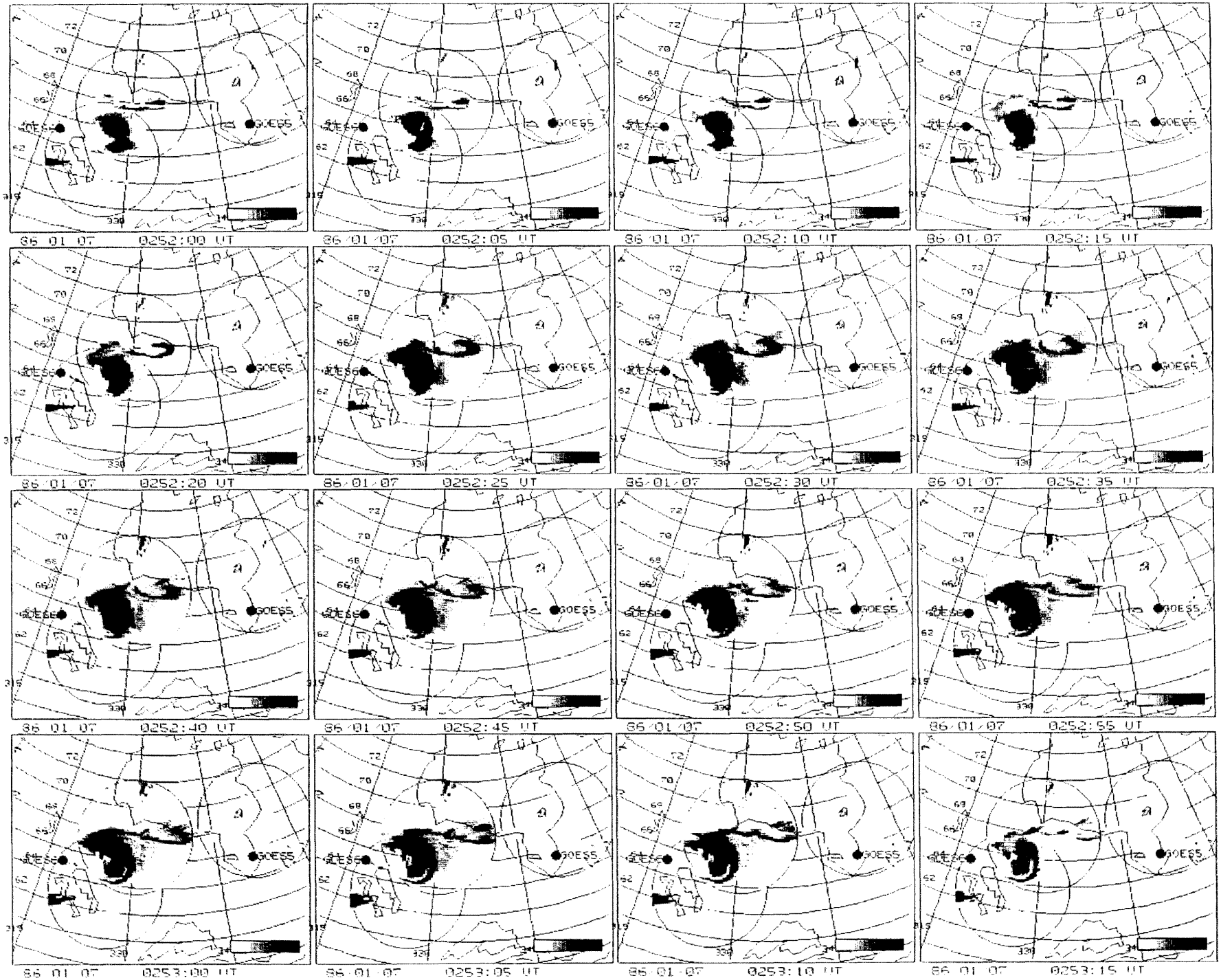

Figure A.2 One example of the processed image, obtained using the image processing system.

The rotation of an auroral vortex is clearly seen.